UNIVERSITY OF SOUTHAMPTON

# Imaging of Mice and Men; Adventures in Multispectral Imaging

by

Paul R. Hoy

A thesis submitted in partial fulfillment for the
degree of Doctor of Philosophy

in the
Faculty of Engineering, Science and Mathematics
Optoelectronics Research Centre

February 2009

UNIVERSITY OF SOUTHAMPTON

ABSTRACT

FACULTY OF ENGINEERING, SCIENCE AND MATHEMATICS
OPTOELECTRONICS RESEARCH CENTRE

Doctor of Philosophy

**Imaging of Mice and Men; Adventures in Multispectral Imaging**

by Paul R. Hoy

Cancer of the brain and CNS account for only 2% of new cancer cases in the UK however it is responsible for 7% of cancer deaths of those aged under 70 years of age. Although surgery falls short of a cure it is the primary method of treatment. Two of the key problems in tumour surgery in the brain are a) that many tumours are visually indistinguishable from normal tissue even for experienced surgeons and b) that the risk of post-surgical neurological deficit is related to the proximity of functional (or 'eloquent') neurological tissue. In collaboration with surgeons at the Southampton University NHS Hospitals Trust we seek to address both of these problems. Firstly there is literature evidence that normal and neoplastic tissue have different spectral characteristics in the visible and near-infrared region. We investigate whether these can be practically imaged intraoperatively to establish disease state. Secondly the redox state of haemoglobin is known to affect it's visible and near-infrared spectral characteristics. This project investigates whether it is possible to identify the haemodynamic response associated with functional activity intraoperatively in the human brain.

Prion diseases are fatal chronic neurodegenerative diseases of animals and man. They have gained notoriety due to recent outbreaks of Bovine Spongiform Encephalopathy (BSE) and the evidence that they can be transmitted between species, including to man. Exposure to BSE infected material has been shown to cause variant Creutzfeldt-Jacob disease in man. Prion disease is also used as a model of other neurodegenerative diseases, such as Alzheimers disease. Remarkably little is known about this class of disease including the specific cause of the neurodegeneration. Prions are a mis-folded protein which have a different conformation than the normal protein. Certain spectral features in the mid infrared region are associated with protein conformation. In collaboration with neuro-biologists within the university and using a synchrotron light source we investigate the application of multispectral imaging in early stage prion disease. By analysis of the protein conformation sensitivity of the mid infrared spectra (with particular interest in the Amide I band) we seek to identify structurally relevant markers in a mouse model before clinical symptoms of the disease are evident. This may lead to better understanding of the disease progression and the neurotoxic element.

# Contents

# List of Figures

# List of Tables

## Academic Thesis: Declaration of Authorship

I, Paul R. Hoy declare that this thesis and the work presented in it are my own and has been generated by me as the result of my own original research

Imaging of Mice and Men; Adventures in Multispectral Imaging

I confirm that:

1. This work was done wholly or mainly while in candidature for a research degree at the University of Southampton;
2. Where any part of this thesis has previously been submitted for a degree or any other qualification at this University or any other institution, this has been clearly stated;
3. Where i have consulted the published work of others, this is always clearly attributed;
4. Where i have quoted from the work of others, the source is always given. With the exception of such quotations, this thesis is entirely my own work;
5. I have acknowledged all main sources of help;
6. Where the thesis is based on work done by myself jointly with others, i have made clear exactly what was done by others and what i have contributed myself;
7. Either non of this work has been published before submission, or parts of this work have been published as:

   Paul R. Hoy, Prof Harvey N. Rutt, William P. Gray and Diederik O. Bulters. Optical intraoperative measurment of function in the human brain. *Frontiers in Optics*, Rochester, 2008. OSA

Signed: _____

Date: _____

# Acknowledgements

First I would like to thank my supervisor Prof. Harvey Rutt who it has been a privilege to work for. He has enabled this project since its inception. His door is always open and how, despite his role as head of school, he still manages to make time his students I may never know.

I would like to thank all my collaborators in medicine and biomedical sciences. Specifically Prof. Liam Gray, Prof. Hugh Perry and Diederik Bulters without whom the collaborations detailed in this thesis would not have been possible.

I would like to acknowledge various funding sources that have helped buy equipment and provide time at a synchrotron. The list of other individuals who have contributed to this project is long and I am unable to mention them all but they include; the other students in the infrared science and technology group, all those that helped in Daresbury and those that have helped proof read this thesis.

Finally I would like to thank my wife Rosie for her love, support, kindness and patience. She is a fantastic mother to our beautiful daughter. Her understanding and forbearance, particularly while writing this thesis, have been invaluable.

Thank you, all.

*To my wife, Rosie and daughter Bethea*

# Abbreviations and selected medical terms

| | |
|---|---|
| $\delta_s$ | Symmetric bending vibrations |
| $\delta_{as}$ | Asymmetric bending vibrations |
| 5ALA | 5-aminolevulinic acid, induces the production of fluorescent porphyrins in affected tissue |
| *in vivo* | Within a living organism |
| AD | Alzheimer's Disease, a fatal neurodegenerative disease of man |
| Adipose | Connective tissue within the body |
| Anatomy | The structure of an organism or part thereof (c.f. Physiology) |
| Angiogenesis | The process involving the growth of new blood vessels |
| Astrocytoma | Most common brain tumour, thought to originate in the glial astrocyte |
| Bitmap | An array of pixel information, limited to 8 bits per pixel for black and white and 24 bits for colour |
| BOLD | Blood Oxygen Level Dependant (signal) |
| BSE | Bovine Spongiform Encephalopathy, fatal neurodegenerative disease in cattle |
| CCD | Charged-Coupled Device, an image capture device consisting of an array of light sensitive capacitors |
| Chronic | A persistent and lasting medical condition |
| CIF | Common Intermediate Format, a video format with 352 pixels by 288 lines, 30 frames per second and 1.22:1 aspect ratio |

| | |
|---|---|
| CJD | Creutzfeldt-Jakob Disease, human fatal neurodegenerative disease |
| $cm^{-1}$ | Wavenumbers, a measure of frequency, defined as the reciprocal of wavelength in centimetres |
| CMOS | Complementary Metal-Oxide Semiconductor, as imaging devices these are active pixel devices that include readout logic within each pixel |
| CNS | Central Nervous System |
| Colposcope | A magnifying and photographic instrument that allows direct observation of the vagina and cervical epithelial *in vivo* |
| CSF | Cerebrospinal Fluid, the clear bodily fluid that occupies the space between the brain and the skull and any empty space within the brain |
| CT | Computed Tomography |
| CWL | Centre Wavelength, the middle of the pass band of a filter |
| DECS | Direct ElectroCortical Stimulation |
| EEG | Electroencephalography, The nerophysiological measurement of electrical activity of the brain |
| Eloquent Cortex | An area of the brain that if removed will result in; loss of sensory processing or linguist ability, minor paralysis, or paralysis |
| Epithelium | Membranous tissue composed of one or more layers of tightly packed cells forming the covering of most of the internal and external surfaces of the body and organs |
| ES | Early Stage, individual with early stage disease |
| fMRI | functional Magnetic Resonance Imaging, c.f. MRI |
| fNIRS | Functional Near Infrared Spectroscopy |
| Focal deficit | A problem in nerve function relating to a specific location (such as the left arm) or a specific function (such as speech) |
| FTIR | Fourier Transform Infrared - a spectroscopic technique |
| FWHM | Full Width Half Maximum, the width of a band pass filter at half the maximum transmission of that filter |

| | |
|---|---|
| GBM | Glioblastoma Multiforme - the most common and most aggressive type of primary brain tumour, a type of malignant astrocytic gliomas (WHO grade IV) |
| GI | Gastro-Intestinal |
| GTR | Gross Total Resection, complete removal of a tumour |
| ICCD | A CCD with coupled to an image intensifier used to detect very low signal levels |
| iMRI | Intraoperative MRI, c.f. MRI |
| InGaAs | Indium Gallium Arsenide, when used as imaging devices these are sensitive from 800nm to around 2$\mu$m |
| INIRS | Intracranial Near Infrared Spectroscopy |
| Intraoperative | Used during a surgical procedure |
| IR | Infrared |
| JPEG | Joint Photographic Experts Group, a commonly used compression standard for images |
| KPS | Karnofskey Performance Status allows patients to be classified as to their functional impairment, values range from normal; 100 to deceased; 0 |
| LS | Late Stage, individual with late stage disease |
| LWP | Long Wave Pass, a filter that passes all light (of interest) with a wavelength longer than a given wavelength |
| Meninges | The membranes that enclose the Central Nervous System |
| Morbidity | A diseased condition or incidence of a disease |
| Mortality | Death rate |
| MRS | Magnetic Resonance Spectroscopy see 4.1.2.5 |
| NBH | Normal Brain Homogenate - used as a control for the prion study |
| NIR | Near Infrared, defined here as the spectral region between visible light and the cut off of silicon sensors, i.e. 700nm to 1$\mu$m |
| Oligodendroglioma | A glial tumour thought to be originating from the oligodendrocytes. Typically WHO grade II or III |

| | |
|---|---|
| Oncology | The study of tumours, this may include the diagnosis, treatment and prevention of tumours |
| PET | Positron Emission Tomography |
| Physiology | The study of the function of an organism or part thereof (c.f. Anatomy) |
| PrP | Prion protein precursor |
| $PrP^c$ | Cellular (healthy) form of PrP |
| $PrP^{sc}$ | Scrapie form of PrP |
| ROI | Region of Interest |
| Sensitivity | The probability of positively identifying a positive sample or 'true positives' (c.f. Specificity) |
| Specificity | The probability of negatively identifying a negative sample or 'true negatives' (c.f. Sensitivity) |
| SPECT | Single Photon Emission Computed Tomography |
| Tomography | Any technique which images planes of a body with the exclusion of material outside that plane |
| TSE | Transmissible Spongiform Encephalopathy |
| $V_s$ | Symmetric stretching vibration |
| $V_{as}$ | Asymmetric stretching vibration |
| VGA | Video Graphics Array, a video format with 640 x 480 pixels and 1.33:1 aspect ratio |
| wavenumbers | see $cm^{-1}$ |
| WHO | World Health Organisation |
| vCJD | Variant Creutzfeldt-Jakob Disease, human fatal neurodegenerative disease caused by exposure to the BSE prion. |

# Chapter 1

# Introduction

This project started by investigating the possibility of developing a low cost device for the remote detection of water in structural materials. This work quickly came to an end as described in Chapter 2. The experience gained in difference spectroscopy enabled the opportunities described in the rest of this thesis. There are two primary strands of this continuing work; the first is investigating an early stage prion disease model in mice, the second is developing neurosurgical intraoperative imaging.

Prion diseases have been observed in animals since the mid 18th Century but it was not until the early 20th Century that the first prion disease of man was described. Prion diseases are currently unique in that the infectious agent appears to contain no nucleic acids; the current understanding is that this agent is a mis-folded protein. The protein in question is termed PrP (Prion Precursor) and is highly conserved between species and therefore, unlike most other diseases, is transmissible between these species. These fatal neurodegenerative diseases cause massive neuronal loss, astrocytosis and the deposition of amyloid plaques of this mis-folded protein. This loss of neurons leaves cavities giving the brain an appearance best described as 'spongy'. Hence the term for these diseases is Transmissible Spongiform Encephalopathies.

Prion diseases are good models for other chronic neurodegenerative diseases such as Alzheimer's Disease. In all of these diseases a significant number of neurons and synapses are dead before the onset of clinical symptoms. However the mechanism for the death of these cells is still unknown. Amyloid plaques are found throughout the diseased brain but whether it is these plaques are neuro-protective, neurotoxic or simply a by-product of neurodegeneration is still questioned. It is this last question that this project seeks to investigate by

attempting to identify these plaques at the point of the earliest signs of degeneration.

The key problem the intraoperative imaging work is trying to address is how to maximise surgical resection of tumours and minimise the risk of post-surgical neurological deficit. This problem arises because tumour tissue is visually indistinguishable from normal healthy tissue, even for experienced surgeons. Brain tissue moves significantly during surgery so the registration accuracy with images taken pre-operatively decreases as surgery progresses. Although still debated the extent of resection has been correlated with increased survival. Therefore there is a significant need for an intraoperative system that can image the tumour boundaries.

Post-surgical neurological deficit arises due to damage to tissue associated with the control of function for example the sensorimotor cortex controls motor function. Physiological differences between individuals and the pathology that these individuals are suffering mean that the precise location of this functional tissue is impossible to predict before surgery; there are diagnostic imaging systems that can identify these regions but they have their limitations including the ones stated above regarding intraoperative registration. These regions can be mapped during surgery (for instance by using cortical stimulation) however again these techniques have limitations.

This project addresses the key problem in two ways; one side of the project looks into identifying tumour margins and the other identifying functional tissue. The aim of this work is to develop a real-time non-contact imaging system which can identify the parameters required and present them in meaningful way.

## 1.1 Thesis structure

The rest of this chapter will briefly introduce some concepts in optical spectroscopy that will added to where needed in the following chapters.

Chapter 2 will outline the work done investigating the detection of water in structural materials. This will introduce the reader to multispectral imaging in the form of a short case study.

The work investigating prion disease will be presented in chapter 3 and will be followed by the work on intraoperative imaging. Finally conclusions will be drawn together and details of future work will be presented in chapter 5.

## 1.2 Spectroscopy primer

All materials absorb light differently, this is commonly known to give materials their colour. This property is not limited to visible light and extends either side of the visible part of the electromagnetic spectrum — figure 1.1 shows an example of an absorbance spectrum. One area of the spectrum of interest is Infrared (IR) particularly with frequencies between 4000 and 400cm$^{-1}$ (wavenumbers). This area is important because all the fundamental vibrations of interatomic bonds in organic compounds appear in this region. These vibrations absorb radiation at different frequencies and intensities. IR spectroscopy involves collecting this absorption information and analysing it in the form of a spectrum.

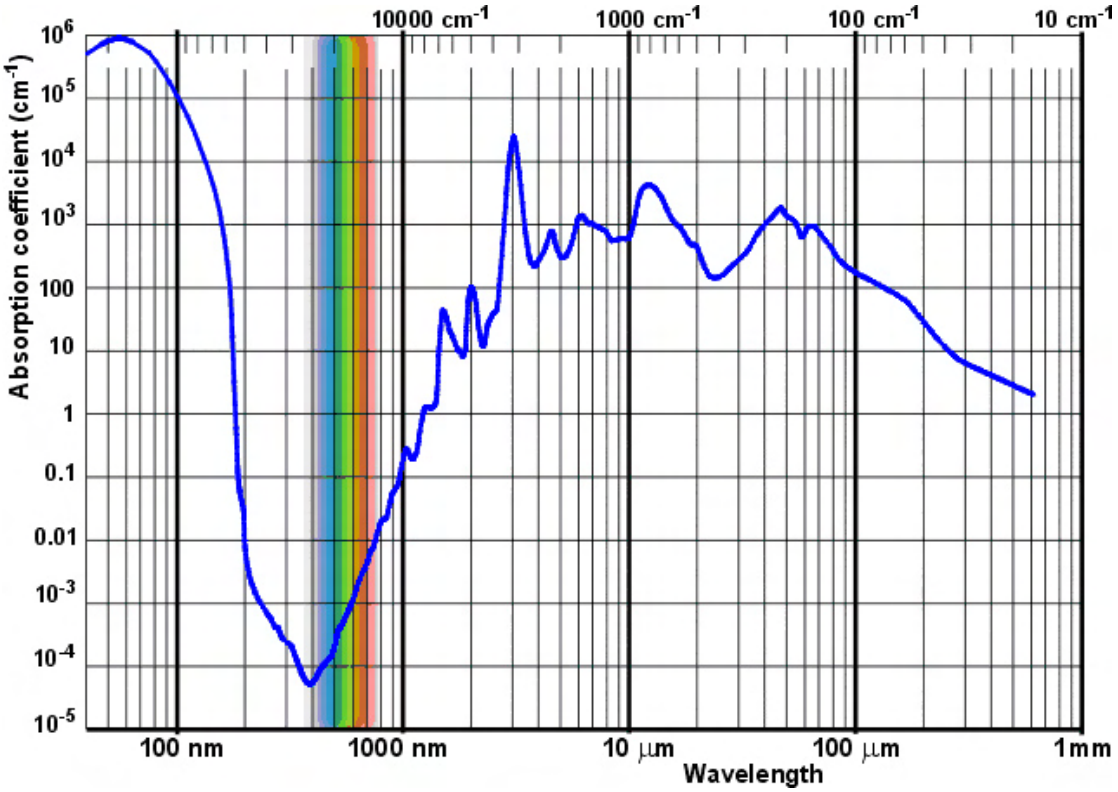


FIGURE 1.1: Absorption characteristic of water (image courtesy of Martin Chaplin www.lsbu.ac.uk/water)

Materials absorb different frequencies of light depending on the characteristics of the material and the mode of absorption. Table 1.1 broadly categorises these different modes of absorption. Electronic absorptions give materials their colour, these absorptions typically require the higher energy photons found in the very near IR and shorter wavelength ranges. Pure rotational absorptions and the more common torsional vibrations (where a full rotation is not possible) have very low energies and so occur in the very long wave IR. Because of the low energies they are very difficult to detect and isolate; in mid IR spectra these

rotations cause additional bands either side of the main absorption peak or broaden the main absorption depending on the type of sample. Vibrations have their fundamental absorptions in the mid IR. These can be further broken down into bending vibrations and stretching vibrations. Stretching vibrations generally have higher energy than bending vibrations and so occur at higher frequencies — the energy of all of these vibrations is dependant on the bond energy and the masses of the atoms involved. Not all vibrations absorb IR radiation; bonds where there is no change in electric dipole with vibration will not be IR active. Raman spectroscopy can also be used to detect material characteristics in the same frequency region as IR spectroscopy. The selection rule for Raman spectroscopy is there must be a change in the polarisability of the molecule with the vibrational molecule. In all but the simplest molecules bonds are typically visible by both IR and Raman spectroscopy but often have differing intensities.

| **Absorption Type** | **Location (wavenumbers)** | **Location (wavelength)** |
|---|---|---|
| Electronic | 12500–50000cm-1 | 800–200nm |
| Vibration | 400–4000$^{-1}$ | 25–2.5$\mu$m |
| Rotation | 10–300cm$^{-1}$ | 1mm–30$\mu$m |

Table 1.1: Location of typical vibration modes in small molecules

This project uses a number of different sensing techniques to build up images of the target scene. The use of a number of images taken of the same scene using different parts of the EM spectrum is called multispectral or hyperspectral imaging. Multispectral imaging is the use of wider spectral bands or the use of spectral regions that are not contiguous. Hyperspectral imaging is the use of many small bands of the spectrum contiguously. The prion imaging work in Chapter 3 is an example of hyperspectral imaging whereas the water and medical imaging work in Chapters 2 and 4 uses specific and discrete absorption bands and so are examples of multispectral imaging.

# Chapter 2

# Low Cost Detection of Water

This chapter looks at a low cost method of detecting water in structural materials. It gives a complete description on the work done on this part of the project. It will describe; the problem and the operating restrictions, how this problem was approached, the prototypes developed, the results and conclusions.

This part of the project is not currently under active development however this is where the project started and is a good introduction to difference spectroscopy.

## 2.1 Background and assumptions

The remote detection of water in structural materials is of importance to a range of customers, from civil and structural engineers to home buyers and do-it-yourself enthusiasts. There is also application in the agricultural sector looking at the hydration of vegetation and the efficiency of irrigation. This project aims to show whether it is possible to create a device that this market will support.

The primary driver for this project is the civil/structural engineering sector. Their current methods of analysis typically measure resistance between two pads or probes placed in contact with or inserted into the material under investigation. This method is very dependant on the material in question and requires direct physical access to the measurement site; this can be a particular problem if the material is difficult to access for example the underside of a motorway bridge. Using these techniques it requires a number of readings to assess an area. To be able to assess larger areas in one go is a step change that will make a significant difference in this field. However it is thought that (Dadachanji (2003 (personnal communication)) this market will not support high

cost devices; preliminary investigations suggest a retail price of around £1000 - this value has been taken as an upper limit for the project cost.

The key issues that need to be addressed are as follows;

- Analysis and understanding of how to remotely detect water.
- Knowledge of the theory and practical uses of various imaging technologies including silicon CCD and CMOS imagers, other materials such as Indium Gallium Arsenide (InGaAs) and any emerging technologies to select the most suitable sensor for the application.
- Design and optimisation of the optical system, including detection methods.
- Image processing to extract the required information.
- Integration of the subsystems into a robust, cheap, easy to use device.

The detection method proposed is difference spectroscopy which typically looks for a particular feature of the IR spectrum by comparing absorption at that feature with the absorption at an area nearby in the spectrum which does not contain that feature. This technique is therefore relatively immune to absolute intensities and does not require a library of sample spectra. Limitations of this technique are that it gives information about a small area of the spectrum and this area must typically selected prior to collection. The choice of spectral region must be carefully made to be sensitive to the target at the exclusion of other materials.

The absorption characteristic of water across the spectrum 200000–10cm$^{-1}$ is shown in figure 1.1; the fundamental vibrations are listed in table 2.1. Overtones (harmonic excitation of a particular vibration above the frequency of the fundamental) and combinations of these vibrations appear at frequencies right up to visible frequencies (see Appendix A for detailed assignment of these overtones). These overtone and combination bands are still detectable into the Near Infrared (NIR) as shown in figure 2.1. The absorption in the visible region is negligible for the depth of water this project is concerned with.

| **Type of absorption** | **Location (cm$^{-1}$)** | **Location ($\mu$m)** |
|---|---|---|
| Asymmetric Stretch | 3756 | 2.66 |
| Symmetric Stretch | 3657 | 2.73 |
| Bend | 1594 | 6.27 |

TABLE 2.1: Location of fundamental vibration modes of water

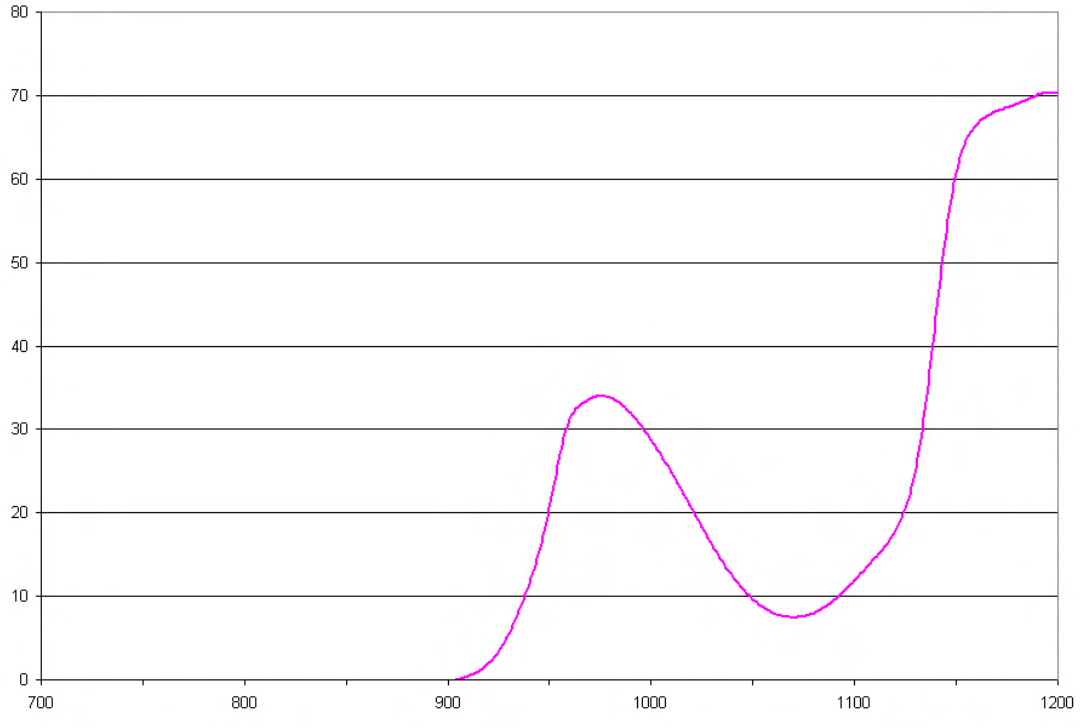


FIGURE 2.1: Measured absorption characteristic of 10mm of distilled water; horizontal axis, wavelength (nm); vertical axis, absorption (%)

## 2.2 Design decisions and experimental strategy

For the proof of principle work the following decisions were made;

- Cheap off-the-shelf imaging sensors will be used instead of a single element sensor scanned across an image. This is a cheaper and mechanically simpler solution and it requires less time to capture an image. However a scanning system may provide better sensitivity, resolution and dynamic range (given the results in section 2.3 of the experiments it may be worthwhile revisiting this decision).
- CCDs are better than CMOS for our purposes. CCDs have higher sensitivity and greater fill factor both are key requirements. The disadvantages of CCDs in regards to power consumption and speed of readout are not critical factors in this application. For a more detailed analysis of the merits of CMOS and CCD imagers see section 4.2.1
- Optical filters will be used to select the required absorption bands. This decision impacts the choice of detector, the filter solution requires a highly sensitive detector as much of the light will be absorbed (or reflected) by the filter.

- A supervised computer based processing system will be used to analyse the images and provide usable output.

The system will use two filters chosen to relate to the spectrum of water, one (on resonance) filter has been selected where water absorbs highly and one (off resonance) where water does not absorb as significantly. The light will be collected and focused onto a camera which records the images and then processed by a computer. The most simplistic processing would be to subtract one image from the other. In reality a number of processing steps are required to improve the signal to noise ratio in the image and to prepare it for display.

The experimental strategy was two-fold. Firstly to construct a series of low cost prototypes and assess their capabilities against a series of targets. The targets progressed from transmission measurements (where the distance travelled through water is controlled and can be as much as a few centimetres) to representative materials. Secondly experiments were conducted investigating the spectra of construction materials with different water contents.

## 2.3 Experimental results

Three different prototype systems were constructed the configuration of these can be found in table table 2.2.

The MK1 prototype was used to quickly gain an appreciation of the key problems. This 'quick and dirty' prototype used stock RG filters and produced results within two weeks of the start of the project. The camera is a CMOS webcam. The camera was modified by removal of the IR cut filter; it is a colour device however the colour filters used on the CMOS chips are almost transparent in the NIR region, as shown in figure 2.2. Quantum efficiency (QE) is defined as the ratio of output quanta to input quanta and in this case is the ratio of photons at a given wavelength incident on a detector to the number of electrons out of the detector. Therefore QE is a measure of the sensitivity of a detector at a given wavelength. The overall decrease in efficiency toward 1100nm is fundamental to all silicon detectors and silicon starts transmitting light around this point so has no sensitivity beyond that.

Figure 2.3 shows a plastic cup partially filled with water. The difference between the on resonance and the off resonance filter (or the 'water signal') is highlighted in red, note that the blue/red circular area in the upper right hand corner of the images are collection artefacts due to reflection of light from the filters. This shows that it is possible to detect water where light is travelling through it.

| | **MK1 Sweex webcam** | **MK1.1 Sweex webcam (improved)** | **MK2 ExView™ camera** |
|---|---|---|---|
| | | Camera Specifications | |
| **Detector Specifications** | CMOS | CMOS | Sony ExView™ CCD with improved sensitivity and optimised NIR response |
| **Resolution** | 352x288 (CIF) | 352x288 (CIF) | 640x480 (VGA) |
| **Dynamic Range** | 6bits (effective) | 6bits (effective) | 8 bits |
| **Interface** | USB1 | USB1 | Composite video and capture card |
| | | Filter Specifications | |
| **Filter Type** | Coloured glass filter | Interference filter | Interference filter |
| **On Resonance** | RG1000 LWP, 50% transmission at 1000nm | CWL = 970nm FWHM = 10nm | CWL = 970nm FWHM = 10nm |
| **Off Resonance** | RG610 LWP 50% transmission at 610nm | CWL = 900nm FWHM = 10nm | CWL = 900nm FWHM = 10nm |
| **Total cost** | £8.97 | £50 | £90 |

Table 2.2: Configuration of prototype water detectors

However this is not a practical situation for detecting water in structural materials. But it is an encouraging result for a £8.97 device.

The MK1.1 device used interference filters which are much better at isolating the water signature. The Full Width Half Maximum (FWHM) or the bandwidth of the interference filters is only 10nm so is much more selective than the long wave pass of both the RG filters used in the MK1, figure 2.4 shows the respective spectral transmission of these filters. Because of the selectivity of the interference filters they are used in all the subsequent systems. Other filtering options include; acousto optical tunable filters or liquid crystal filters both of these devices provide electronically controllable wavelength selection however they are currently expensive, have a limited tunable range and require the transmitted light to be polarised, all of these factors make them unsuitable for this project.

Selectivity can be defined as the ability to distinguish between wanted and unwanted signals. The selectivity to water of the optical filters used in the prototypes is dependant on the spectral bandwidth of the filters and the absorption of water in that bandwidth. So by decreasing the bandwidth of the filters and ensuring that their spectral location is in the area where water absorbs most strongly it is possible to maximise the amount of signal due to the water absorption. However reducing the bandwidth means that less light is incident on the detector making it more difficult to detect. The RG filters shown

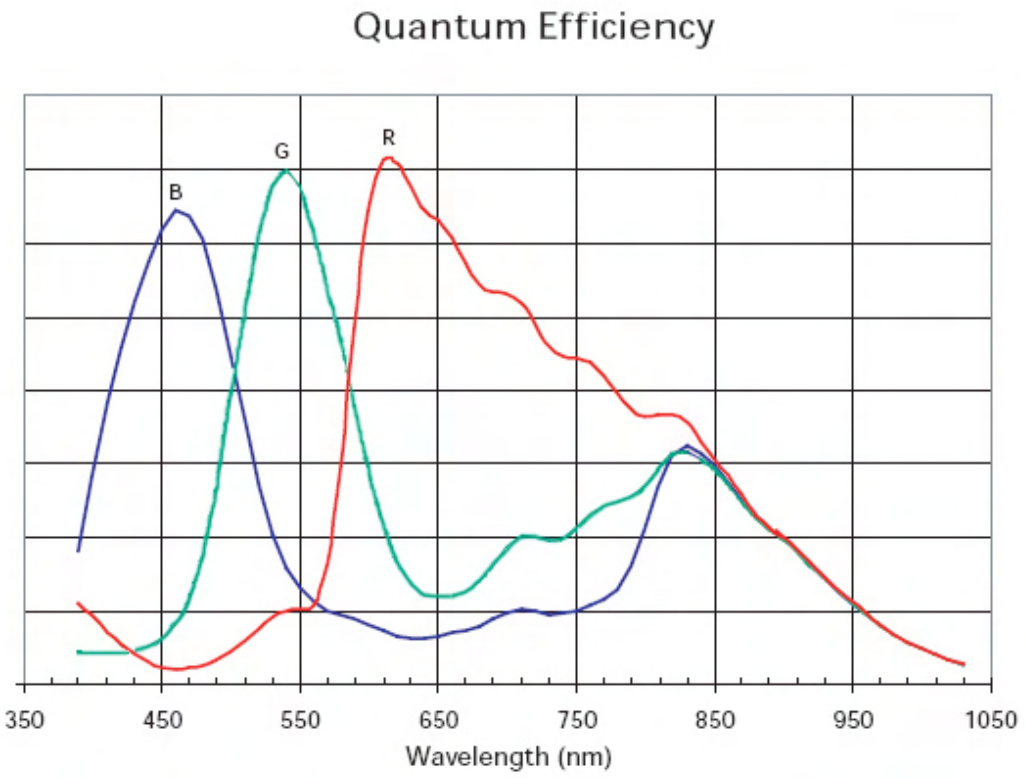


FIGURE 2.2: Typical colour sensitivity of a CMOS imaging sensor without IR blocking filter (image taken from data-sheet for MT9V012 manufactured by Micron)

in figure 2.4 have a very wide bandwidth and so do not select the water band well but allow a lot of light onto the detector. In contrast the interference filters labelled I900 and I970 have a higher selectivity but block much of the incident light requiring a more sensitive detector.

Figure 2.5 shows that the water signal is significantly more obvious (it is again highlighted in red) and the images have reduced artifacts. The darkness around the edge of the images in due to vignetting - the small diameters of the filters cutting off the edges of the image. One key problem with this prototype is that the interference filters due to their selectivity cut out around 99% of the available light. This means that the images collected are more limited by the noise and the dynamic range of the detector. For this reason this prototype still could not detect films of water on test materials where the water signal is significantly smaller.

The MK2 device has a higher effective dynamic range (around 2 bits, a factor of 4, greater) than the previous two prototypes, lower noise figures and greater sensitivity in the region of interest. It uses the same interference filters as MK1.1 so has the same selectivity advantage over the first prototype. These advantages

(a) output of off resonance filter (RG610)

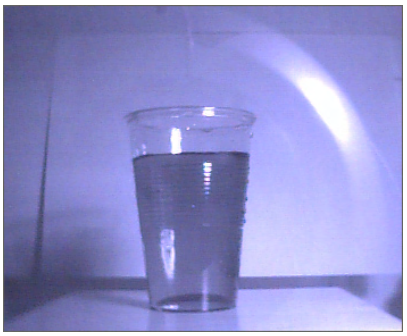

(b) output of on resonance filter (RG1000)

(c) processed output showing water content

FIGURE 2.3: Images showing the output of the MK1 prototype and the water content of a cup of water

are shown by the ability of this device to detect water absorbed onto cardboard as shown in 2.7 which the previous prototypes were unable to do. The image sensor (a Sony ExView$^{TM}$ sensor similar to the ICX258AL — the device was destroyed in the Mountbatten fire of 2005 and therefore impossible to give the actual part number) is optimised for IR sensitivity and is logically a black and white sensor — which also improves sensitivity. The spectral sensitivity is shown in figure 2.6, this is normalised to the maximum response, in practice this is typically higher than CMOS devices and is particularly apparent in comparisons with the cheap CMOS webcam of the MK1 prototypes. The higher spectral sensitivity is due in part to the size of the active area of the device. CMOS sensors use an active pixel architecture which adds logic components to each pixel hence reducing 'fill factor' (the light sensitive area expressed as a

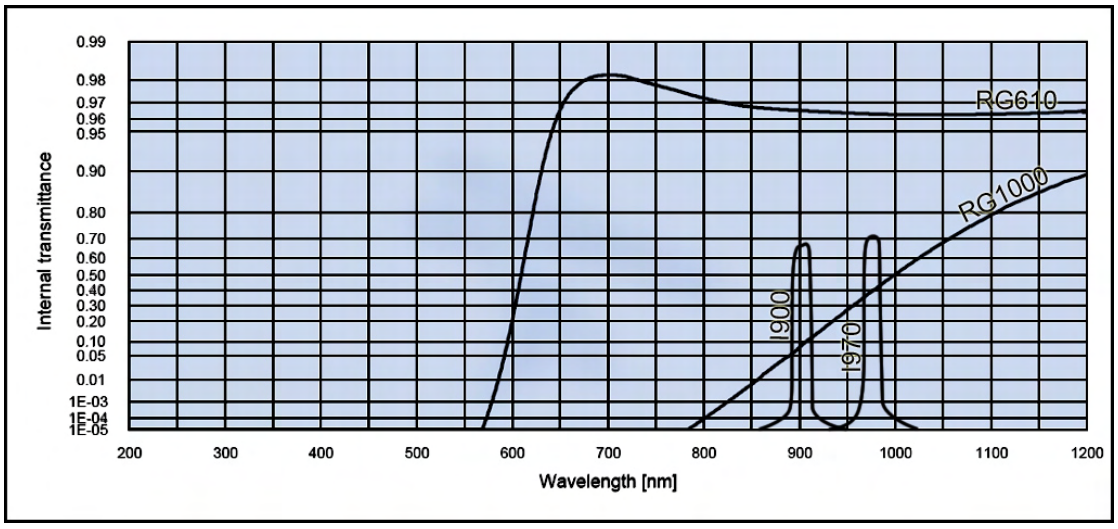


FIGURE 2.4: Spectral characteristics of the filters used in the MK1 and MK2 prototypes, showing both RG filters (RG610 and RG1000) and representations of the interference filters used (I900 and I970) (source for RG filters www.schott.com).

percentage of the total incident area). For the CMOS sensor in the spectral camera used in Chapter 4 this is 60% - which is considered high for a 1Megapixel CMOS sensors without micro-lenses. A CCD sensor however can achieve 100% fill factor, for example the Apogee camera used in Chapter 4 achieves this.

Figure 2.7 shows a piece of wet cardboard, it can be clearly seen an area of the cardboard has been highlighted as containing a water signal. In figure 2.7(c) the water is highlighted red, there is an obvious red area to the left of the cardboard, this is due uneven illumination (the light source is above and to the right of the image).

The Mk2 prototype shows that it is possible to identify areas of water in an image. This prototype and the output image shown in figure 2.7(c) exploited the technique of averaging a number of images to increase the effective dynamic range. The increase in dynamic range scales with the square root of the number of images averaged, the image in figure 2.7(c) was created by averaging 32 images together (giving an effective dynamic range of 11 bits and increased noise immunity) and was calibrated for the conditions at the time. Even with these algorithmic improvements there are only about 4 grey levels (2 bits) associated with the water signal, suggesting that the signal is of the order of 1 in 500. To achieve this level of dynamic range in something approaching real-time requires a more sophisticated camera, these are much more expensive (10bit cameras normally retail at over £1000). There are other techniques available to increase the dynamic range by taking multiple exposures. These techniques are adequate for recompressing the dynamic range to a limited format like a JPEG or Bitmap however they provide a very non-linear response and so are unsuitable.

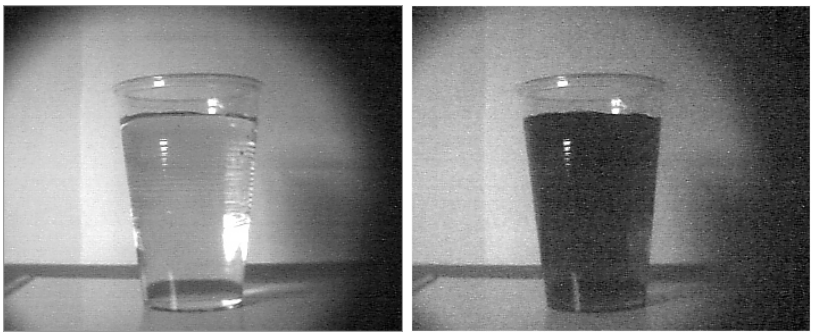

(a) output of off resonance filter (900nm) (b) output of on resonance filter (970nm)

(c) processed output showing water content

FIGURE 2.5: Images showing the output of the MK1.1 prototype and the water content of a cup of water

The low signal suggested that light incident on the subject was travelling through a very small amount of water before reaching the sensor. Figure 2.8 shows a number of interactions between light and matter, it is the third mode from the top that gives rise to the water signal. This signal is small which is intuitively reasonable as at 970nm the absorption coefficient of water is around $3\%\text{mm}^{-1}$ and the distance travelled through the water is short. Measurements were taken on a Varian Spectrophotometer of various building materials to better understand the absorption characteristics of different materials with varying water content. The results of this suggested that the test case of wet cardboard is representative and very low signal levels should be expected (less than 0.1% in some cases). However these data were lost in the fire and as this part of the project is not under active development the measurements have not

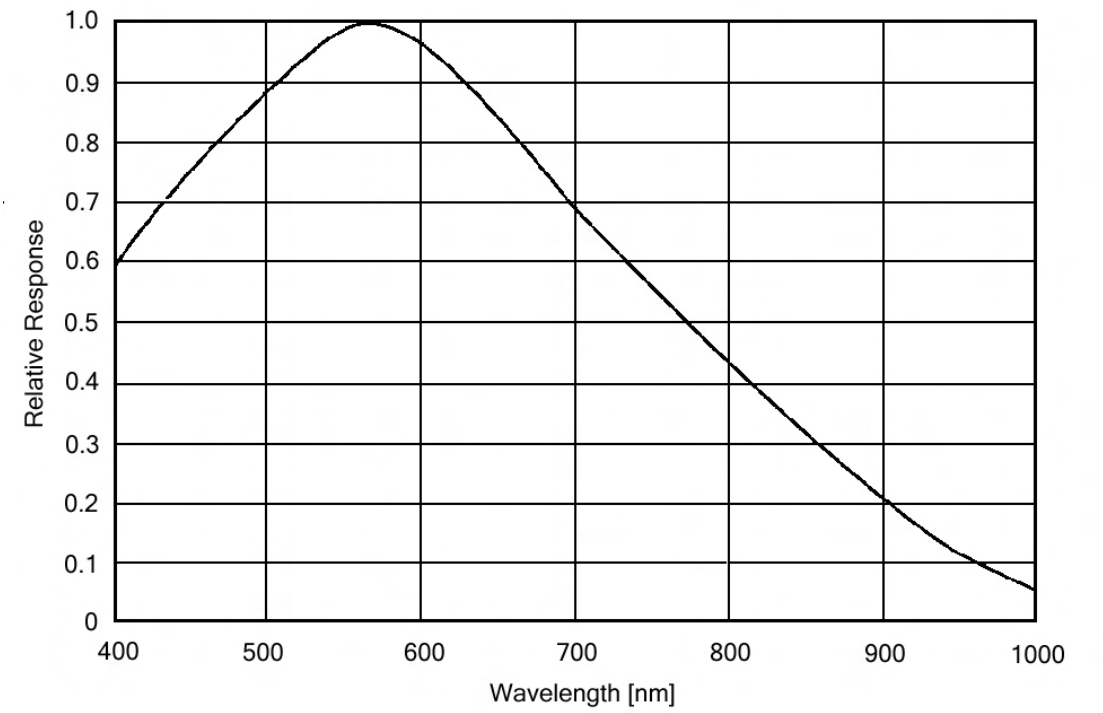


FIGURE 2.6: Spectral Sensitivity of the ExView$^{TM}$CCD

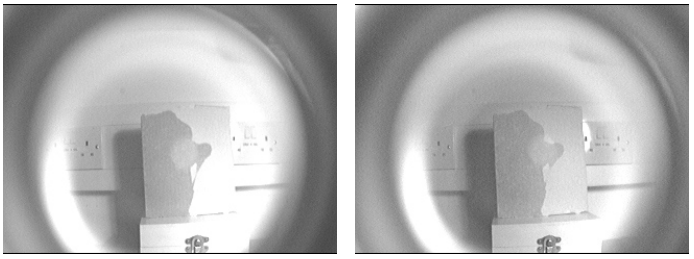

(a) output of off resonance filter (b) output of on resonance filter

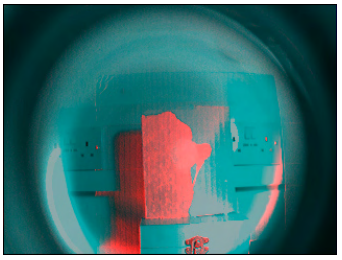

(c) processed output showing water content

FIGURE 2.7: Images from the mk 2 camera correctly identifying damp cardboard

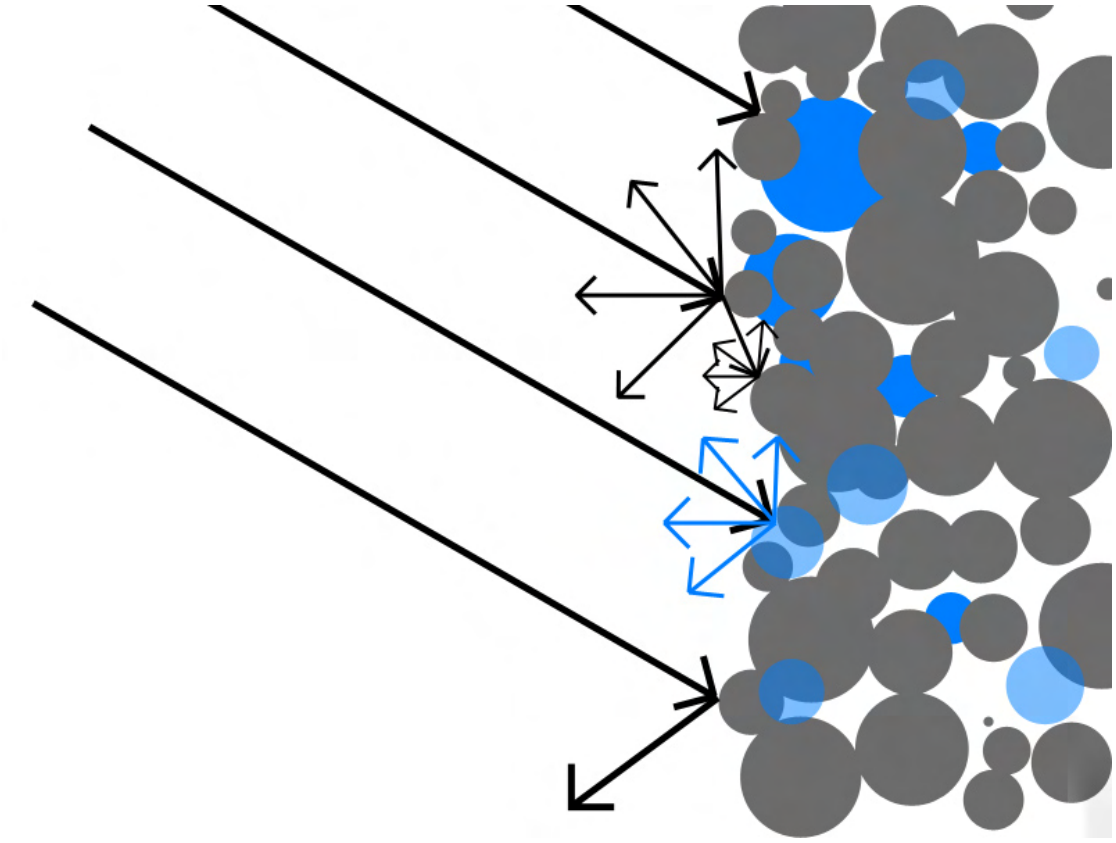

FIGURE 2.8: Modes of scattering and absorption, from top; Absorption, Scattering, Water absorption and scattering, Specular reflection

been repeated.

## 2.4 Conclusions

This part of the project set out to investigate the possibility of developing an imaging device that can detect water in structural materials and that can be produced for under £1000.

The prototypes developed have shown that it is possible to detect water by the spectrum of the diffusely reflected light. However it is difficult and requires imaging capabilities with a dynamic range of in excess of 11bits. The practicalities of the imaging sensors at this level of sophistication are that they are expensive and are in excess of the self imposed £1000 budget. Further work may be undertaken to establish if this budget is realistic or whether the market will support greater costs for such a device.

Further work may be done on using a single element sensor instead of a focal plane array since this should provide higher dynamic range. Using a mirror to

scan across the scene a resolution broadly similar to the prototype systems may be achieved. It may also be engineered to provide a lighting solution that does not rely on ambient light. This system would be more difficult to manufacture and would be more sensitive in operation. The requirement to scan the scene rather than capture in parallel would put practical resolution limits on this technique.

This work has proved that it is possible to use filters to detect relatively small changes in the spectrum of diffusely reflected light and infer from that properties of that material. This may well have application in other areas.

# Chapter 3

# Prion

In collaboration with the CNS Inflammation Group in the School of Biomedical Sciences this project has investigated the multispectral identification of early stage prion disease in tissue samples. Prion diseases are fatal chronic neurodegenerative diseases. They have gained notoriety due to the outbreaks of Bovine Spongiform Encephalopathy (BSE) and the realisation that causative agent of BSE can be transmitted to humans via the food chain and cause variant Creutzfeldt-Jakob Disease (vCJD).

The CNS Inflammation Group within the University is using a prion disease in mice as a model for Alzheimer's Disease (AD) in humans. AD has many of the same characteristics as a prion disease including; fatal chronic neurodegeneration and aggregates of mis-folded protein. Over 26 million people worldwide are estimated to have AD, and it affects around 417,000 people in the UK (Brookmeyer et al. (2007); Alzheimer's Society (2009)) .

One characteristic common to all prion diseases and AD is the accumulation of amyloid plaques containing mis-folded protein. These plaques are composed of many protein molecules which occur naturally in the brain but for some reason are mis-folded and become much more difficult to break down and are possibly neurotoxic. In both AD and prion diseases the normal proteins are associated with cell membranes and have a primarily $\alpha$-helical structure whereas the mis-folded protein has a primarily $\beta$-sheet structure. In pure protein samples these different structures have unique spectral features which enable their identification. This project seeks to identify these features in early and late stage disease *ex vivo*.

## 3.1 Background

This section seeks to establish the literature background to prion diseases in general. It will give a primer on Fourier Transform Infrared (FTIR) spectroscopy and literature background associated with the specific data processing techniques generally known as "resolution enhancement". Finally it will briefly consider the synchrotron radiation source and why this is important.

### 3.1.1 Prion disease

Scrapie was the first recognised Transmissible Spongiform Encephalopathy (TSE). The earliest descriptions of this disease date from the mid 18th Century (Aguzzi (2006)) although it was not known to be transmissible until 1936 when Cuillé and Chelle demonstrated this by intra-ocular injection (Cuille and Chelle (1936)). The demonstration of transmissibility between species followed in Cuille and Chelle (1939) where Cuille demonstrated transmissibility from sheep to goats. In the first part of the 20th Century other TSEs were identified including; the first possible cases of Creutzfeldt-Jakob Disease (Creutzfeldt (1920); Jakob (1921)) and Kuru in the Fore people of Papua New Guinea (Gajdusek and Zigas (1957)). Transmissibility was demonstrated into more species such as scrapie into mice (Chandler (1961)) and CJD into chimpazees (Gibbs et al. (1968)). It wasn't until 1967 when the 'protein-only' hypothesis was proposed by Griffith that the current mechanism for transmission was described (Griffith (1967)). The term 'prion' describing this 'proteinaceous infectious particle' was coined by Prusiner in 1982 (Prusiner (1982)) shortly after which the BSE crisis in the UK brought prion diseases to the public attention.

TSEs are now defined by the transmission and involvement in neuropathogenesis of abnormal forms of prion protein $PrP^c$ (Caughey and Baron (2006)) a list of recognised TSEs can be found in table 3.1. $PrP^c$ is a glycoprotein which is normally monomeric in structure, protease-sensitive and expressed at the cell surface of neurons and glial cells. The purpose of $PrP^c$ is still not known but it is highly conserved within species indicating that it does have an important role to play. The high affinity of $PrP^c$ to bind to Copper and Zinc presents one possibility; that $PrP^c$ may be a sensor or a scavenger of these metals (and these metals have been found near deposits of amyloid plaques in terminal disease, Miller et al. (2006)). $PrP^c$ also appears to be involved in processes which restructure cells whether during learning, cellular differentiation or response to injury and stresses, Caughey and Baron (2006). Mice bred without the PrP gene have various abnormalities including interruption of circadian rhythms leading

to; the inherited prion disease fatal familial insomnia (Tobler et al. (1996)), problems with synaptic function such as epileptiform activity (Collinge et al. (1994)) and increased susceptibility to infection Watarai et al. (2003). It may be the latter observation that provides the greatest insight that $PrP^c$ is associated with the immune response as the brain is particularly intolerant of inflammation. $PrP^c$ is also expressed in lymphoid tissue associated with the immune system (PrP is highly expressed in the human tonsils which may lead to a diagnostic test Hill et al. (1997)) and challenges to the immune system have been shown to increase progression of these diseases, Cunningham et al. (2005b).

| **Host** | | **Disease** | **Cause** |
|---|---|---|---|
| **Animal** | | | |
| | Sheep / Goats | Scrapie | Infection in genetically susceptible sheep; oral transmission; sporadic |
| | Cattle | Bovine Spongiform Encephalopathy (BSE) | Infection with prion-contaminated food; possibly sporadic |
| | Deer / Elk | Chronic Wasting Disease | Unclear, possibly similar to scrapie |
| | Mink | Transmissible Mink Encephalopathy | Infection with contaminated meat from sheep and cattle |
| | Cat | Feline Spongiform Encephalopathy | Infection with contaminated bovine tissue and food |
| **Human** | | | |
| | CJD | Creutzfeldt-Jakob Disease | |
| | fCJD | Familial CJD | Inherited (mutation in the PrP gene) |
| | sCJD | Sporadic CJD | Unknown possibly spontaneous conversion of $PrP^C$ into $PrP^{Sc}$ |
| | iCJD | Iatrogenic CJD | Acquired from contaminated instruments, dura mater grafts or growth hormone |
| | vCJD | Variant CJD | Acquired (infected by bovine prions) |
| | Kuru | | Limited to the Fore tribe of Papua New Guinea, acquired through cannibalistic rituals |
| | GSSS | Gerstmann- Straussler-Scheinker Syndrome | Inherited (mutation in the PrP gene) |
| | FFI | Fatal Familial Insomnia | Inherited (mutation in the PrP gene) |

TABLE 3.1: Overview of the human and animal TSEs (adapted from Kretlow et al. (2006))

If prion disease is transmitted by transforming the host $PrP^c$ to a different conformation (the 'protein-only' hypothesis) then an individual devoid of $PrP^c$ would be immune to the disease. This appears to be the case when tested with mice bred without the PrP gene where inoculation with infected brain homogenate does not induce disease of any kind (Bueler et al. (1993)). It would also be expected that a small amount of $PrP^{sc}$ introduced into brain homogenate *in vitro* would increase, this was demonstrated in Castilla et al. (2005). These observations add weight to the 'protein only' hypothesis however still do not eliminate other mechanisms, for example an unidentified virus.

Although they are poorly defined structurally the abnormal PrP must be consistent enough to allow inter species transmission. Abnormal PrP has been given various names including; $PrP^{tse}$, $PrP^d$, $PrP^{tox}$ and $PrP^{res}$, each of these emphasise different characteristics of the abnormal prion such as disease state or

protease resistance. This document will use $PrP^{sc}$ denoting the scrapie form of the PrP protein. $PrP^{sc}$ forms structures ranging from non-fibrillar oligomers to large amyloid plaques. These large amyloid plaques are apparent in late stage disease and occur throughout the brain; however it is not known whether these are neuroprotective, neurotoxic or simply the detritus of the neurodegeneration. There is a general trend that small-to-intermediate oligomers, equivalent to between 14 and 28 PrP molecules, are the most affective initiators and the more toxic elements (Caughey and Lansbury (2003)) . However there are still questions about the minimum infectious element, a mass greater than that of 5 PrP molecules has been presented by Silveira et al. (2005) however it is possible that is not purely $PrP^{sc}$. The mechanism which disables and kills neurons is still unknown (Caughey and Baron (2006); Aguzzi (2003)).

$PrP^{sc}$ is not amenable to high resolution structural techniques such as X-ray crystallography and NMR, Collinge (2005). It has however had its conformation studied by FTIR and the major difference being that $PrP^{sc}$ is predominantly $\beta$-sheet whereas $PrP^{c}$ is mainly $\alpha$-helix (Pan et al. (1993)). Some drugs can break down the larger amyloid plaques however that may leave the smaller oligomers which have been shown to be more infectious.

Transmissible is not the same as infectious; infectious implies that it is readily communicated which is not the case in prion disease. Experimentally a number of modes of transmission are used, including intra-cerebral injection and orally administered infected brain homogenate. Iatrogenic disease has been transmitted in humans from infected meningeal transplants and hormone products derived from infected tissue. The most troubling mode of transmission reported is through blood transfusion (amongst others, Peden et al. (2004)) intravenous injection of infected brain homogenate has been shown to be as infectious as intracerebral injection Lasmezas et al. (2001). However the transmission reported here by Peden was of whole blood suggesting that contact with cerebral materials is not required. This transmission occurred prior to the raft of measures introduced in the late 90s to reduce the risk of transmission via national blood banks, Wilson and Ricketts (2004). However the long incubation times which are increased due to the so-called 'species barrier' may mean that an epidemic has not yet been avoided, Aguzzi (2006).

Initial transmission between species takes longer than transmission of native prion material (Prusiner (1997)). Unlike the native disease where the progress is notably consistent and all animals will succumb; primary interspecies transmission is variable and not all of the animals will develop the disease, Collinge (2005). For example mice inoculated intracerebrally with BSE brain extracts required over a year to develop disease (Fraser et al. (1992)) whereas

native prions take a consistent 140days (Cunningham et al. (2003)). The species barrier only occurs only on the first transmission, new prion created in the new host is then identical to the native prion in that host — this adds considerable weight to the 'protein only' hypothesis. The method of transmission also influences the incubation time and the species barrier, for instance pigs can be infected by intra-cerebral injection of BSE but not orally, Lasmezas et al. (2001) (an alternative interpretation is that the species barrier by this route is longer than the lifetime of the host).

The species barrier is very much dependant on genotype and there also appears to be a strain component, Lasmezas et al. (2001). For example; BSE only transmits efficiently to a range of species, transmission of sporadic CJD to mice is very difficult with long incubation periods however mice expressing the human PrP gene are highly susceptible and react as if it were a native prion. VCJD transmits more readily to wild type mice than sporadic CJD and is relatively more difficult to transmit into transgenic mice with human PrP Collinge (2005). Most of the cases of vCJD to date (of which there have been 164 in the UK, peaking in the year 2000, The National Creutzfeldt-Jakob Disease Surveillance Unit (2009)) have been of a particularly susceptible genotype with short incubation periods to BSE prions. It is possible therefore that these cases are a genetic subpopulation and the vCJD outbreak is over or more pessimistically that it has not yet started.

The mechanism of neurodegeneration is still under debate, Aguzzi (2006). Evidence that $PrP^{sc}$ is toxic to cultured neuronal cells has been presented (Forloni et al. (1993)) and not confirmed elsewhere (Kunz et al. (1999)). Interestingly cells expressing $PrP^{c}$ are required for neurotoxicity, this was demonstrated by a homozygous graft of brain over-expressing $PrP^{c}$ into a mice devoid of the $PrP^{c}$ gene followed by an inoculation of infected homogenate. Despite the mice having graft derived $PrP^{sc}$ throughout their brain and the graft suffering classic neurodegeneration the mice were still alive and well 16 months after inoculation (Brandner et al. (1996)). It is therefore possible that it is the conversion between $PrP^{c}$ and $PrP^{sc}$ that is neurotoxic, possibly due to some intermediary or depletion of $PrP^{c}$ into the aggregates.

Alzheimer's disease is the most common form of dementia with clinical symptoms of memory loss, disorientation in person, time and place, and cognitive decline. Neuronal and synaptic loss, and the formation of amyloid plaques typifies the damage at a cellular level. This leads to cortical atrophy, narrow gyri, widened sulci and enlarged ventricles at the level of gross anatomy. The amyloid plaques share many of the same characteristics as the prion plaques seen in the diseases mentioned above. Benzinger et al. (1998) demonstrated that the

primary component of the amyloid plaques of Alzheimer's disease is the 39-44 amino acid peptide Beta-amyloid. As with the prion diseases however the role of these plaques in the neurodegeneration is still unknown, Choo et al. (1996). Mutations in this beta-amyloid have been shown to relate to earlier onset and more severe phenotype, Benzinger et al. (1998). Due to prion diseases presenting many of the same morphological and pathophysiological features as AD except in their transmissibility (Aguzzi (2003)) they make a good model for AD .

The prion model used in this project is the murine prion ME7. Clinical signs in mice such as poor coat condition, hunched posture, urinary incontinence and weight loss have an onset around 20 weeks post-inoculation. The animals are normally euthanised around three weeks after the onset of clinical symptoms otherwise the disease course would last for 35 weeks. At the onset of clinical symptoms a significant amount of brain damage has already occurred, maybe as much as 50% of the neurons have been damaged Jeffrey et al. (2000). The earliest this loss of neurons can be detected is at 14 weeks. MRI has also been shown to be able to detect changes before onset of clinical symptoms Dubois et al. (2003). Cunningham et al. (2005a) presents measurable behavioural traits of prion infected mice. The first of these in ME7 infected mice occur at 12 weeks. Spontaneous behaviours such as glucose consumption, nesting, and burrowing are affected first, followed by increased open field activity and cognitive impairments measured in passive avoidance and T-maze spontaneous alternation experiments. Motor impairments (balance, coordination, and strength) occur toward the late stages of disease.

### 3.1.2 Fourier transform infrared spectroscopy

Infrared spectroscopy is a chemical analysis technique which detects the vibrational characteristics of chemical bonds. As mentioned earlier chemical bonds have different vibrational modes: stretching, bending and torsion. The frequency of these vibrations principally depends on the mass of the atoms and the strength of the bond; the environment is also important for example a C–H bond has a different frequency depending on whether it is part of a $CH_2$ or $CH_3$ group.

Fourier Transform Infrared (FTIR) spectroscopy is a technique which encodes the wavelength emission of a source in time, this light then interacts with a sample (e.g. reflection or transmission) and some of this light is absorbed. The remaining light is detected in the time domain, it is then inverse Fourier transformed in a computer. This provides the spectra of the source and sample multiplied together, from which the source spectra (or background) can then be

removed (by repeating the process without a sample). The wavelength encoding is typically performed by a Michelson interferometer and it is the parameters of the spectrometer that determine the fundamental resolution of the output spectra.

In contrast with traditional dispersive techniques where the wavelength information is encoded spatially (e.g. with a prism) and an aperture and detector are scanned spatially to acquire the wavelength information. The Fourier transform technique acquires all of the wavelengths at the same time (the so-called multiplex or Fellgett's advantage). Also the aperture of the Michelson interferometer does not determine the resolution as it does with a dispersive instrument so a much higher intensity is found at the detector giving a greater signal to noise (the throughput or Jacquinot advantage).

FTIR spectroscopy allows the collection of spectra with high resolution and high signal to noise across a range of wavelengths in a reasonably short period of time. A single scan typically takes of the order of a second to complete and scans are normally averaged to improve signal to noise (typically of the order of 100 scans are averaged). Most of the fundamental stretching and bending vibrations of organic molecules are found in the 800–4000 wavenumber region, wavenumbers are the inverse of wavelength in centimetres, denoted $cm^{-1}$.

The absorption bands of the amide bond are of interest when investigating proteins. The amide bond is part of the peptide backbone that links amino acids together to form polypeptides and proteins. A list of the various amide bands, their frequency and assignment are given in table 3.2. The amide I band is of particular interest as it is sensitive to the hydrogen bonding in its local environment. Therefore this bond changes frequency dependant on the conformational structure of the protein. Interestingly in Raman spectroscopy the amide III band is much stronger, it is also sensitive to conformation and so is used in preference using this technique (Surewicz and Mantsch (1988)).

The amide I band is broader than many bands with typical bandwidth around $50cm^{-1}$. In purified simple proteins and polypeptides the predominant conformation can be identified readily as there are distinct changes in the shape of the band. In more complex proteins this is more difficult due to the line-width of the components (figure 3.1 shows some example proteins). However in tissue samples it is almost impossible to identify without further data processing due to the overlapping nature of all of the amide I absorptions.

| **Designation** | **Approximate frequency ($cm^{-1}$)** | **description** |
|---|---|---|
| Amide A | 3300 | NH stretching |
| Amide B | 3100 | NH stretching |
| Amide I | 1600—1690 | C=O stretching |
| Amide II | 1480-1575 | Out of phase CN stretching and NH bending |
| Amide III | 1229-1301 | In phase CN stretching and NH bending |
| Amide IV | 625-767 | OCN bending |
| Amide V | 640-800 | Out-of-plane NH bending |
| Amide VI | 537-606 | Out-of-plane C=O bending |
| Amide VII | 200 | Skeletal torsion |

TABLE 3.2: Characteristic infrared bands of peptide linkage, adapted from Kong and Yu (2007).

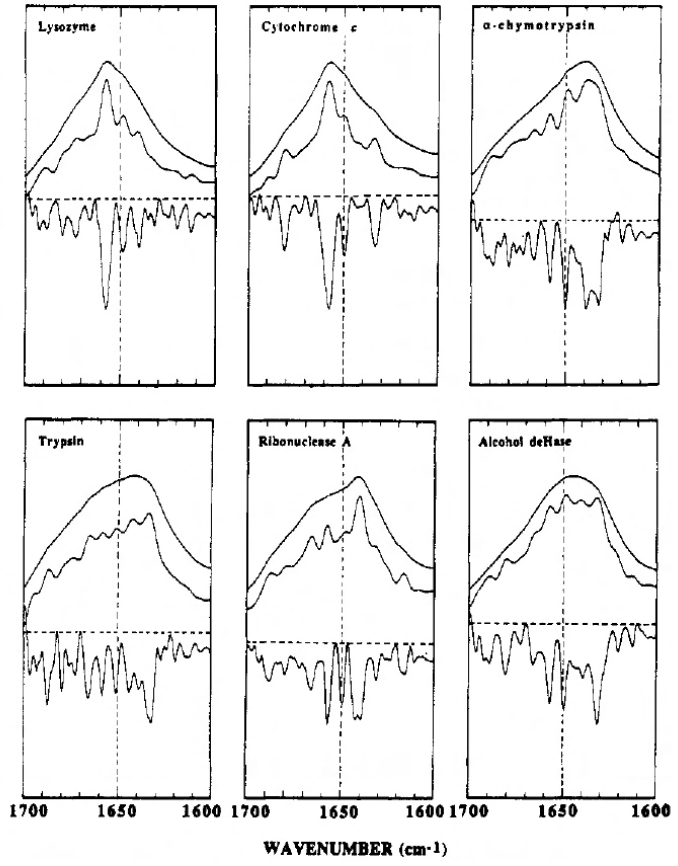


FIGURE 3.1: Image from Dong et al. (1992) demonstrating various amide I band shapes, in each image the upper, middle and bottom trace represent absorption, Fourier self-deconvolution and second derivative spectra. The primary component of each of the proteins is as follows (X-ray crystallographic structural assignments) , Lysozyme – $\alpha$-helix (45%), Cytochrome C – $\alpha$-helix (48%), $\alpha$-chymotrypsin – $\beta$-sheet (50%), Trypsin – $\beta$-sheet (56%), Ribonuclease A – $\beta$-sheet, Alcohol dehydrogenase – $\beta$-sheet (45%)

#### 3.1.2.1 Data processing

FTIR spectroscopy is now a commodity technique even though the machines first became available in the 1970s. There was an interest in resolving the component of the amide I band and given the signal to noise advantage over previous techniques this appeared to be possible. Beginning in the 1980s a number of techniques were developed, Fourier self-deconvolution and even-order derivatives being the two most commonly used. These techniques have moved the precision of FTIR spectroscopic determination of protein secondary structure to a point between modelling and molecular coordinate approaches (Jackson and Mantsch (1995)). FTIR also allows this determination in various conditions including in solution and under changing temperature and pressure for example Meersman et al. (2002).

Fourier self-deconvolution and the derivative techniques are generally called 'resolution enhancement'. This term is not strictly accurate, the fundamental resolution is set by the machine at the time of data collection. These techniques do not increase the resolution but increase the separation between features by narrowing the line-width, thus allowing easier visualisation. The accuracy of the location of these narrower features is still determined by the machine resolution. The cost of narrower line-width is a decrease in signal to noise. A more accurate term may be 'contrast enhancement' and is the term that will be used in this document.

Fourier self-deconvolution was presented by Kauppinen from the observation that a major component of line-broadening had a consistent Lorentzian shape and therefore can be removed (Kauppinen et al. (1981)). Before the Fourier transform of the acquired spectra the intereferogram is divided by the Fourier transform of a Lorentzian of a given width. The choice of parameters is important and may affect how the results are interpreted Surewicz et al. (1993). Details of this technique have been covered in much more detail elsewhere Surewicz and Mantsch (1988); Susi et al. (1985); Byler and Susi (1986).

Even-order derivatives have also been shown to increase contrast as first reported in Susi and Byler (1983) and further in Susi and Byler (1986, 1987); Krimm and Bandekar (1986). Derivatives of output spectra are calculated rather than processing the interferogram. Any derivative will increase the contrast, the advantage of even-orders is that the maximum intensity of component vibrations will occur at the maxima rather than zero-crossings as would happen with odd-order derivatives. Increasing order derivatives are more sensitive to noise, second-order derivatives are most commonly used. Smoothing is routinely used with all derivative processing.

These techniques are often presented together and provide very similar information. The choice of which technique to use seems to depend on the end user rather than technical merit. Cameron and Moffatt (1987) demonstrates that even-order derivatives yield higher signal to noise than convolution techniques. However Fourier self-deconvolution does not change the integrated areas of the different components making comparison with other techniques easier Goormaghtigh et al. (1990).

X-ray crystallography is generally considered the gold standard for protein structural analysis. However crystallographic data on a protein cannot easily be extrapolated to protein properties in solution Kong and Yu (2007). Also not all proteins form crystals, $PrP^{sc}$ appears particularly difficult to crystallise and many membrane proteins present similar difficulties. A question must be raised regarding whether the conformation of a protein in a crystal is identical to that of the protein in its native environment. This is not a problem for most proteins however PrP seems to have two separate stable conformations. Another technique for determination of secondary structure is nuclear magnetic resonance spectroscopy, but the interpretation of nuclear magnetic resonance spectra of a large protein is difficult.

Comparison between contrast enhanced FTIR determination of structural components with X-ray crystallography has been made with many different proteins Kong and Yu (2007); Prestrelski et al. (1991); Goormaghtigh et al. (1990); Oberg and Fink (1998); Fabian et al. (1992); Lee et al. (1990). These reports of components generally agree with crystallography to an accuracy of between 4–7%. Computational models have also been compared with FTIR structural analysis Torii and Tasumi (1992); Perez-Pons et al. (1995), as has circular dichroism Gorga et al. (1988) and again forms a general consensus. Although FTIR alone is not sufficient to assign complete secondary structure (Wilder et al. (1992)) and assumptions are made on the molar absorptivity of components in the amide band (these have been shown not to be equal de Jongh et al. (1996)) it is useful and generally compares well with other physical techniques.

Spectral assignments are widely reported and while there is little contradiction the *exact* assignment must be considered for each protein individually. One structure which is rare but has a unique position in the band is the $3_{10}$ helix (Kennedy et al. (1991)), whereas others have been found not to have a unique position for example the parallel $\beta$-sheet (Khurana and Fink (2000)). A table listing many of the assignments from various sources is presented in table 3.3 or is adequately summarised in table 3.4.

| **Amide I frequency ($cm^{-1}$)** | **Assignment** | **Reference** |
|---|---|---|
| 1624 ±0.5 | $\beta$-sheet | Dong et al. (1990) |
| 1623 | Antiparallel $\beta$-sheet | Susi and Byler (1987) |
| 1626 | Parallel $\beta$-sheet | Susi and Byler (1987) |
| 1627 ±1.0 | $\beta$-sheet | Dong et al. (1990) |
| 1628 | $\beta$-sheet | Susi and Byler (1987) |
| 1631 | Parallel $\beta$-sheet | Susi and Byler (1987) |
| 1632 ±1.0 | $\beta$-sheet and extended chain | Dong et al. (1990) |
| 1632 | Antiparallel $\beta$-sheet | Bandekar (1992) |
| 1634 | Antiparallel $\beta$-sheet | Susi and Byler (1987) |
| 1635 | $\beta$-sheet | Susi and Byler (1987) |
| 1636 | Parallel $\beta$-sheet | Susi and Byler (1987) |
| 1638 ±1.0 | $\beta$-sheet | Dong et al. (1990) |
| 1639 | Parallel $\beta$-sheet | Susi and Byler (1987) |
| 1639 | Antiparallel $\beta$-sheet | Susi and Byler (1987) |
| 1642 ±1.0 | $\beta$-sheet | Dong et al. (1990) |
| 1645 | Parallel $\beta$-sheet | Bandekar and Krimm (1988) |
| 1648 ±2.0 | unordered | Kong and Yu (2007) |
| 1650 ±1.0 | unordered | Dong et al. (1990) |
| 1651 | unordered and $\alpha$-helix | Perez-Pons et al. (1995) |
| 1652 ±1 | $\alpha$-helix | Susi and Byler (1987) |
| 1654 ±4 | $\alpha$-helix and loops | Surewicz et al. (1993) |
| 1656 ±2.0 | $\alpha$-helix | Dong et al. (1990) |
| 1658 | $\alpha$-helix | Bandekar (1992) |
| 1663 ±3.0 | $3_{10}$-helix | Kong and Yu (2007) |
| 1666 ±1.0 | $\beta$-turn | Dong et al. (1990) |
| 1667 | Rippled sheet | Bandekar (1992) |
| 1671 | Antiparallel $\beta$-sheet | Susi and Byler (1987) |
| 1672 ±1.0 | $\beta$-turn | Dong et al. (1990) |
| 1673 | Parallel $\beta$-sheet | Susi and Byler (1987) |
| 1675 | Parallel $\beta$-sheet | Susi and Byler (1987) |
| 1679 | $\beta$-sheet | Susi and Byler (1987) |
| 1680 ±1.0 | $\beta$-turn | Dong et al. (1990) |
| 1685 ±2.0 | $\beta$-turn | Kong and Yu (2007) |
| 1688 ±1.0 | $\beta$-turn | Dong et al. (1990) |
| 1691 ±2.0 | $\beta$-sheet | Kong and Yu (2007) |
| 1694 | Parallel $\beta$ sheet | Bandekar (1992) |
| 1696 ±2.0 | $\beta$-sheet | Kong and Yu (2007) |

TABLE 3.3: A list of amide I band assignments

FTIR analysis of both prion diseases and AD have been reported. Choo et al. (1996) reported on a synchrotron study of AD samples taken from terminal cases. Choo found extreme differences in the spectra associated with the large amyloid plaques found in these cases. The peak frequency found in this report is higher than synthetic amyloid however the measurements are consistent with other

| **Structure** | **Amide I frequency cm$^{-1}$** |
|---|---|
| aggregated strands | 1610-1628 |
| $\beta$-sheet | 1625-1640 |
| unordered | 1640-1648 |
| $\alpha$-helix | 1648-1660 |
| $3_{10}$-helix | 1660-1666 |
| antiparallel $\beta$-sheets or aggregated strands | 1675-1695 |

TABLE 3.4: Summary of structural assignments of frequencies in the amide I band.

proteins in the same spatial region of the sample. However it was already known that there are large amyloid deposits in the terminal brain of both AD and prion.

Kneipp has demonstrated that is is possible to identify prion disease (263K strain) in a hamster model Kneipp et al. (2000, 2002, 2004). However the spectroscopic characteristics are markers of general disease or neuronal death and not specifically related to prion disease. The most significant markers found are located between 1000–1300cm$^{-1}$, a region primarily associated with the phosphate backbone of nucleic acids and not directly related to prion tissue. Although these markers were found before the onset of clinical symptoms, this mirrors disease progress identified elsewhere. In terminal disease of the same model Kretlow et al. (2006) identifies a prion specific marker relating to the $\beta$-sheet content of PrP$^{sc}$ however there is significant overlap with the control tissue indicating that there may be regions of more 'normal' tissue within the diseased samples. Normal tissue has a range of frequencies associated with it, which follows intuitively given the differing constituents of the samples which contain whole cells and have a number of resolution elements across them.

### 3.1.3 Synchrotrons

FTIR spectrometers use an infrared emitting source, standard bench top instruments typically use a glo-bar which is similar to a filament light bulb without the glass enclosure. The key parameter of the source is radiance which is directly related to the overall throughput of the machine.

A synchrotron is a cyclic particle accelerator. As these particles (often electrons) accelerate, as they do when they are bent around the ring, they emit radiation. Due to the relativistic speeds these particles are travelling at this radiation is emitted in a beam tightly confined in the plane of the ring. Various insertion devices such as wigglers and undulators can control the spectral characteristics of the output radiation. Synchrotrons are most commonly used in the short

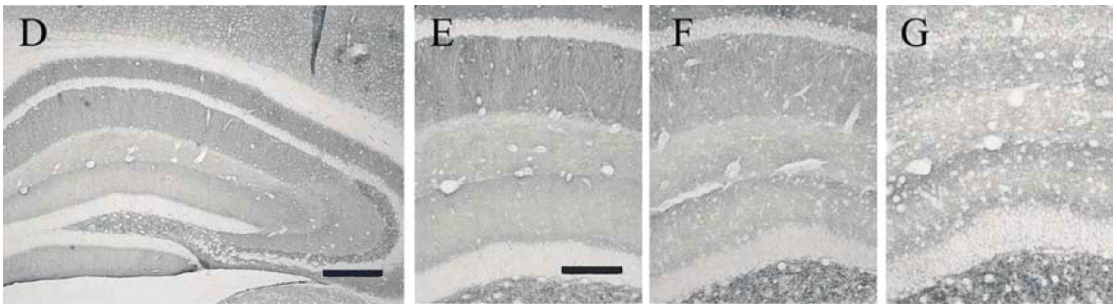


FIGURE 3.2: Extract from Cunningham et al. (2003) showing the NBH mouse hippocampus (D), and the CA1 region of NBH (E), early stage (F) and late stage (G). Scale bars 200$\mu$m D and 100$\mu$m E–G

wavelength region where they are many orders of magnitude brighter than other available sources. In the infrared region they are around 100 times brighter than glo-bar sources used in FTIR instruments, Reffner et al. (1995). The glo-bar does provide more power but over a wider angle and is therefore the choice for large apertures and focal-plane arrays, Miller and Smith (2005).

High spatial resolution spectra with reasonable spectral resolution are required for investigating these prion diseases. As mentioned above the protein content is integrated over an aperture including both diseased and normal proteins. To maximise the chances of identifying a plaque of prion protein the spatial resolution must therefore be maximised this was observed in Dubois et al. (2003).

## 3.2 Experimental setup

Despite the research into prion diseases there are still a number of questions yet to be answered. This project is most interested in why the accumulation of the abnormal $PrP^{sc}$ protein causes the neurodegeneration and mechanism by which this occurs. By studying the earliest phase at a point when the earliest signs of neurological deficit occur, i.e. the first behavioural effects, it may be possible to define the first pathology. Using IR spectroscopy in the region of the brain associated with these first deficits, the hypocampus, the project seeks to identify relevant spectral markers associated with the deposition of $PrP^{sc}$. In the late stage of the disease these deposits are prevalent throughout the hippocampus, in the early stage they are sparse and barely detectable by immunohistochemistry. The immunohistochemistry detects aggregates large enough to bond with the fluorescent marker, IR spectroscopy may be able to detect the $PrP^{sc}$ in the smaller oligomers.

Tissue from normal C57 mice and from animals infected with the ME7 mouse prion agent was collected in accordance with UK Home Office Licence. Tissue

was taken from mice inoculated with Normal Brain Homogenate (NBH) and brain homogenate infected with ME7 at early (13wks) and late stages (18wks) of the disease. The use of individuals inoculated with NBH ensures that any features identified are not associated with surgical damage. Further details regarding the animal husbandry can be found in Cunningham et al. (2003). Images of the hippocampus and evidence of neurodegeneration are shown in figure 3.2. Fresh frozen coronal sections were taken at the level of the dorsal hippocampus, approximately 1.5mm caudal to bregma[1]. Fresh frozen sections were chosen over formalin-fixed parrafin embedded sections as these ensure that any information in the lipid region of the spectrum is maintained. The sections were mounted on Barium Fluoride slips which enabled the use of transmissive mode spectroscopy. The spectral information collected was limited to above 850cm$^{-1}$ due to the absorption of Barium Fluoride beyond this point, however this retains the known important regions of the spectra.

The regions of interest (ROIs) to be sampled are illustrated in figure 3.3. A line 20um x 100$\mu$m passing along the axis of the pyramidal cells in CA1 (3.3 i), an area 70 x 70$\mu$m located in the stratum radiatum of CA1 (3.3 ii), a line passing across the dentate granule cells and the hilus of the dentate granule cells (3.3 iii). The rationale for choosing each of these regions is as follows. ROI (i) contains the cell body, dendrites and synaptic connections of the CA1 pyramidal cells which are known to degenerate at late stages of disease. ROI (ii) contains a relatively homogeneous field of synaptic contacts from CA3 cells to the CA1 cells and it is known that synaptic degeneration occurs early in this region in the absence of immunohistochemically detectable PrP$^{sc}$ deposition. ROI (iii) contains the cell bodies of dentate granule cell neurons which are not affected by the disease but are surrounded by PrP$^{sc}$ at early and late stage disease.

Spectra were collected at the Daresbury Synchrotron facility on a Nicolet Nexus FTIR spectrometer coupled to a Nicolet Continuum IR microscope. The spectra were collected from a 10x10$\mu$m region with a 10$\mu$m pixel spacing. These spectra had a spectral range of 850–4000cm$^{-1}$, a spectral resolution of 1cm$^{-1}$ with a zero filling factor of about 2, yielding a data spacing of 0.12cm$^{-1}$. The spectra were calculated by an average of 128scans and normalised by background spectra taken prior to collection of the image which was an average of 512scans, thus improving the signal to noise by a factor of $\sqrt{2}$. After collection, the images were converted to a local format with equivalent dynamic range.

The data processing was conducted using the same image processing toolkit developed for the medical imaging work detailed later in section 4.2.6. Specific processing included using the Laplacian of Gaussian second derivative filter also

[1] a known standard reference point

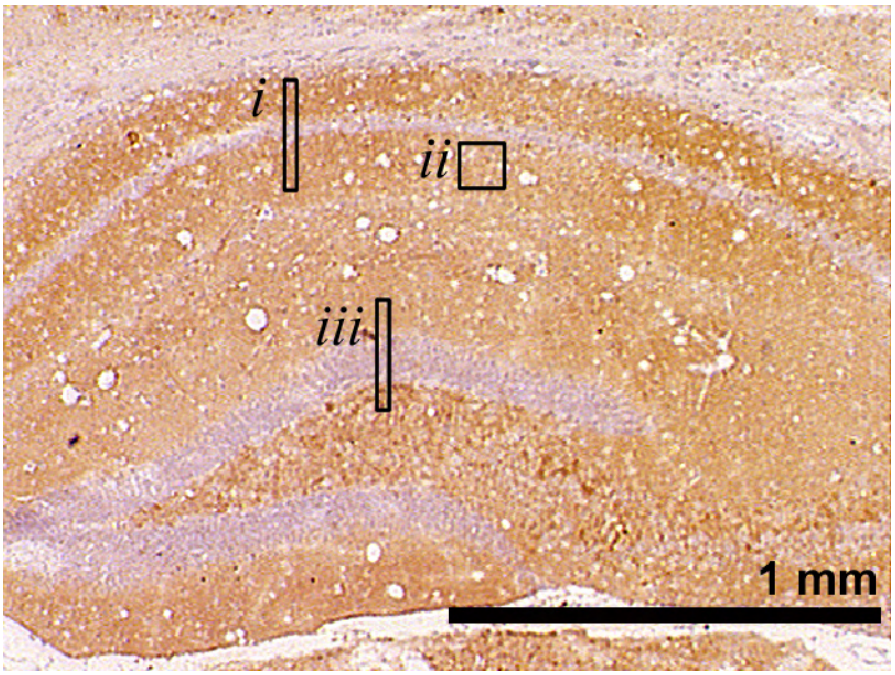


FIGURE 3.3: Hippocampus of ME7 infected mouse at 22 weeks, showing data collection areas.

known as the Marr-Hildreth operator which is common in image processing, Marr and Hildreth (1980). This filter calculates the second order differential and also incorporates Gaussian smoothing.

A linear search algorithm was also implemented to automatically find differences in the spectra that separate NBH from Late Stage (LS) individuals in a training set. These spectral features were then compared with a test set including the Early Stage (ES) individuals. This search algorithm compares different band positions and widths to find pairs of bands which separate the NBH and LS groups in the training set. The metric used related the size of the group to the distance between the centres of the groups. This process is computationally expensive and so this application was threaded, using the pthread library, to leverage the additional processing capacity of multiprocessor machines. Even so on a quad-core AMD Opteron$^{TM}$ running at 2.4GHz a typical processing run took a number of hours.

Due to the high cost of running synchrotron facilities, time is allocated via an application and funding process. This project twice applied for time on the beamline and was granted 5 days on each occasion. The first of these periods was first rescheduled and then interrupted by machine failures and a further 2 days was allocated to make up this time. Thanks go to the Engineering and Physical Sciences Research Council for the allocation. Acknowledgement must go to the beamline scientist James Nicholson and other staff at CCLRC Daresbury

Laboratory. Also thanks to all the neuroscientists from the CNS Inflammation Group and colleagues within the ORC who helped run the data acquisition around the clock for a total of 10 days, who include; Ayodeji Asuni, Suzanne Campion, Kathryn Hilton, Vincent O'Connor, Jack O'Sullivan, Hugh Perry, Harvey Rutt, Zuzanna Siskova, Jedrzej (Andrew) Szelc and others.

## 3.3 Results

Spectra were collected in three collection sessions. These consisted of 9, 6 and 15 individuals respectively. Due to operational reasons the samples for the second set (6 individuals) were not specifically prepared for this project. These samples were prepared some time previously and were not as high quality as those in the first and last set. That the preparation of samples is vitally important has been reported elsewhere (Roggan et al. (1999)). Unfortunately these data proved not to be good enough to make any quantitative deductions. The standard deviation (calculated per wavelength) of one of these images 4.5 times greater than that of the typical image from the other sets.

Sample spectra of control and late stage tissue are shown in figure 3.4. The noise burst at around 2300cm$^{-1}$ is due to poorly controlled $CO_2$ bands in the purge gas - this however is the only significant affect of this problem as $CO_2$ does not absorb in the same spectral regions as amide I. It can be seen that these two spectra are similar, indicating that there is no major change in the overall composition of the tissue which is as expected.

Before further processing it is standard practice to normalise and baseline the amide I band. This process allows consistent comparison between spectra independent of source illumination intensity and in this case sample thickness which will affect overall transmission. Normalisation was performed using the peak of the amide I band and the minimum on the high wavenumber side (typically around 1720cm$^{-1}$). Baselining is particularly important when comparing contrast enhanced spectra, the minima either side of the amide I band are automatically found and the baseline removed, in line with literature Susi and Byler (1986). Figure 3.5 shows an example baseline.

Figure 3.6 shows example second derivative spectra calculated with a Gaussian smoothing $\sigma$=4cm$^{-1}$. As discussed above there has been a significant amount of work done on the assignment of particular Amide I band frequencies to structural conformations, this is summarised in table 3.5.

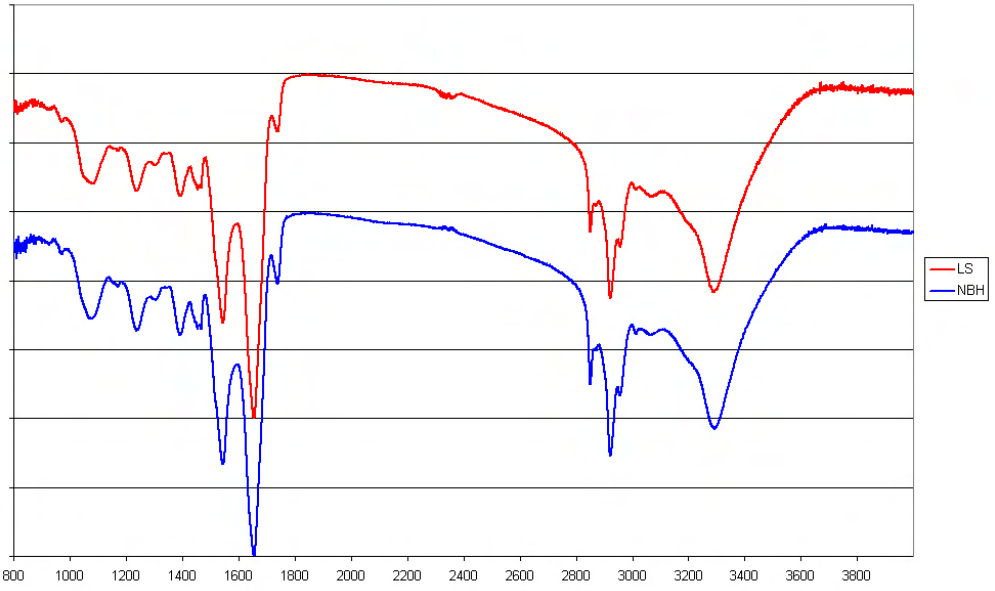


FIGURE 3.4: Transmission spectra of NBH and late stage individuals, vertical offset added for clarity, horizontal scale in $cm^{-1}$

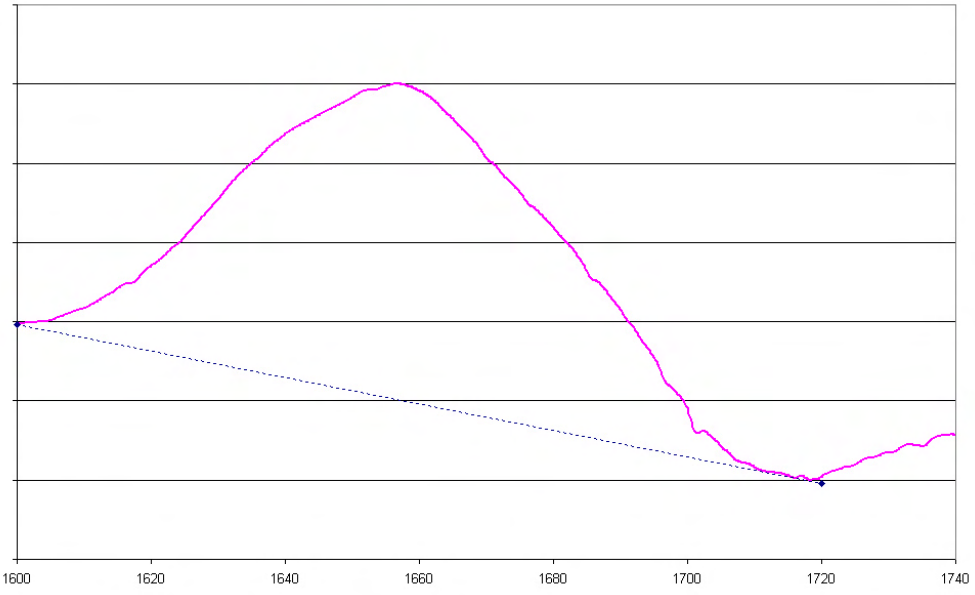


FIGURE 3.5: Example amide I band showing baseline before further processing, horizontal scale $cm^{-1}$, vertical scale arbitrary

Initial processing on group 1 using the linear search algorithm to separate the three groups (control, early and late) identified four spectral areas of significance. These areas are specified in table 3.6. This table shows a good correlation with bands associated with $\beta$-sheets assignments referenced above. Therefore these factors identified are likely to be structurally relevant. Figure 3.7 shows how well the groups separate, clearly demonstrating that the groups are generally separable with a low number of structurally relevant factors. This graph shows

| **Structure** | **Amide I frequency cm$^{-1}$** |
|---|---|
| aggregated strands | 1610-1628 |
| $\beta$-sheet | 1625-1640 |
| unordered | 1640-1648 |
| $\alpha$-helix | 1648-1660 |
| antiparallel $\beta$-sheets or aggregated strands | 1675-1695 |

TABLE 3.5: Approximate structural assignment of amide I bands

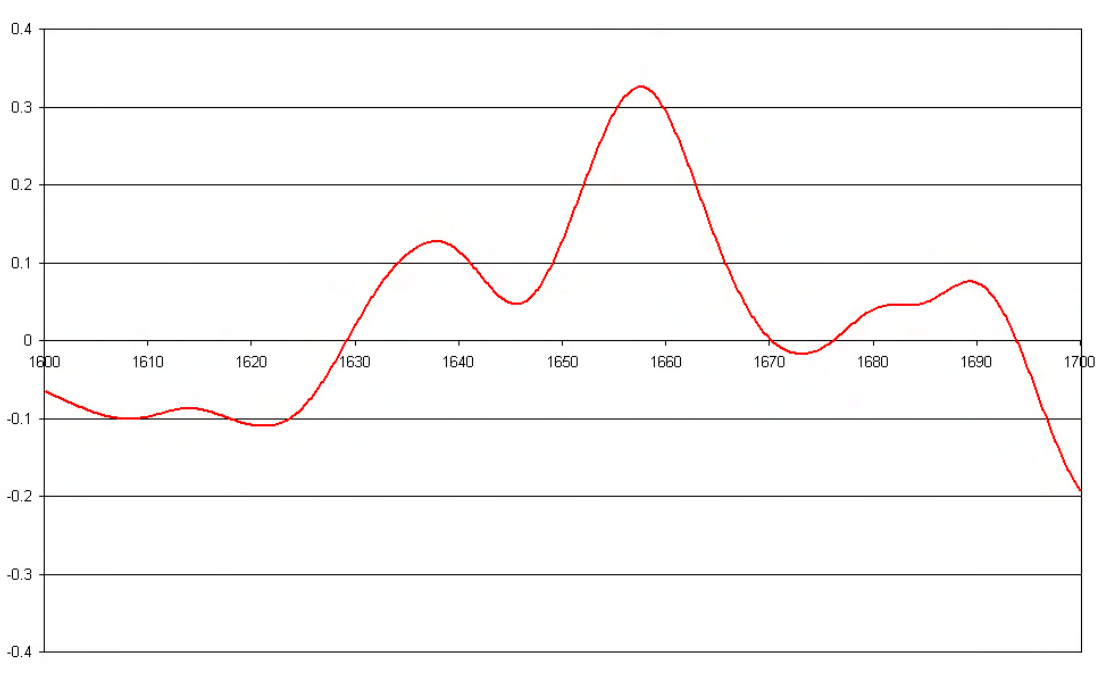


FIGURE 3.6: Second derivative of the Amide I absorption spectra of NBH tissue calculated by a LoG filter with $\sigma$=4cm$^{-1}$.

| **Factor** | **Region (cm$^{-1}$)** | **Processing done** |
|---|---|---|
| 1 | 1614–1623 | Second Derivative (4cm$^{-1}$) |
| 2 | 1635–1643 | Second Derivative (2cm$^{-1}$) |
| 3 | 1636–1644 | Second Derivative (4cm$^{-1}$) |
| 4 | 1657–1669 | Second Derivative (2cm$^{-1}$) |

TABLE 3.6: Amide I frequency regions identified as being helpful in the separation of the groups

some overlap between the control and early tissue groups, this is entirely expected as the disease process is continuous and not all the tissue particularly in the ES group would be diseased. Also evident is some overlap between the late stage and early stages again due to the continuous nature of the disease progression this is to be expected.

The images in figure 3.8 show a false colour representation of the metric

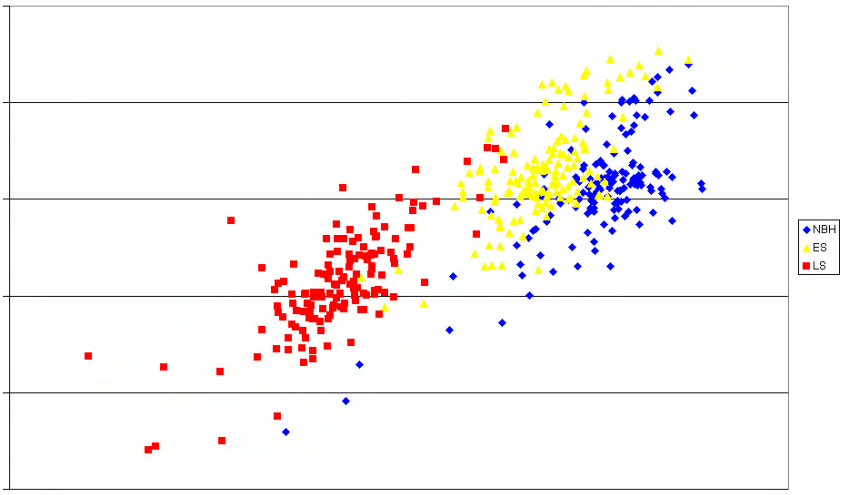


FIGURE 3.7: A plot of the clustering of the groups; horizontal axis is the product factors 2 and 3, vertical axis the ratio of factors 4 and 1 from table 3.6, absolute values are arbitrary

identified. This metric is calculated from the average of the spectra within the regions specified in table 3.6, it is proportional to factors 2—4 and inversely proportional to factor 1. Clearly showing that it is possible to identify the differences between the groups. This metric also shows interesting differences with the regions, figure 3.9 shows the ROI 3 of a late stage individual clearly showing a difference between the neurons and the synapses.

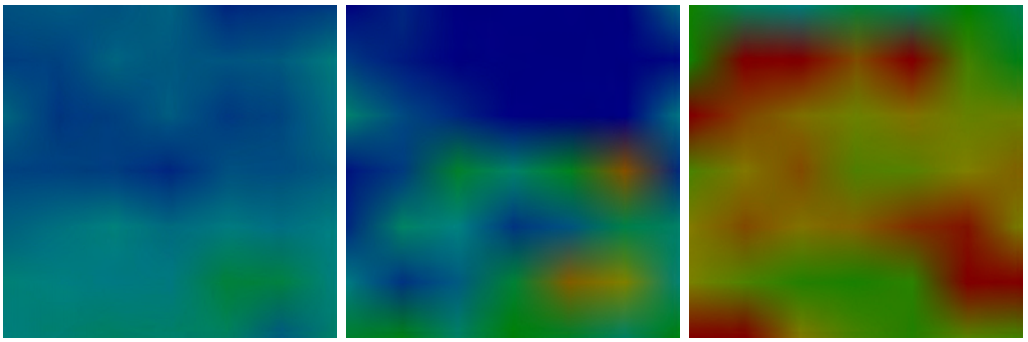

(a) Control (b) Early stage (c) Late stage

FIGURE 3.8: Region 2 demonstrating the difference between control, early and late stage tissues. Scale from blue to red proportional to factors 2, 3 and 4 and inversely proportional to factor 1 from table 3.6.

Unfortunately due to the failure of set 2 to provide data of similar quality to set 1 (the training set used in the above). The predictions of the search algorithm were unable to be tested until another set of data was collected. After collection of set 3 these factors were not all found to correctly assign disease state except one. The one factor that still had some power to predict the disease state of the

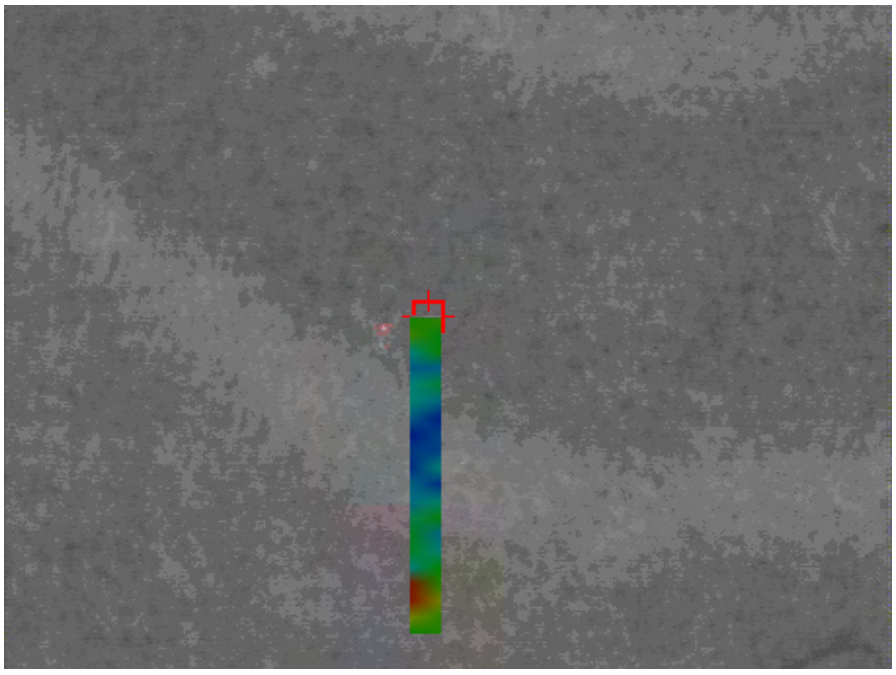

FIGURE 3.9: Region 3 of a late stage individual demonstrating the differences within the CA3 region. Same scale and metric as figure 3.8.

test set this was the second derivative between 1635–1643cm$^{-1}$. The training set only contained a total of 6 NBH and LS individuals whereas the test set contained 10 so the failure to accurately predict the larger test set is not particularly surprising.

The search algorithm was rerun on a larger training set comprising at total of 12 NBH and LS individuals (6 from set 1 and 6 randomly from set 3), the test set comprised the remaining 4 individuals from set 3. Only one band was identified which was between 1639–1643 with contrast enhancement ($\sigma$=4cm$^{-1}$); this bands can be seen in figure 3.10 which shows the mean plus and minus the standard deviation. In this figure this small band around 1640 is the only region which shows the means greater than one standard deviation apart.

This band shows convincing separation of the test set as well as the training set, the combined frequency graphs can be seen in figure 3.11. As expected the early stage samples are also found between the NBH and late stage. This band is in a spectral region recognised as $\beta$-sheet and so must be considered structurally relevant. Another metric which one would expect if there is a change in the ratio of $\beta$-sheet to $\alpha$-helix is that the location of the peak of the amide I. A decrease in the frequency of the peak absorption indicates an increase in this ratio. This has been observed elsewhere and also demonstrated here and shown in figure 3.12. This is a structurally relevant feature associated with a decrease in $\alpha$-helix and increase in $\beta$-sheet.

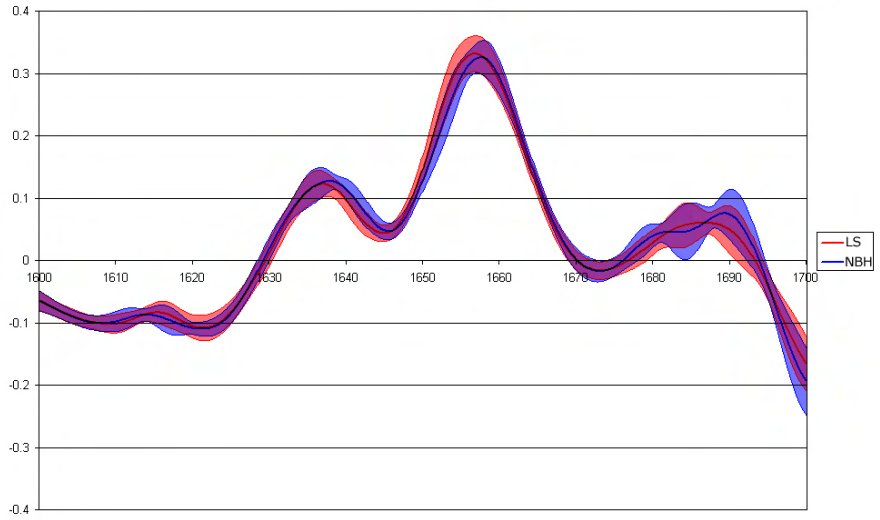


FIGURE 3.10: Average plus and minus one standard deviation of a contrast enhanced ($\sigma$=4cm$^{-1}$) averaged spectra of LS and NBH

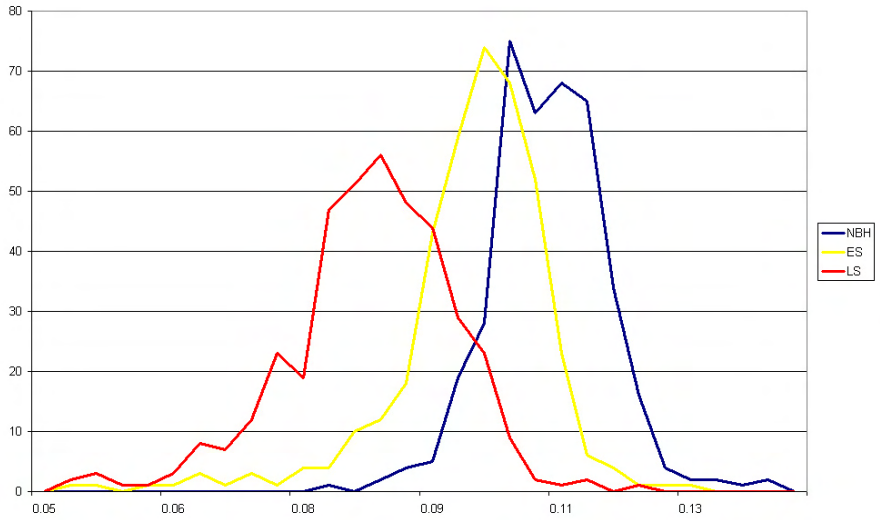


FIGURE 3.11: Demonstrating the power of the 1640 band to assign disease progress, horizontal scale arbitrary, vertical number of pixels.

The most interesting feature of the spectra of these groups is in the region around 1740cm$^{-1}$— the metric used is the average between 1735–1752 contrast enhanced with $\sigma$=4cm$^{-1}$. This is not associated with the amide I band and so not a direct measure of PrP$^{sc}$ accumulation in tissue. In common with the amide I band it is associated with the C=O stretch (carbonyl group) however not the hydrogen bonded form found in the peptide backbone but that found in carboxylic acids and saturated aldehydes. Of the 20 standard amino acids only two contain a carbonyl groups on their side chains, glutamic acid and aspartic acid and there are no aldehydes. Therefore this band is associated with proteins with glutamic and aspartic acid side chains, any free amino acid and other

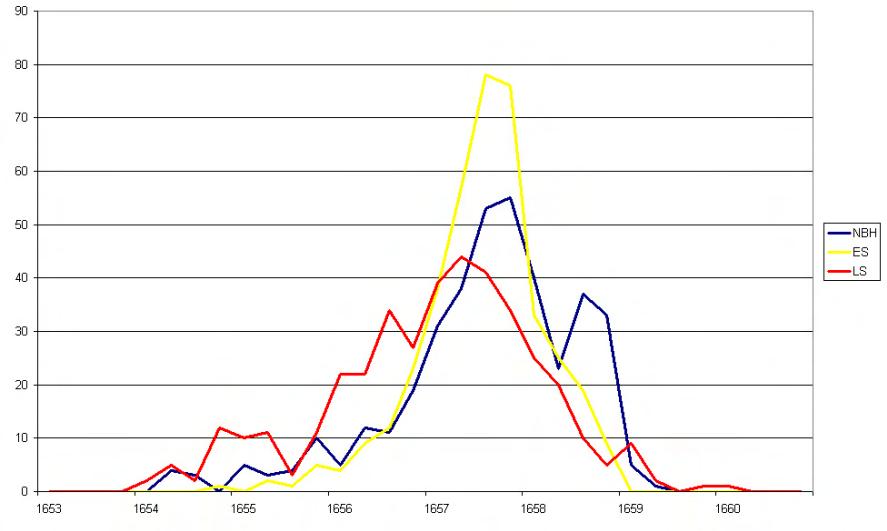


FIGURE 3.12: Demonstrating that the peak location of amide I is related to disease progression, horizontal scale amide I position ($cm^{-1}$), vertical number of pixels at a given position

compounds with carbonyl groups (notably tricarboxylic acid (TCA) and lactic acid). This band is twice as sensitive to free glutamic and aspartic acids as it is to other amino acids. It is the association with amino acids which is most interesting, for this absorption to be solely protein side-chains (of which glutamic and aspartic acids will only account for of the order 10%) a massive change in the amount of protein would be observed. This is not the case, overall protein levels are reasonably consistent across the groups (demonstrated by little change in the intensity of the amide absorptions relative to other bands, this is shown in figure 3.13). Finally it is unlikely that the signal observed is associated with TCA and lactic acid as in this ROI these will be primarily metabolised in mitochondria of glial cells which increase in number as the disease progress (a process called astrocytosis).

Notably glutamic acid is a neurotransmitter provided to neurons by astrocytes and used in synapses. Glutamic acid is used in the vast majority of fast excitory synapses in the brain, gamma aminobutyric acid (also with a carbonyl group) is the next most prevalent neurotransmitter and is used in the vast majority of fast inhibitory synapses. Glutamic acid is produced in synapses from glutamine, it is then stored in vesicles near the synaptic terminal. On activation the synapse releases this glutamic acid activating receptors of the post-synaptic density. Some of this glutamic acid escapes into extracellular space where if it was not removed would kill the synapse (a process called excitotoxicity). In healthy tissue astrocytes would collect all of the glutamic acid, convert it back to glutamine and pass it back to the neuron. Kleene et al. (2007) has associated depletion of PrP with decreased transport of these amino acids by astrocytes . As shown in

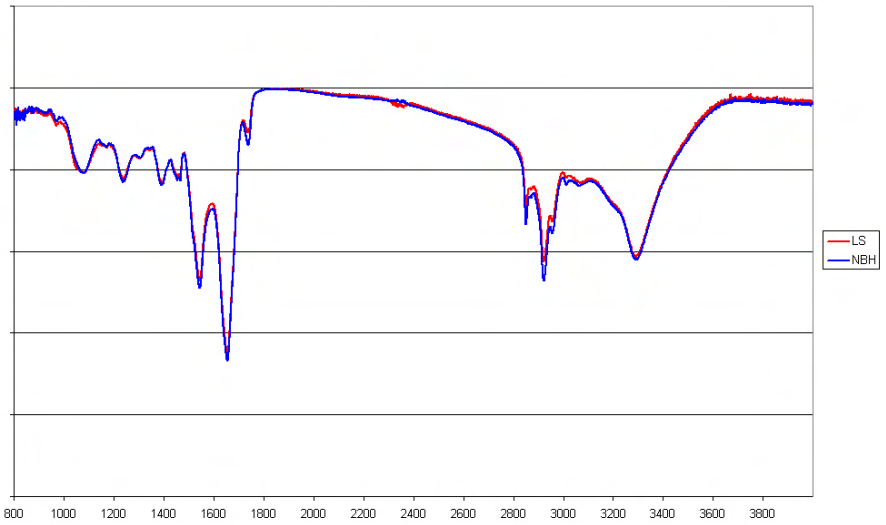


FIGURE 3.13: Transmission spectra of LS and NBH overlaid, normalisation to maximum value, horizontal scale $cm^{-1}$, vertical scale arbitrary.

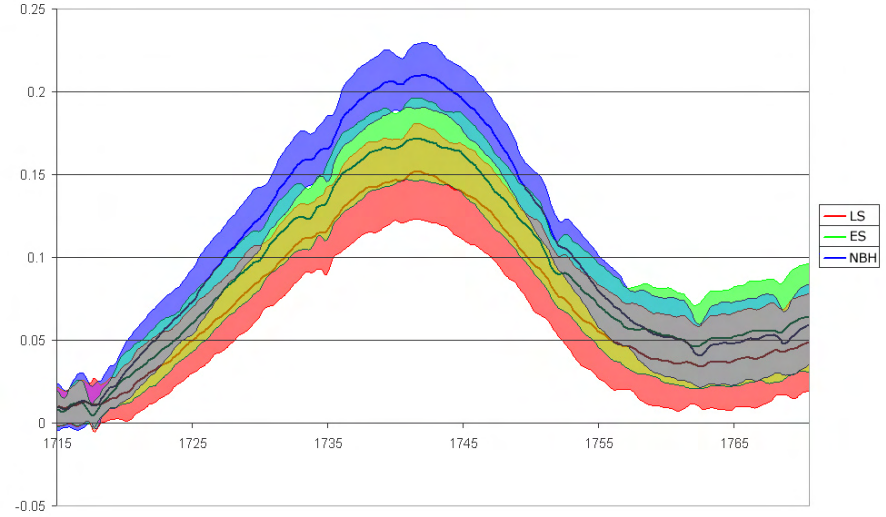


FIGURE 3.14: The average plus and minus one standard deviation of the absorption spectra of LS, ES and NBH tissue is shown (red green and blue respectively) in the carbonyl region, horizontal scale in $cm^{-1}$, vertical scale arbitrary.

the background section 3.1.1 many of the neurons are already damaged before the onset of clinical symptoms, the synapses of these neurons are damaged first with 40% fewer synapses found at 12 weeks relative to NBH (Perry (2009)).

The average and standard deviation of this band are shown in figure 3.14, the spectra presented here were normalised to the maximum of the amide I band and baselined as described. Even with this minimal processing of the spectra it can be seen that these bands will separate. Contrast enhancement makes this marker easier to identify. With contrast enhancement this marker separates the NBH and LS groups by almost 3 standard deviations, and NBH and ES by over 2, this

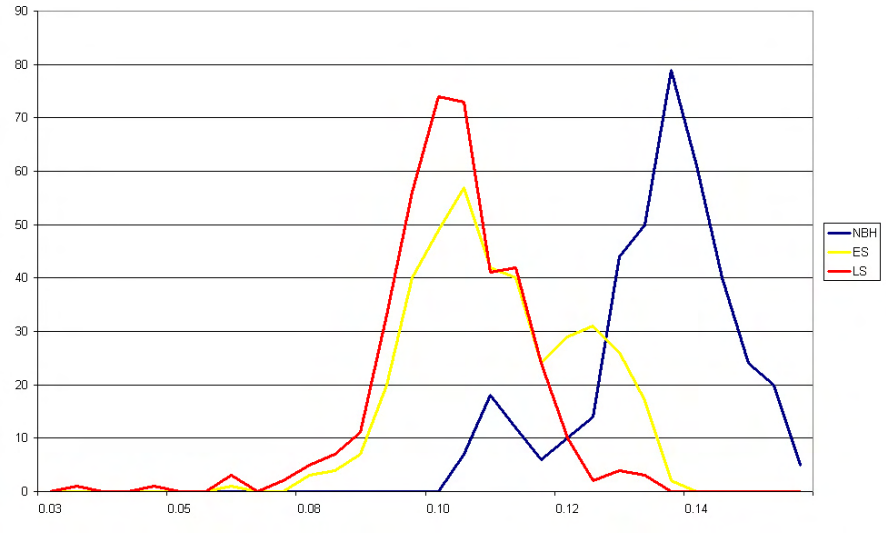


FIGURE 3.15: Frequency plot of the intensity in the carbonyl region, horizontal scale is measure of the intensity, vertical scale is number of pixels

is shown in figure 3.15. The similarity in shape and mean suggests that the first evidence of this feature occurs far earlier in the disease progress than the structural features identified associated with $PrP^{sc}$ deposition. If this can be shown to be correlated with the neurotransmitter glutamic acid this signal could used as an indicator of synapse loss in the earliest stages of the disease.

Finally separation of the groups is possible using the metrics identified. Figure 3.16 shows the grouping of the three groups using two of the metrics identified (the average of the bands 1735–1752cm$^{-1}$ and 1636–1643cm$^{-1}$ contrast enhanced with $\sigma$=4cm$^{-1}$). As can be seen the NBH and LS groups have good separation with the ES group between them as expected.

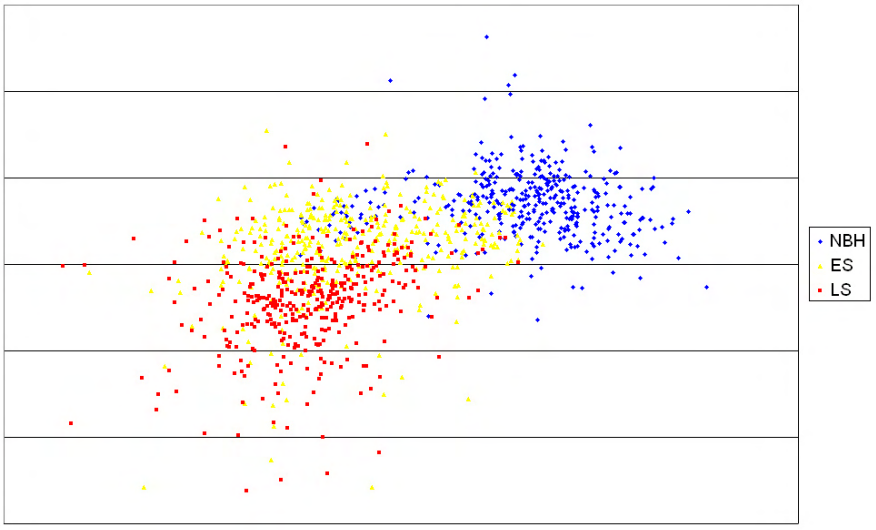


FIGURE 3.16: Separation of the three groups using two metrics, horizontally the average between 1735–1752cm$^{-1}$, vertically the average between 1636–1643cm$^{-1}$, both bands contrast enhanced with $\sigma$=4cm$^{-1}$

# Chapter 4

# Intraoperative imaging of human brain

The possibility of optically imaging the human brain intraoperatively to assist surgeons identify diseased tissue arose out of a meeting with Prof. Liam Gray of the Southampton General Hospital and the University School of Medicine. He presented that even experienced neurosurgeons are unable to visually distinguish between many brain tumours and normal tissue. Tissue also moves during surgery reducing the accuracy of the registration with images taken before the operation. This makes it more difficult to balance greater removal of tumour with higher risk of post-operative deficit.

This project approaches this problem in two ways; firstly to identify the boundaries between tumours and normal tissue, and secondly to delineate functionally useful areas. This project will attempt to find differences in the spectra of normal and tumour tissues and develop a system able to identify these differences. It will also attempt to identify the time varying characteristics which are associated with the use of brain tissue.

This chapter will begin by detailing the relevant literature regarding the medical background of this project. This section considers in some depth the debate about how much tumour should be removed and whether this correlates with increased survival. This issue is key to this project as if there is no medical benefit in removing more tumour then surgery should only be performed for palliative reasons. The background will continue by looking into current and developing imaging systems.

Then the details of the systems and software developed will be presented. This will be followed results from these systems demonstrating that it is possible to both delineate tumour and areas of functional tissue intraoperatively.

## 4.1 Background

The background to this project will be considered in three sections; a medical review and a review of current and developmental systems. The medical review will establish the need for intraoperative imaging to delineate both tumour and function. The following sections will discuss imaging technologies that are currently available and those that are still in development.

### 4.1.1 Medical review

This section seeks to establish the medical need for this work. There is a large amount of literature in the field, this section will review the most relevant of this literature. The treatment of tumours particularly in the brain is a contentious issue where there is significant debate; this thesis attempts to represent both sides but also presents the authors opinion. What follows is a brief overview before going into more depth in the following sections.

Currently about 1 in 4 people in the UK will die of cancer. Four types of tumour; lung, bowel, breast and prostate account for approximately 50% of these deaths. These are principally in older people; 74% of cases are diagnosed in patients over 60 years of age, a group which accounts for only about 22% of the UK population. Primary tumours of the brain and CNS are rare, they account for only 2% of new cases in the UK (approximately 4500 people per year) however they are responsible for 7% of the cancer deaths in patients under 70 years of age. The rate of incidence has remained uniform for about 20 years but critically the survival rates have not changed either. These survival rates are low. One year survival is currently around 30%, 5 year around 10% and these rates correlate strongly with age with older patients having very low survival. (Statistics from Cancer Research UK (2009))

In contrast breast cancer has seen a consistent increase in survival with 1 year survival currently over 90% and 20 year survival at over 60%. There are a number of reasons why the survival rates of tumours of the brain and CNS are so low;

1. Tumours of the brain and CNS typically present late in the disease progress. A number of factors including the plasticity of the human brain allow the tumour to grow without symptoms for a significant period of time. Presenting symptoms commonly include seizures, headaches and focal deficits - these are ‘mass affects’ due to the growing tumour.

2. Brain tumours infiltrate surrounding normal brain. Recurrence often occurs near the original tumour site. For this reason surgery is in the vast majority of cases not a cure.

3. The blood brain barrier limits chemotherapy options.

Survival may be the most important metric in tumour treatment, although it is not without limitations. For example progression or disease-free survival may be more useful for patients seeking to understand how long before a tumour comes back. There are a number of neurological performance metrics and quality of life metrics which can be used to measure 'quality time' before further treatment. All of these metrics have a common problem that earlier detection equates to longer survival times. At diagnosis a brain tumour patient may have been living with a slowly growing tumour for many years before the tumour mutates and starts causing symptoms. These symptoms are typically caused by an increase in growth thus increasing cerebral pressure leading to diagnosis. A patient may only live for a few months after diagnosis but may have lived with this tumour for 20 years. However there is of course no other time point from which to start measuring survival. Within this survival gap exists a lack of understanding of tumour growth. This presents a difficulty in treatment particularly of low grade tumours - will they all mutate into higher grade tumours, and how does surgery affect this outcome?

Current opinion is that in all but the lowest grade of tumour (grade I) the tumour will return. Grade II tumours may take 10 years to do so, the most malignant (grade IV) may take less than 6months. For these tumours, surgery falls short of a cure but is the primary method of treatment. However during surgery the tumour resembles healthy tissue so closely to be indistinguishable by even the most experienced surgeons (Albert et al. (1994)).

Even with the most sophisticated pre-surgical imaging and careful planning of surgical treatment there are two key problems limiting the effectiveness of the surgery;

1. Movement of the brain tissue reduces the registration accuracy with the pre-operative imaging. Movements as large as 10mm have been observed with the average being reported as 5.6mm (Maurer et al. (1998)), figure 4.1 shows an example of this imaged by iMRI. This movement is seen as soon as the dura is opened and is a result of the internal pressure put on the brain by the growing tumour. The reverse is also true as during surgery the tissue dehydrates and relaxes and deforms as resection continues. These

factors seriously degrade the registration between the guidance system and the tissue.

2. Functional tissue in the region of the resection must be avoided to prevent neurological deficit after surgery. The current protocol for assessing this is described later (4.1.1.6) but has poor spatial resolution and takes time to perform.

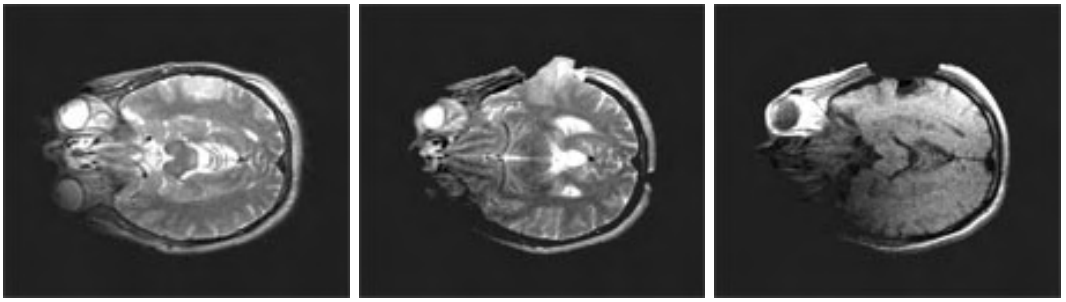

FIGURE 4.1: Images taken by an intraoperative MRI during craniotomy showing movement of brain tissue (images taken from Morton (2005))

#### 4.1.1.1 Infiltrating nature

Bernsen et al. (2005) documented a case of gliomatosis cerebri[1] which although rare does highlight the extent to which a tumour can infiltrate normal tissue. The patient presented as a 68-year-old man with cognitive dysfunction with sudden onset. CT showed a large hypointense region in the left hemisphere, MRI showed a similar hypointense region which did not enhance with Gd contrast. CT images taken 4months later showed increased hypodensity in both hemispheres, these images are shown in figure 4.2. The patient died days after the second set of imaging of an unrelated cause, autopsy showed a highly diffuse tumour in both hemispheres. This highlights the fact that angiogenesis is not always associated with tumour growth, this lack is associated with the lack of MR-imaging contrast. This also poses a problem for therapy as this tumour or non-enhancing portions of other diffuse infiltrating tumours are likely to be unresponsive to antiangiogenic treatment.

80 years ago Dandy (1928) described the hemispherectomy (removal of half the brain) — possibly the most extreme treatment for malignant glioma. The few patients that survived this extreme treatment died of recurrent disease. Dandy noted that the tumour tissue invaded deep into the midline of the brain and

[1]Gliomatosis is a rare neoplasm, defined by the WHO-2000 classification of tumors of the nervous system as a diffuse glial tumor infiltrating the brain extensively, involving more than two lobes, frequently bilaterally, and often extending to infratentorial structures.

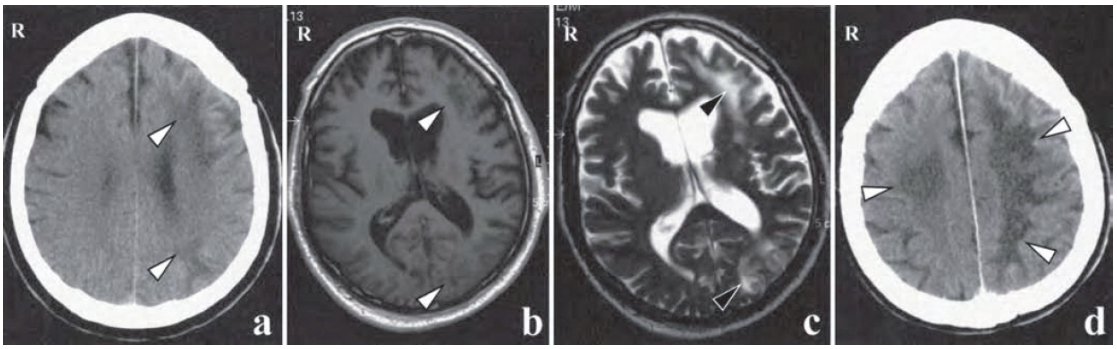


FIGURE 4.2: Figure from Bernsen et al. (2005) indicating the extent of infiltrating margins, a; CT image with large hypointense region indicated taken at first admission, b and c; $T_1$ and $T_2$ MRI with Gadolinium enhancement indicates large hypointense area that is non-enhancing with contrast, d; CT obtained 4 months later demonstrating hypodensity in both hemispheres.

infiltrated the overlying dura so these cases were extreme. However visible tumour was found well away from the primary site demonstrating in the early part of the $20^{th}$ Century that glioma had no discrete margin and also that surgery was not a cure. Over 50 years later Burger et al. (1983) demonstrated with modern neuroimaging that glioma infiltrates diffusely centimetres from the primary site and even into the other hemisphere.

#### 4.1.1.2 Assessment of extent of resection

Before commencing the discussion of how much tumour should be removed during surgery it must be noted how the assessment technique used influences the outcome of the studies. As noted earlier brain tumours are visually indistinguishable from normal tissue and their infiltrative properties make achievement of complete removal difficult. This is also the case for assessment of the extent of resection.

The estimation of extent of resection by the operating surgeon has been shown to be a poor predictor of resection assessed by either intraoperative MR or early post-operative MRI or CT. Martin et al. (2000) demonstrated that using an iMRI system increased the extent of resection in 57% of the 30 patients studied and assisted in avoiding critical vessels in 4 (13%) of the remaining cases. Schneider et al. (2005) stated that the extent of resection was increased in 29% of the 31 patients. These 31 patients were operated on using current techniques until the resection was judged complete, MR imaging was then used to assess the extent of resection and surgery continued as necessary.

Early post operative imaging is the most important technique for identifying the extent of resection and understanding the pattern of regrowth. Forsting et al.

(1991, 1993) demonstrated that scans must be collected within the first four days after surgery, beyond this point surgically induced enhancement prevents clear visualisation of residual tumour. Forsting also observed a much higher incidence of progressive disease, 75% in those with residual tumour immediately post-operatively compared with only 36% in those without. Forsting went on to work with Albert to further quantify the importance of early post-operative MRI (Albert et al. (1994)), particularly with Gadolinium enhancement. Gadolinium enhancement within 72hrs identifies any remaining tumour better than either CT (with or without contrast) or surgeons estimation. This timing continues to avoid visualisation of surgically induced enhancement and minimises interpretation difficulties. In his study Albert also found that the majority of tumour regrowth initiates from the same location as post-operative MRI enhancement.

Later work (Ryska et al. (2005)) has confirmed this and also investigated the affect of methemoglobin, a product of haemoglobin degradation, which presents as hyperintensity on T1 MRI and could be mistaken for residual tumour. Albert and Forsting (2003) commenting on Lacroix et al. (2001), demonstrated the importance of an appropriate post-operative MR imaging protocol that images within the first 72 hours. Emphasis was also given to conducting this imaging using Gadolinium contrast enhancement. This method is a valuable tool in determining extent of resection and should be the standard for assessment of residual tumour, this unfortunately is not always the case.

#### 4.1.1.3 Aims of resection

The optimum amount of tumour removed (or alternatively the amount of tumour left behind) is currently the subject of some debate and has been so for some time. Intuitively one would think that greater resection increases the risk of post-surgical neurological deficit, less resection decreases the progression-free survival. The presented data has not always backed this up. This section will look at the reasons for surgical intervention, the next two sections will consider the debate for both high grade and low grade tumours.

The first surgical resection of a primary brain tumour has been attributed to Bennet and Godlee in 1888 (Pang et al. (2007)). Although this was over 130 years ago there still remains considerable controversy and discussion about the surgical treatment of primary brain tumours. Patient survival was reported in the 1930's as less than 2 years, today's situation is not much different, Pang et al. (2007)

There are a number of aims of surgical intervention that cannot be ignored. These have been enumerated in a number places including Pang et al. (2007) and Nazzaro and Neuwelt (1990)

1. Symptomatic relief - relief from mass effect and obstructed cerebrospinal fluid circulation are clear benefits. Distortion of the brain and compression of the local structures contribute to both general symptoms and focal deficits which are likely to show some improvement with resection.
2. Neurological improvement - global symptoms such as headache, nausea, vomiting and general malaise often show dramatic improvement following surgery. This may be due to the reduction in intracranial pressure or may be due to a reduced tumour burden.
3. Oncological reduction to augment adjuvant therapy - reducing the tumour load increases the efficacy of adjuvant therapy such as radio and chemotherapies and reduces the number of tumour cells available for proliferation.
4. More accurate diagnosis - the accuracy of the diagnosis is dependant on the size of the tissue sample particularly where the mass is heterogeneous.

However the possibility of achieving long-term survival for malignant tumours is remote even with multi-modal therapy.

So where should the line be drawn between resection and minimal damage? The fact that such a fundamental question is still unanswered is remarkable. A large number of authors have attempted to draw together conclusions from the extant literature for example Ryken et al. (2008); Claes et al. (2007); Jacobs et al. (2005); Keles et al. (2001); Whittle (2004). To accomplish this is difficult as there are significant differences in classification criteria, distributions of co-variants, patient selection bias, and various methodological differences.

It has been observed that the level of published evidence regarding the extent of resection is not high. Proescholdt states that there are no studies with a high level of evidence, Proescholdt et al. (2005). This may be primarily due to the lack of randomised trials and the moral difficulties in setting up such a trial.

One of the few randomised trials Vuorinen et al. (2003) presents a small study of 23 elderly patients with malignant glioma. Vuorinen did not find a significant relationship between the extent of resection and survival however this study was particularly small and only considered patients over 65 years and so this may limit interpretation. Stummer et al. (2006) describe a randomised study of the

extent of resection and it's effect on survival using 5-aminolevulinic acid (a fluorescence inducing agent). This study is probably the most significant to date and states that a complete resection (defined by post-operative MRI) is correlated with increased survival in glioblastoma multiforme. However this trail was critically flawed in that it excluded neuronavigation in the control group, it is also questionable whether the selection bias was too significant. Both of these factors will be discussed below.

The current standard for surgery is using neuronavigation. Neuronavigation exploits pre-operative imaging to aid the surgeon resect as much tumour as possible. Preoperative imaging has limitations as described earlier on page 44 however neuronavigation has been shown to increase the chances of gross total resection (as assessed by early post-operative MRI) in approximately 26% and 12% of cases Kurimoto et al. (2004); Wirtz et al. (2000) respectively. Stummers' 2006 study and the additional work presented in 2008 which further adjusted for bias in the study are critically flawed as they excluded neuronavigation in their control group (Stummer et al. (2006, 2008)). Neuronavigation was only permitted in planning and initial tumour localisation and by implication not during resection. Stummer achieved an increase in the chance of GTR in 29% of patients. This increase does not appear to be much larger than that achieved by neuronavigation alone.

The study was also highly selective regarding both the position of the tumour away from hard to resect areas and eloquent tissue and the observation of the tumour on preoperative MRI where a ring of enhancement and indication of necrosis was required. This selectivity is probably due to the limitations of the 5-aminolevulinic acid induced porphyrin fluorescence used. There is some debate as to whether 5ALA can cross the blood brain barrier or whether this technique depends on the compromised blood brain barrier in high grade tumours. Studies such as Terr and Weiner (1983) suggest that it only crosses into the brain where the barrier is compromised; others like McGillion et al. (1975) that it will cross (although the techniques of the latter have been questioned, Hebeda et al. (1998)). The conclusions may be drawn that a compromised blood brain barrier is the primary means for 5ALA to enter the brain but not the sole method (Novotny and Stummer (2003)) so to quote Hebeda;

> Probably Astrocytoma will behave differently form oligodendroglioma, and grade II tumours could be completely incomparable to grade III or IV tumours

This would pose a serious problem where the tumour is not homogeneous. This is confirmed by Utsuki et al. (2006) where non-fluorescing samples were

demonstrably infiltrating tumour. In summary Stummer's work on the extent of resection guided by 5ALA induced porphyrin fluorescence performs similarly to neuronavigation in a subset of the highest grade of malignant glioma.

The achievable extent of resection has been greatly improved by better intraoperative imaging. Intraoperative Magnetic Resonance imaging has been particularly useful, Knauth et al. (1999) demonstrated that iMRI significantly increases the rate of complete tumour resection. In their study of 41 operations (not a large number but probably sufficient for the conclusions drawn) they first conducted the surgery with a normal neuronavigation and when judged complete imaged intraoperatively before continuing where appropriate; over 50% of the cases judged complete by the surgeon showed residual tumour on the iMRI. IMRI in this case increased the complete resection of enhancing tumour by 36.6% (judged by early post-operative MRI), this result was statistically significant. However this paper also serves to highlight the fact that in this iMRI setup the time taken to perform each MR examination was about an hour.

The risks of surgery are not inconsiderable North et al. (1990) in a retrospective study of 77 patients noted that one adult was left moribund a further two died within 3 weeks of surgery and 9 of the 18 children had cognitive impairment (IQ $\leq$70). Sawaya et al. (1998) reported major post-surgical morbidity as 8.5% in his study of 400 craniotomies (327 patients). Greater morbidity was present in patients with tumours in or near eloquent tissue, 13% of patients with tumour in an eloquent region suffered major neurological complications even though these patients were less likely to have a gross total resection. Other factors which correlate with morbidity include age and low KPS.

#### 4.1.1.4 Extent of resection of high grade tumours

This section will consider the literature background regarding the resection of high grade tumours. There is still a significant amount of debate in this subject. Some of the factors hindering the assessment of literature in this area are the assessment criteria, eligibility criteria and the definition of GTR.

Table 4.1 shows the increasing weight of recent studies favouring gross total resection for high grade (WHO grades III and IV - typically anaplastic astrocytoma (AA) and glioblastoma multiforme (GBM)). This demonstration that recent studies have shown an increase in the amount of literature favouring GTR is probably indicative of better post-surgical imaging protocols. This report will now go on to select some of the more interesting papers to review in more detail.

| Authors and Year of Publication (no. patients grade IV/III) | | | |
|---|---|---|---|
| **≤1990** | **1991-1995** | **1996-2000** | **2001-2008** |
| ***statistics favour more extensive resections*** | | | |
| Ammirati et al. (1987b)(21/10) | Nitta and Sato (1995)(68/33) | Daneyemez et al. (1998)(72/48) | Kurimoto et al. (2004)[1](76) |
| | | Keles et al. (1999)(92/0) | Laws et al. (2003)[2](413/147) |
| | Albert et al. (1994) | | Martinez et al. (2008)(80/30) |
| | | | Mineo et al. (2007)(340/0) |
| | | | Stummer et al. (2006)[3](250/9) |
| | | | Vuorinen et al. (2003)[3](19/4) |
| | | | Lacroix et al. (2001)(419/0) |
| | | | Stummer et al. (2000)(51/0) |
| | | | Jeremic et al. (2003)(175/0) |
| | | | Schneider et al. (2005)(31/0) |
| | | | Brown et al. (2004)(191/29) |
| | | | Ushio et al. (2005)(105/0) |
| | | | Wisoff et al. (2006)(56/75) |
| ***statistics do not favour extensive resection*** | | | |
| Coffey et al. (1988)(64/27) | Kreth et al. (1993)(115/0) | Kowalczuk et al. (1997)[4](52/23) | |
| | Prados et al. (1992)(0/357) | | Kreth et al. (1999)[2](228/0) |
| | Quigley and Maroon (1991)[5](5691) | | |
| | Salcman et al. (1994) | | |

TABLE 4.1: A historical summary of literature either favouring or not gross total resection.

[1] Only the total number of patients available
[2] Early postoperative MRI/CT not used
[3] Randomised trial
[4] Early postoperative MRI/CT used within 10days
[5] A review of prior literature

In Albert et al. (1994), a prospective study of 60 patients all eligible for gross total resection, it was found that GTR assessed by Gadolinium enhanced early post-operative MRI was the most predictive factor in patient survival, larger than both performance status and age. Using this imaging technique patients with residual tumour had a median progression free interval and median survival of 2 and 9months respectively. Whereas the patients without residual tumour were disease free for 14 and median survival was 16months (a conservative estimate as 4 patients from this group were still alive at publication). This was one of the key papers establishing early-post operative MRI for the assessment of residual tumour.

Even before post-operative MRI became the method of choice for determining the extent of resection there was some evidence that total resection improved prognosis. Ammirati et al. (1987a) demonstrated that the performance rating and extent of resection were the most important factors for life expectancy in patients undergoing repeated surgery for high grade glioma.

In a retrospective study looking at 416 patients between 1993 and 1999 Lacroix et al. (2001) investigates the affect of age, Karnofskey performance scale, extent of resection and degree of necrosis on pre-operative MR. The extent of resection was assessed by early post-operative MRI. Resection of greater than 98% demonstrated a significant ($p<0.0001$) increase of median survival of 4months (median survival time of 13months, compared with 8.8months for resections less than 98%). The extent of resection was found to be more significant than any other factor and confer the most advantage to those patients whose other predictive factors are favorable.

Kowalczuk et al. (1997) uses post-operative CT for the assessment of extent of resection but only collects this within 10days of surgery in their retrospective study of 77 (23 Anaplastic astrocytoma, 52 Glioblastoma multiforme). Post-operative CT within that time period would show surgically induced enhancement, therefore this was assessed using two criteria; where enhancement was nodular and in a 'probable location of residual tumour' is was assigned as residual tumour. This work did not find that extent of resection was a significant prognostic factor.

Nitta and Sato (1995) observes in his retrospective study of 101 patients that there is no significant difference between 'subtotal' and 'partial' resections (here defined as between 100% and 75% and less than 75% respectively). He demonstrates that patients with a gross total resection (resection equal to 100%) have a significantly longer survival. Results that subtotal resection performs similarly to biopsy have been reported elsewhere.

Other prognostic factors have been suggested, for instance; Hammoud et al. (1996) found necrosis, oedema, and degree of enhancement to be significant. Martinez et al. (2008) correlates two neurological functional tests; the Neurological Performance Scale and the Sawaya Functional Grade (as used in Sawaya et al. (1998)). These functional factors were shown to predict disease-free time and survival whereas extent of resection only correlated with survival. They performed better than all other factors in predicting survival and disease-free progression. These factors assess how much functional tissue is involved in the tumour and this may affect the extent of resection. The association of extent of resection and other clinical variables (such as age, clinical location and clinical status) has been demonstrated in Mineo et al. (2007), the functional parameters proposed by Martinez may be measures of these variables. Andreou et al. (1983) demonstrates using postoperative CT that where greater resection is possible prognosis is better, age was also found to be a significant factor.

In Burger and Green (1987) histological factors affecting survival of Glioblastoma Multiforme (GBM) are presented. This study did not consider extent of resection to be a prognostic factor. Burger found a strong negative correlation between increasing age and length of post-operative survival. Other factors were related to age; the presence of necrosis, extent of vascularisation, smaller cell size, however these factors did not offer a full explanation of the observed age effect.

Given the very short life expectancies after diagnosis of older people and probable extant conditions which make surgery more complicated and recovery times longer, many oncologists may recommend limited cytoreductive surgery and palliative care. For these reasons older people are typically excluded from analysis. Mangiola et al. (2006) attempts to put forward the view of equal treatment options for patients over 65 years of age. Mangiola looked particularly at the role of radiotherapy, chemotherapy and surgery in this group of 34 patients. All patients underwent resection, 79% received a gross total resection, the remainder a partial resection. The tumour location was not analysed, it has been shown elsewhere that tumours in functional areas and those in more inaccessible areas are more difficult to resect completely. 10 patients did not receive any adjuvant therapy due to 'treatment refusal or particularly poor conditions', this will prejudice any survival metrics which consider this group. This paper while advocating non-discrimination based on age (which has been consistently been shown to be a predictor of poor prognosis) does not analyse their results sufficiently accurately to draw any significant conclusions. It has been shown that non-surgical treatment options also influence outcome, the influence of radiotherapy on survival performed better than age and KPS in Mineo's study of 340 GBM patients reported in Mineo et al. (2007).

There is still much debate within the literature; Barker and Chang (2006) questions the scientific basis for GTR stating that patients where GTR has been performed typically have other favourable factors. This criticism may be valid and may correlate with the function performance scales that also seem to be indicative of prognosis. However Barker seems to ignore the evidence presented by papers which only select patients where GTR would be appropriate. Barker makes the following statement; "the survival benefit of complete removal of enhancing tumour is modest at best". Any demonstrable improvement is likely to be beneficial and an increase in survival of up to 70% (reported by Albert et al. (1994)) is unlikely to be referred to as modest so a question must be raised as to what Barker is basing this statement on.

Anderson et al. (1983) is often cited as a criticism of the analysis of GTR, this paper outlines the shortcomings of a simplistic analysis of chemotherapy data particularly in assignment of significance to these data. This paper observes two problems in the traditional analysis of medical intervention;

1. Patients must survive long enough to be identified as responding to treatment whereas any patients who die before this point are identified as non-responders
2. It is very difficult (or impossible) to differentiate between cases where response prolongs survival or simply acts as a marker for patients with a favourable prognosis.

In respect to item 1 Anderson observes that survival curves for non-responders and responders can still be useful in the clinical management of patients where a patient with a poor prognosis may be treated differently than those with a favourable prognosis. This criticism is less relevant to surgical intervention than medical, Anderson identifies that where "most patients who respond do so early and very few patients die in this early period ... the results of the incorrect methods [come] close to those of the correct methods." Surgical intervention can be considered to be the extreme where patients respond immediately (or not at all) and no patient dies before this point (surgical mortality is invariably discounted from any prognostic analysis).

Anderson's criticism is however relevant to some literature; one example is Mangiola et al. (2006) where they analysed a group of 34 patients aged over 65 years for prognostic factors in the treatment of glioblastoma multiforme. Mangiola considers the effect of a second surgical intervention and determines that this is of statistical significance, although the time points where the second intervention took place are not stated the implication is that it is not immediate.

Operating after any post-operative MRI enhancement has dissipated would mean that the delay would be at least three months at which the survival has already dropped to 70%. This effect, particularly when combined with the small group size, means that these results have to be seriously questioned.

The problem defined in 2 could be restated that "Gross total resection is only possible in patients with a favourable prognosis". This is increasingly being recognised in the literature;

> tumour resectablity may be a surrogate factor for tumour behaviour. Molecular cytogenetic profiles may be different for multifocal, deep tumours located in eloquent areas of the brain, compared with those lesions located near the cortical surface in noneloquent areas. Laws et al. (2003)

Study of how these tumours develop and an understanding of the features which make them more aggressive may help mitigate this problem.

Even where all patients are eligible for GTR and the extent of resection is accurately assessed Anderson's criticism may still be valid. Eligibility criteria can be set up to attempt to ensure that all patients are equally likely to have a GTR. This can be done by excluding from the study certain tumours including those difficult to reach (basal ganglia, brain stem, corpus callosum etc.) and those adjacent to functional areas (sensorimotor cortex, speech region etc.). Accurate measurement of residual tumour is required and is possible with early post-operative MRI. The only way to resolve this criticism is to randomly assign gross total or partial resection to a population of patients and pursue gross total resection at whatever expense. However this would be totally unethical and against the oath which all surgeons undertake (Hippocrates (ca. 400BC)). One of the closest to this is Albert et al. (1994) which dates from before neuronavigation became standard practice, this paper looks at assessing both surgeon's estimation of resection extent and the survival advantage conferred by GTR. The surgeon's estimation was therefore the only method to intraoperatively assess the extent of resection. Albert used early post-operative MRI for assessment of residual tumour and had reasonable exclusion criteria for difficult tumours. Surgeon's estimation was shown to be a poor assessment of the extent of resection (this is supported elsewhere, Nazzaro and Neuwelt (1990); Keles et al. (2001)). Also the extent of resection was shown to be a strong predictor of survival, however even without neuronavigation and depending on surgeon's estimation which means that the extent of resection may be more likely to be randomly distributed there is no way to prove this.

By similar reasoning papers such as Claus et al. (2005) where the aim is to achieve GTR (in this case using iMRI) and only accept partial resection when functional tissue is involved is critically flawed in that the ability to perform GTR could be a prognostic indicator rather than the treatment.

Selection bias can be a particular problem, for example high risk patients are more likely to have a biopsy than undergo the more aggressive total resection, this tends to distort the statistics in favour of resection. Attempts have been made to mitigate selection bias, for example Laws et al. (2003) states in their retrospective study of outcome data from 788 patients that the biopsy group were considered to have negative risk factors (age >60 years, KPS <70, presence of multifocal tumours). Therefore to accurately assess whether patients undergoing biopsy actually have a poorer outcome or if it is simply associated with their existing high-risk factors some adjustment must be made. Laws mitigates this bias by removing the "poor-risk" patients from analysis. Although this reduces the size of the data-set it increases the validity of the data. Laws observes an increase in the significance of extent of resection with successive attempts to analyse only the "good-risk" patients from both resection and biopsy groups for both GBM and AA.

Care must be taken in analysis of the existing literature as there seems to be a large amount of comment but little new data and some of the data presented needs to be carefully considered. For example Hess (1999) continues the debate but does not add significantly to it. This paper, published in 1999, considers data collected in the early 90s, the latest data point is from 1996. The publication of this paper appears to lag the collection of the data by an unacceptable margin even though the data relates to higher grade tumours where the prognosis is poor and so not requiring particularly long follow-up periods. Similarly Jeremic et al. (2003) uses data collected before 1993 considers a cohort of 175 patients with GBM of whom the maximum survival was 60months. A large number of factors were considered in this work and most found to be of some relevance, the extent of resection the greatest of these factors however the assessment protocol was not stated. One might assume given the publication date that a post-surgical imaging technique would be used however the patient cohort dates from before this saw wide adoption.

Differences in the definition of the extent of resection present interpretation difficulties. The results of Ammirati et al. (1987a) must be called into question based on the measurement of the extent of resection, that GTR is not possible in all patients and that almost certainly that GTR would indicate those with a favourable prognosis

#### 4.1.1.5 Low-grade tumours

Low grade gliomas are the most benign of the primary brain tumours. The World Heath Organisation classifies these as grade I and II. The more common grade I tumours are pilocytic astrocytoma, dysembryoblastic neuro-epithelial tumours, pleomorphic xantho-astrocytoma, neurocytoma and ganglioglioma. The more common grade II tumours include astrocytoma, oligodendroglioma and mixed oligostrocytoma Whittle (2004). These definitions are important as grade I tumours can generally be cured by surgical excision Luyken et al. (2003). Whereas grade II are tumours generally incurable but have long median survival times of >5 years. Equally oligodendrogliomas typically have a better prognosis than astrocytomas partially due to gene deletions which make them particularly susceptible to chemotherapy, Shaw et al. (2002).

Low-grade gliomas commonly present with seizure disorders and are difficult to classify even with the best MRI so first an accurate diagnosis must be obtained. After diagnosis a number of management options other than surgery present themselves; a "watch and wait" policy may be most appropriate for patients who are asymptomatic or whose symptoms can be controlled medically (e.g. with anticonvulsants); radiotherapy and chemotherapy have been shown to improve prognosis, Karim et al. (2002). However the timing is still debatable as Olson et al. (2000) has shown that there is little difference between post-operative or delayed radio/chemotherapy. Surgery is complicated by the large number of these low-grade gliomas which are diffusely infiltrating, figure 4.3 demonstrates the difficulty, this patient underwent a sub-total resection and which completely stopped her seizures. However a complete resection in this patient even using awake craniotomy would almost certainly be followed by major neurological disabilities.

Whether the extent of resection is associated with longer survival times is still a subject of some debate. Claus et al. (2005) investigates this question but the confidence intervals presented in this paper are too large for any significant conclusions to be drawn from it. Hall (2004) documents a long-term study correlating extent of resection with survival in 65 patients with low-grade glioma (29 oligodendrogliomas and 36 astrocytomas). Lo et al. (2002) found that the only significant prognostic factors in their study of 65 patients with low-grade glioma were extent of resection and whether the tumour was enhancing on preoperative imaging. In this study little difference was observed between those patients with subtotal resection and those who only underwent a biopsy. This study has not attempted to adjust for the inherent selection bias in the bias/subtotal resection groups.

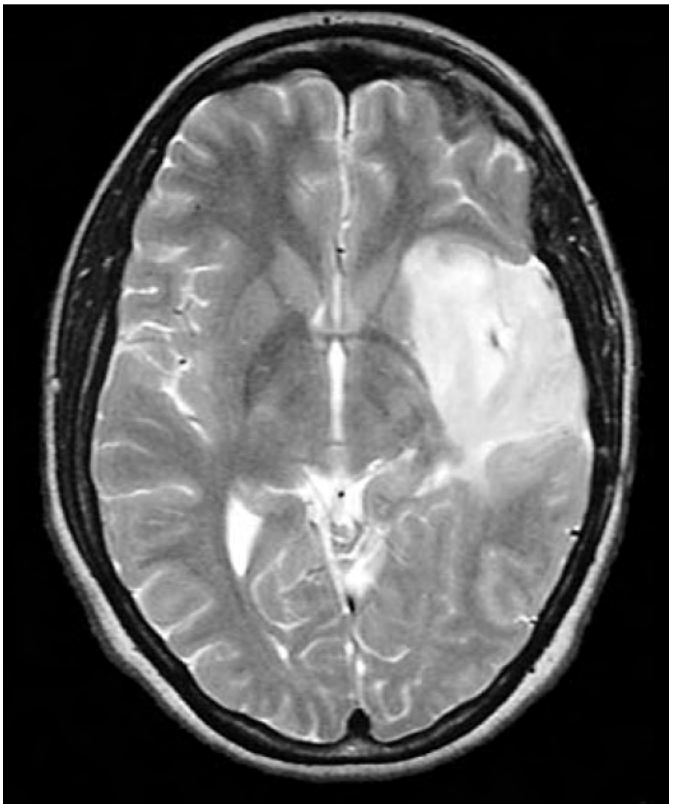

FIGURE 4.3: A T2-weighted MRI scan of 28 year old woman with complex partial seizures but no focal deficit. The lesion did not contrast enhance and radiologically fits the classical appearance of low-grade glioma (from Whittle (2004))

Similarly to the high grade tumours there are a number of prognostic factors associated with survival. Nicolato et al. (1995) retrospectively analysed 76 patients diagnosed with low-grade astrocytoma in the CT-era and found a large number of significant prognostic factors listed in table 4.2. A number of these factors are likely to be inter-dependant, for example the shape and the edge definition are likely to be correlated. This study has a relatively small number of cases so it is inappropriate to over-emphasise this study however it does highlight the same factors as other papers. Age, size, KPS and histology are recognised in Pignatti et al. (2002) as significant in one of the rare larger randomised studies - the specific aim of this study however was to investigate the effect of postoperative radiotherapy and although not randomised with respect to the extent of resection its conclusions are still interesting.

| **Significant factors by univariate analysis** | **p Value** |
|---|---|
| Extent of surgery | 0.0001 |
| Preoperative KPS Score | 0.0001 |
| Age (≤50 years) | 0.0006 |
| Well defined edge | 0.002 |
| Regular shape | 0.003 |
| Tumour diameter (CT) | 0.004 |
| Presence of cyst | 0.01 |
| Postoperative KPS Score | 0.02 |

TABLE 4.2: Univariate prognostic factors in low-grade glioma from Nicolato et al. (1995)

| **Authors and Year (no. patients astrocytoma/oligodendroglioma or mixed)** | |
|---|---|
| **≤2000** | **2000-2008** |
| ***statistics favour more extensive resections*** | |
| North et al. (1990) | Lo et al. (2002)(65) |
| Nicolato et al. (1995)(76) | Pignatti et al. (2002)(395/215) |
| Miralbell et al. (1993)(67) | Yeh et al. (2005)(46/47) |
| | Hall (2004)(36/29) |
| | Shaw and Wisoff (2003)[1](1600) |
| ***statistics do not favour extensive resection*** | |
| Lote et al. (1997)(379) | Shaw et al. (2002)(64/139) |

TABLE 4.3: A historical summary of literature either favouring or not gross total resection for low grade glioma

[1] Review of 5 prospective clinical trials

Selection bias seems to be more evident regarding patients with low-grade glioma.

> Every neurosurgeon has seen patients with low-grade astrocytomas who are fully functional, have no neurological deficit, and who survive for long periods of time without any form of treatment Laws (2001).

Laws suggests that these patients are very unlikely to be entered into a trial of any sort. There has not been any significant attempt to mitigate this selection bias.

In spite of the various problems within the literature, including; selection bias, differing definitions, lack of randomised trials, this author thinks that attempting

to achieve gross total resection in high grade tumours improves patient prognosis. The weight of recent literature using post-operative MRI indicates an increasing trend towards this same conclusion. Low grade tumours pose more of a problem particularly if their symptoms can be controlled with medication and ultimately it probably depends on the patient. The author does not entirely agree with the statement below from Laws (2001). If the patient is asymptomatic or adequately controlled then a 'watch and wait' policy may well be the best option; however if resection is chosen then this author advocates maximal safe resection.

> this strategy of recommending radical resection of gliomas of the brain is probably a sound one, based on what we currently believe to be the pathogenetic mechanisms associated with gliomas. Clearly, the more cells at risk, the more likely a tumour is to undergo the series of genetic events that ultimately leads to a more aggressive or malignant glioma. For that reason, the traditional oncological principle of cytoreduction must be considered appropriate until proven otherwise. Laws (2001)

If Anderson is correct in his statement that it is the ability to perform total resection rather than the resection itself that is prognostic then attempt the resection and remove any doubt. Whatever happens the tumour seems likely to return, and a better understanding of the prognosis is likely to assist the patient even if this prognosis is not favourable. If this author were the patient, whether the tumour was a low or high grade, he would opt for maximal resection

#### 4.1.1.6 Function

Neurosurgeons seek to minimise post-operative neurological deficit which means that they do not operate solely on anatomy but also on physiology. There are a number of techniques to assess the function of tissue both preoperatively and during surgery. There is more information about these methods in 4.1.2.

Duffau et al. (2008) demonstrates the amazing potential for the brain to reorganise function or 'plasticity'. He studied 77 consecutive patients undergoing surgery for Low-Grade Glioma in principle functional areas including the sensorimotor cortex and temporal language areas. 92% of these tumours were extensively or totally resected and all patients had immediate post-operative deficit. However all but 5% of cases suffered no long-term morbidity. This plasticity shows how it is possible that all of the patients studied presented without functional deficit despite significant tumour masses within typically

eloquent areas. Also that these deficits experienced immediately post-operatively were due to resection of tumour infiltrated regions which are associated but not essential to function. This decreases the risk of post-surgical morbidity. It presents an opportunity to surgeons to increase the extent of resection into eloquent areas but leaves the difficult question of knowing what functionality can be compensated for.

The gold standard for localizing functional areas is direct electrocortical stimulation (DECS). At the beginning of the procedure, after the brain has been exposed the surgeon stimulates the cortex with bipolar probe. This probe consists of two metal contacts about 2mm in diameter separated by approximately 7mm. This is applied to the exposed cortex and current pulses are injected. The awake patient is able to communicate and perform tasks, where the probe is applied to eloquent tissue it will inhibit function in this tissue hence stopping the task. As the surgeon does not stimulate into the sulci this could be considered an incomplete map also stimulation cannot always be performed for clinical reasons. Therefore new ways of assessing the location of eloquent tissue are of interest.

Functional MRI has the potential to be of some use in identifying functional tissue however the correlation between fMRI and electrocortical stimulation has yet to be proven. Xie et al. (2001) calls into question the validity of all measurements by BOLD-fMRI by suggesting that a change in deoxy-haemoglobin does not always accompany neuronal activation. Pouratian et al. (2003a) questions the correlation between perfusion-related imaging (such as optical intrinsic imaging and fMRI) and activity. Pouratian notes that the signal often seems to "spread" possibly due to; subthreshold activity in adjacent tissue, super threshold activity of non-essential tissue, or the non-exact colocalisation of activity and perfusion. Larsen et al. (2007) quantifies the correlation of DECS and fMRI in a single case study, Larsen demonstrates that stimulation finds a subset of the areas defined by fMRI. This may be due to active tissue in the sulcus or could be the activation of tissue that is associated with but not critical for a given activity. Krings et al. (2001) has correlated fMRI with Transcranial Magnetic Stimulation (TMS), DECS and PET. Krings presents that fMRI correlates with both the electrophysiological methods (TMS and DECS) and the metabolically based method (PET) however the limited spatial resolution of these techniques and Krings' definition of a miss as >2cm raises questions. Krings also uses a different technique for DECS — a monopolar (presumably a return is located elsewhere on the patient) stimulator on anesthetized patients to elicit muscular movement (monopolar stimulation is broadly similar to bipolar stimulation Kombos et al. (1997)). Hill et al. (2000)

which defines significant errors as >10mm in their comparison of fMRI and stimulation and determines that fMRI is not suitable for functional delineation for surgical use. Hill cites brain deformation during surgery and motion artifacts during imaging at the primary causes of error.

There is some interest in integrating fMRI systems with other imaging or point measurement modalities. Gore et al. (2006) investigates the integration of fMRI, and event-related potentials, and recognises that there could be considerable advantages in integration of the varied techniques for functional imaging. However the cost in additional complexity seems to make this sort of integration somewhat unlikely.

Michael Haglund currently at Duke university has pioneered the optical imaging of function in humans. His work built on that of Grinvald working in the Weizmann Institute of Science in Israel, Grinvald developed this technique in mammals both awake and anesthetized (publications include Grinvald et al. (1986, 1991)). Although there was some question as to the origin of the signal, optical imaging of function was demonstrated in the sensorimotor cortex by activity and stimulation by Haglund and colleagues in 1992 (Haglund et al. (1992)). Haglund has continued working in this field and has expanded it to observe spontaneous epileptic seizures, Haglund and Hochman (2004). Haglund typically uses wavelengths between 650 and 700nm.

The sources of the intrinsic signal include reflectance changes from several optically active processes which correlate indirectly with neuronal firing. The main parameters that affect this signal are summarised by Zepeda et al. (2004) as;

1. Changes in the blood volume
2. Chromophore redox, including the oxy/deoxy haemoglobin ratio, intracellular cytochrome oxidase and electron carriers
3. Light scattering

The first two factors are simply dependant on the metabolic rate of the cerebral tissue and thanks to the autoregulation of blood flow in the brain these signals are very localised. Neuronal activity uses oxygen which is initially supplied by the local capillaries and a highly localised dip in the oxy/deoxy ratio (initially evidence to support this was lacking however it was demonstrated in Vanzetta and Grinvald (1999) and subsequently confirmed elsewhere). During brain activation regional cerebral blood flow greatly increases ($\sim 30\%$) within 1–2 seconds, whereas the metabolic rate only increases moderately ($\sim 5\%$), assessed

in healthy volunteers using PET, Fox and Raichle (1986); Fox et al. (1988). This decoupled response means that during neuronal activity deoxyhaemoglobin concentrations decrease while oxyhaemoglobin increases. It is this increase in oxygen delivery which is observed in fMRI and referred to as the "Blood Oxygen Level Dependant" (BOLD) signal and can be interrogated optically.

The third factor was first reported in Hill and Keynes (1949) from the scattering of a crab leg nerve. Although this is undoubtedly present and potentially yields information with a higher temporal and spatial correlation, particularly as this effect does not expand to surrounding areas. It dominates the other affects in the near-infrared 850—700nm region. However it does not seem to have significant interest in the current literature possibly due to its low value relative to the scatter of the surrounding tissue.

Building on work first reported by this group in 2002 (Sato et al. (2002); Nariai et al. (2002)) Sato and colleagues use Xenon illumination and a filter of 605 ±5nm to correspond with the maximum difference between the oxy/deoxy haemoglobin spectra. Work presented in Sato et al. (2005) and Nariai et al. (2005) observed the somatosensory cortex of 14 patients undergoing a craniotomy and stimulated either the digits of one hand or the maxillary nerve. Their patients were anesthetized so they correlated their results with somatosensory-evoked potentials. In this study even though brain surface was stabilized with a glass plate some movement artifacts were reported. The size of the craniotomy in the figures presented is somewhat larger than one would expect even given the requirement for functional mapping of the cortex near the tumour. Acquiring a map required 8 blocks of 3 stimulation/control cycles taking in total about 10 minutes, another 5 minutes was required for initial processing. Areas of functional activation corresponded with stimulation. These areas were slightly overlapped but generally well separated.

Cannestra et al. (2001) presents work establishing the co-localisation of fMRI, Optical intrinsic signal and evoked potentials. This paper strengthens the spatial correlation between fMRI and optical imaging of function. It also highlights the difference in temporal location with fMRI lagging optical imaging by approximately 2–3seconds. The same group previously reported (Cannestra et al. (2000)) that optical imaging and electrocortical stimulation were colocalised in the regions associated with speech and language. This paper also presents differences in the temporal profile of the optical signal relating to sensory and motor cortices which may add additional information to the analysis. Further work from the same group was presented in Pouratian et al. (2002) highlights the fact that fMRI is a volumetric tool instead of the 2-D optical imaging and demonstrates that the spatial correlation is not exact.

Epileptic events are of particular interest to optical imaging due to the high temporal and spatial resolution possible with intraoperative optical imaging. Schwartz (2003) describes imaging of simulated seizures in the ferret visual cortex and exploits the ability to map function in the vicinity. Suh et al. (2005) investigated the effect of epileptiform events and observed in an animal model that these events unlike normal physiology increase the metabolic rate beyond the capabilities of the brain to supply it. If this event is short then the increase in local blood flow will eventually supply enough and an increase will be observed. They observed the dip in oxyhaemoglobin in human patients with electrocortical stimulation (which is not unlike an epileptic event).

Intraoperative optical imaging is invasive and optical means are being sought to determine function through the skull. Schroeter et al. (2005) demonstrates that an intracranial functional Near Infrared Spectroscopy (fNIRS) system is capable of assessing functional response in tissue as deep as 1cm into the cortex. He correlated this with fMRI and continued recording until the relative haemoglobin levels returned to pre-stimulation values which took approximately 30s.

Various techniques to improve the signal to noise in optical functional maps exist including Schiessl et al. (2008). There also attempts to increase the functionality of such a optical system, Dunn et al. (2002) integrates functional imaging with laser doppler to add sensitivity to blood flow to the total haemoglobin concentration and oxygenation in mice.

Imaging of the haemodynamic response is not the only optical technique that may be relevant to delineation of function. Husson et al. (2007) presents a technique sensitive to flavoprotein autofluorescence which derives from proteins involved in the mitochontrial electron transport chain and is therefore a more direct measurement of function than the haemodynamic response. They have shown that this signal is present in both cats and rodents and follows activation but precedes the BOLD signal. This paper acknowledges some of the limitations of this technique, that it requires a large amount of illumination and long integration times to capture sufficient fluorescence for mapping, the amount of background fluorescence is not mentioned but is likely to limit the signal to noise ratio.

### 4.1.2 Current Imaging methods

A number of imaging technologies are in current oncological use. Many of these have been mentioned in Section 4.1.1 this section will provide a brief introduction into these methods. This section will focus specifically on the use of

| **Category** | **Imaging Method** |
|---|---|
| Structural | |
| | X-ray Computed Tomography (CT) |
| | Magnetic Resonance Imaging (MRI) |
| | Magnetic resonance angiography |
| Functional | |
| Noninvasive | Positron-emission tomography (PET) |
| | Single photon-emission computed tomography (SPECT) |
| | Functional Magnetic Resonance Imaging (fMRI) |
| | Electroencephalography (EEG) |
| | Magnetoencephalography (MEG) |
| | Transcranial Magentic Stimulation (TMS) |
| Invasive | Electrocortiography |
| | Depth electrodes |
| | Cortical Stimulation |
| | Optical signal imaging |

TABLE 4.4: A summary description of imaging methods.

these technologies for diagnosis and will provide some of the pros and cons of these methods. These techniques either give information about the tissue structure (anatomy) or the tissue function (physiology) the advantages of this will also be highlighted. Table 4.4 shows broadly what techniques can be used for anatomical and physiological delineation. Figure 4.4 summarises graphically the spatial and temporal resolution of some of these techniques.

#### 4.1.2.1 Radiological

Most people are familiar with radiology for diagnostic purposes and it is the primary means of anatomical imaging (with the exception of in the brain). The simplest form of which is the diagnostic X-ray which involves directing radiation upon a specific part of the body and collecting radiation that has passes through. Increasingly digital sensors are replacing the traditional cassette and photographic film. X-rays passing through the body are more absorbed or scattered by dense tissues (bones, tumours etc.) and relatively less absorbed through less dense tissue (muscle, fat etc.). These radiological techniques are primarily an anatomical technique as tissue density varies with tissue type and not function. Tumour tissue is typically more dense than non-malignant tissue and in addition more advanced tumours can show calcification which can be detected.

Computed Tomography (CT or commonly as "cat") uses an X-ray generating source opposite a detector (normally an array of detecting elements). This source

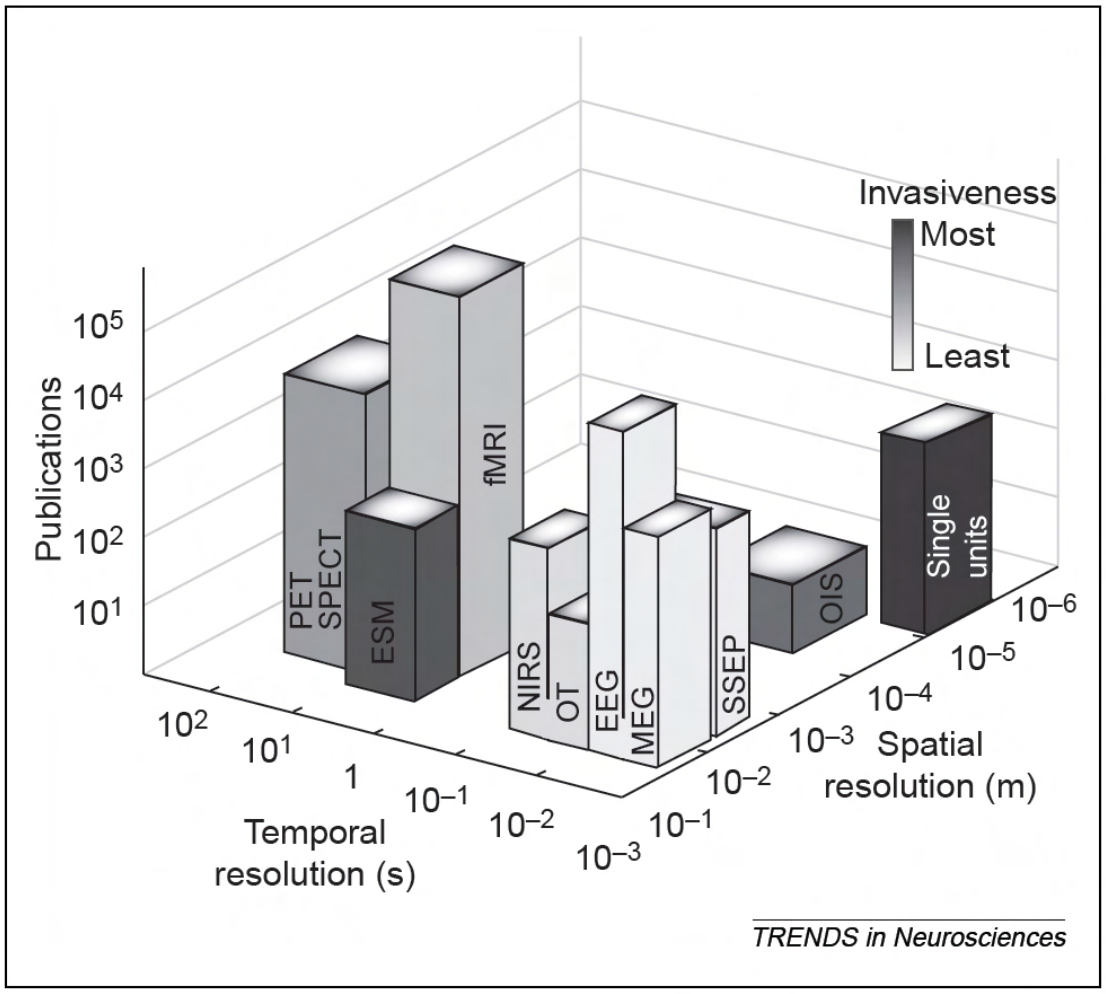


FIGURE 4.4: Spatial and temporal comparision of functional human brain mapping techniques (image from Pouratian et al. (2003b))

detector pair are then rotated axially around the patient and a computer is used to reconstruct this information into a three dimensional model and generate cross-sectional images. Intravenous contrast agents can be used to enhance the appearance of arteries and veins in CT scans which enables the anatomy of these, otherwise low contrast, vessels to be viewed.

With the introduction of spiral CT systems in the mid 1990s a new technique called perfusion CT was made possible. A small amount of reasonably innocuous contrast agent is administered intravenously and then frequent scans give the perfusion of tissue under investigation. This is primarily used in strokes and oncology. Perfusion CT use in strokes can identify areas of brain which are being deprived of oxygen prior to surgical intervention i.e. areas where the blood flow is below a threshold. In oncology perfusion CT can identify the relative increase in blood flow due to the angiogenesis (or neovascularisation) of the tumour bed. Although this is not extensively used in neural oncology, possibly due to the

poor contrast of cerebral anatomy when compared with MRI, it certainly has it's uses (for more information Miles and Griffiths (2003) is an interesting review and two cases studies can be found in Teksam et al. (2005)).

Intraoperative CT although demonstrated in the early 80's has not achieved a significant role in neurosurgical practice. Mobile CT has improved the situation in certain fields, for example in intensive care units where moving the patient would be detrimental to their welfare. This has made intraoperative CT more practical. However CT uses ionizing radiation, has limitations on plane orientation and has poorer contrast than MRI (Martin et al. (2000)). For these reasons and the development of iMRI in the mid 90's intraoperative CT has not made a significant impact.

Fluoroscopy is another radiological technique that has significant impact in the field. Fluoroscopy should not to be confused with fluorescence techniques using intrinsic or extrinsic fluorophores and optical excitation. This technique uses a constant stream of X-rays onto a fluorescent screen or image capture device. This is often used intraoperatively to aid guidance during procedures however is not a tomographic technique so has limited utility.

Radiological techniques are minimally invasive. All patients will receive a radiation dose. Currently it is assumed that all radiation doses present risk to the individual however small the dose. The contrast agents used in CT scans present some risk to patients particularly those with kidney impairment. The scan takes some time, maybe as much as 30 minutes, through which the patient should be as still as possible. The CT is enclosed in a ring and so the environment is relatively open and so is not as intimidating as MRI, and is also suitable for patients with metal implants (e.g. cochlear implants, aneurysm clips, pacemakers, replacement joints).

#### 4.1.2.2 Nuclear medicine

Nuclear medicine involves the use of radioactive isotopes to diagnose disease. Radioisotopes ('tracers') are integrated into radiopharmaceuticals with a known behaviour and administered intravenously or inhaled by the subject. These radiopharmaceuticals act characteristically in the body therefore these isotopes collect in specific tissues or organs giving a measure of function (or physiology) not anatomy.

Positron Emission Tomography (PET) was developed in the mid 1970's although was not in clinical until the late 1980's (Mazziotta (1994)). PET uses positron emitting tracers which annihilate an electron and produce a pair of gamma rays

travelling in opposite directions, detecting these gamma rays allows tomographic images to be produced. Typical uses include fluorine-18 labeled fluoro-L-thymidine and fluorodeoxyglucose for monitoring glucose consumption and DNA synthesis respectively, amino acid transport can be monitored using carbon-11 methionine and oxygen-15 can be used to monitor oxygen metabolism. The short (about 2mins for $^{15}$O up to 110mins for $^{18}$F) half-lives of these isotopes require local production in a cyclotron which makes this technique particularly expensive. PET can provide information about cerebral metabolism, blood flow and volume, oxygen use, neurotransmitter synthesis and receptor binding.

Single Photon Emmision Computed Tomography (SPECT) is very similar to PET, the key difference being that the tracer emits a gamma photon rather than a positron. SPECT instruments were developed in the 1950-60s and immediately applied to cerebral function. Typical tracers used include xenon 133, iodine 123, technetium 99. SPECT can provide generally similar information to PET including cerebral perfusion, blood volumes, and receptor distribution. It is also used in applications such as thyroid function assessment and bone imaging. Although it has lower spatial resolution than PET the longer half-lives of the radioisotopes mean that local production is not necessary.

Similar to radiological techniques all patients receive a radiation dose generally about the same as a diagnostic X-ray. These techniques are minimally invasive typically requiring no more than an intravenous injection. They do take a significant amount of time, following the injection of the radionuclide a patient may have to wait a number of hours for the tracer to reach it's destination. The scan itself takes some time (maybe as much as 30 minutes) during which movement of the patient is detrimental to the image.

#### 4.1.2.3 Magnetic resonance imaging

Magnetic Resonance Imaging (MRI) has it's origins in the chemistry technique Nuclear Magnetic Resonance, a spectroscopic technique that is used to provide microscopic chemical and physical information about molecules. MRI was introduced clinically in the 1980s. It is particularly useful in neurooncology due to the excellent spatial resolution and high contrast between gray and white matter.

MRI uses a large, often superconducting, electromagnet (commercial clinical devices range from 0.1Tesla up to about 3T) to align the nuclei of atoms that exhibit spin, one such nuclei is hydrogen. Once aligned the atoms are then excited using Electromagnetic (EM) waves of the appropriate frequency (for

Hydrogen in a 1T machine this is 42.58MHz). The excitation is then removed causing the excited atoms to relax and emit radiation at the same frequency which can be detected.

The contrast of MRI images can be tuned to a number of different tissue properties (unlike radiological methods whose only contrast mechanism is the optical properties of tissue in the X-ray region). There are three main parameters that are used; Spin-Lattice Relaxation time ($T_1$), Spin-Spin Relaxation time ($T_2$) and Spin Density ($\rho$). These parameters vary with tissue type, some pathology has the $T_1$ value similar to that of normal tissue whereas the $T_2$ values may differ - some relaxation times and density values for tissues found in the human head are shown in 4.5. The details of how the MRI is tuned to these values are not pertinent to this document and are explained better elsewhere (for example http://www.cis.rit.edu/htbooks/mri/index.html).

Kelly et al. (1987) demonstrates that T2-weighted MRI imaging reveals greater tumour volumes than contrast enhancement and low-attenuation boundaries on CT. Biopsy of 195 samples revealed that contrast enhancement indicated tumour; hypodensity related to normal tissue infiltrated with tumour cells or in some instances low-grade glioma or oedema; and isolated tumour cell infiltration extended at least as far as T2 enhancement on MR images. MRI is very sensitive to high grade tumours particularly with the use of contrast enhancement, however this contrast agent exploits a compromised blood brain barrier which is not present in low grade tumours. Due to this lack of contrast agent, the presentation as hypodensity and presence beyond the T2 enhancement MRI is not particularly sensitive to these low grade tumours.

| **Tissue** | **$T_1$ (s)** | **$T_2$ (ms)** | $\rho^\star$ |
|---|---|---|---|
| CSF | 0.8 – 20 | 110 – 2000 | 70 – 230 |
| White | 0.76 – 1.08 | 61 – 100 | 70 – 90 |
| Gray | 1.09 – 2.15 | 61 – 109 | 85 – 125 |
| Meninges | 0.5 – 2.2 | 50 – 165 | 5 – 44 |
| Muscle | 0.95 – 1.82 | 20 – 67 | 24 – 90 |
| Adipose | 0.2 – 0.75 | 53 – 94 | 50 – 100 |

$^\star$Based on $\rho$ =111 for 12mM aqueous $NiCl_2$

TABLE 4.5: shows the range of values $T_1$ $T_2$ and $\rho$ found in magnetic resonance images of the human head Fletcher et al. (1993)

MRI is mainly used as an anatomical technique but also has the ability to detect functional characteristics of the brain by detecting the BOLD signal. The Blood Oxygen Level Dependant (BOLD) signal is a function of the activity of a section of brain tissue. Using the BOLD signal MRI is able to establish where an area is eloquent (an area of the brain that if removed would result in loss of ability).

This technique is called functional MRI (fMRI). In common with other functional techniques the patient must be conscious and able to perform the tasks required. FMRI has the advantage over radiological techniques (e.g. SPECT), which can detect similar signals, in that it does not expose the patient to ionising radiation. FMRI does not have the temporal resolution of Electroencephalography (EEG) but has better anatomical sensitivity.

MRI takes some time to capture an image but it does not expose patients to ionising radiation like radiological or nuclear techniques. Due to the tremendous magnetic fields present in the MRI there are limitations placed on the local environment including medical instrumentation. There is an infamous case of a 6year old boy killed when struck by an oxygen cylinder which was attracted by an MRI. This also limits patients with metal implants such as cochlear implants, aneurysm clips, pacemakers, hip replacements etc. as even small amounts could present a hazard and will distort the image. A contrast enhancing agent is often administered intravenously, a Gadolinium compound is common in neurooncology; normally this is tolerated exceptionally well but may not be advisable in patients with poor renal function. As with all the tomographic techniques the patient must stay as still as possible during the scan although the images collected by MRI can be registered post acquisition to reduce motion artefacts. The patient will be totally enclosed during the scan which may preclude its use for those with claustrophobia and scans can be very noisy particularly with older instruments.

#### 4.1.2.4 Intraoperative MRI

Intraoperative MRI (iMRI) is a developing technique that has significant potential in the field of neuro oncological surgery. The possible impact of this technology is such that it deserves individual attention. Current image guidance systems rely on images taken pre-operatively and so as tissue is resected and anatomical structures move these systems become increasingly inaccurate. These systems cannot provide the surgeon with any new information. Intraoperative MRI however can provide real-time information similar to fluoroscopy, however iMRI is a tomographic technique and does not use ionising radiation with the added benefit of better resolution. This enables the surgeon to establish the extent of resection and provide image guidance on the current anatomical state of the tissue. However there are significant limitations on these systems not least the extent that the surgical routine is affected. The region around the MRI and often the whole operating theatre must be completely free of ferromagnetic

instrumentation and even instruments that are non-ferrous may be repelled or attracted by the strong magnet or cause artefacts in the images.

The intraoperative MRI was developed in a collaboration between the Brigham and Women's Hospital and General Electric starting in 1990. The prototype system was deployed into an operating theatre in 1994 the development was documented in Black et al. (1997). The development of this system included significant testing of which instruments can safely be used within the vicinity of the imager. This imager has a split coil with a 54cm gap, allowing the surgeon and assistant to access the patient between the vertically oriented rings (see figure 4.5). This allows images to be collected while the surgery is in progress. The 0.5T field does not provide the resolution of more powerful diagnostic imagers (typically 1.5T) but is described as 'sufficient for intraoperative guidance' (Martin et al. (1998)). Similar split rings are available such as that demonstrated in Germany by Schneider et al. (2005). The split coil does have disadvantages, the gap between the coils is small and limits access to at most 2 people, may limit the positions that the patient can orientated, all the instrumentation used must be MRI compatible. Even though the smaller imagers yield lower resolution images they do provide real-time imaging.

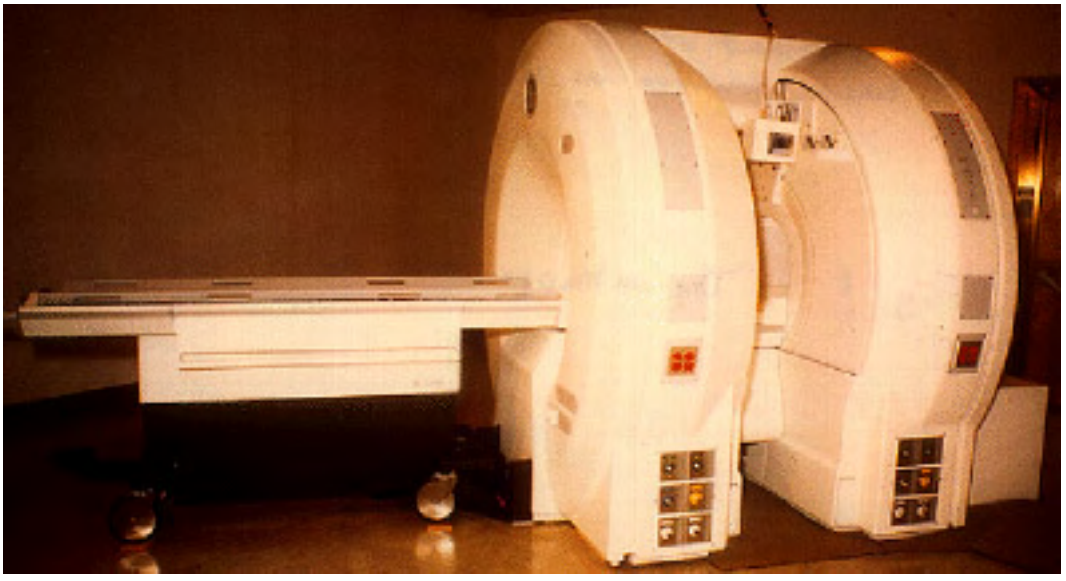

FIGURE 4.5: Image of split coil MRI note the size of the gap between the rings (image from Martin et al. (1998))

Intraoperative MRI systems come in a number of different shapes and sizes. In Martin et al. (2000) an iMRI system is described that consists of a 1.5T high field unit with a operating table that can slide in and out both sides of the ring. The theatre has an area of high-field where only MR compatible equipment can enter, outside this area normal equipment can be used. The ring is not split so surgery cannot be performed while imaging but can be performed near the

imager within the high field region using MR compatible equipment, or in a more traditional theatre environment in the low-field region (see figure 4.6). Imaging typically takes 10–15 minutes and the imager provides similar capabilities, in terms of both resolution and range of imaging, to a diagnostic imager. The imaging performance of this system is superior to typical split ring configurations due to the higher field, it also allows use of normal instrumentation (although care and correct procedures must be implemented). It does however require a larger operating theatre than split ring iMRI configurations and has the disadvantage of additional time required to move the patient to the imager. These disadvantages must be weighed against the improved contrast and other functionality of the higher power imager such as fMRI and FLAIR. These high field imagers do seem to be becoming more common, Nimsky et al. (2004) demonstrates a 1.5T short bore MRI and an increase in resection of up to 39%.

FIGURE 4.6: An iMRI suite showing the short-bore 1.5T MRI towards the left, the arrow indicates 4 MRI-compatible screens, the bed can slide between the MRI and a pedestal on the right surrounded by conventional instrumentation (image from Martin et al. (2000))

One option where a full iMRI system may be unaffordable or there are other constraints is to position the operating theatre adjacent to a full diagnostic MRI system. This can allow the patient to be transfered to this system for imaging, this may take up to 40 minutes but provide important information. This system suggests that a full-time MRI system is not required but does introduce other problems such as maintaining the sterility of this system. This system is in use and recognises that an MRI is not required throughout the whole procedure and

so potentially one MRI system could be shared between a number of operating theatres.

IMRI shares the same limitations as diagnostic MRI however there are also concerns that iMRI can increase the amount of post-operative morbidity as total resections are pursued at the expense of functional areas. Muragaki et al. (2005) presents a significant correlation between the first 46 patients operated under iMRI and the previous 50 patients operated using traditional techniques. Although this paper does observe a significant increase in post-operative morbidity the rate of permanent morbidity did not differ significantly. This paper also observes a significantly reduced amount of residual tumour. Others, for instance Schneider et al. (2005), have not reported any increase in morbidity.

#### 4.1.2.5 Developing MR techniques

Magnetic resonance imaging techniques are still under active development. There are two emerging techniques of particular interest; the first is MR Spectroscopy; the second is Diffusion Weighted MRI.

Magnetic Resonance Spectroscopy exploits the fact that the resonant frequency of a 'MR visible' nuclei (for example $^{13}$C, $^{23}$Na, $^{19}$F) is dependant on it's local chemical environment. The change is small, of the order of $10^{-6}$, so a known reference must be used. Because MRS is dependant on frequency shifts another method of excitation is required to enable tomographic data collection, this can be achieved by use of phase encoding the dimensions of interest. Specific chemical signatures can then be extracted which can be used to assign tissue properties or characteristic tissue types Urenjak et al. (1993). The image shown in figure 4.7 shows on the left healthy brain tissue displaying the normal high N-Acetyl-Aspartate peak (NAA). The right is a spectrum of brain appearing normal on MRI (without Gadolinium contrast enhancement). This spectrum however shows an absence of NAA indicating a loss of viable tissue and an increase in choline indicating high cell proliferation often found in tumours Liney (2009).

The contrast mechanism in diffusion weighted MRI is based on endogenous contrast using a technique discovered by Stejskal and Tanner (Stejskal and Tanner (1965)). This technique applies two field gradients with equal amplitude and opposite polarity over a given time interval. Stationary nuclei will be equally phased and dephased however nuclei that have moved will suffer a net phasing and therefore enable detection. By using fields of sufficiently high amplitude microscopic levels of motion can be detected. Full 3D diffusion measurements

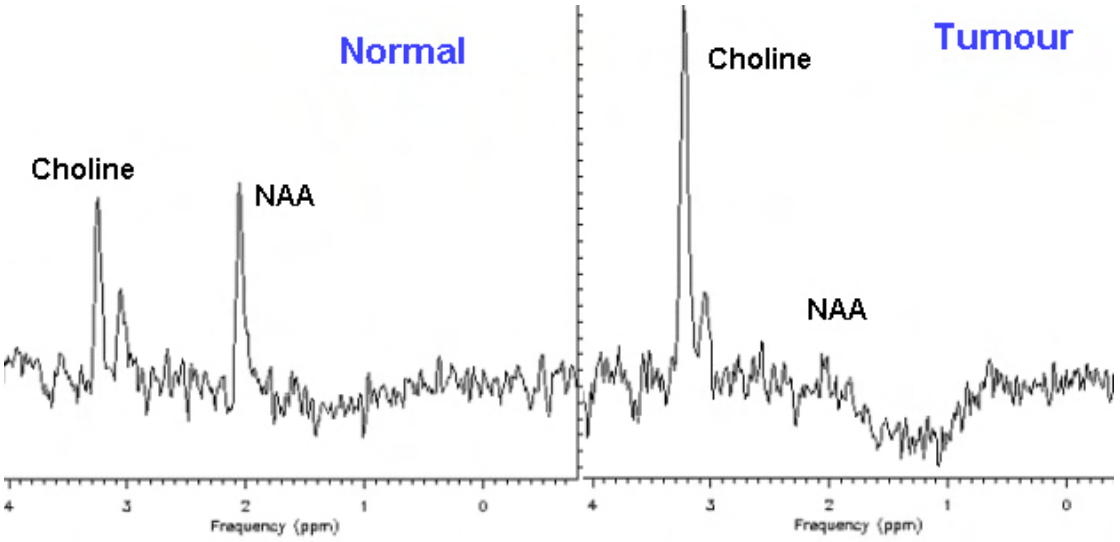


FIGURE 4.7: Example of a single voxel proton MRS in normal and malignant brain tissue (image from Liney (2009))

can be made and require 13 scans with different settings. The major advantage of this imaging technique is the ability to visualise movement due to the preferential diffusion along structures and fibres such as white-matter tracts. Figure 4.8 shows an image courtesy of Liney (2009) showing the possibilities of diffusion weighted MRI to identify white matter tracts. This technique could reduce post-surgical neurological deficit in neuronocological surgery but to date the major clinical use is to identify areas of ischemia (lack of oxygen) due to a stroke, diffusion weighted imaging can identify this earlier than any other diagnostic technique. However Smith et al. (2005) reports that post-operative diffusion weighted MRI should be handled with care but could be useful in long term monitoring.

#### 4.1.2.6 Ultrasound

Diagnostic sonography is a well established technology in certain fields, obstetric care is the typical example particularly prenatal scans. However ultrasound can also be used to image almost any soft-tissue in the body; cardiac, muscular, tendons, renal and liver it even has opthalmic uses. Ultrasound has seen little exploitation in the neurological field mainly due to the poor signal to noise ratio of transcranial ultrasound. There are niche applications for example neonatal ultrasound can be key in identifying and monitoring various conditions. There is some indication that ultrasound may be helpful in diagnosing Parkinson's disease (Stern (2008)),

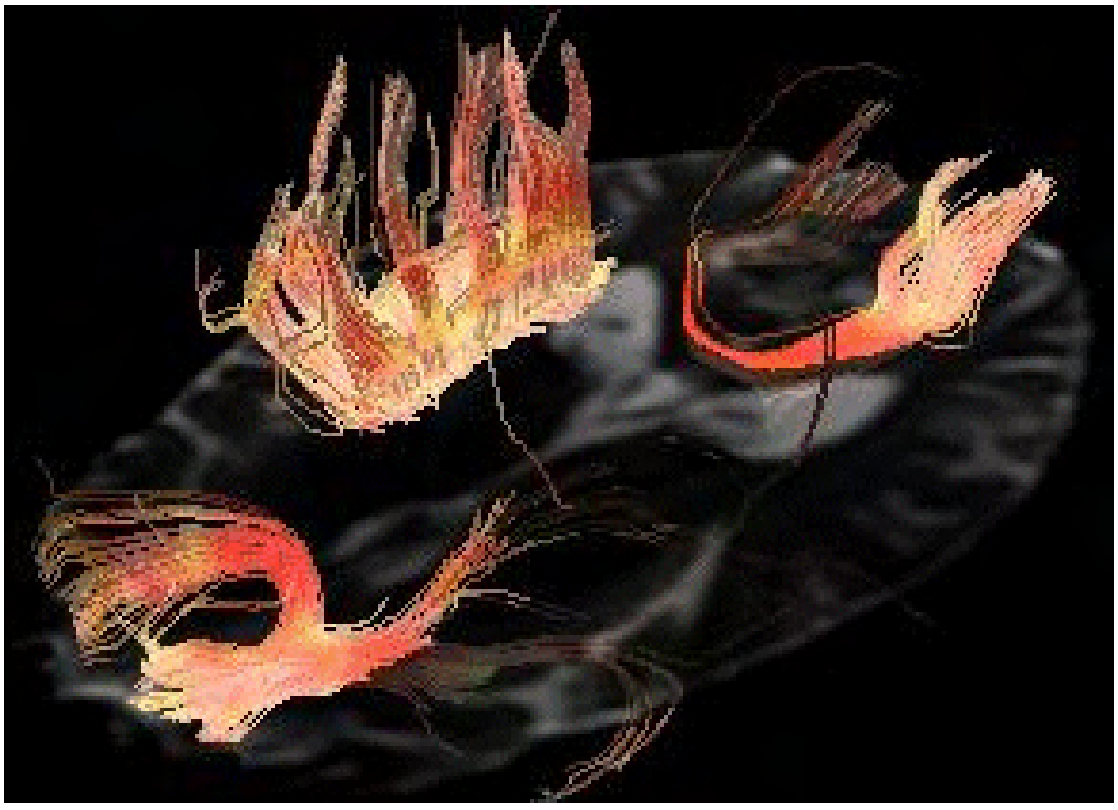

FIGURE 4.8: Example of white-matter tracts in a normal subject imaged by diffusion weighted MRI. Image from Liney (2009)

.

Intraoperative ultrasound can be difficult to correlate with preoperative imaging as almost all preoperative imaging is conducted with CT or MRI which have different contrast mechanisms (Martin et al. (2000)). A group in Norway (Unsgaard et al. (2002)) has demonstrated a three-dimensional ultrasound imager with a neuronavigation system utilising pre-operative imaging although this technique hasn't seen significant adoption many of the problems limiting earlier systems seem to be solved.

#### 4.1.2.7 Electroencephalography and magnetoencephalography

Electroencephalography (EEG) was developed and used clinically in the early part of the 20th Century. It measures the weak electrical potentials created by neuronal activity. Averaging and statistical analysis of components of the EEG signal have significantly improved the signal to noise and EEG currently has a wide range of uses. Measurements can be taken on the surface of the head, the surface of the cortex or by use of 'depth electrodes' into the sulci. The later two are obviously limited to patients undergoing a surgical procedure but provide improving spatial resolution as they are not limited by the distortion introduced

by the skull. The temporal resolution is uniformly excellent and of the order of neuronal events (milliseconds). Intraoperative measurement of evoked potentials is a very similar technique.

Magnetoencephalography (MEG) has been in development since the 1960s and works by measuring the induced magnetic fields created by the weak electrical currents created by neuronal activity. The extremely low magnitude of these signals makes this difficult requiring supercooled devices and a shielded environment. Unlike the electrical fields measured in EEG magnetic fields are not distorted by the intervening matter Mazziotta (1994). MEG has exquisite temporal resolution which is comparable to neuronal events. The spatial resolution is continuously improving as the significant technical challenges are overcome.

#### 4.1.2.8 Intra-cranial near infrared spectroscopy

In this context Intra-cranial Near Infrared Spectroscopy (INIRS) will be a term used to describe intracranial measurement of tissue parameters by using infrared spectroscopy, fNIRS is a functional implementation of this method. This technique suffers from three major problems;

1. *Partial volume effect* — due to the difference between the volume sampled and the volume exhibiting a change in properties (i.e. activation) INIRS therefore underestimates the concentration changes. Correction factors can be used to help account for this, factors of the order of 10 have been reported Strangman et al. (2002).
2. *Cross talk* — the path length in tissue is wavelength dependant, if this is not adequately determined changes in oxyhaemoglobin concentration can mimic those of deoxyhaemoglobin. This can be reduced to a few percent when using optimal wavelength combinations Steinbrink et al. (2005).
3. *Extracellular blood volume changes* — to sample the brain the scalp and skull must be traversed hence any changes in the blood volume in these tissues will also be detected. Using multiple detector/source pairs and methodological techniques (i.e. avoid systemic responses to stimulation) help reduce this effect.

Typically INIRS systems use light emitting diodes as sources, these are available in a sufficiently wide range of wavelengths and powers. Laser systems have been used to achieve a similar effect and have similar problems. Sase et al. (2006)

demonstrates a non-contact system tested against a phantom. By using time-gating in the hundred picosecond region this system is able to to detect objects buried up to 20mm in a scattering medium. However this system is currently impractical for clinical measurements, two Ti-Sapphire lasers were used with pulses in the 15ps region with a time-resolved intensifier operating with a 600ps time gate which is a physically large, complex and costly system. The signal to noise was generally poor, spatial resolution was approximately equal to the depth of the object. The dependence of this system on backscatter requires the time-gating system, whereas separated source-detector systems do not collect backscatter. Coupling into the head will be a particular problem for this system, hair will scatter or absorb almost all of the signal and limit this technique to hairless portions of the head.

fNIRS has struggled to consistently measure the decrease in deoxyhaemoglobin concentrations, for example Boas et al. (2000). It has also been noted that patients with brain disorders may have a different response from healthy adults Xie et al. (2001). It has been suggested that an increase in cerebral blood flow will not necessarily remove the deoxyhaemoglobin from the vessels or that a sufficient increase in oxygen use may compensate for the change in blood flow. Both of these possibilities would have affects on fMRI which can only measure activation by changes in the deoxyhaemoglobin concentration. During activation region blood flow increases by up to 50% however the oxygen consumption increases by no more than 5% therefore neuronal activity leads to a decrease in the extracted fraction of oxygen. Deoxygenated haemoglobin concentrations decrease in the cerebral vessels, including capillaries and veins, while oxygenated blood concentrations increase Xie et al. (2001).

### 4.1.3 Systems and techniques in development

This section will discuss the systems and techniques in current and recent literature.

#### 4.1.3.1 Fluorescence

Fluorescence is an established technique in all sorts of histopathological and *in vitro* biological applications. This section will focus on the *in vivo* applications and it's use in oncology in which fluorescence is a developing technique with limited commercial exploitation. There are some surgical procedures that already use fluorescence techniques for example fluorescence angiography NICE (2004) and NICE (2006). Labelled antigens have been developed for certain

cancers (prostate cancer and adenocarcinoma for example) and for specific detection of many proteins (see section 3 for another example).

Fluorescence occurs when a molecule absorbs a photon of high energy light (often ultraviolet) promoting the molecule into a higher energy state which then relaxes into a lower energy state emitting a photon of a lower energy (longer wavelength). The difference in energy of the high and low energy states is taken up by other changes of state within the molecule, for example vibrational or electronic states. There are two types of fluorophores in use, extrinsic (or exogenous) fluorophores and intrinsic (endogenous or autofluorescence). The use of extrinsic fluorophores requires the introduction of labelled drugs, proteins, antibodies or other entity into the patient or tissue sample. Intrinsic fluorescent systems exploit the natural fluorescence of the material or part of the material under investigation. Systems are in development that exploit both of these types of fluorophores, some only one, others integrate this information with other sources to enable diagnosis.

Xillix Technologies Corp (2007) have developed a number of systems based on their 'LIFE' core, where LIFE stands for Light Induced Fluorescence Endoscopy. Their LIFE-Lung system has completed it's clinical trials (in the US) and has been released commercially. They also have a Gastro-Intestinal (GI) and an Ear Nose and Throat system in development. These systems are all used in addition to white-light endoscopy and consist of an intensified CCD with red and green filters and a blue light source. They have shown that changes in the red/green ratio are related to tissue abnormality. The endoscopes used for these systems are fibre-bundles and so are considerably larger than top of the range endoscopes which typically have an imager on the patient end of the endoscope and only electrical signals pass down the body of the endoscope. The results have been published by the US Food and Drug Administration (the regulating body for medical instruments in the US) and showed an increase in per patient sensitivity from 0.37 to 0.75 (sensitivity is the probability of positively identifying tissue) but a decrease of specificity from 0.78 to 0.42 (specificity is the probability of a negative test of normal tissue) meaning a increase in overall detection but also an increase in false positives. A number of papers have been written documenting the testing these devices (including Kusunoki et al. (2000); Sokolov et al. (2002)) although in 2007 the LIFE core was sold on to Novadaq (Novadaq (2009)) after Xillix entered receivership. Novadaq has been exploiting fluorescence for the assessment of coronary angiography since 2002 Canada (2002) and markets the LIFE-lung system as Pinpoint.

Other groups are also targeting lung tissue, Zeng et al. (2004) have used a fibre bundle endoscope and coupled that to a normal colour 3CCD camera and via

optical fibre have coupled a spectrometer to the centre of the image. They demonstrate the use of the camera for white light endoscopy and fluorescence imaging and the spectrometer for point measurements of tissue. This system is using a fibre bundle endoscope these are physically larger and have a limited range of movement when compared with more modern endoscopes which place a camera at the end of the endoscope. A number of groups have investigated inserting a fibre down the instrument channel of a standard endoscope for point measurement. This is likely to result in a much more flexible and clinically useful device than Zeng et al. suggest.

Epithelial tissues (surface tissues) are an obvious target for all oncological instruments due to the ease of access and the majority of tumours start in these tissues. Skin is the most accessible of these and a device that can detect skin cancer under the name of Dermlite (2009) is already on the market based on polarised illumination. In other areas Tumlinson et al. (2003) shows the development of a endoscopic system for the colon, however no human tests have been completed to date. This probe — unlike the LIFE system — is small enough to go down the instrumentation channel of most endoscopes (typically greater than 2.8mm diameter for colonoscopy and GI, smaller for the lungs down to about 2mm diameter, source Olympus KeyMed Group (2009)). A complete endoscopic system with integrated white light and fluorescence imaging has been demonstrated by Wang et al. (1999).

Fluorescence laser scanning confocal microscopy has been demonstrated (Astner et al. (2008) building on work in Meyer et al. (2006)) to be useful for *in vivo* histological diagnosis of actinic keratosis (a premalignant skin condition) and bassal cell carcinoma (the most common skin cancer). This investigation uses an exogenous fluorophore, in this case sodium fluorescein which is an organic dye and used for various purposes in medicine but with repeated exposure will illicit an immune response. The use of this fluorophore which has an excitation maxima at 450nm (longer than most flavins and porphyrins) enables fluorescence confocal microscopy by providing better contrast than the endogenous fluorophores.

Gastro-intestinal epithelial tissues are another target for fluorescence investigation, Chwirot et al. (1997) demonstrates *ex vivo* that there are diagnostic differences between normal, malignant and pre-malignant tissue samples. Renal tissue has also been investigated; Parekh et al. (2005) uses both fluorescence and diffuse reflectance to distinguish between normal and tumorous renal tissue with a high sensitivity and selectivity (both >90%).

Cervical and ovarian tissues are subject to a lot of interest as ovarian cancer accounts for the highest death rate of all the gynaecological cancers at around

6% of female cancer deaths (source Cancer Research UK (2009)). Brewer et al. (2001) shows that fluorescence may have the ability to differentiate between malignant and normal excised tissues of the ovary using an exogenous fluorescent agent. Later work by the same group (Brewer et al. (2004)) showed that there were diagnostic differences dependant upon excitation frequency. They presented a confocal fluorescence imaging device with 270 and 340nm excitation which can be inserted down the instrumentation channel of a normal endoscope. This group is continuing with this programme and in Kanter et al. (2006) published results using the same technique on a rat model of ovarian cancer showing statistically significant ($p < 0.05$) changes in the fluorescence signal for neoplastic tissue.

A fluorescence and white light colposcope (a device to aid the examination of vaginal and cervical epithelia) for detecting cervical cancer has been demonstrated in Benavides et al. (2003). This device uses a normal 8bit colour CCD camera and either white light or specific excitation frequencies for the fluorescence. This device does not require measurements to be taken in the dark nor does it require a significant deviation from normal practice and does not require the administration of exogenous fluorophores. The sensitivity and specificity are reasonably high (greater than 0.6). This device appears to be an excellent example of this technique in operation and is highly exploitable. The aim of this device is to assist the physician and with further development may help reduce the requirement for biopsy. Brookner et al. (2003) looks at improving the diagnostic accuracy of fluorescence diagnosis of cervical tissue by analysing other biological factors effecting the fluorescence emission of this tissue. A device exploiting the differences in fluorescence and diffuse reflectance spectra of normal and neoplastic cervical tissue has been presented in Schomacker et al. (2006). The device demonstrated here is near clinical use and can identify grades 2 and 3 dysplasia.

Fluorescence techniques have also been applied in neurosurgery. Bottiroli et al. (1998) uses intrinsic fluorescence to attempt to identify tumour margins intraoperatively with a point measurement technique, this paper does identify a need for a solution to this problem. Croce et al. (2003) present differences in both the spectral shape and signal amplitude between neoplastic and normal (both white and grey) brain tissue. Croce present point measurement or discrimination techniques and finds significant differences between normal, marginal and tumour tissue in a small study of high grade tumours. Toms et al. (2005) presents a point measurement dual modality fluorescence and diffuse reflectance spectroscopic system which has sensitivity and specificity of 0.94 and 0.93. This device must be held in contact with the patient, each sample taking about 30seconds to complete and must be conducted in complete darkness. Yang

et al. (2003) takes this a step further developing an imaging system comparing five different fluorescent bands to identify malignant tissue and ITM during brain surgery. Tests were done with only six patients and an extrinsic fluorescent agent, however some correlation was found, the system was also able to determine absolute fluorescence levels with a 10:1 signal-to-background ratio. With the exception of Bottiroli, all of these techniques use extrinsic contrast enhancing agents.

Butte et al. (2005) show with high sensitivity and specificity (>0.89 and 1 respectively) a method of diagnosing meningioma by fluorescence. Meningioma are typically slow growing, low grade, fairly benign tumours of the meninges which is the system of membranes which surrounds and protects the brain. Surgery, in contrast to most other primary brain tumours, is often a cure for meningioma. Therefore although this research is interesting and meningioma is one of the most common primary brain tumours it is not particularly useful in a diagnostic setting as this tumour is currently being successfully treated.

Fluorescence when combined with diffuse reflectance has shown power to discriminate between normal and tumorous tissue by Lin et al. (2000). Fluorescence intensity is not the only factor which could be diagnostically useful. Marcu et al. (2004) demonstrated that fluorescence lifetime also varied with disease state in *ex vivo* human brain tissue, and might therefore be useful for diagnosis but requires more sophisticated measurement equipment. Marcu did not however specifically consider tumour margins.

5ALA induced protoporphyrin fluorescence guided surgery in a high grade tumour rabbit model has been demonstrated to greater resection than white light alone, Bogaards et al. (2004a). Although there are questions regarding the validity of tumour models in small mammals they do allow histological analysis of the residual tumour to be conducted. Bogaards observes a significant increase in extent of resection however this conclusion would be more relevant if conducted in a human cohort which is possible for example by intraoperative MRI. Bogaards has extended the use of 5ALA in relation to photodynamic therapy where protoporphyrin can be used as a light induced toxic element Bogaards et al. (2004b).

Fluorescence guided resection of high grade glioma is becoming an established technology principally developed by Walter Stummer, Stummer et al. (2000, 2006, 2008, 1998) although others have also published in this field including (Sugawara et al. (2003)). This technique uses 5ALA induced porphyrin as a fluorophore and can identify high grade glioma tissue, this has been extensively reviewed above, in section 4.1.1.3. Infiltrating tumour margin has been shown to

be non-fluorescing (Utsuki et al. (2006)) and therefore this technique is likely to leave residual tumour.

There are some papers which give the idea that fluorescence has the ability to image tumours through large amounts of scattering tissue. While it is possible for fluorescence to identify specific molecular markers present in for example DNA, it is not practical to do this through more than a few mm of tissue. Ntziachristos et al. (2002) uses a number of animal models and specific fluorescent agents to image tumours using systems that look at the whole animal. All the models used are mice where the tumour site is not far from the surface and acquisition times of minutes are used with bright illumination.

There are still a number of problems with fluorescence spectroscopy *in vivo* that limit application. The first is detection of the small fluorescence signal, approaches to this are two fold; increase the excitation power and use intensified imagers (often ICCDs). Both of these approaches are limited by the background autofluorescence of tissue under investigation. The second problem is selection of the fluorophores specific to the application and the greater challenge of understanding the biochemical basis of fluorescence spectroscopy and the other factors that influence the fluorescence signal. Despite significant work in this field there is still no mathematical model of how fluorophores are modulated by the disease process.

Mahmood et al. (1996) observes that nonspecific exogenous fluorescent agents often accentuate non-specific differences such as permeablity or perfusion. This results in relatively low target to background ratios (usually <4:1). Mahmood goes on to develop near-infrared fluorescence probes which are only fluorescent after interaction with specific enzymes.

#### 4.1.3.2 Spectroscopic techniques

In 2003 the opportunities and limitations of optical intrinsic signal imaging relating to function were eloquently established by Pouratian et al. (2003b). Pouratian's comparison of the temporal and spatial resolution of various techniques is shown in 4.4. This technique has helped define the relationship between the electrophysiology and perfusion related signals and define the plasticity of sensory and language cortices. The limitations listed include image registration issues (minimisation of registration during collection and post registration) correlation between differing modalities and sensitivity. Although only a year earlier Pouratian recognises that this technique was solely in the research domain (Pouratian et al. (2002)) he anticipates that this methodology

will be useful in the near future with improving CCDs and image processing techniques.

Infrared, Raman and Near IR Spectroscopy are used extensively in the physics and chemistry fields to identify what materials are present in samples. Chapter 3 has a more detailed example of a specific use of this IR spectroscopy. These technique are of great potential use in the medical field and spectra of different tissue types have been reported. For example Torricelli et al. (2001) reports the NIR spectrum of skin tissue samples from various parts of the body.

The specific details of spectral differences in the long wave region in specific cancers are reported in a number of places in the literature. Using the Colon as investigated by Jianqiu et al. (2001) in the 1300—900cm$^{-1}$ waveband using exfoliated cells, the following differences were found;

- Changes in the Phosphodiester group is probably associated with changes in the phosphate backbone of nucleic acids and destruction of hydrogen bonds. The peak of the symmetric stretch ($V_sPO_2^-$) normally located 1082cm$^{-1}$ shifted 3cm$^{-1}$ to high frequency and the asymmetric stretch ($V_{as}PO_2^-$), normally 1241cm$^{-1}$, was shifted by 2cm$^{-1}$ to low frequency. This brings the peaks of the $V_sPO_2^-$ and $V_{as}PO_2^-$ closer together in cancerous cells compared to normal tissue.
- Changes were identified in the region 1150–1180cm$^{-1}$, particularly the ratio of the peaks at 1174cm$^{-1}$ and 1155cm$^{-1}$. This change can be attributed to a change in the number of C–O bonds stretching vibrations and a change in the amount of hydrogen bonding in the C–OH groups.
- Descreases in the C–OH bond of glycogen indicating lower levels in cancerous cells (although not statistically significant). Observed by a weaker glycogen band at 1025cm$^{-1}$.
- Additional band peaks. An additional peak presented at 970cm$^{-1}$ in the cancerous tissue.

The same conclusions are found elsewhere and in different tissues for example Salman et al. (2001) and Rigas et al. (1990) both in the colon, Wood et al. (1995) gives the glycogen more weight and also uses the C—O whereas Mordechai et al. (2004) uses the glucose/phosphate and a RNA/DNA ratios (1121/1020cm$^{-1}$) for their respective diagnostic tools in cervical cancer. Yano et al. (2000) also gives glycogen more weight and introduces cholesterol for detection of cancer in the lungs. Fujioka et al. (2004) adds the Amide III

grouping and the $\delta_{as}CH_3$ and $\delta_s C(CH_3)_2$ bending vibration in gastric tissue. Eckel et al. (2001) in addition to some of the previous metrics observes a difference in the secondary structure of proteins in breast tissue using the Amide I band. The spectra of brain tissue has been reported in Krafft et al. (2004, 2006) and Steiner et al. (2003) both of whom find diagnostic differences. FTIR techniques have successfully distinguished between normal and malignant gastric, colon, cervical, breast, lung and brain tissues (amongst others) using these metrics. Mordechai suggests that not all of these measures are found in all tissue but that some metrics may be more generic than others for example the ratio of nucleic acids calculated using wavenumbers 1121cm$^{-1}$ and 1020cm$^{-1}$.

Infrared spectra have been used for grading of tumour tissue; this is a useful application but does have it's limitations. Andrus and Strickland (1997) have shown that the DNA/RNA ratio (1121/1020 cm$^{-1}$) and the presence of a distinct peak at 1121cm$^{-1}$ is correlated with the grade of lymphoid tumours. Morris et al. (1995) have shown that there is a progression of spectral features with grade in cervical specimens. Jackson et al. (1999) have shown through multiple regression analysis changes in spectra correlated with grade in breast tissue. These methods are not however perfect, the accuracy of the reported grading is at best 90% and shows evidence of classifying high grade tissue as low or non-malignant tissue, therefore it should not currently be used in isolation.

Near Infrared spectroscopy is in some ways more interesting as the technology becomes cheaper and traditional materials can be used for the optics ('normal' glass is opaque on the low wavenumber side of 3000cm$^{-1}$). The NIR spectroscopic characteristics of human brain tissue have been investigated by a group in Vanderbilt University. Their work is of particular interest to this project as they are operating using similar methodology. Using a combination of fluorescence and diffuse reflectance on fresh frozen samples with blood removed Lin et al. (2000) achieved a sensitivity and specificity of .96 and .93 respectively on a total number of 127 sites from 20 patients (in 4 of which the primary cancer was located elsewhere in the body so not relevant as these are easy to distinguish from brain tissue). Removal of the blood means that this technique requires some development before it is becomes a useful technique. Some of this work was done in Lin et al. (2001a) which reduces the effect of superficial blood contamination for the combination of fluorescence and diffuse reflectance. The trial presented in Lin et al. (2001b) investigated another 120 sites in 34 patients (again, 7 of which did not have primary brain cancer) and concluded that using a combination of diffuse reflectance and autofluorescence it is possible to distinguish normal tissue from infiltrating tumour margins. This work was continued in a larger study in Toms et al. (2005) where the sensitivity and specificity are quoted at .80 and 0.89

for distinguishing solid tumour from normal tissue and as high as .94 and .93 for normal tissue and ITM. There is report that there has been a follow-up pilot study Toms et al. (in preparation) but is yet to be published. The key problem and limitation in all the work from this group is the point measurement nature of their measurement technique. This would imply that the surgeon either has to probe every cut surface (in a number of places) or have an idea about where the tumour has not been completely resected. An imaging technique would remove this limitation but would be more difficult to implement.

Visible and very near IR spectroscopy (including diffuse reflectance spectroscopy) has been used. Cervical tissue has been investigated by Collier et al. (2003) who found that there is a difference in diffuse reflectance between normal, precancerous and malignant tissues. Ali et al. (2004) observes diagnostically significant differences in the water content of normal and malignant prostate tissue. Ali also observes a difference in the polarisation of light reflected from these tissues, this polarisation signal is independent of the absorption of the tissue and relates more to the physical construction of this tissue. The malignant tissue was less ordered than the normal and was identified by a drop in the polarisation signal. This may also be present in the brain where the tissue is highly structured, however no investigations into this have been published.

Raman spectroscopy is a complimentary technique to FTIR. In Infrared spectroscopy a sample is illuminated with infrared light, different bonds absorb this light at different frequencies and, some of, the remaining light is collected to form a spectrum. In Raman spectroscopy the sample is illuminated with a laser so the light is monochromatic. This brings the energy levels in the molecules to a virtual high energy state from which the molecules relax back down to vibrational energy level with the emission of a photon (see Figure 4.9). Normally the photon has a lower frequency than the laser (Stokes Raman scattering) sometimes it is higher (Anti-stokes Raman scattering) but in practice only Stokes scattering is normally measured. The difference between the frequency of the laser and the scattered photon is called the Raman shift and it is this that corresponds to structural features of the molecule. Even though these techniques both involve molecular vibrations they do not provide the same information. IR spectroscopy probes vibrations during which an electrical dipole moment changes, Raman spectroscopy detects those where the electrical polarisability changes. Taking $CO_2$ as an example the asymmetric stretch is IR active as there is a change in dipole (and little change in the polarisability) and the symmetric stretch is Raman active as there is a change is polarisability (and no change in the dipole). Although in larger molecules the vast majority of bonds are both IR and Raman active although the intensity can vary greatly.

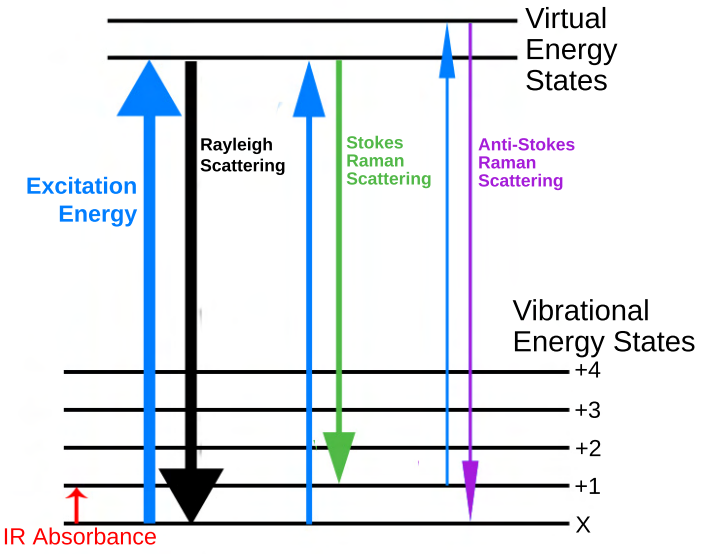


FIGURE 4.9: A diagram showing Rayleigh, Stokes and Anti-Stokes scattering

Raman spectroscopy has it's advantages, for microspectroscopy the achievable spot size is significantly smaller than FTIR. Water which dominates the IR spectrum shows a very weak signal in Raman spectroscopy and so Raman can penetrate some tissues deeper than IR spectroscopy. However Raman spectroscopy also has it's limitations, and they are severe, about only 1 in 10,000,000 photons will produce a Raman shift whereas all the other photons are either absorbed, transmitted or reflected. This means that much more illumination or time are required. One key factor that influences the Raman signal is the choice of excitation frequency, there has been some work done in this area including by Utzinger et al. (2001); Huang et al. (2003); Min et al. (2004). A short summary of the characteristics of each technique are given in table 4.6.

| | **IR spectroscopy** | **Raman spectroscopy** |
|---|---|---|
| Spatial resolution | >10$\mu$m | >1$\mu$m |
| Signal-to-noise | High | Low |
| Effect of Fluorescence | None | High |
| Sensitivity to; | | |
| Water | Strong | Weak |
| Amides | Strong | Medium/Weak |
| Phosphates | Strong | Medium |
| C–C, C=O, C≡O | Medium/Weak | Strong |
| O–H | Strong | Weak |

TABLE 4.6: General features of Raman Spectroscopy and Infrared Spectroscopy

Raman spectroscopy has been used in neurology to identify glioblastoma and necrotic tissue, the technique presented by Koljenovic et al. (2002) shows microspectroscopic maps of a malignant and normal tissue and shows that they

can be distinguished. Identifying necrotic tissue is of particular interest for follow-up surgery after radiotherapy. Koljenovic used a 100mW laser for excitation and took 10seconds to collect each pixel of the maps (the maps presented include between 1000—5000 pixels equating to between 3 and 15 hours for collection). More work has been done in the area of lung cancers, Huang et al. (2003); Kaminaka et al. (2002); Min et al. (2004) all present work on the Raman spectrum of normal and malignant lung tissue. The conclusion of these papers is that it is possible to distinguish between normal and malignant lung tissue using a point measurement endoscopic technique. Utzinger et al. (2001) presents work on the Raman spectroscopy of cervical pre-cancer cells showing that there are significant differences in the spectra and suggests that it may be possible to use this method for grading. Min et al. (2004) reported the NIR Raman spectra of normal and cancerous fresh lung tissue concluding that it is possible to discriminate these tissues with 1060nm NIR multi channel Raman spectroscopy. These are all point measurement techniques and so are limited in application.

#### 4.1.3.3 Optical mammography

Due to the number of publications in this area it deserves some consideration. This area has seen significant investment, breast cancer is the highest incidence of all cancer in the UK, 16% of all cancer cases are breast cancer (Cancer Research UK (2009)). X-ray mammography is currently used as a screening test and can help with diagnostics. The case against X-ray mammography is that it does expose the individual to ionising radiation and that it is not as effective at testing the denser breast tissue of the under 50s. However the radiation dose is typically 0.7mSv (or 70mrem) which is less than the average person would pick up in 3 months from background radiation and secondly the incidence and mortality of people under 50 is significantly lower than that of the over 50s (although the rate drops even more under 40).

There are papers that have investigated the optical properties of breast tissue; Cerussi et al. (2000); Peters et al. (1990); Grosenick et al. (2005) to name three. These broadly agree on the magnitude of the absorbance and scattering coefficients, taking as an example Cerussi et al. quote the absorption coefficient ($\mu_a$) as .05mm$^{-1}$ and the scattering coefficient ($\mu_s$) as 1mm$^{-1}$ at about 700nm. This leads to the question of the probability of a single photon a second being transmitted without scattering (T) through length (l) of breast tissue is as follows;

$$T = e^{-\mu_a l} \cdot e^{-\mu_s l}$$

Then the probability of a single photon getting through 5cm of tissue is of the order of $10^{-22}$ which means that to stand an even chance of having a single undiverted photon a second through the tissue it would need to be irradiated with about 100W. Which is clearly impractical and would certainly cause thermal damage.

The example above is emphasising the case against and it is not really as bad as this case would suggest. Techniques such as time gating can select photons which have travelled the shortest distance through the tissue. However the break-through was the development of Diffuse Optical Tomography by a group in University College London. Diffuse propagation through bulk tissue is complicated, the light will spread out through the tissue in a highly non-linear way depending on the optical properties of the tissue. By using multiple sources and detectors it is possible to solve the 'inverse problem' and calculate the optical properties of the tissue (Leff et al. (2008) is a recent review). However the spatial resolution of this technique is still not sufficiently good for an oncological diagnostic technique and is in the authors opinion unlikely to be in the foreseeable future. van der Mark et al. (2008) presented an optical tomographic technique which used spectroscopic and fluorescence and was supported by Philips, technically the system was very impressive however the inability to achieve the required spatial resolution led to the programs discontinuation.

Diffuse Optical Tomography does have applications that are potentially very useful and difficult to achieve in other ways. These applications do not have such stringent spatial resolution requirements. One example is monitoring cerebral perfusion of neonates which could provide non-invasive bedside monitoring for a number of life-threatening complications of premature babies.

## 4.2 Systems developed

The problem that this project has attempted to address can be summarised as follows;

To develop an imaging system that;

1. Is non-contact
2. Provides real-time imaging of the whole field at a resolution equal to or better than the precision of the surgeon's cut
3. Will automatically identify the required tissue/features with minimal cross-sensitivity

4. Will have minimal impact on the surgical environment
5. Does not have prohibitive cost or infrastructure requirements

Initially this project only set out to identify tumour and tumour margins however it became apparent that it would also be possible to investigate functional activation. The key to this work was a collaboration between the Prof. William Gray and Diederik Bulters both of the Southampton University Hospitals NHS trust and the author and his supervisor Prof. Harvey Rutt both of the University of Southampton Optoelectronics Reasearch Centre. All the collecting of images was done with informed consent and under appropriate ethical approval.

This work developed two separate system, first one which was designed to be sensitive to tumour and then one sensitive to functional activation. These two systems will be presented separately.

### 4.2.1 Development strategy - tumour systems

To obtain the required spatial (defined by Prof Gray as 0.25mm) and temporal resolution (towards real-time) the technique must be an optical system. The visible and near infrared has been shown to contain diagnostically relevant differences between normal, malignant and marginal tissue shown in figure 4.10. This region is also the most cost-effective spectral range as silicon imagers can be used and no exotic optical materials are required.

There are other features which may make it possible to detect malignant tissue *in vivo*. These tissues have a higher metabolic rate than surrounding normal tissue and therefore use more oxygen and have a higher vascularisation. This vascularisation is disordered and often leads to hypoxia and can result in necrosis of the centre in high grade tumours. This hypoxia may be detectable (Dachs and Tozer (2000)) as the spectral characteristics of haemoglobin are well known and shown in figure 4.11. Tumour hypoxia is a secondary effect and does not directly identify the tumour. This technique is very similar to the contrast mechanism in fMRI and this led to the work presented later in 4.3.2 investigating functional activation.

One other feature which may be diagnostically useful is a change in polarisation. In general nerve tissue is highly ordered, this order combined with structures which are long and thin indicate that there may be some anisotropic behaviour relative to polarisation. This is speculative, there is some evidence from other ordered tissues that tumours appear disordered Ali et al. (2004) — this has also

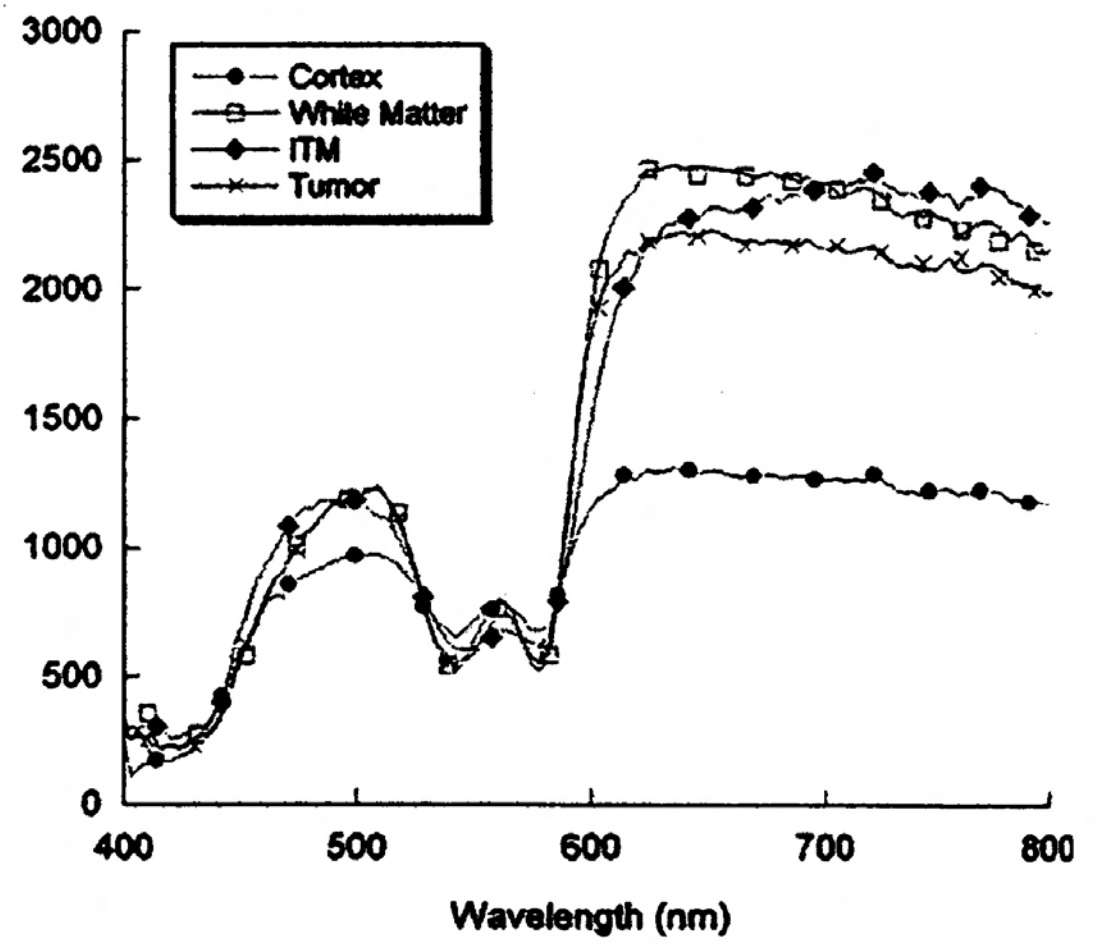


FIGURE 4.10: Diffuse reflectance spectra of different brain tissues collected by fibre-coupled spectrometer intraoperatively reproduced from Toms et al. (2005)

shown that the polarisation signal is independent from any spectral characteristics.

Visible light has a very shallow penetration depth in tissue which is primarily due to the high scattering of tissue which dominates absorption. Given that scattering is much larger than absorption ($\mu_s >> \mu_a$) the reduced scattering coefficient ($\mu_s'$) is normally used which allows for anisotropic scattering. Coefficients of absorption and scattering can be found in the literature (Gebhart et al. (2005) amongst others) where a typical value for the reduced scattering coefficient of white matter at 700nm is found to be 4mm$^{-1}$. While this is related to the wavelength this typical value is a reasonable estimate across the wavelength range and differing tissues. The inverse of this factor gives the 'reduced mean free path' and is a measure of the depth of penetration of this wavelength of light. Therefore at 700nm the systems developed will only be sensitive to the first 250$\mu$m of tissue, or about 6 cells. Moving towards longer wavelengths will increase this, also the use of polarised illumination and a

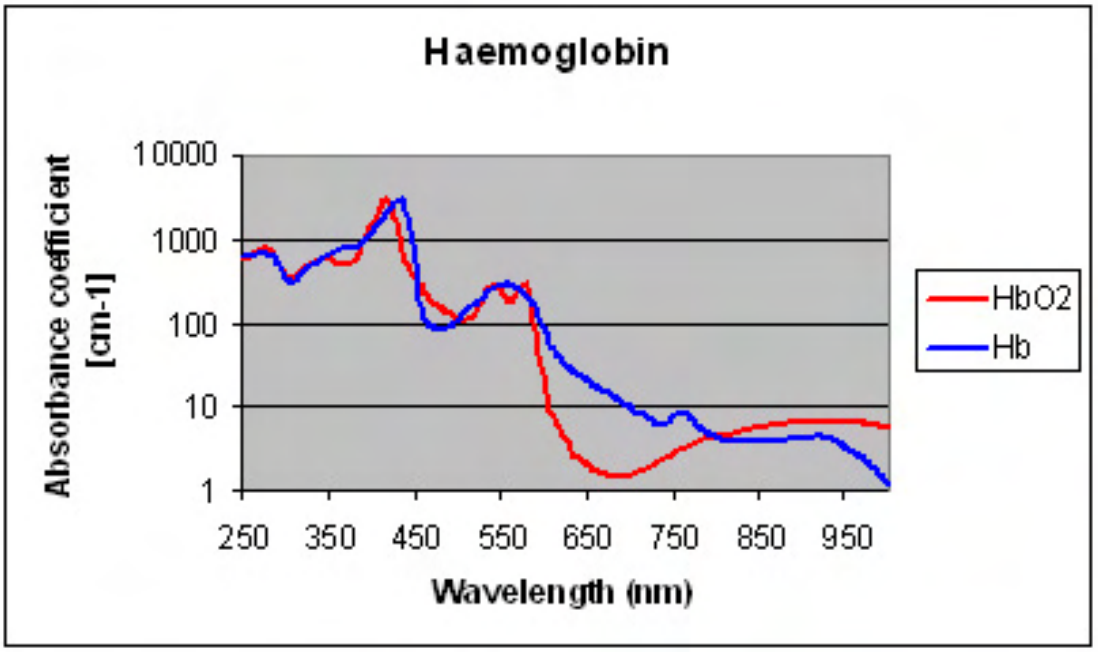


FIGURE 4.11: The visible and near infrared spectra of haemoglobin taken from Prahl (2001)

polarised filter in the camera will preferentially select photons which have been multiply scattered, therefore increasing the average depth.

The requirement to have minimal impact on the operating theatre environment means that the camera system should operate under normal theatre illumination, should be as automatic as practical should take a minimum amount of time to set-up and operate. To minimise registration issues resulting from the camera moving it requires a stable platform to operate from. This platform should have a minimal impact on the theatre and provide sufficient range of movement for the camera.

The signal level of the diffusely reflected signal is small, variously reported as approximately 1 in 1000. This requires a imaging device which has sufficient signal to noise.

There are two types of visible/NIR imagers in widespread use, these are the Charge Coupled Device (CCD) and Complimentary Metal Oxide Semiconductor imagers (CMOS - this name actually refers to a device fabrication technology and not specifically an imaging device however it is common usage and is unambiguously used in this report to refer to an imaging device). Visible/NIR CCD and CMOS imagers both share the same basic operation, they capture photons of light converting these photons to a charge; this charge is then measured and assigned a digital value. They are both band-gap devices made from silicon, the bandgap of 1.14eV determines the wavelength sensitivity cut off,

photons with less energy will not be able to excite an electron across this gap and therefore will not be absorbed or detected. For silicon this cut off is around 1.1$\mu$m.

There are some key differences between the two types of imager which affect the performance. CCDs are constructed with only a photodiode making up each pixel, the electrons produced by absorbed photons (or the dark current associated with the photodiode — a noise source) are collected in potential wells. These potential wells are then read out one row at a time into a shift register where each well is then transfered out of the sensor into a single charge-to-voltage converter. CMOS imagers have what are called 'Active Pixels', in each pixel in addition to a photodiode there is clear and readout circuitry typically consisting of 3 transistors. The charge-to-voltage conversion occurs in each pixel.

| **Feature** | **CMOS** | **CCD** |
|---|---|---|
| Responsivity | ✓ More on chip gain gives CMOS the marginal lead | |
| Noise | | ✓ Less on chip circuitry and common charge-to-voltage circuitry give CCDs far noise performance |
| Uniformity | | ✓ The CMOS onboard amplifiers improve sensitivity but greatly increase non-uniformity |
| Dynamic range | | ✓ Far superior in CCDs due to lower noise |
| Global shutter | | ✓ Shuttering is superior in CCDs than CMOS while maintaining pixel size. The most sensitive imagers use external shutters |
| Windowing | ✓ Random access allows dynamic changing of window parameters | |
| Speed (frame-rate) | ✓ More on chip circuitry allow shorter propagation delays and faster readout | |
| Power consumption | ✓ CCDs consume several times more power than CMOS | |
| Cost | ✓ While not achieving the very low costs promised by using standard CMOS production facilities CMOS still has the marginal edge | |

TABLE 4.7: A comparison of the features of CCD and CMOS imagers

Some of the features of CMOS and CCD imagers are compared in table 4.7. The key parameters for this application are the noise and dynamic range which are closely related and are determined by the physical parameters of the imager including well depth (the number of electrons a potential well can hold) dark

current and read-out noise; all of these factors are better in CCDs than CMOS imagers. Dynamic range is defined as the ratio between the smallest and the largest possible values. CMOS imagers have the advantage in speed and power consumption, where the additional on-chip circuitry makes significant differences. CMOS sensors typically use a rolling shutter; the exposure time is defined as the time between the clearing and the readout of each row and the rows are cleared in sequence. This means that the first row is exposed before the last row, a global shutter exposes all the rows at the same time. The problem with a rolling shutter occurs where there are changing features in the scene. At their conception CMOS imagers were expected to be significantly cheaper than CCD imagers due to the similarity of their manufacture with volume products such as RAM, however this has not become reality and the manufacture of these devices require short production runs with dedicated equipment. For these reasons CCD imagers are used throughout the camera systems in this project, specific selection of a given imager will be detailed where appropriate.

### 4.2.2 Tumour camera system 1

A prototype imaging system has been developed to investigate the spectral signatures intraoperatively. Our medical partners have applied for and the project has been awarded ethical approval a process which took a considerable amount of time (almost 12months) and effort. The table given in 4.8 gives details of the specification of the components of this system. To avoid confusion the terms 'Apogee camera' will refer to the imaging camera, 'spectral camera' will refer to the Specim spectral camera and 'camera system' will refer to the whole prototype.

The Apogee CCD camera is designed specifically for astronomy and so has particularly low dark noise (assisted by the Peltier cooler) and readout/digitisation noise. The full well size is up to 500,000 electrons so the dynamic range is limited by noise at 14 bits or 1:16384. As the digitisation level is greater than this level the achievable dynamic range can be increased by averaging a series of images. These parameters are constantly improving and now a similar priced camera can deliver 2-3 times better noise performance.

The Spectral camera consists of a grating and an imaging device. The grating separates the spectral components of a line across the scene onto the imager. This camera was purchased as a single device specified to provide the spatial and spectral resolution given in table 4.8 however the device did not perform as specified. This camera collects the light from a small area of the scene separates that light spectrally onto a imager, naturally the amount of light falling on each

| | |
|---|---|
| **Imaging Camera** | |
| Model | Apogee U260 camera |
| Sensor | Kodak KAF-0261E CCD |
| Sensor format | 1inch |
| Cooling | 3 stage peltier cooled -40°C |
| Resolution | 512x512pixels |
| Pixel Dimensions | 20x20$\mu$m |
| Digitisation range | 16 bits (65536 levels) |
| Lens focal length | 70mm |
| Lens minimum working distance | 50cm from front of system |
| Dark noise | $1e^-$/pixel/sec |
| Readout noise | $15e^-$ |
| **Spectral Camera** | |
| Model | Specim V10E Spectral Camera |
| Sensor | CMOS |
| Resolution | 1280(Spatial) x 1024(spectral) |
| Dynamic Range | 12 bits (4096 levels) |
| Wavelength Range | 400-1000nm |
| Spectral Resolution | 2.8nm |
| **Mounting** | |
| Tripod | Vinten 3796-3 Aluminium tripod and dolly |
| Max Height | 200cm |
| Head | Vinten Vision 8 |
| Max Weight | 25Kg |

TABLE 4.8: Specification of the first prototype tumour imaging camera

pixel is small. Therefore the integration times for this device are large — seconds or even higher. One would expect therefore that the imager would be specified for a low dark current suitable for such low light imaging — this however was not the case and the images from this device were too poor to be of use even with the bright theatre illumination. The spectral camera has subsequently been used by Jack O'Sullivan fitted with a more appropriate CCD imager from the Prosilica range.

The prototype camera system was designed to ensure that both cameras had a co-axial view by the use of a flipping mirror, the filters and polarisers were mounted in separate filter wheels in front of the imaging camera and polarisers were mounted in front of the spectral camera. All of the filter wheels were motorised and the electronics would also control the mirror and a pair of class I lasers to assist in alignment. These electronics had a software interface into the software running on the controlling computer.

Software interfacing to both cameras and the control electronics was written to allow the capture process to be as automated as practical. The maximum

acquisition time was set at five minutes and included moving, aligning and focussing the camera and collecting a complete set of images. The software includes a user interface displaying the captured image to allow focusing, it auto-exposes the camera (algorithm based on Farrell (2004)) for each filter using previous values and records each image with the appropriate information about the camera status.

Although this camera did produce interesting results which have not been reported elsewhere it did have some shortcomings;

- The Apogee camera although providing excellent noise performance and dynamic range was slow to readout providing a maximum frame-rate of approximately 2 fps. When one considers the requirement to auto-expose each image and time to change filters the frame-rate decreases further to as low as 0.3 fps.
- The Apogee camera is a large format sensor requiring large lenses, large filter diameters and large filter wheels.
- Both the Apogee and the spectral camera are physically quite large devices (the Apogee 150x150x62.5mm and the spectral camera 60x60x235mm) and when combined with the filter wheels and associated electronics result in a large camera system.
- The tripod posed problems, although relatively easy to move around it was large and this restricted the angle the camera can achieve to the patient limiting imaging options.
- This camera system did not integrate well with the sterile drapes used in theatre as this was not considered a priority in initial discussions. It was therefore limited in how close to the patient it could approach.

### 4.2.3 Tumour camera system 2

The second camera was designed to overcome many of the limitations of the first camera. The physical size of the first camera system was the greatest limitation and associated with that was the inability of that camera to collect images looking directly down, which was a requirement developed through the use of the first camera. Therefore the second camera system was based around a much smaller imager described in table 4.9.

Due to the smaller format of the imager (the format is associated with the dimensions of the imager and is given as the diameter of the equivalent vidicon

| **Camera** | |
|---|---|
| Model | Prosilica GC1290 |
| Sensor | Sony ICX440 ExView CCD |
| Sensor format | 1/3 inch |
| Resolution | 1280x960pixels |
| Pixel Dimensions | 3.75x3.75$\mu$m |
| Maximum frame-rate (full frame) | 32 fps |
| Physical dimensions | 46x33x60mm |
| Lens focal length | 15mm |
| Lens minimum working distance | 12cm |

TABLE 4.9: Specification of the first prototype tumour imaging camera

tube — a type of cathode ray tube used as an imaging device in video cameras until the 1980s) which relates to area where the image is formed; the lens required for this camera is physically much smaller (25mm diameter in contrast to the 60mm diameter of the Apogee). This means smaller filters can be used, smaller filter wheels are easier to move meaning smaller electronics. The complete camera system is now only 200x100x100mm. The requirement for vertical imaging has been met by using an old microscope base with the camera mounted on an adjustable arm. Photographs of the camera and microscope base can be found in figure 4.12.

The proximity electronics for this camera are necessarily more complicated than the first camera. As space was at a premium, smaller geared motors were used in place of the larger stepper motors that were used in the first system. This means that the filter-wheels required indexing, and the maintenance of the state of these wheels was off-loaded to the camera. A further requirement to mechanically adjust the focus was introduced due to the draping requirements of working in an operating theatre. An AVR microprocessor was used for the control the hardware and interface to the image acquisition software.

The speed issue was also addressed in this second camera system. Using the microscope base significantly reduces the amount of setup time required. The full-frame readout speed of the prosilica camera is 32 fps (frames per second) which can be increased by binning the image however this reduces resolution. The practical frame-rate was limited by the data acquisition system to a continuous 12 fps or a burst of approximately 200 frames at full speed. Smaller filter-wheels allow the time to change filters to be reduced to around 200ms. Overall the frame-rate to collect a set of images is around 1 fps. This camera has also been designed with the requirements for draping and so is easy to drape with standard equipment used in theatre.

(a) Front view without enclosure

(b) Rear view without enclosure

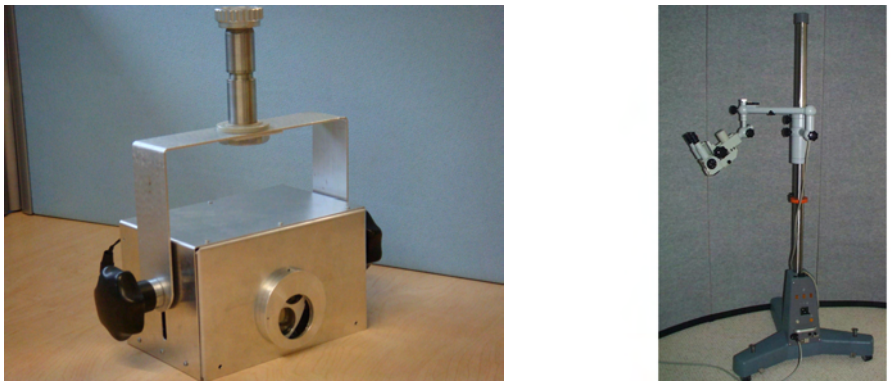

(c) Front view with enclosure

(d) Microscope base

FIGURE 4.12: Photographs showing different views of the camera system and the microscope base (before removal of microscope)

### 4.2.4 BOLD imaging system

The early results of the first tumour camera raised the possibility of optically identifying functional activation of tissue intraoperatively. FMRI already exploits changes in the oxygenated/deoxygenated haemoglobin ratio to infer function as described in section 4.1.1.6. While fMRI uses a change in the magnetic properties to assess the concentration of deoxygenated haemoglobin there is also a change in the optical properties. A number of people have investigated this effect but despite over 15 years since Haglund demonstrated intraoperative imaging of activity in the human brain (Haglund et al. (1992)) there is still no clinical use of this technology. This project aims to categorically demonstrate this technology working alongside the current gold standard for intraoperative functional delineation.

The visible and NIR spectra of haemoglobin changes dependant on it's oxygenation state as shown in figure 4.11. These data can be presented to highlight the contribution of each oxygenation state to the absolute absorption

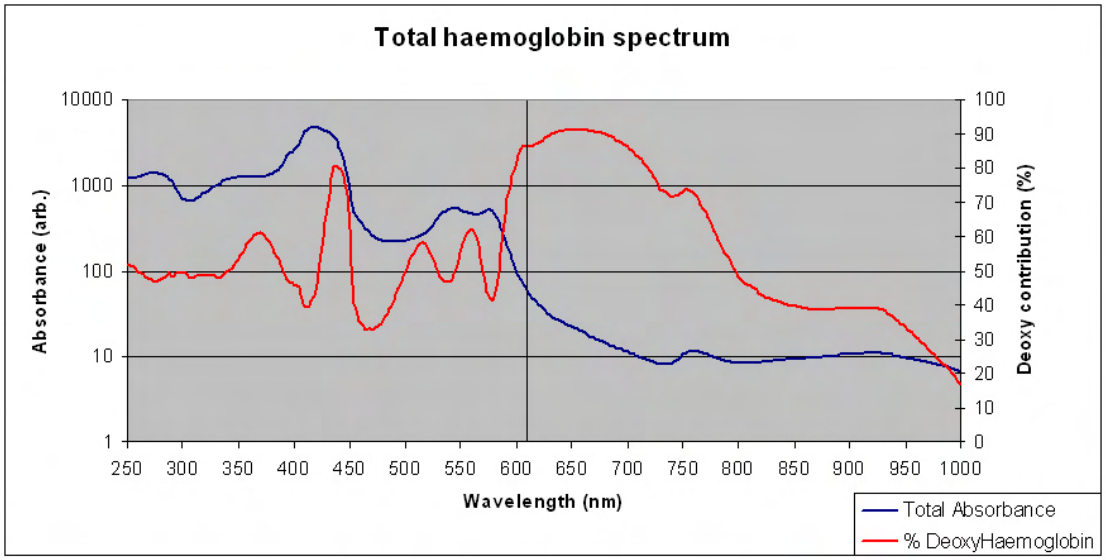


FIGURE 4.13: Visible and NIR spectra of total absorption of haemoglobin (left axis) and percentage contribution to this absorption from deoxyhaemoglobin, vertical line denotes 610nm (data from Prahl (2001))

as shown in figure 4.13. As can be seen there is a region between 600–700nm where deoxygenated haemoglobin dominates the absorption.

There is only a requirement to measure one wavelength; functional activation will be detected as a change of the signal over time. Otherwise the requirements are similar to that of the tumour cameras; high dynamic range, low noise etc. Framerate is more important as temporal resolution better than twice the heart rate removes the requirement to synchronise image acquisition with the heart rate. The single wavelength means that there are no moving parts and hence a much simpler camera. This camera uses an adapter to a standard Zeiss neurosurgical microscope which is already in use in theatres in Southampton General Hospital. The imaging device is the same model as that used in the second tumour imaging camera. The whole system makes minimal impact on the theatre environment and on surgical procedure.

### 4.2.5 Image capture

The requirements for the image capture system were that it be portable, has sufficient interface and storage bandwidth and that it has a suitable user interface including visual display. A laptop computer is used to meet this requirement as a common image acquisition system. All of the cameras communicate via USB2 or gigabit ethernet (GigE or 1000base-T). USB2 is used by the Apogee and the original spectral camera posed some problems due to the limited cable lengths of only 5m between hubs/boosters. Ten metre cables have

been used with all the cameras therefore these cameras requiring a commercial signal booster making the use of the camera system more cumbersome. GigE is used on the prosilica cameras and has a 100m maximum cable length.

All of the image data is stored on the laptop prior to permanent storage on university owned computers. The frame-rate limit mentioned in section 4.2.4 is due to the maximum sustained bandwidth of the hard disk which is approaching 30MB/s, to achieve the maximum stated frame-rate a bandwidth of 80MB/s would be required. These bandwidths have been achievable for some time in desktop devices and more recently in laptops mainly in the very high end devices aimed at high performance gaming.

A custom application has been developed to control each of the camera systems. These have used the manufacturer's software development kit (SDK) to interface to the camera and provide the maximum automation at the user level. SDKs are provided by manufacturers to provide access to camera functions, typically these are very low level interfaces some down to the level of bytes and bits. These interfaces have been wrapped to provide an object with high level functionality such as; auto-exposure, initialisation, image capture. This object can then be fully tested before it is used in a programme to capture a complete set of data. This is good software engineering practice has been followed throughout this project. Just the interface to the cameras without any of the controlling software contains 4500 Source Lines of Code (SLOC).

The control applications use configuration files to ensure consistent settings across each data acquisition session. These applications allow full control over the camera hardware at a high level. They provide the operator a visual display of the images as they are acquired. This allows the operator to ensure that the camera is set up correctly and that high quality images are being collected.

Due to the different requirements of each of the camera systems a custom application was written for each system. These applications build on the camera abstraction layer and the same imaging framework. This framework will be described in more detail in section 4.2.6.

The tumour cameras' acquisition software interfaces with the hardware controllers on the cameras. The software then presents a live image to allow the camera to be targeted at the required region. It then auto-exposes and collects and image using each of a sequence of filters/polariser combinations which had been previously defined by the user.

The software for the functional imaging camera unlike the tumour cameras only interfaces with the camera. However this application has been optimised to

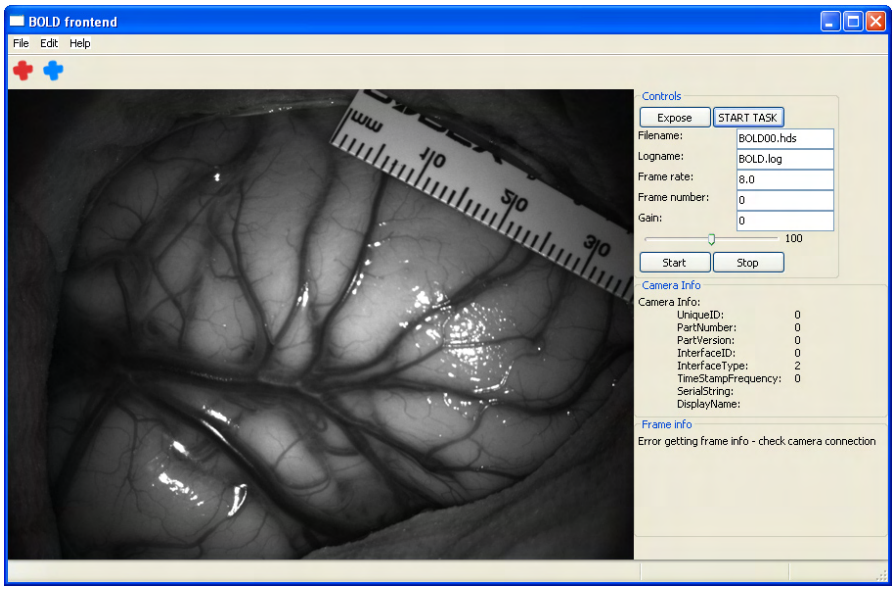


FIGURE 4.14: A sample view of the application used with the functional camera

obtain the maximum bandwidth from the camera as well as providing real-time display to the operator of the region of interest. This optimisation has required using multiple threads in both the top level application and at the camera level to maximise the image-capture bandwidth. Multi-threading allows a single program to conduct multiple tasks at the same time as if these tasks are running in parallel (processors use time-division multiplexing and the context switching is sufficiently fast that it can be conducted during high latency operations such as reading from memory). This application also allows the user to record information about how cortical stimulation was performed and what the outcome of this stimulation; i.e. a given site was stimulated and whether this site was determined to be eloquent or not. This ability to record information alongside the images makes correlation of these separate data sources much more simple, figure 4.14 shows a sample view of this application.

### 4.2.6 Image processing

The image processing requirement of the data collected should allow statistical analysis of the data and should visually enhance the collected images such that one can appropriately identify areas of interest. Visual enhancement is required for two reasons; the dynamic range of standard display devices does not match that of the image acquisition devices used in this project; secondly that the human vision system would not be able to identify those differences even if displayed. Although a large field, a basic understanding of the limitations of the

human visual system is essential in designing the image display system. Some examples of these limitations include the following;

The bottom row of the image to the right has 8 evenly spaced levels of grey, the next level up shows 16 levels .... Typically the human eye cannot distinguish between more than about 32 levels or the third level up. This can be represented by only 5 bits, the Apogee camera can capture 14 bits, or over 500times more. (Note that this image is well within the colour gamut of most printing and display devices.)

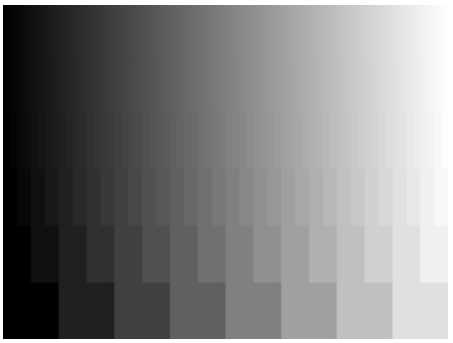

FIGURE 4.15: Demonstration of the limited dynamic range of the human eye

The figure on the right shows three pairs of boxes with the same absolute intensity on different intensity backgrounds. The boxes on the lighter background appear darker than those on the darker background. This figure demonstrates how the relative contrast affects how the absolute value is interpreted.

FIGURE 4.16: Demonstration that observed intensity is contrast dependant

The pattern on the right is stationary (definitely so if printed) yet it is often perceived to expand, particularly if one is not looking directly at it, e.g. reading this text. This is one of the many variants of the "snake illusion" made famous by Akiyoshi Kitaoka. This image demonstrates that even movement can be simulated in a stationary image.

FIGURE 4.17: A variant on the "snake illusion" by Akiyoshi Kitaoka

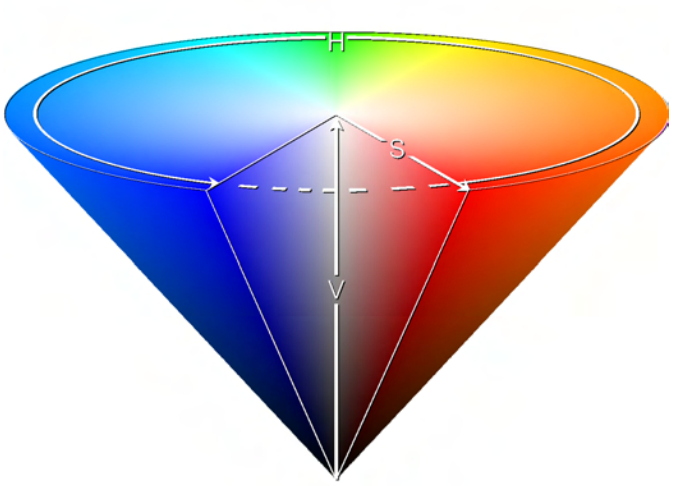


FIGURE 4.18: Conical representation of the HSV colour space. (Reproduced under the GNU Free Document Licence version 1.2, original author; moongateclimber)

An image processing toolkit has been constructed specifically for this project. This toolkit makes up a third of the total amount of software written for this project (approximately 9000lines). All of the camera systems use the same image format which is capable of storing an arbitrarily large image or stack of images. An image stack is a commonly used concept in multispectral imaging which collects all the images in a single file. This concept is not dissimilar to the concept of storing red green and blue images to create a colour image. A video processing toolkit has also been developed using a similar format to the still image work and can exploit all of the functions in the still image toolkit.

The primary aim of the image processing is to highlight the differences between a pair of images and present that difference in a way that the user can identify it. The differences between images are calculated by the equation shown in equation 4.1, due to the small differences typical in the images used a gain $G$ is added as in equation 4.2. In these equations $R$ and $D$ are images, $R(x, y)$ is the pixel at row $x$, column $y$ of image $R$. These equations can trivially be extended to work with more than one image pair.

$$D = \frac{\Delta R}{R} \tag{4.1}$$

$$D(x, y) = 2G\frac{R_1(x, y) - R_2(x, y)}{R_1(x, y) + R_2(x, y)} \tag{4.2}$$

For display this difference information is typically converted into an 8bit representation and mapped into the Hue, Saturation and Value (HSV) colour space.

The collection of images takes time, ranging from tens of seconds in the case of the tumour systems (section 4.3.1) up to several minutes of video in the BOLD system (section 4.2.4). Any movement of the tissue relative to the camera over this period of time will produce registration inaccuracies between the images. As the primary algorithm for identifying differences in tissue is sensitive to changes in pixel intensity these registration inaccuracies must be minimised. To accomplish this one image from a sequence is chosen as a 'key frame' and all other images are registered to that image. This provides a dataset where a single pixel position relates to the same piece of anatomy in each image. The data from the tumour systems often does not require registration as the patients are normally asleep and the head is held in a stereotaxic frame. The data from the BOLD system typically requires registration due to movement of the patient, in this case the first frame is normally chosen as the key frame. The BOLD data is also particularly sensitive to the amount of time taken for each registration as there are often many thousands of frames to register.

There are a number of transformations which can occur due to movement of the camera or of objects in the scene. Some of these are affine transforms that comprises of a linear transformation and then a translation. The properties of an affine transform are that collinearity is maintained (i.e. three points in a line before the transformation will still be on a line afterwards) and that the ratios of the distances between these points will stay the same. These transforms are illustrated in figure 4.19, they are typically associated with camera — scene movement for example translation occurs when the scene moves laterally, scale where the camera move towards or away from the scene. Transforms 4.19(g) – 4.19(i) are associated with movement of objects within a scene or a surface changing shape as occurs intraoperatively. Barrel distortion is often associated with fish-eye lenses but also occurs due to a distortion of the surface of the scene, this occurs during surgery as the cortical surface swells and contracts with each heartbeat. Object movement occurs due to a portion of the scene or an object within the scene moving, this occurs frequently intraoperatively as objects are introduced and subsequently removed from the operating field. With object movement there is also often occlusion where part of the scene is hidden from view.

One of the key capabilities of the imaging toolkit and as mentioned above is particularly important for the video processing required by the functional imaging camera is image registration. The task of image registration is to translate a pair of images taken at different times or from different relative positions into the same coordinate system. This is fundamental in image processing. Image registration is a problem which humans excel at but is a

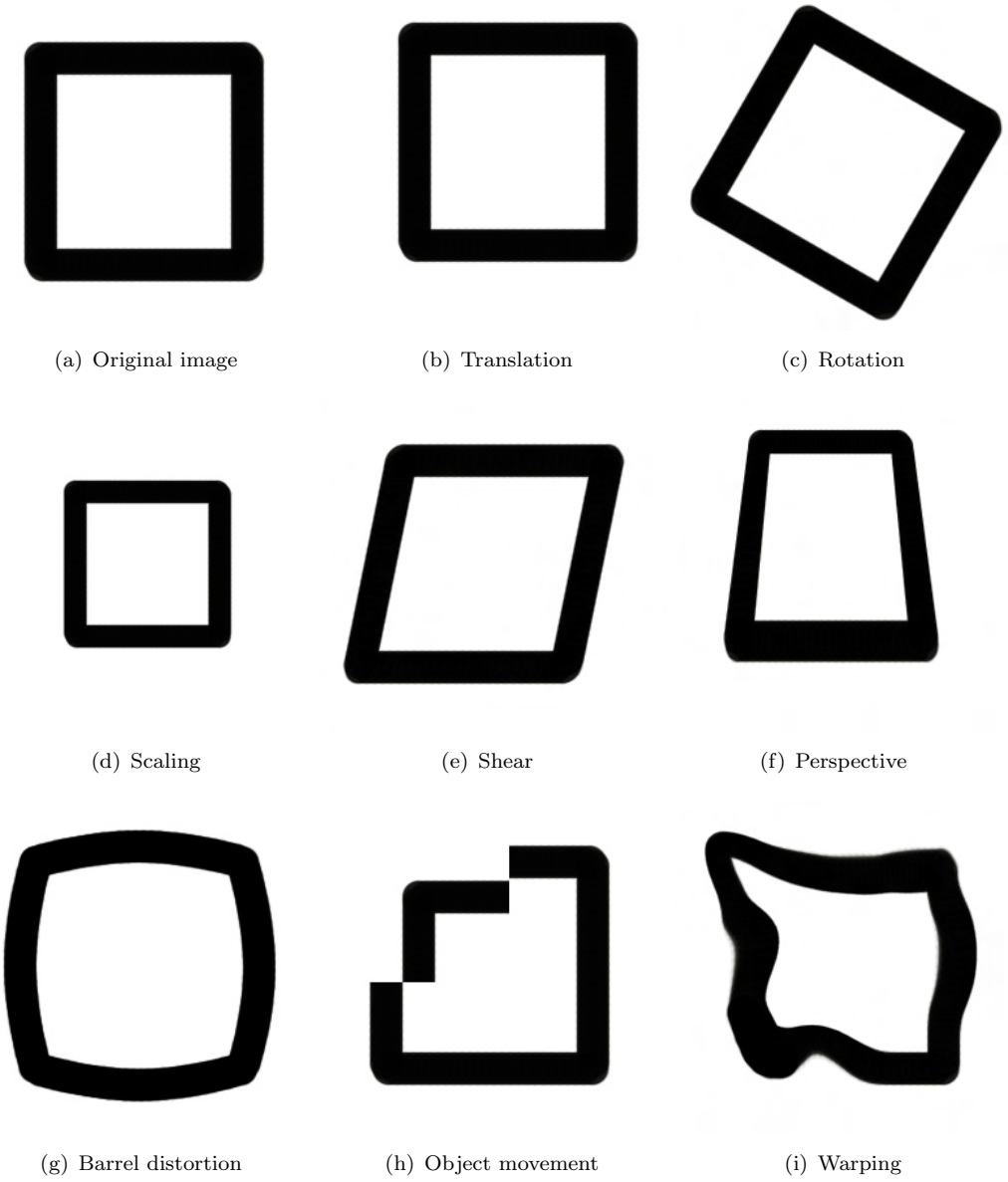

(a) Original image (b) Translation (c) Rotation

(d) Scaling (e) Shear (f) Perspective

(g) Barrel distortion (h) Object movement (i) Warping

FIGURE 4.19: Representations of different types of transform, figures 4.19(b)–4.19(f) are affine transforms, figures 4.19(g)–4.19(i) are not affine transforms

subject of current research interest, currently there is no one optimised set of algorithms which satisfy the requirements. Image registration methods can loosely be broken up into the following categories;

1. Methods that use the pixel values directly, e.g. cross-correlation methods. Benhimane and Malis (2004)

2. Algorithms which use the frequency domain, e.g. Fourier transform based methods, phase correlation. Including De Castro and Morandi (1987); Chen et al. (1994); Reddy and Chatterji (1996); Averbuch and Keller (2001, 2002); Keller et al. (2005)

3. Feature based methods that use low-level features such as edges and corners. Bajura and Neumann (1995); Bentoutou et al. (2005)

4. Feature based methods that use high-level features such as objects or the relationships between features. Wong and Clausi (2007)

These methods have different characteristics; the frequency domain methods (2) are typically illumination and noise resistant (Wang et al. (2007)) but can only recover a limited class of transformations — currently translation, rotation and scale. Methods directly using pixel values (1) have problems with noise and are illumination sensitive and computationally expensive (although reducing the computational expense is also being researched Chen et al. (2005)). Both of the feature detection methods depend heavily on the consistent identification of features which can be problematic. For a more comprehensive review of image registration techniques see Brown (1992) and more recently Zitova and Flusser (2003).

This project has investigated both image registration by Cross-correlation which uses pixel values directly and a frequency domain technique based of the Fourier-Mellin Transform. The cross-correlation equation as defined by Garhart et al. (1999) is;

$$r(m,n) = \frac{\sum_x \sum_y \left(w(x,y) - \overline{w(x,y)}\right)\left(t(x-m,y-n) - \bar{t}\right)}{\left(\sum_x \sum_y \left(w(x,y) - \overline{w(x,y)}\right)^2 / \sum_x \sum_y \left(t(x-m,y-n) - \bar{t}\right)^2\right)^{\frac{1}{2}}} \quad (4.3)$$

Where r is the result matrix, $\bar{t}$ is the average of value of the template, $\overline{w(x,y)}$ is the average value of the portion of the window match image currently coincident with the template $t(x,y)$. The template is defined as the original image and the match image which requires registration to the template. This searches a window $(x,y)$ over an area $(m+x, n+y)$ and generates an array $r$ containing the correlation values. The computational expense of this technique is correlated with the size of the search area $mn$ and the size of the window $xy$. The maximum value of the result array should be the translation of the matching image to the template, this maximum should satisfy various statistical tests e.g. should be greater than any other local maximum by $\frac{1}{4}\sigma$ (where $\sigma$ is the standard deviation). This algorithm was found to be unreliable for finding a match even with feature enhanced images such as edge detection. Cross-Correlation scales as $O(k^2n^2)$ where k is the search space and n is the size of the image. Therefore large translations require large search spaces and increase computational expense. Scale and rotation introduce further complexity and require a much larger search spaces. This was determined to be impractical, particularly for the

large number of registrations required for the functional work. However cross-correlation can in principle recover most of the transforms presented, even barrel distortion and warping, however object movement and occlusion can not be recovered and must be excluded by the statistical tests.

A frequency domain technique based on the Fourier-Mellin invariant descriptor was found to successfully register a pair of images. The Fourier transform of an infinite image is translationally invariant, i.e. it does not matter where the 'origin' of the image is. A finite image which has been appropriately windowed to reduce edge effects can exploit this property to extract the amount of translation. The method is as follows (the first and second images are denoted $a$ and $b$;

1. Calculate the Fourier transform of $a$ and $b$ let these be $A$ and $B$
2. Generate a third image from $A$ multiplied by the complex conjugate of $B$
3. Inverse Fourier transform the result

This algorithm results in a delta function at the location that correlates with the translation of both images and approximately zero elsewhere. The Mellin transform introduces a conversion from Cartesian to log-polar coordinates for both $A$ and $B$ before repeating the process from step 1. This gives an output which is a delta function at a location which correlates to the rotation and scale. The log-polar transformation conceptually converts both scale and rotation into linear factors which are mutually perpendicular and can be extracted in a similar way to translation. For more information about the log-polar conversion consult Young (2000). The Fourier Mellin transform was presented in Chen et al. (1994) however the author found Reddy and Chatterji (1996) more accessible.

The Fourier Mellin transform scales as $\mathrm{O}(n \log n)$ due to the Fourier transforms of which at least 3 transforms are required and 2 reverse transforms. There are other operations required but all scale better than the Fourier transforms so that these dominate. This image registration algorithm has been demonstrated to be highly resistant to noise, illumination changes and object occlusion. The major criticism of these techniques is the limit on the class of transform which can be recovered, however the transforms that can be recovered are the most likely to occur in the specific imaging scenario under investigation.

In total over 28,000 source lines of code have been written for this project. Jack O'Sullivan has written approximately 1500 of these lines. For comparison this is about twice as large as this thesis. All of the code is on the CD enclosed.

| **Centre Wavelength** | **Filter Set 1** | **2** | **3** | **4** | **5** |
|---|---|---|---|---|---|
| 410nm | ✓ | | | | |
| 440nm | ✓ | | | | |
| 470nm | ✓ | ✓ | | | |
| 580nm | ✓ | ✓ | ✓ | | |
| 610nm | ✓ | ✓ | ✓ | ✓ | |
| 630nm | | | ✓ | ✓ | ✓ |
| 700nm | | | | ✓ | ✓ |
| 750nm | | | | | ✓ |
| 800nm | | | | | ✓ |
| 900nm | | ✓ | ✓ | ✓ | ✓ |
| 970nm | | ✓ | ✓ | ✓ | ✓ |
| Patients | 1 | 6 | 4 | 1 | 3 |

TABLE 4.10: The different filter sets used in the tumour imaging cameras and the number of patients investigated with each

## 4.3 Results and discussion

This section will discuss some of the results from the different camera systems. Where appropriate it will also highlight some of the processing involved. It will start by considering the tumour systems and move on to look at the results from the functional systems.

### 4.3.1 Tumour systems

There have been a number of different filter sets used on the tumour imaging systems. These can be found in table 4.10, all of the filters have a 10nm full width half maximum, or bandwidth, these filters typically have a 60% maximum transmission and have of the order 0.01% transmission out of band. In addition to these filters the cameras have a 'clear' filter which has a transmission of 1% this low transmission value is comparable to the overall transmission through the coloured filters when integrated over the entire sensitivity of the CCD. There are also polarisers in the each of the cameras, the first camera had polarisers covering the 400–700nm range the second camera has polarisers covering the complete 400-1000nm range. The selection of filters has evolved and is continuing to do so. The initial filter set was quickly changed to accommodate 900/970 combination that are sensitive to water, this required the removal of the 410nm and 470nm filters which were giving the poorest imaging of the set and presented little contrast with 580nm. The addition of more 600-800nm filters is due to the research presented in Toms et al. (2005).

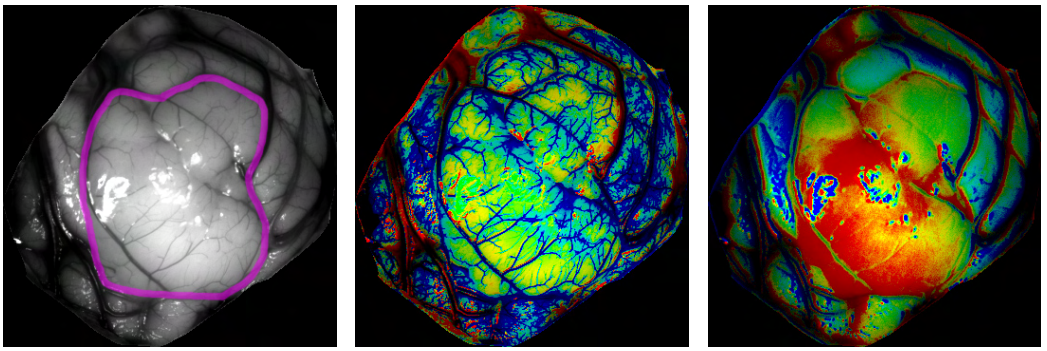

(a) Clear image (b) $\delta$610–580nm (c) $\delta$970–900nm

FIGURE 4.20: Images captured using the first tumour imaging system and filter set 2 in patient 2283840. 4.20(a) shows the tumour margin in magenta

This project has been awarded grant funding to continue work by the National Institute for Health Research (NIHR). The NIHR is part of the NHS and this project will be funded under the New and Emerging Applications of Technology programme (NEAT). The main aim of this fund is to address the funding gap for translational research and development in new and innovative technology. It only funds projects aligned with a clinical need and so provides more evidence that there is a wider acknowledgement that this is an important area of study. The application submitted for this funding can be found in Appendix B.

The data presented here is from a low number of cases. With the wide range of neuropathological condition which require surgery there is little coherence across the data set and little duplication of tissue types. This project is not in the position to be able to state that there are 'X' spectral characteristics which relate to 'Y' tumours as yet. In fact correlation with tissue type is an extant problem with all of the data presented here. Pre-operative imaging poorly differentiates infiltrating tumour margins and there is currently a problem registering preoperative data with the images collected by the camera systems. It is possible to project tumour extents based on pre-operative images into the field of an operating microscope, however this equipment is not currently available at the hospital (allowance has been made for it within the grant funding). The problem of poor diagnostic imaging of infiltrating tumour margins presents more difficultly in correlation. The only solution to this is extensive sampling and diagnosis by pathology which requires agreed assessment criteria for these specimens and a strong relationship with the pathology department. For consistency this may require a single pathologist to analyse these cases as there has been shown to be some variation between pathologists. The pathological assessment of these cases is in the process of being established.

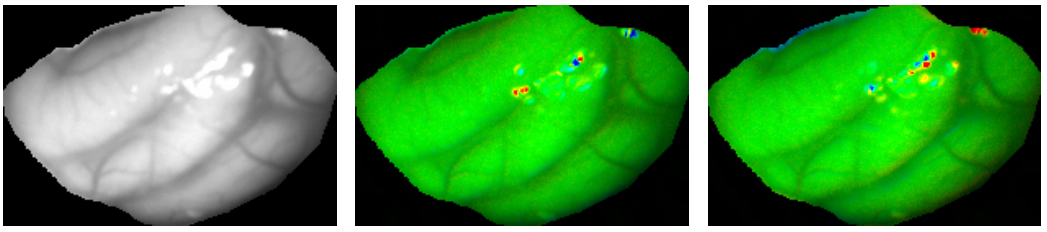

(a) Clear image (b) $\delta$610-580nm (c) $\delta$970-900nm

FIGURE 4.21: Three images of a normal brain from patient 4700075 these have undergone identical processing to those in figure 4.20

The images shown in figure 4.20 are from patient number 2283840[2]. This is a grade III tumour and as is clear in Figure 4.20(a) is visually indistinct from the surrounding normal tissue. Figure 4.20(a) shows the clear image without a colour filter, the magenta outline defines the tumour as seen by pre-operative imaging. The centre panel shows the difference between 610 and 580nm filters, the panel on the right shows the difference between 970 and 900nm. The differences in these images have been presented in a false colour, blue–cyan–green–yellow–red (this colour mapping will be used consistently throughout this report). Artifacts can be seen in some of these images; 4.20(a) shows reflections as bright white areas where the camera pixels were saturated - there is a loss of information in these regions. Figures 4.20(b) and 4.20(c) show artifacts around particularly high contrast regions such as vasculature, again these artifacts are not considered to contain information.

Figure 4.20(b) shows the difference between two bands associated with the rapidly changing absorption of haemoglobin as seen in figure 4.11. Therefore the contrast in this image can be attributed to changes in the vasculature and neovascularisation due to tumour growth. The extent of the contrast is somewhat larger than that from pre-operative imaging particularly to the top of the image between two vascular structures. Vasculature in the brain is generated as needed and so highlighting a larger area of changing vascularisation is not unreasonable but may also indicate tumour margin however angiogenesis is not always associated with tumour growth, Bernsen et al. (2005). The differences in the 970-900 region are shown in figure 4.20(c) this has a higher correlation with the preoperative margin, the area that is highlighted in the green-red colours again however there is some indication in the top and bottom of the image that the same spectral characteristics can be found elsewhere.

For comparison with the images presented in figure 4.20 the images shown in figure 4.21 show unquestionably normal tissue. This patient was undergoing

[2]The first six patients were anonymised by assignment of unique 7 digit random numbers, this proved to be cumbersome and subsequent patients were sequentially numbered from 1, the prefix PT is used.

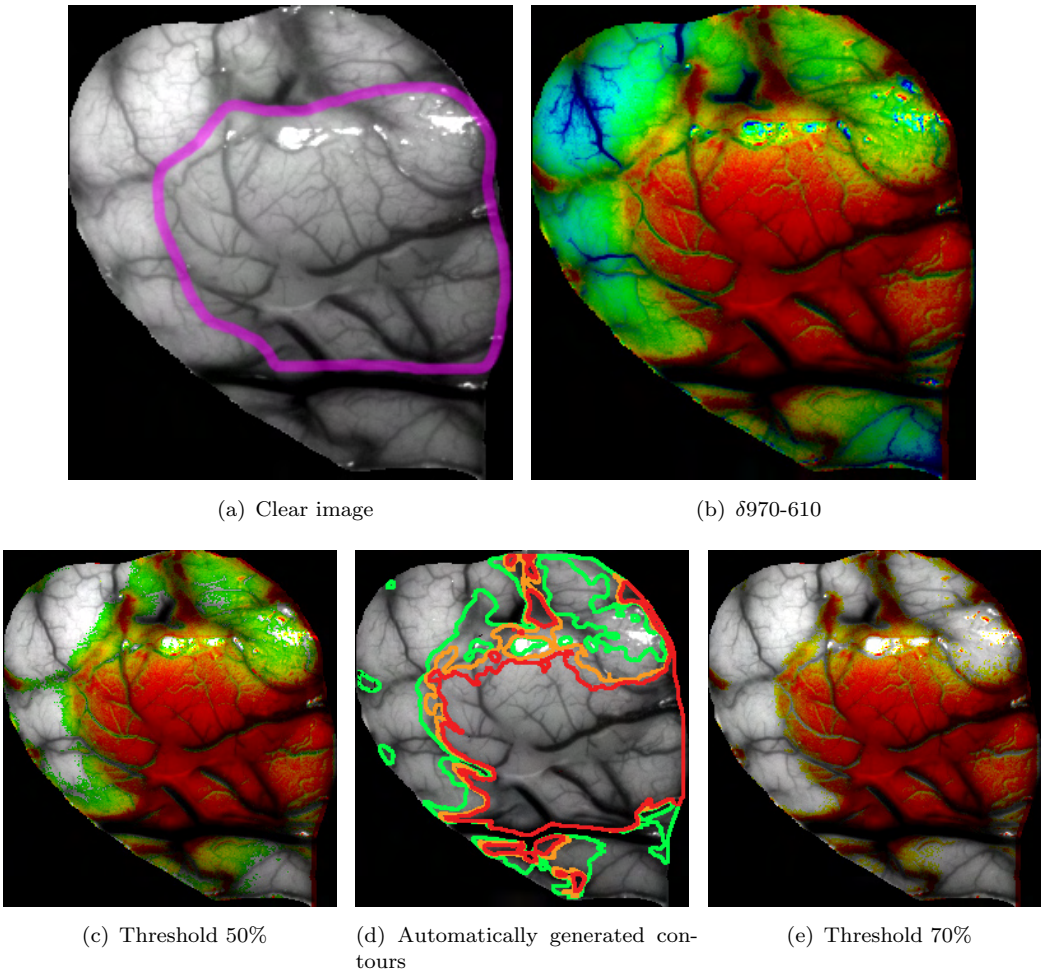

(a) Clear image

(b) $\delta$970-610

(c) Threshold 50%

(d) Automatically generated contours

(e) Threshold 70%

FIGURE 4.22: A selection of images from PT1. 4.22(a) shows the clear image with the resection extent marked in magenta; 4.22(b) shows the difference between 970 and 610nm; 4.22(c)–4.22(e) shows a series of threshold values applied to 4.22(b)

surgery for epilepsy, which involved small resection deep inside the brain. There was no involvement of the brain surface with this condition. The image processing conducted in both figures 4.21 and 4.20 is identical — including the gain as specified in equation 4.2. Processing includes a normalisation step to remove global changes which makes the system insensitive to factors such as the spectrum of illumination and camera sensitivity. The flat green seen in figure 4.21 is indicative of no contrast in these wavelengths, this is not stating that the reflectivity of the tissue is equal at each wavelength but that there is no change across the field. Consistent reflectivity changes across the entire field will be removed by the normalisation. The consistency seen in these is maintained even at much higher gain settings.

Patient 1 had a left frontal oligodendroglioma grade II. Figure 4.22 shows a series of images from Patient 1 the outline in 4.22(a) indicates the resection extent, this was generated using pre-operative imaging. There is clearly contrast

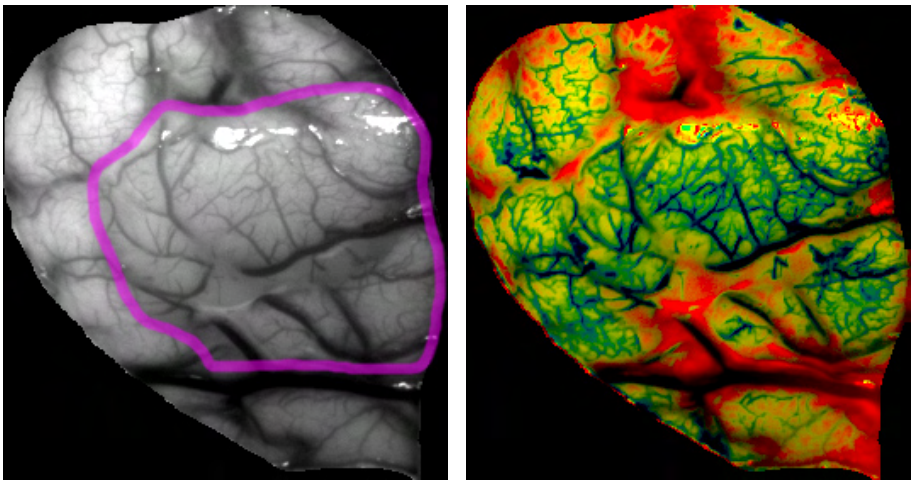

(a) Clear image (b) $\delta$610-580nm

FIGURE 4.23: Images from PT1, 4.23(a) shows the clear image with surgical margin shown; 4.23(b) shows the difference between 610 and 580nm

in the difference between 970 and 610 bands this correlates with the surgical extent. Thresholding the differences can visually enhance the results, figures 4.22(c)–4.22(e) show only the differences above a given value. Figure 4.22(d) shows automatically generated contours after median filtering of the difference image in 4.22(b), while the processing conducted on this image is still fairly basic it does show one possible method of visualisation during surgery giving confidence levels (in this case the green represents 65%, orange 75% and the Red 85%). Note that figure 4.22(e) demonstrates a high correlation with the surgical margin (shown in 4.22(a)).

The images shown in figure 4.23 are shown for comparison with similar images in 4.20(b). The images from Patient 1 show little contrast associated with the surgical margin, this may be due to a lack of angiogenesis associated with this tumour or alternatively the angiogenesis extends outside of the surgical margin as in 4.20(b) to the point where we are unable to resolve the boundaries. As mentioned above the current system of camera and processing is not powered to resolve global differences and so is not able to compare these on an intra patient basis however the possibility that the edges of the infiltrating tumour margin have not been reached exist.

Filter sets 1 and 2 perform particularly badly where there is an excess of blood in the field. This is often the case with high grade glioma due to the breakdown of the blood brain barrier. It is also the case in reoperation, even for low grade tumours.

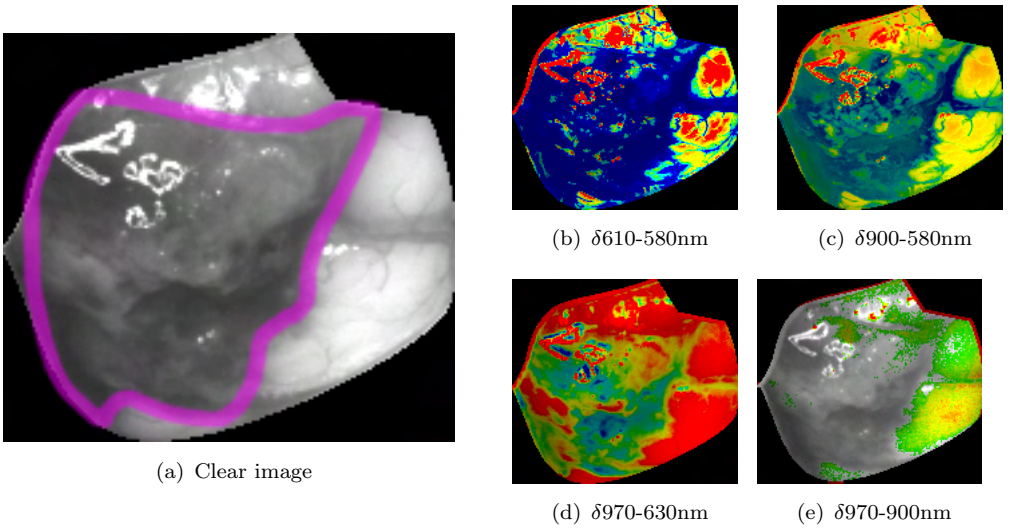

(a) Clear image

(b) $\delta$610-580nm

(c) $\delta$900-580nm

(d) $\delta$970-630nm

(e) $\delta$970-900nm

FIGURE 4.24: Images from PT4 highlighting the blood contamination in high grade glioma; 4.24(a) shows the clear image with resection contour in magenta the very dark areas are blood contamination; 4.24(b) shows the difficulty of imaging vascularisation in this region; 4.24(c) shows that the longer wavelengths are less sensitive to blood contamination; 4.24(d) shows much better contrast achieved with a pair of longer wavelengths; 4.24(e) with a threshold applied highlights what may be normal tissue.

Figure 4.24 shows how a damaged blood brain barrier can affect the imaging. The longer wavelengths are relatively less affected by the blood due to the lower, and spectrally flatter, absorption of haemoglobin in this region (Zijlstra et al. (1991)). The images shown in 4.24(d) and 4.24(e) demonstrate that it is possible to obtain relevant contrast in the presence of blood.

Tissue movement during surgery was highlighted as an issue in the background section (page 44) where reports detailing average movements of around 5.6mm were described. It is this author's experience is that is a real issue, after performing the craniotomy on patient 2283840 (of which some images are presented in 4.20) the surface of the brain moved to be almost level with the skin. This displacement would be of the order of 10mm but was not measured. Figure 4.25 demonstrates graphically how much these tissues move during surgery. This figure shows two images (4.25(a) and 4.25(b)) from before and after resection, the lower two images are the same images with areas coloured to allow discussion of these areas. The green and blue areas correlate in the two images, it can clearly be seen that these areas change shape and position during resection. Additionally the magenta area in the before resection images disappears from the after resection images as this tissue has moved out of the surgical field. These three regions highlight the difficulty of registering the tissue with pre-operative data as resection progresses. Finally the yellow area in the after resection image indicates a surgical instrument used to temporarily hold tissue out of the field, this is an example of occlusion mentioned in section 4.2.6.

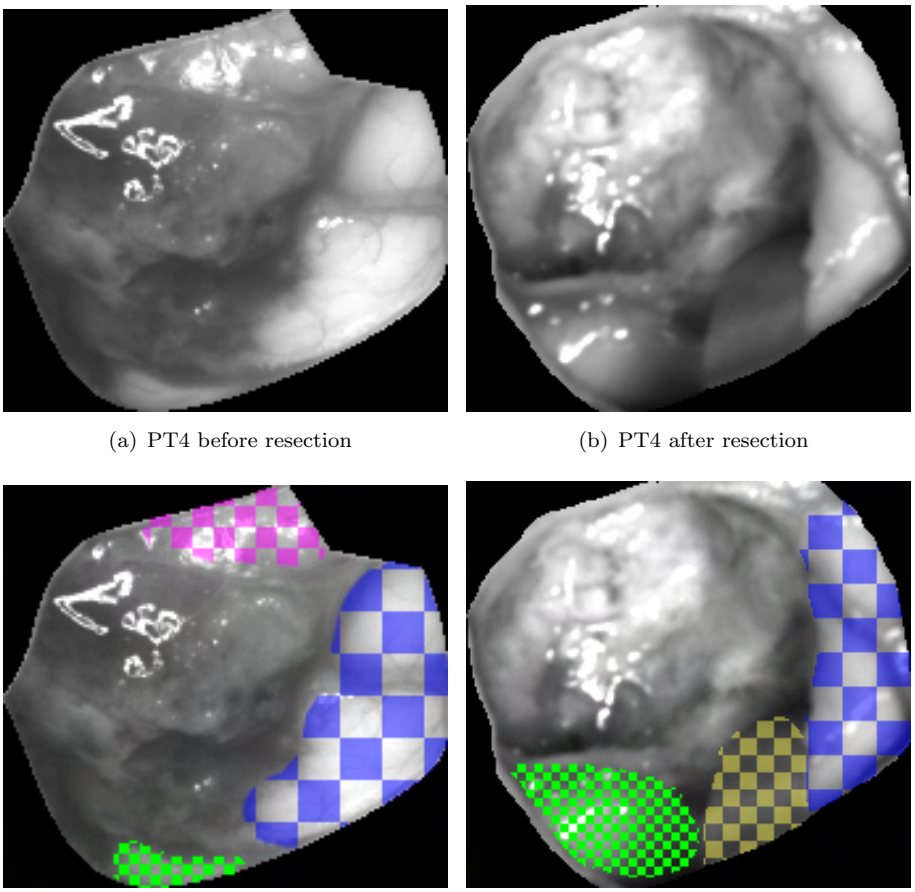

(a) PT4 before resection

(b) PT4 after resection

(c) PT4 before resection

(d) PT4 after resection

FIGURE 4.25: This figure demonstrates the amount of tissue movement during resection. The top two images (4.25(a) and 4.25(b)) are black and white visible images taken before and after resection. The bottom two images (4.25(c) and 4.25(d)) are the same images with certain areas highlighted; the green and blue hatched areas correspond to the same piece of tissue but has been moved and deformed, the magenta area in 4.25(c) is a section of tissue that was not removed during surgery but is not visible in the post-resection image, the yellow hatched area in 4.25(d) shows a surgical instrument (a retractor) holding the tissue in place (an example of occlusion as seen in figure 4.19

Some of the potential utility of this technique during surgery is demonstrated in figure 4.26. Imaging of the bottom of the resection cavity may indicate the extent of resection and could be sensitive to low grade and infiltrating tumour which other techniques are not sensitive to. Also this will not require registration with preoperative imaging. Figure 4.26 shows a detectable difference the tissue at the bottom of the resection cavity indicated by the blue colours in 4.26(b). There is also an area which shown in figure 4.26(c) which shows a particularly strong signal in the difference between the 610 and 970nm bands which has been shown above to correlate with resection margin (figure 4.22). However without the associated pathology assessment this is currently impossible to assess whether the bottom of the cavity contained infiltrating tumour.

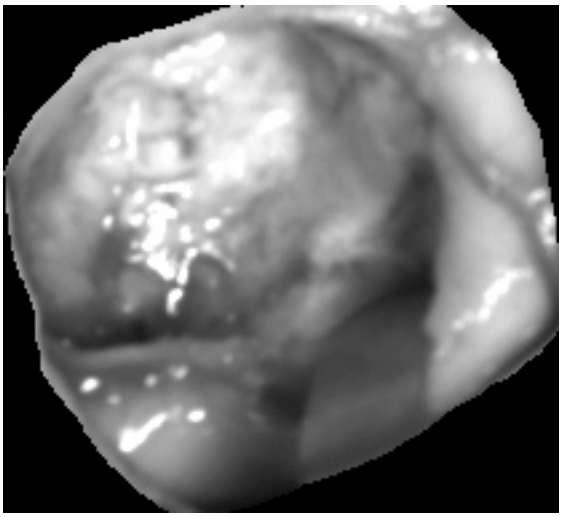

(a) Clear image

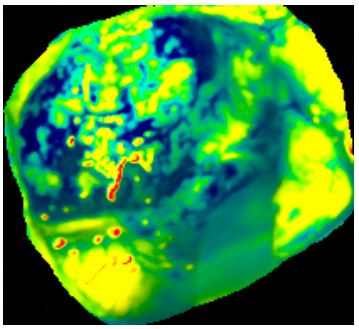

(b) $\delta$610-580nm

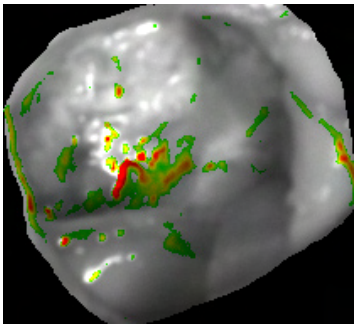

(c) $\delta$970-610

FIGURE 4.26: Images take after resection in PT4 show some contrast; 4.26(a) shows the clear image for reference; 4.26(b) shows some contrast between the cortical surface and the resection cavity in the difference between 610 and 580 nm — blues at the bottom of the resection cavity and yellows at the cortical surface; 4.26(c) shows an area of distinct contrast (this image has been threshold filtered for visual appearance) at the bottom of the resection cavity.

Patient 12 was undergoing surgery on a tumour which was had previously been operated on as a grade II glioma. This second surgery graded the tumour as a grade III oligodendroglioma. Figure 4.27 shows some of the images from this patient. Near letters A and B of figure 4.27(a) there some saturation in some of the images, this would manifest in the difference images as solid green areas indicating no difference. These difference images shown in 4.27(b)–4.27(d) indicate in red very similar regions which correlate well with the resected margin (shown in figure 4.27(a) in magenta). These difference images show that there are consistent differences in a number of spectral bands all associated with tissue inside the resection margin. The largest area of tissue not resected was that in the top right corner this correctly identified in 4.27(b)–4.27(d) indicated by yellow/greens and even blue colours demonstrating little or no spectral difference between these bands.

Another way to visualise these images is shown in figure 4.28. This shows the intensity at two different wavelengths plotted in the X and Y axis, the colours relate to the tissue type; all pixels are plotted in blue, pixels designated as normal have green added, those designated tumour have red added. This

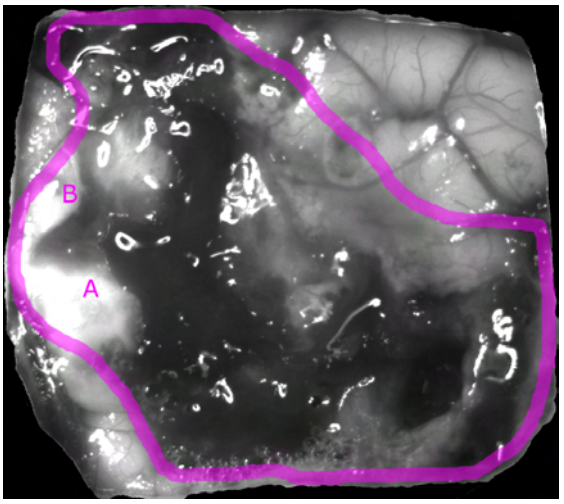


(a) Clear image

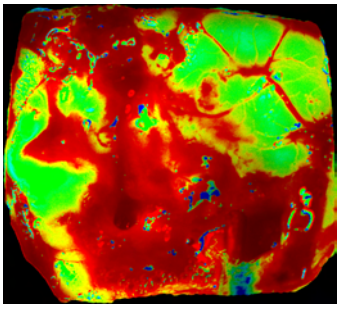

(b) $\delta$630-700nm

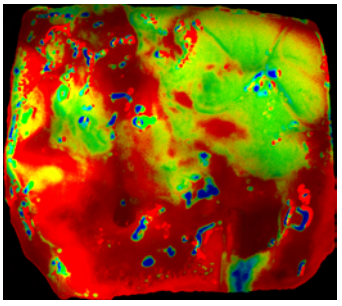

(c) $\delta$800-700nm

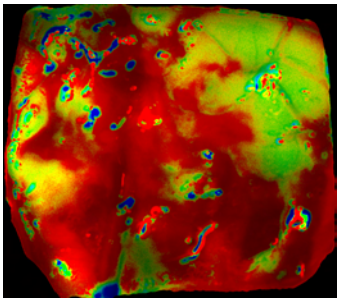

(d) $\delta$970-700nm

FIGURE 4.27: Images from PT12 undergoing a second surgery for oligodendroglioma collected using filter set 4 and tumour camera 2; 4.27(a) shows the clear image with the resection extent in magenta; 4.27(b)–4.27(d) show the differences of different spectral bands indicated by the $\delta$X-Ynm

therefore presents normal pixels as in blue–green (including cyan), and tumour as blue-red (including magenta). Yellow or white pixels indicate that the spectral characteristics of the tissue types are not separable. Some cross-over is expected due to the continuous nature of these variables and that these images are only considering two wavelengths. Figure 4.28(a) shows clearly that there is a distinct area of magenta which is separate from the cyan this is indicating that the tissue designated tumour has a distinctly different spectral character from the normal tissue — in this case indicating differences in the water content. Figure 4.28(b) again shows two areas one clearly cyan and one magenta, there is more cross-over in this image indicating that the differences are not as distinct however again a line can be drawn separating tumour from the normal groups.

The results from patient 2283840 appear to be separable with the tumour and normal tissue existing in different areas of this space. This is generally the case. This is obviously dependant on the selection and the designation of the areas. This has been done conservatively with a gap between that designated tumour

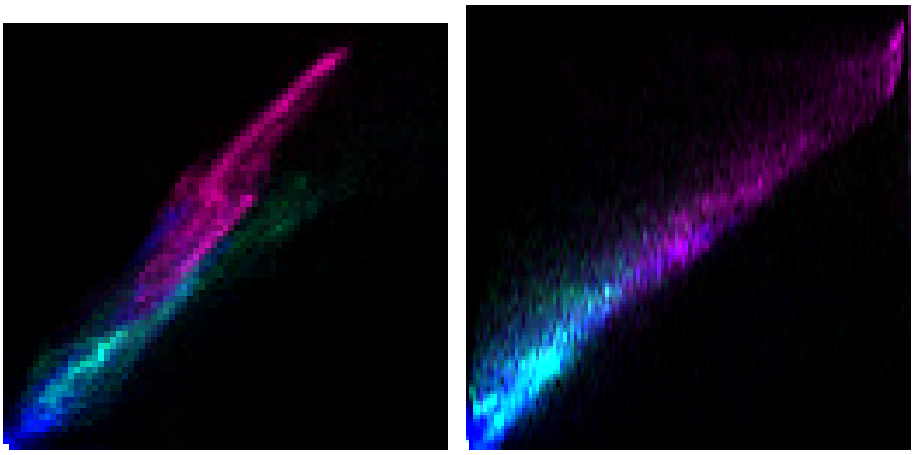

(a) X=970nm, Y=900nm (b) X=580nm, Y=610nm

FIGURE 4.28: An alternate visualisation of the images from patient 2283840 allows assessment of the grouping of the pixel values between the diseased and normal tissue (magenta indicates tumour, cyan normal, blue for the remaining pixels); 4.28(a) shows the values at 970nm and 900nm in the X and Y axis respectively; 4.28(b) shows values at 580 and 610nm in the X and Y axis

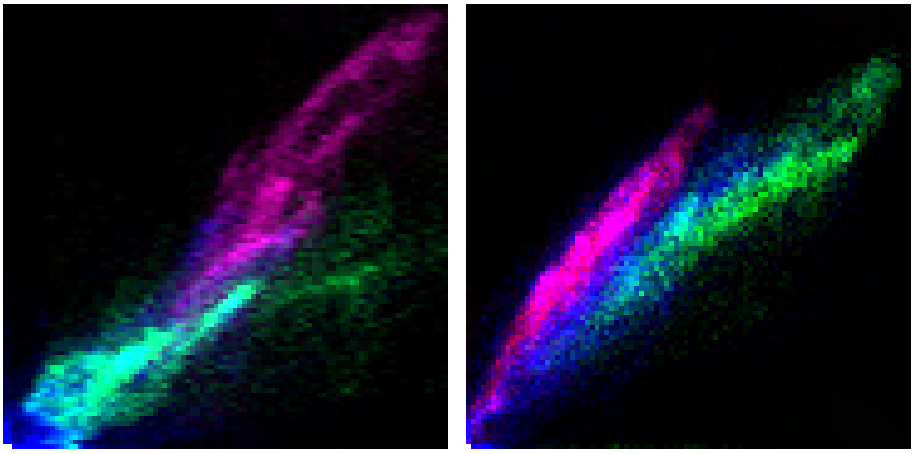

(a) Patient 2283840 (b) Patient 1

FIGURE 4.29: Two images representing the spectral content of the 970 and 610 in the tumour and normally designated tissue in different patients; 4.29(a) from patient 2283840; 4.29(b) from patient PT1

and normal but no large areas have been excluded from the analysis. Angles in these images are dependant on the relative normalisation between the two axis and therefore arbitrary. Figure 4.29 shows side-by-side two of these images from different patients demonstrating similar trends.

### 4.3.2 Bold systems

The opportunity to image functional activation of exposed cortex became possible because of the high dynamic range imaging and the narrow band filters able to select specific wavelength regions. Initially the first tumour camera was used as a data collection system. In addition to the other limitations of this camera a low frame-rate introduced aliasing affects into the collected images. However the results were encouraging.

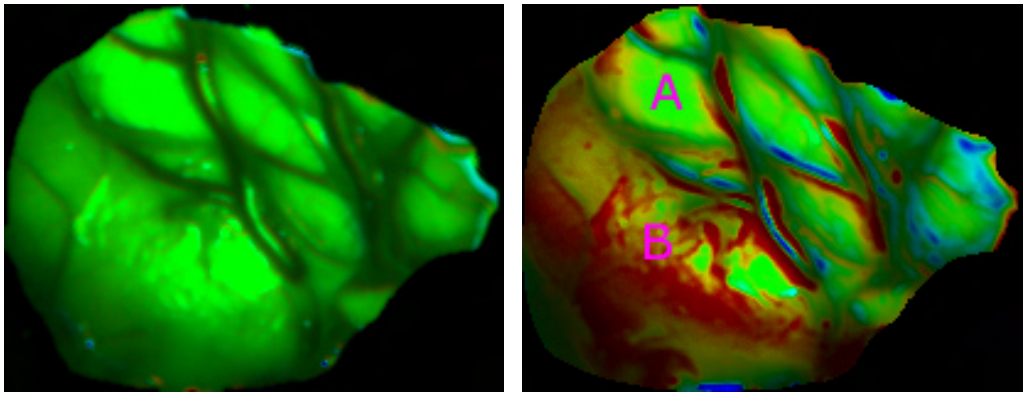


(a) At rest (b) Activation

FIGURE 4.30: Functional images taken using the first tumour camera in patient 5015360; 4.30(a) shows the at rest period; 4.30(b) shows the active period.

Figure 4.30 shows some of the images collected by this system. Patient 5015360 was undergoing surgery for a relatively benign tumour in the temporal cortex. In the bottom left of the image 4.30(b) labelled B is tumour. There is some saturation in the area labelled A which unfortunately means that there is a loss of information in region. The area labelled A was also identified as eloquent by electrocortical stimulation. The tumour showing as active in these images is interesting and could be interpreted in a number of ways including; that it shares a blood supply with the active region or that it contains some non-critically useful tissue. Vascular structures should be ignored in these images as any slight registration inaccuracy will create large signals in these regions. Functional activation can be seen clearly when plotted through time as shown in the figure 4.31, this shows two periods of activation, one starting at around frame 10 lasting for 15frames, the second starting around frame 60 and finishing around frame 140.

It can be clearly seen in figure 4.31 that the traces are not smooth, this is probably due to the frame-rate of the camera system being similar to the heart rate of the patient and therefore aliasing this changing signal. Patients imaged

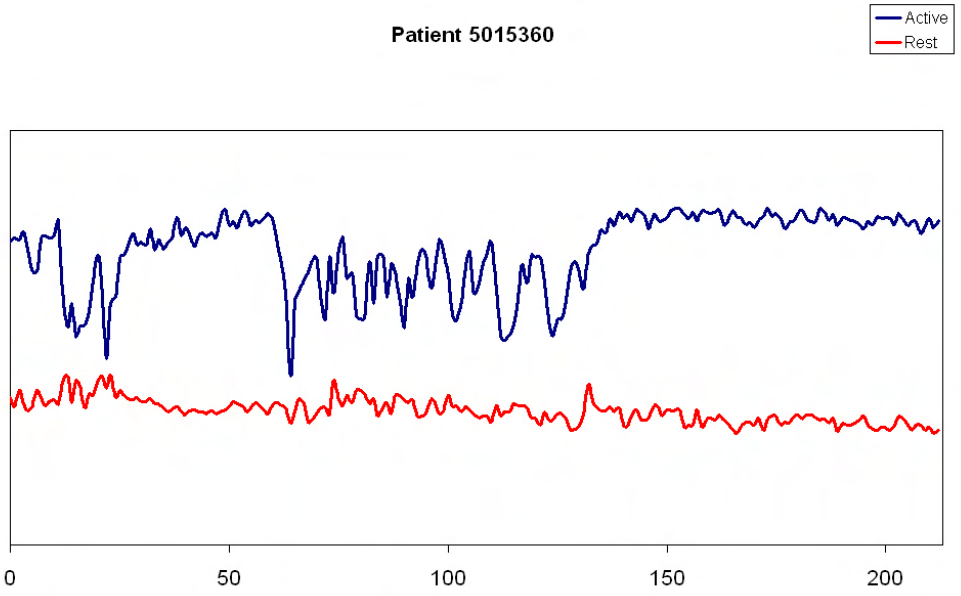


FIGURE 4.31: Two pixels plotted through time from patient 5015360, the x-axis denoting frame number collected at approximately 2 fps; Blue trace is from an active area; Red trace from an inactive area. Offset introduced to aid clarity.

where there was no eloquent tissue found by cortical stimulation did not show any signal.

These results were sufficiently encouraging that a new system described in section 4.2.4 was built which has a much faster frame-rate and can be attached to a standard Zeiss operating microscope. This allowed a better perspective on the imaging not limited by the physical constraints of the first tumour camera, much more of a "surgeon's-eye view". The images collected by this new system has more serious registration inaccuracies than the first system and due to the higher spatial resolution and frame-rate so computational expense is also an issue. A unfortunate side-affect of the poorer registration is that the non-uniform illumination of the operating microscope becomes a significant factor. In fact the relative change of the illumination relative to the field is more significant than any change in the absorption of the tissue.

The light field generated by the microscope is shown in figure 4.32 this field can be modelled effectively by a fourth order polynomial. However as the field does not change with the zoom of the microscope the size and position of the field must be extracted from each data-set individually. The registration algorithms used elsewhere can be exploited for this purpose. The size or scale of the light field can be recovered by using a Fourier-Mellin transform which is spatially invariant. Then the location can be recovered by the standard phase correlation method. An example of images before and after light field subtraction are presented in figure 4.33.

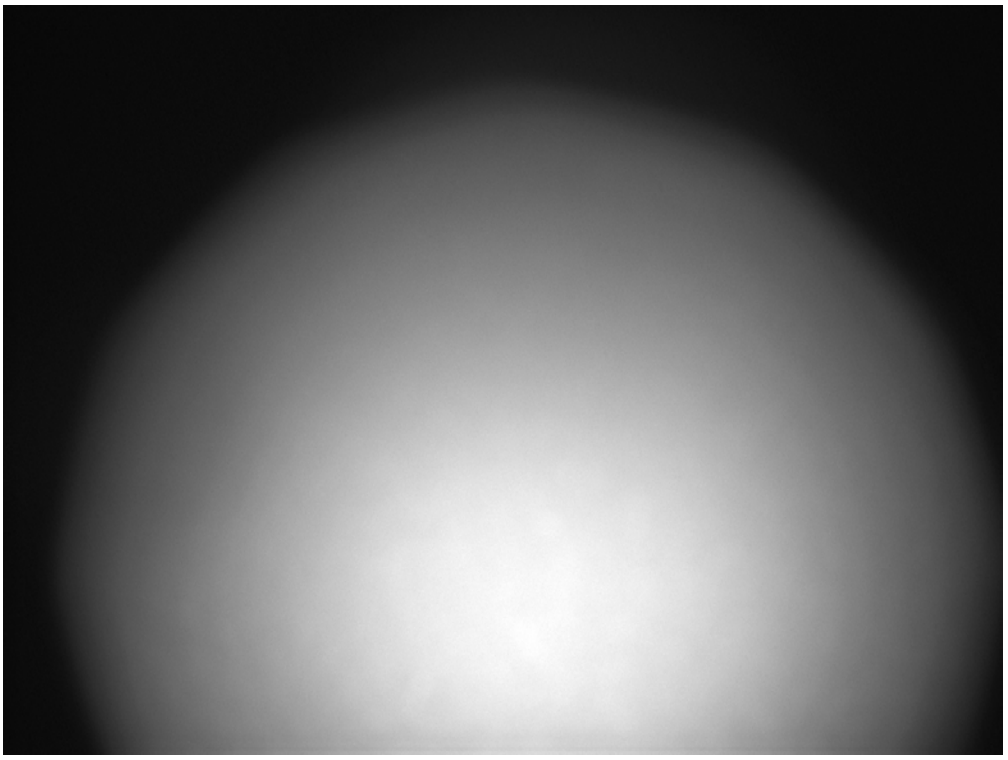

FIGURE 4.32: An example of the light field generated by the Zeiss operating microscope

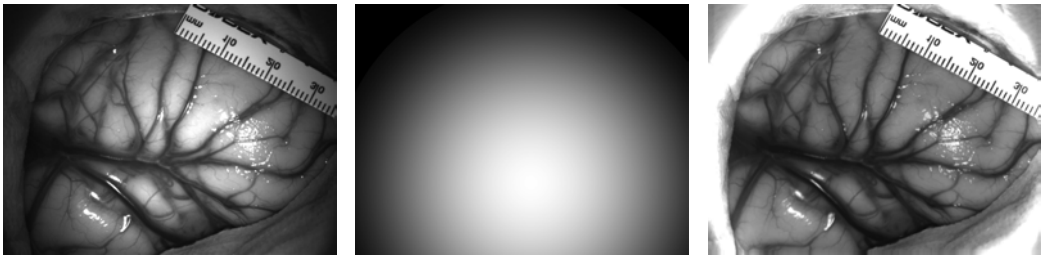

(a) Before subtraction (b) Calculated light field (c) After subtraction

FIGURE 4.33: Images taken from patient PT9 before and after subtraction of the light field calculated and shown in 4.33(b)

Patient 9 was undergoing surgery for a oligoastrocytoma near the sensorimotor cortex. Figure 4.34(b) shows the differences between a period of rest and a period of activation. This image has been thresholded to improve the visual appearance, the area in the top left of the image clearly shows some differences between activation and rest. There are strong signatures around some of the vascular structures this is primarily due mis-registration. Surface deformation is a large contributor to the mis-registration. In this case the activation was arm movement. These are the first results of an active map with this camera and the results are encouraging however there is still much work to do improving the images.

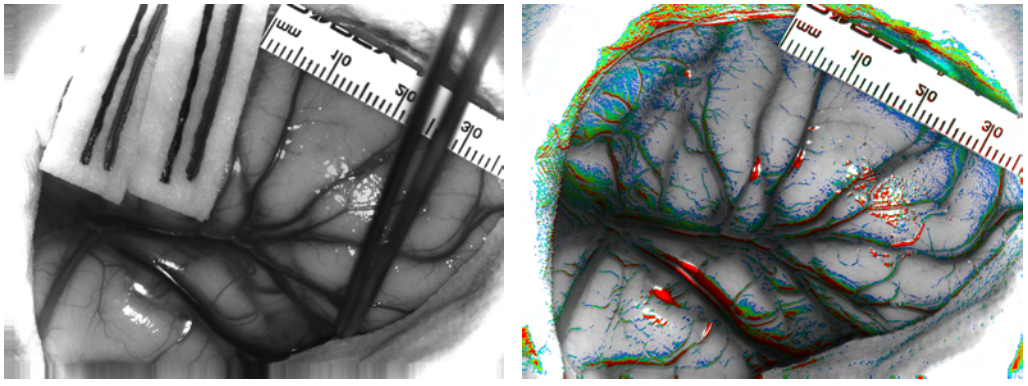

(a) Reference image (b) Active image

FIGURE 4.34: Images from PT9 showing functional activity; 4.34(a) the surgeon indicates with patties the area defined as eloquent by stimulation; 4.34(b) an image displaying the difference between periods of rest and activity

# Chapter 5

# Conclusions and future work

These conclusions are specific to the areas of the work, so will logically be presented separately.

## 5.1 Prion

Prion diseases are characterised by the deposition of mis-folded protein in amyloid plaques. This mis-folded protein has a primarily $\beta$-sheet conformation in contrast to the primarily $\alpha$-helix conformation of the prion precursor protein.

By using synchrotron illumination and Fourier transform infrared spectroscopy this project has found structurally relevant bands associated with the deposition of $PrP^{sc}$. A change in both the intensity of the $\beta$-sheet component around $1640cm^{-1}$and a decrease in the location of the peak of the amide I band are both associated with the change between normal $PrP^{c}$ and $PrP^{sc}$. This change demonstrates the deposition of $PrP^{sc}$ at both the early and late stage of disease progress (12 and 20 weeks post inoculation).

Also identified as a significant marker of disease progression is the band around 1740 associated with the carbonyl group. The most significant contributor to this absorption is likely to be glutamic acid which is known to be a neurotransmitter. This neurotransmitter is stored in synapses which are the earliest casualties of the neurodegeneration. Data presented in this thesis suggest that this marker will be identifiable much earlier in the disease progress and may be able to track the decline in synapses before any neuronal loss.

The use of a linear search algorithm was demonstrated to identify the structurally significant bands. Contrast enhancement was also demonstrated to improve the identification of these bands.

The absorption relating to the carbonyl group has not been reported previously be associated with prion disease and may be the earliest optical marker yet observed. Unlike the prion markers which have been shown by others to only be detectable at high spatial resolution, collection of the carbonyl data does not necessarily require synchrotron illumination as the area of high synaptic density is sufficiently large, evenly distributed and the absorption strong enough to allow lower resolution imaging. This should enable this to become a laboratory technique. Further data collection from earlier in the disease progress may identify the earliest loss of synapses. This could provide critical information about the disease mechanism and eventually result in methods to combat the disease.

## 5.2 Intraoperative identification of tumour margins

The need for intraoperative delineation of tumour margins stems from the fact that many primary brain tumours are visually indistinguishable from healthy tissue. Therefore it is difficult to accurately assess the extent of resection during surgery. Pre-operative imaging has been shown to help but as surgery progresses the registration accuracy of these images decreases so it is of limited utility. Also while pre-operative imaging is very good at identifying high grade tumours is not as sensitive to low grade tumours or even the infiltrating margins of the high grade tumours. This is potentially an area in which the systems developed within this project will excel.

Spectral differences from point measurements have been demonstrated elsewhere. This project has demonstrated for the first time that diffuse spectral *imaging* can resolve the differences between normal and malignant brain tissue. These differences have been correlated with resection margins. The location of these spectral differences is associated with the type of disease. Spectral regions including 970, 900, 800, 750, 700, 630, 610, 580 and 470nm have been shown to have evidence of spectral differences. Imaging of tumour angiogenesis appears possible by using the shorter wavelengths where haemoglobin absorbs strongly. Other features and deeper penetration is possible with the longer wavelengths; including in the 970–900nm band which is associated with water content differences. Blood from compromised blood brain barriers can interfere with the spectral imaging, correct selection of wavelengths can minimise this impact however further investigation is required.

This project has succeeded in developing a camera which is suitable for use in theatre, has minimal impact on the surgical routine, and has adequate spatial

and spectral resolution and dynamic range. The software toolkit has proved versatile and powerful.

The future of this project is guaranteed by three year grant funded by the National Institute for Health Research (NIHR). The application for which was entirely based on the work detailed in this document (the application can be found in appendix B). More data is required and routine histopathological analysis must be established. This analysis of the tissue types around the resection margin and at the bottom of resection cavities will establish the validity of the margins delineated by the camera. The collaboration with the pathology department that will enable this is developing and will allow definite statements about the pathological state of the tissue under investigation.

Investigations further into the infrared may yield interesting results; proteins, lipids and various other tissue constituents have a unique spectral features in the mid infrared region. There is some evidence in the literature that these features can be diagnostically useful. This is another area that would benefit from further research and something that the continued project aims to investigate.

## 5.3 Intraoperative delineation of function

Identification of functionally useful areas of brain is already conducted intraoperatively using point measurement techniques which have poor spatial and temporal resolution when compared with optical techniques. The identification of function is important to help minimise post-surgical neurological deficit due to damage of those areas. It is particularly important in tumour surgery as functional areas can be moved by a growing tumour. It may also have application in other areas of neurosurgery including epilepsy.

This project has developed a camera that attaches to a standard neurosurgical operating microscope and so is clinically straightforward and simple to use and integrates seamlessly with the operating theatre environment. This project has solved the image registration and uneven light-field problems for this application.

The results have demonstrated that it is possible to identify functional activity with a single cycle of activation. Previous reports have averaged over multiple cycles. This project has demonstrated that the areas delineated by this system correlate with the current standard for intraoperative measurement of function.

Again this work will continue under the grant awarded by the NIHR. Data from more individuals is required. Follow-up of the patients should be able to

correlate any immediate and long-term deficits with the proximity of the resection margin to identified functional tissue.

Different wavelengths should be considered as longer wavelengths will give greater penetration and possibly greater signal to noise. Other applications of the same technology are also worth investigation, epilepsy is one potential target, another is surgery for aneurysms where the blood supply to an area of brain may be disrupted real-time monitoring of the oxygen content of that region could potentially give vital information.

# Appendix A

# Assignment of the IR vibrational absorption of liquid water

| **Wavelength** | **Wavenumber** ($cm^{-1}$) | **Assignment** |
|---|---|---|
| 0.2mm | 50 | intermolecular bend |
| 55$\mu$m | 183.4 | intermolecular stretch |
| 25$\mu$m | 395.5 | L1, librations |
| 15$\mu$m | 686.3 | L2, librations |
| 6.08$\mu$m | 1645 | v2, bend |
| 4.65$\mu$m | 2150 | v2 + L2 |
| 3.05$\mu$m | 3277 | v1, symmetric stretch |
| 2.87$\mu$m | 3490 | v3, asymmetric stretch |
| 1900nm | 5260 | av1 + v2 + bv3; a+b=1 |
| 1470nm | 6800 | av1 + bv3; a+b=2 |
| 1200nm | 8330 | av1 + v2 + bv3; a+b=2 |
| 970nm | 10310 | av1 + bv3; a+b=3 |
| 836nm | 11960 | av1 + v2 + bv3; a+b=3 |
| 739nm | 13530 | av1 + bv3; a+b=4 |
| 660nm | 15150 | av1 + v2 + bv3; a+b=4 |
| 606nm | 16500 | av1 + bv3; a+b=5 |
| 514nm | 19460 | av1 + bv3; a+b=6 |
| Note that a and b are integers, >=0 | | |

# Appendix B

# Intraoperative Multispectral Imaging of Brain Tumours (iMSI)

APPLICATION NUMBER L032

Lead Applicant:
W. P. Gray
Professor of Neurosurgery
School of Medicine
University of Southampton

Joint Applicant:
H. N. Rutt
Head of School
School of Electronics and Computer Science
University of Southampton

Named Contributor:
P.R. Hoy
Optoelectronics Research Centre
University of Southampton.

Total requested:
£436,398

## B.1 Layman's summary

Brain tumours account for 7% of cancer deaths in patients under 70 years of age in the UK . Surgery remains the single most effective therapy, with the amount

of tumour removed being strongly predictive of outcome . However accurately identifying tumour boundaries during surgery is difficult, as they are often visually indistinguishable from normal tissue . Removing a surrounding rim of normal brain may be undesirable, if it has an important function like speech or movement. Preoperative imaging is of limited utility, as deformation of the brain during surgery causes significant inaccuracy. There is a pressing need for a non-invasive, real time tool that can be used during surgery to accurately identify tumour and eloquent tissue for maximising tumour removal and minimising loss of function.

The ability to perform high-resolution imaging of multiple spectra across the visible and infrared spectrum has only recently become technologically available. Intraoperative Multispectral Imaging utilises absorption in multiple parts of the electromagnetic spectrum from visible into the infrared, to identify tumour tissue from normal brain. In patients undergoing awake surgery this system can also detect a signal related to deoxygenated blood allowing the identification of functionally useful areas as these areas use more oxygen. This information can then be presented in real time in a relevant manner to the operating surgeon to maximise safe tumour resection.

A PhD project has demonstrated the feasibility of the technique using multiple visible and near infrared spectra but it requires further development to demonstrate proof of concept. Our objectives are to identify combinations of spectra, ranging from the visible to the infrared, that are specific for brain tumours. By the end of the project we hope to be in a position where a clinical tool integrated into a standard operating microscope could be further developed commercially.

## B.2 Purpose and outcomes

The purpose of the iMSI project is to provide proof of concept that the application of multispectral visible/infrared imaging has intrinsic value for identifying tumour tissue intraoperatively.

Although the infrared spectrum of brain tumours (wavelengths from 2-10$\mu$m) is known from point measurement techniques , it has not been previously imaged during surgery. The infrared spectra of frozen brain tumour tissue sections has shown significant differentiation of tumour grade and tumour tissue from normal brain as the origin of the infrared spectrum is governed by factors directly related to tissue makeup (C-N bonds that reflect protein composition, C-H bonds that reflect lipids). We will perform imaging at high resolution across the whole

operating field to generate an operative picture in real time. These images will be generated from combinations of spectra across the complete visible and into the infrared to maximise diagnostic accuracy — a technique that has not been applied to tumour imaging but has shown value in defence and satellite imagery. Because of our unique development of a multispectral tumour imaging system we will also be able to incorporate BOLD imaging of functional brain tissue in awake patients. This will represent a fundamental advance in the technology used to identify brain tumours intraoperatively and will pave the way for the development of a clinically useful system. This project will also provide phase 1 clinical data to support these outcomes.

Specific outcomes will be:

- Identification of combinations of visible and infrared spectra that accurately identify human brain tumour tissue.
- Construction of a multispectral camera system sensitive to these spectral features.
- Demonstrate a high correlation between preoperative imaging, histopathology and the iMSI system.
- Demonstrate a correlation between existing techniques such as 5-ALA and the iMSI system.
- Correlate functional imaging with intraoperative corticography.
- Develop both systems to the point where commercial R&D can be undertaken.
- Develop relationships with potential exploiters of the technology.

These outcomes will be exploited by applications to i4i for further funding in collaboration with an industrial partner and a user group from the Society of British Neurological Surgeons to develop a clinically usable device that delivers the relevant information to the operating surgeon in real time in a user-friendly manner. We foresee patentable possibilities in the complete device, and the spectral band combinations and processing used to interpret the spectral data and display the functional images. Finally, funding for a clinical trial using the device to demonstrate more complete and cost effective tumour resection with a lower complication rate than standard surgery will be applied for from joint industry and research council funding. Approximately 2000 craniotomies for intrinsic tumours are performed in the UK each year and a substantial market for such devices exists both nationally and internationally.

## B.3 Background

Primary brain tumours diffusely infiltrate surrounding brain. Therefore although surgery improves both life expectancy and quality of life, it rarely results in cure. This has led to a debate over how much tumour should be removed as conservative resection leads to earlier recurrence rates while aggressive resection may lead to more post operative neurological deficits. The goal should be to remove all tumour without any surrounding brain. However the infiltrative nature of these tumours means that tumours can resemble healthy tissue so closely that even experienced surgeons cannot visually distinguish them . Nor is it possible to differentiate eloquent from non-eloquent cortex. Preoperative imaging is used extensively in planning resection and is presented to the surgeon using an image guidance system that is integrated with the surgical microscope. This is of limited use during surgery as tissue deforms by as much as 15mm and accurate registration with preoperative images is lost. Figure B.1 demonstrates the extent of this tissue deformation.

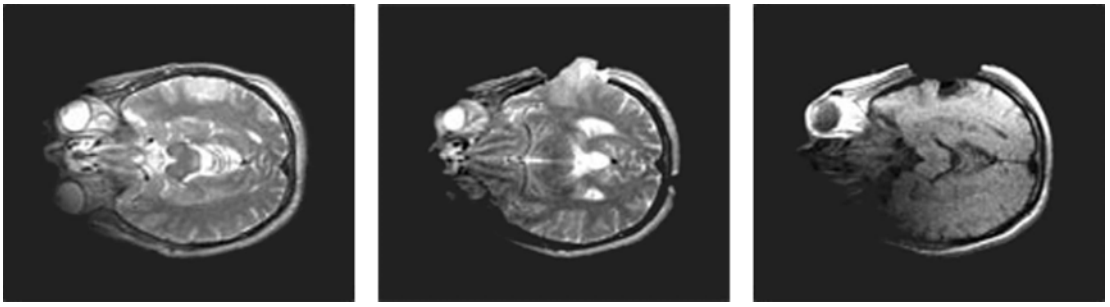

FIGURE B.1: Images taken using intraoperative MRI during a craniotomy demonstrating the extent of tissue movement during surgery Morton (2005).

Intraoperative MRI has been developed to improve the accuracy of resection , however this technique is prohibitively expensive and imposes significant restraints on the operating environment. Fluorescence techniques show promise (one example is ) and there are products on the market, however this technique is only of value in high grade gliomas where resection margins are relatively easier to identify and the prognosis is poorer than the low grade gliomas, which are found in a younger patient population . Fluorescence imaging is limited by the autofluorescence of tissue and often requires the injection of extrinsic fluorophores, the wavelength selection is limited and the technique is sensitive to stray light so the operating theatre must be darkened. Spectroscopic techniques have shown high sensitivity and specificity , however this is a point measurement technique and so has significant resolution and speed limitations.

The optical absorption of a material, including biological tissue, is determined by the physical constituents of this material and its structure. In the visible and

near infrared (defined here as 300-1000nm) the absorptions are primarily electronic transitions; i.e. the energy in a photon is enough to promote an electron to a higher energy state, thereby absorbing that portion of the spectrum, e.g. red dye absorbs blue and green light leaving the red light to be reflected (or transmitted) and observed. In the mid and long wave infrared (defined here as 1-5$\mu$m and 5-10$\mu$m respectively), the absorption is primarily due to the chemical bonds in the material. There are a number of different mechanisms for this absorption, however there is a direct correlation between absorption at a given wavelength and a given chemical bond e.g. the CH bond in a fat or the amide bond in a protein. Figure B.2 gives an example of this. Combining these wavelength regions may provide information about the tissue which was not obvious in any one of the bands in isolation. The technique of imaging a number of distinct wavelengths (either within a wavelength region or between regions) is called multispectral imaging.

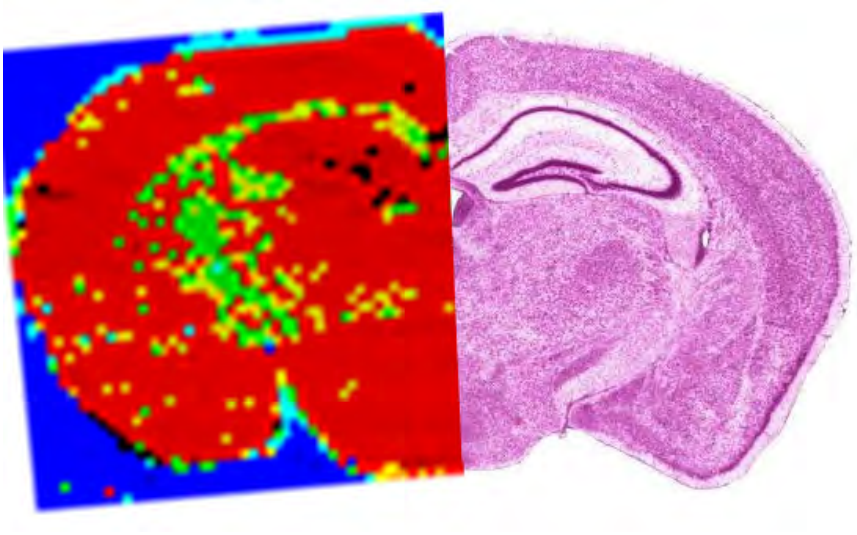

FIGURE B.2: An image of a mouse brain, the left hand side was imaged using mid and long wave infrared spectra and processed to distinguish between protein and fat, the right hand side has been stained to increase the tissue contrast.

Multispectral imaging compares the information content in a number of different spectral bands and presents this in a method that is relevant to the user; the technique originated in military applications where it has a strong track record. There is evidence in the literature that normal and malignant brain tissue have different spectral characteristics (i.e. the tissues absorb differing amounts of light at specific wavelengths). This evidence is based on *in vivo* measurements using point measurement spectroscopic techniques and *in vitro* techniques mentioned above. We have evidence that this information can be used in an imaging modality and this proposal seeks to continue and develop this work.

The iMSI project started with a PhD project investigating the applications of multispectral imaging. This work has established collaboration between engineers in the University of Southampton Electronics and Computer Science department and academic neurosurgeons at both Southampton University and Southampton General Hospital. We have been awarded ethical approval for taking multispectral images during surgery. A camera system has been developed which is sensitive to light in the visible and near infrared bands. This camera is very sensitive to small changes in reflected light and by using narrow band filters can accurately select which part of the absorption characteristic it is sensitive to. This project has also developed the software required to analyse the collected images. Figure 3 shows one set of intraoperative results. The scale bar on the right shows high probability of tumour in red and a low probability in blue. This image is an early result using a single pair of wavelengths but shows indications in the red and yellow areas that discrimination is possible, additional bands improves this differentiation as seen below (Figure B.4).

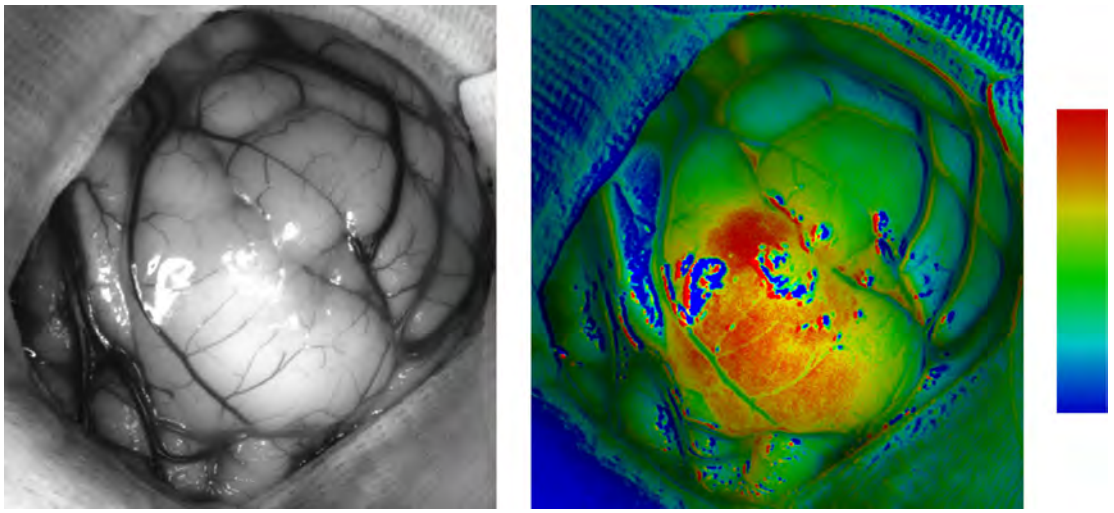

FIGURE B.3: Images taken intraoperatively. Left: shows a black and white visible view of the cortical surface. Right: shows a false colour image highlighting the tumour tissue.

The images shown in Figure B.4 show a patient undergoing their second surgery for high grade glioma; the false colour image on the right highlights tumour in green to red and normal tissue in blue. This image had a good correlation with the preoperative data (shown in the centre image) and clearly shows a high level of contrast between the normal and the diseased tissue. The rightmost image is a multispectral image composed of two different spectral bands and demonstrates better contrast than the central image which only uses one spectral band. This shows the advantage of using multispectral imaging to differentiate between normal and tumour tissue. These improvements were obtained within the visible

and near infrared; there is good literature evidence that extension to longer wavelength infrared will produce substantial further improvement.

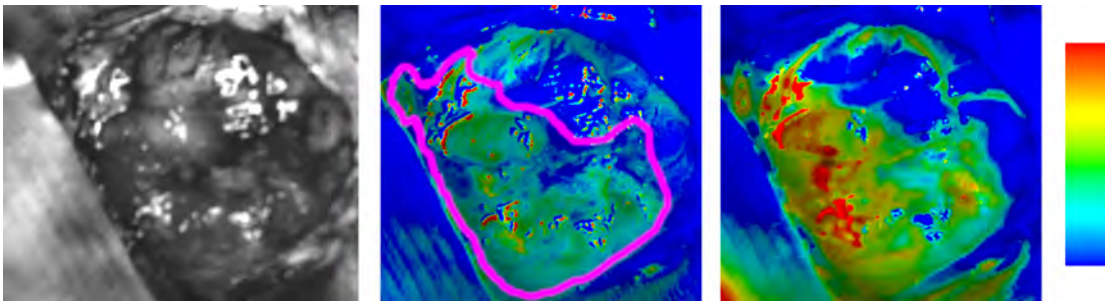

FIGURE B.4: Multispectral images taken intraoperatively. Left: black and white visible image. Centre: false colour image of tumour tissue using a single spectral band (blue low probability of tumour, red high probability of tumour) tumour outline shown in magenta. Right: false colour image using two spectral bands (multispectral).

To date, this work has enrolled 13 patients in the tumour study. One of the image sets had to be discarded due to a technical failure. About half of the remaining patients were undergoing surgery for a tumour. Using multispectral imaging, abnormal tumour tissue was identified in most cases (sensitivity 83% - rising to 100% in later patients due to developmental improvements, compared to 50% with single spectrum analysis). It was our impression that multispectral imaging also improved the extent of tumour identified (see Fig. 3) but we require a microscope integrated head-up display on our navigation system to combine the MRI tumour margin with the visible image to accurately quantify this. The specificity of our multispectral imaging was 100% as no tumour spectra were identified in patients undergoing non-tumour surgery.

Another problem that the iMSI project will address is the lack of intraoperative functional imaging. The current techniques for establishing function during surgery (somatosensory evoked potentials and electrocortical stimulation) are slow, low resolution point measurement techniques. The preoperative techniques, functional MRI and PET, take a considerable amount of time and may involve injection of radionuclides. The iMSI system hopes to identify functionally useful areas of the brain using the same Blood Oxygen Level Dependant (BOLD) signal used by fMRI. This signal can be accessed optically at higher resolution than fMRI and intraoperatively across the operating field in near real-time. The iMSI system developed is sensitive to this signal. Figure 5 shows a part of the temporal cortex, the region labelled 1 was found to be associated with speech by electrocortical stimulation, region 2 was tumour. The image on the right hand side of Figure 5 highlights the BOLD signal. It is clear that the eloquent region shows a strong signal, however the tumour region also has a high response indicating the presence of functioning cortex within the tumour. This

demonstrates the potential for an intraoperative functional capability with this technique.

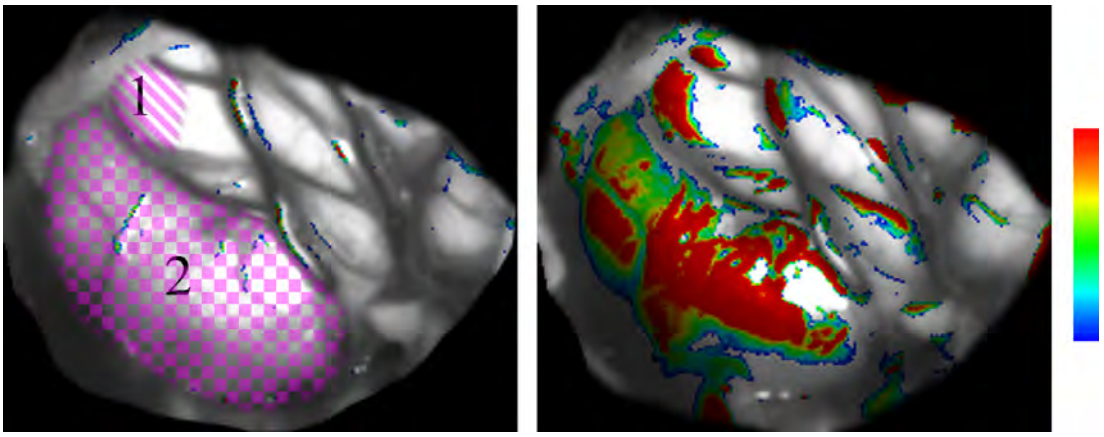


FIGURE B.5: Intraoperative functional images taken with the iMSI system. Left: black and white visible image showing region 1 and 2. Right: output of iMSI system.

The BOLD image is collected as a series of images; a representation of this series can be seen in Figure B.6. This shows the signal from a single point through time, the red bars at the bottom indicate a period of stimulation (in this case the patient was asked to read words from a card), the blue bars indicate periods of rest. It can be clearly seen that there is an increased signal during the periods of stimulation; this correlated well with the electrocortical stimulation results.

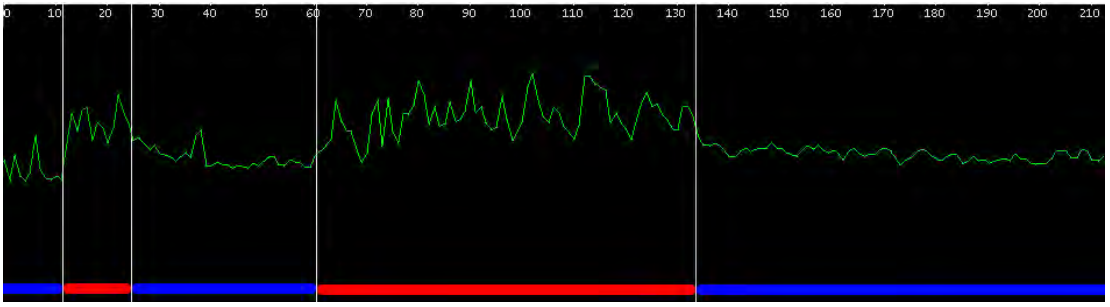


FIGURE B.6: Demonstrating the BOLD signal of a single point through time.

To date, 3 patients have been enrolled in the intraoperative functional imaging study and a sensitivity and selectivity of 100% has been demonstrated. This work will soon be presented at the OSA Frontiers in Optics Conference.

Normal cortex and white matter are highly organised structures at a microscopic level. We therefore expect that light at some wavelengths will be polarised which may allow differentiation between nerve fibre tracts in the brain, which could significantly improve the safety of resective surgery which can also result in deficit by severing critical connections between cortical areas of function. This structure is also lost in tumours and could produce more information about

tumour margins deep in white matter. The iMSI camera will incorporate polarisers to investigate this possibility.

FIGURE B.7: An Example neurosurgical microscope, the red box indicated by the arrow is indicative of the size of the finished iMSI system.

It is standard practice during neurosurgery to use an operating microscope similar to that shown in figure B.7. These microscopes can be integrated with a guidance system (IGS) which projects the tumour outline generated from preoperative imaging data straight onto the surgical field. This is a valuable addition to the microscope but as noted earlier this preoperative data loses registration as the surgery progresses; having a system that can integrate with the current technology and provide real-time information about the tumour boundaries would be a significant improvement. The completed system may be no larger than the red box shown in Figure 7. The size is dependant on the number of bands required for accurate delineation but this will be comparable to the size illustrated (and certainly be available as a microscope attachment). If mid and long wave infrared technology is used in the final system this would

increase the size somewhat, however it could still be integrated with the microscope head.

The complete system will operate as pictured in Figure B.9. The software could completely integrate with current guidance systems which present preoperative data allowing seamless switch over between preoperative and intraoperative imaging.

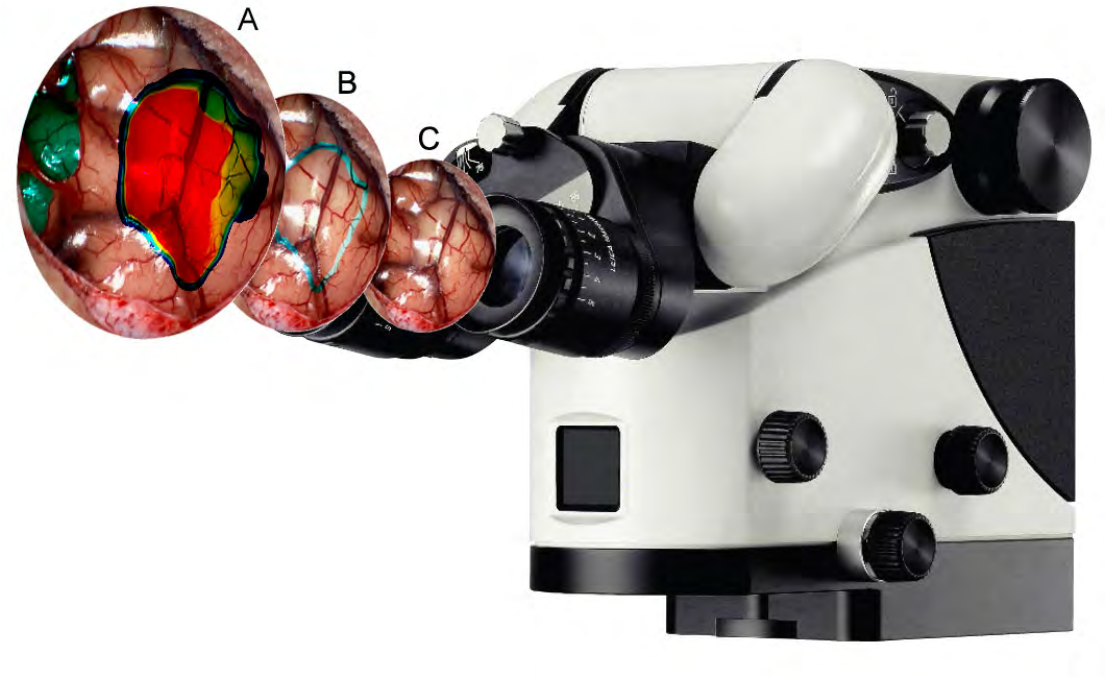


FIGURE B.8: Microscope head showing a number of different views. A: the tumour boundary highlighted in red-blue, bold highlighted in cyan, B: outline based on preoperative data, C: operates as a normal microscope.

**Cost Benefits:**

Complete resections (MRI guided) are associated with an age-adjusted five-fold reduction in mortality risk over a five-year period for low-grade gliomas . This has obvious potential direct patient benefits with both reduced postoperative deficits and significantly improved disease free survival times, especially with low-grade gliomas. However, iMSI is likely to be more cost-effective (commercial system likely to cost approx £50k) than intraoperative MRI (£1 million per installation) and will certainly be easier and more user-friendly in theatre. In addition, iMSI may well be applicable to other areas of tumour surgery outside of neurosurgery. Healthcare providers will also accrue both immediate direct cost savings in reduced hospital stay from less deficits as well as longer term savings as redo operations for suboptimal resections are minimised.

**Novelty of the proposed work:** The main novelty of this proposal lies in the multispectral analysis across the visible to infrared spectrum to provide a high-resolution image of tumour probability and functional cortex in the operative field. This has been made possible by the recent development of high-resolution infrared camera technology as well as the emerging utility of multispectral analysis for useful information extraction.

The infrared spectra of frozen sections of brain tumour tissue sections has shown significant differentiation of tumour grade and tumour tissue from normal brain but the lack of high resolution infrared imaging has prevented the processing of these data into an operative image to delineate tumour.

Multispectral analysis by combining, e.g. electronic transitions from the visible spectrum, with water content from the near-infrared and protein and lipid content from the mid and longwave infrared spectra will significantly enhance the detection of abnormal tumour tissue and in combination with BOLD imaging will simultaneously detect eloquent cortex to guide safe surgical resection. Multispectral analysis will also provide information on many other indices of tissue structure and content such as cell density and DNA/RNA ratios which may also be useful. Multispectral imaging has not been applied to tumour imaging, but has shown value in defence and satellite imagery.

We will perform this visible and infrared imaging at high resolution across the whole operating field to generate a real time picture. These images will be generated from combinations of spectra across the complete visible/infrared range to maximise diagnostic accuracy. Because of our unique development of a multispectral tumour imaging system, we will also be able to incorporate simultaneous BOLD imaging of functional brain tissue in awake patients. This combination of simultaneous structural and functional imaging has not previously been achieved.

The development of an iMSI device will thus be a fundamental paradigm shift / advance in intraoperative brain tumour imaging.

## B.4 Research plan and methodology

We have ethics approval for this project REC 06/Q1704/139.

Based on our outcomes, our research plan is as follows:

1. **Identification of combinations of visible/infrared spectra that accurately identify human brain tumour tissue.**

Initially, published infrared spectra of gliomas will be used to choose pilot bands and appropriate filters will be constructed for high-resolution infrared imaging. We will also perform a complete visible and infrared spectral analysis on fresh frozen tumour tissue to confirm literature results and extend the analysis into other tumour types that have not been previously reported. Control spectra of normal cortex will be performed on normal tissue excised during non—tumour epilepsy surgery performed by Prof Gray (REC 07/H0504/195).

2. **Construction of a multispectral camera system sensitive to these spectral features.**
   Filters will be selected based on section 1. Where available, these filters will be purchased commercially (COTS). However these off-the-shelf filters do not cover the complete infrared spectrum and where unavailable we will have to construct these specifically which is a costly process. We are providing two high-resolution infrared cameras worth (£50k each) for this project however these will need to be built into a camera system. This system will include coaxial optics for all of the imagers and the selected filters and polarisers. The construction of a camera system is complicated by 'normal' glass being opaque in the mid and long wave infrared, so more exotic materials must be used (e.g. Calcium Fluoride or Germanium); this significantly increases the cost of optics in this region.

3. **Demonstrate a high correlation between preoperative imaging, histopathology and the iMSI system.**
   Over 100 craniotomies per year for intrinsic supratentorial tumours are performed by Prof Gray and colleagues at the Wessex Neurological Centre. Of these approximately 40% are performed under awake conditions. The prototype iMSI system developed to date has been successfully used in 13 cases and will be extended to image the infrared. The iMSI camera is mounted on a separate microscope stand. Currently we do not have microscope integration of the Stealth image guided system and cannot obtain through-the-microscope photographs of the operative field with the tumour outline projected onto it. Purchase of the Stealth heads up microscope display will generate these images, providing co-registration with the iMSI camera visible images, corrected for parallax errors. These fused images will allow accurate comparison of the initial MRI generated surface tumour boundaries (before shift) with the spectral characteristics of the operative field. Each point (pixel) in the operative field will undergo an acquisition across the complete spectral bands. Post processing of the visible images and spectra will then be carried out to generate a probability

density map of tumour tissue for individual and selected combinations of spectra and the performance across patients and tumours will be quantified and statistically analysed with respect to tumour extent (MRI), and type (histopathology). This will be an iterative process with continuing refinement of the spectral combinations used to maximise the accurate (sensitivity and specificity) identification of tumour tissue. Patients will undergo MRI scanning within 72h of surgery to assess the presence and location of residual tumour tissue in the operative bed. Neurological deficit and survival will be recorded in all patients as linked-anonymised data.

4. **Demonstrate a correlation between existing techniques such as 5-ALA and the iMSI system.**
   For high-grade gliomas, patients will be given 5-ALA orally three hours before surgery and tumour tissue visualised using fluorescent visualisation using the iMSI system and a fluorescent light source. Porphyrin fluorescence will be imaged with the iMSI camera and compared to the spectral emissions as above, at set points during and at the end of resection, to see how the iMSI system performs for identifying high-grade gliomas tissue. All patients will undergo MRI scanning within 72h of surgery to assess the presence and location of residual tumour tissue in the operative bed. 5-ALA is not suitable for Grade 3 gliomas, nor for low grade gliomas where multispectral imaging may perform well because of its sampling of different aspects of the tumour across multiple spectra (see above).

5. **Correlate functional imaging with intraoperative corticography.**
   In cases undergoing awake craniotomy and intraoperative mapping of cortical function, both in epilepsy surgery and tumour surgery cases, identified areas of critical function (using an Ojemann bipolar cortical stimulator) will be marked using a visible light image from the iMSI system and compared with the multispectral information collected.

We expect to recruit at least 100 patients to the study over three years from a total operative population of 300 patients for that period.

The Gantt chart in Figure B.9 shows how we plan to progress the project and sequentially add more infrared and multispectral capability with continuous collection and analysis of the data across all spectral bands. It also shows regular periods of review and reporting. The functional imaging and visible spectra will be quick to start given the previous work.

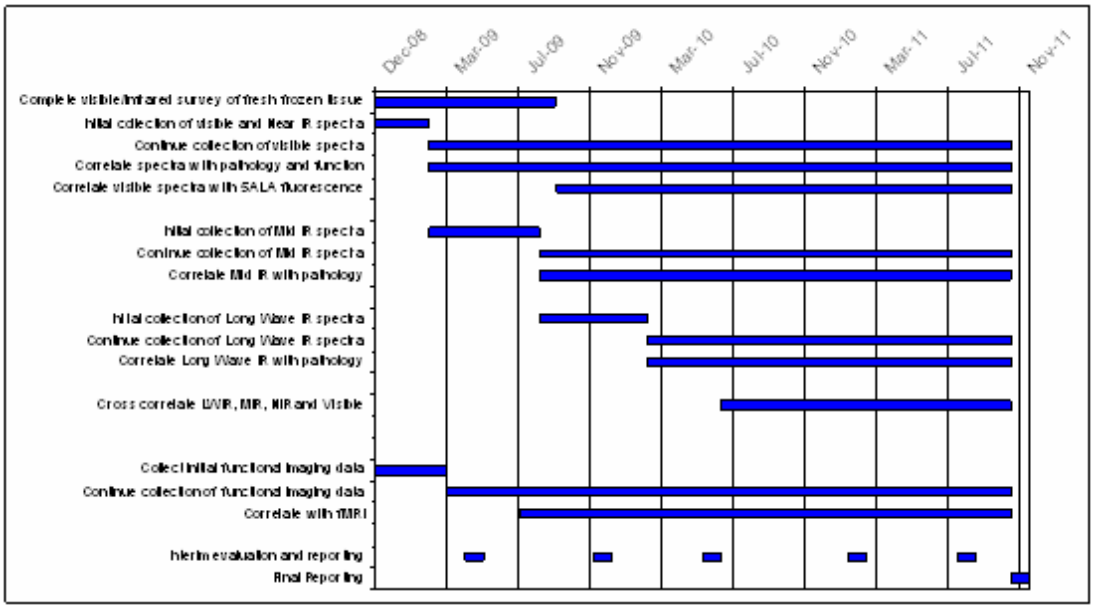


FIGURE B.9: Gantt chart showing project progression.

## B.5 Dissemination, implementation, route to market

Any intellectual property developed will reside within the University of Southampton which will commercially exploit this technology by seeking industrial partners principally among existing manufacturers of surgical microscopes (for example Zeiss and Leica). Information that may be beneficial to the wider scientific community (but which will not prejudice the commercial position) will be submitted to relevant journals (such as Neurosurgery, British Journal of Neurosurgery, Lancet Neurology, Journal of Biomedical Optics) and presented at appropriate conferences (e.g. the European Conference of Biomedical Optics, BIOMED, and Medical Imaging).

## B.6 Consumer involvement

Neurosurgeons would be the primary users. They require means of providing safer and more accurate surgery which multispectral imaging promises to provide. Through providing safer and more accurate surgery, patients are likely to experience fewer complications (such as paralysis and speech deficits) as well as reducing their postoperative recovery and tumour recurrence. This will reduce the burden on carers and costs to the NHS.

The Primary investigator on this project is a neurosurgeon with 10 years operative experience at consultant level and this project is already collaborating

with other neurosurgeons in Southampton General Hospital. Once proof of concept has been established we will apply to i4i for development of a clinical device and will involve a user group of surgeons from the Society of British Neurological Surgeons and patient groups with brain tumours.

## B.7 Skills of research team

The main outcome of this project is to provide sufficient information to enable the commercial development of a system which can identify eloquent areas of cortex and provide information about resection margin. We believe the team, combining practising neurosurgeons with an experienced engineering focussed optoelectronics group is exceptionally well placed to target a practical outcome.

Professor William Gray obtained an honours medical degree from University College Cork, Ireland in 1986, Fellowship of the Royal College of Surgeons in 1990, MD by thesis in 1993 and his Fellowship in Surgical Neurology in 1995. He was appointed Senior Lecturer in Neurosurgery in 1998 after completing two years of stem cell research at post-doctoral level. He was appointed to the University Chair of Neurosurgery at Southampton in January 2006. He established a functional epilepsy surgery programme in Southampton in 2000 using awake craniotomy and cortical mapping to guide excision of tumours and cortical lesions causing drug refractory epilepsy. His research interests are in cerebral physiology, Health Technology Assessment in Neuroscience and Adult neural stem cell biology. He has had a number of research grants with the Research Councils and Industry. He is Secretary of the UK Chapter of the International League Against Epilepsy (ILAE) and is Chairman of the Academic Committee of the Society of British Neurological Surgeons (SBNS).

Professor Harvey Rutt took a first class honours degree in Electronics Science at the University of Southampton in 1968, followed by a PhD in Optoelectronics in 1971. After spending three years in Brazil setting up a laser research group in a federal University, he returned to join the UKAEA Culham Laboratory, eventually becoming Division Head of Beam Science & Technology, with some 75 staff. Technical interests included novel lasers, high power lasers, and high brightness ion beams. Since 1992 he has been the Rank Professor of Infrared Science and Technology, with wide ranging interests in infrared materials, lasers and instrumentation. He was Deputy Director of the Optoelectronics Research Centre, University of Southampton for nine year from 1998, prior to becoming Head of School for the University‘s School of Electronics and Computer Science in 2007. Prof Rutt has experience of exploitation of IP resulting from University

research via Directorships of University spin-out companies and licensing negotiations.

## B.8 Costs

We are able to provide well-equipped facilities for this research, including a wide background of the infrared equipment needed; including e.g. FTIR microscope facilities costing in excess of £100k. No large equipment items are included in our costings, and we will provide two high specification infrared cameras for the prototype work.

Please see attached detailed Costings with inflation in Appendices.

### B.8.1 Research and development costs

Justification:

The major costs are staff costs for the three-year appointment of Mr Hoy to perform optics and spectral research. Mr Hoy has designed and built the current system and is a named researcher on the ethics award.

The Consumable costs are necessary for the construction of the appropriate filter sets. The Stealth Microscope interface is necessary to produce an image of the operative field with the MRI guided tumour outlines at the operating focal plane for co-registration with the iMSI Camera images to measure the sensitivity and specificity of the iMSI system for tumour detection.

### B.8.2 Service support and treatment costs

There are no additional procedures or resources for this project above standard clinical care for this proof of concept study. We are obtaining optical data during surgery for later off-line analysis and image generation. The images obtained will not be available to the operating surgeon and will not influence patient care or management decisions.

## B.9 References

[References included in main bibliography]

## B.10 Signatures

I declare that the information given on this form is complete and correct.

Signed _____

Name _____ date _____

Signed _____

Name _____ date _____

Position _____

## B.11 Appendices

CV and list of grants for Prof. Gray and Prof. Rutt.

**Curriculum Vitae**
Prof. William P. Gray
MB.B.Ch. B.A.O., M.D., F.R.C.S.I., F.R.C.S.(SN)
Division of Clinical Neurosciences,
School of Medicine, University of Southampton.
Room LD74, Level D, South Academic Block,
Southampton General Hospital, Southampton, SO16 6YD, England
Email: w.p.gray@soton.ac.uk
Tel: 02380 794271
Fax: 02380 794542

**Qualifications**
M.B. B.Ch. B.A.O. (hons); M.D., F.R.C.S.I., F.R.C.S.(S.N.) **GMC Reg:** Full. GMC, No. 4051787, 23rd August 1993.

**Posts Held** 2006 – present Professor of Neurosurgery, University of Southampton

1998 – 2005 Senior Lecturer in Neurosurgery, University of Southampton

**Resume**

Professor William Gray obtained an honours medical degree from University College Cork, Ireland in 1986, Fellowship of the Royal College of Surgeons in 1990, MD by thesis in 1993 and his Fellowship in Surgical Neurology in 1995. He was appointed Senior Lecturer in Neurosurgery in 1998 after completing two years of stem cell research at post-doctoral level. He was appointed to the University Chair of Neurosurgery at Southampton in January 2006. He established a functional epilepsy surgery programme in Southampton in 2000. His research interests are in cerebral physiology, Health Technology Assessment in Neuroscience and Adult neural stem cell biology. He has had a number of research grants with the Research Councils and Industry. He is Secretary of the UK Chapter of the International League Against Epilepsy (ILAE) and is Chairman of the Academic Committee of the Society of British Neurological Surgeons (SBNS). He has established a training programme in academic Neurosurgery in Southampton (one of three nationally), obtaining a Walport Clinical Lecturer, two Walport ACFs and three academic F2 training positions in academic neurosurgery.

Current research includes investigation of the effects of neuropeptides on adult neural stem cells funded by the MRC, an analysis of cytokines and gene expression in neural stem cells after brain injury funded by the MRC and GlaxoSmithKline and characterisation of Adult Human Neural Stem Cells in 3D culture (EPSRC). He has written a number of book chapters and reviews on adult neural stem cells and brain Injury. His external collaborators include Prof. Helen Scharfman, Columbia University, New York (BDNF and adult neural stem cells), Prof. Herbert Herzog, Garvin Institute, Sydney, Australia (NPY receptor knockout mice), Prof. Annette Beck-Sickinger, Univ Leipzig, Germany (NPY receptor pharmacology), Prof. Christian Steinhauser, University of Bonn and Prof. Frank Kirchoff, MPI, Gottingen (gial and neural stem cells) and Prof. Claude Wasterlain, UCLA (Galanin and neurogenesis). He also has collaborative industrial research links with the stem cell group at GlaxoSmithKline.

**5 most recent Publications:**

Watkins, A.J., Wilkins, A., Cunningham, C., Perry, V.H., Seet, M.J., Osmond, C., Eckert, J.J., Torrens, C., Cagampang, F.R., Cleal, J., Gray, W.P., Hanson, M.A. & Fleming, T.P. (**2008**) Low protein diet fed exclusively during mouse oocyte maturation leads to behavioural and cardiovascular abnormalities in offspring. The Journal of physiology, 586, 2231-2244.

Gray, W.P. (**2008**) Neuropeptide Y signalling on hippocampal stem cells in health and disease. Molecular and cellular endocrinology; *288,* p52-63.

Scharfman, H.E. & Gray, W.P. (**2007**) Relevance of seizure-induced neurogenesis in animal models of epilepsy to the etiology of temporal lobe epilepsy. Epilepsia, 48 Suppl 2, 33-41.

Laskowski, A., Howell, O.W., Sosunov, A.A., McKhann, G. & Gray, W.P. (**2007**) NPY mediates basal and seizure-induced proliferation in the subcallosal zone. Neuroreport, 18, 1005-1008.

Howell, O.W., Silva, S., Scharfman, H.E., Sosunov, A.A., Zaben, M., Shatya, A., McKhann, G., 2nd, Herzog, H., Laskowski, A. & Gray, W.P. (**2007**) Neuropeptide Y is important for basal and seizure-induced precursor cell proliferation in the hippocampus. Neurobiology of disease, 26, 174-188.

Grants Prof W.P. Gray 2003- 2008 **Research grants and contracts**

| Dates | Award Holder(s) | Funding Body | Title | Value |
|---|---|---|---|---|
| Jan 2004 – June 2005 | H.V. Wheal, W.P. Gray, L.E. Sundstrom, V. O'Connor | Epilepsy Research Foundation | Studies on hippocampal neurogenesis | £60,000 |
| Oct 2004 – Sept 2007 | W.P. Gray | FQMS PhD studentships x2 | | £150,000 |
| Oct 2004 – Sept 2007 | W.P. Gray, V. O'Connor | **MRC** | Neuropeptide control of adult hippocampal stem cell proliferation | £236,000 |
| Sept 2005 – August 2008 | C. James, W.P. Gray | LSI PhD Studentship | Seizure Prediction | £30,000 |
| Oct 2005 – Sept 2008 | W.P. Gray, A.A. Chang | **MRC** CASE studentship | Regulation of neural stem cell proliferation - analysis of cytokines | £36,000 |
| Oct 2006 – Sept 2009 | W.P. Gray, E. Redhead | Epilepsy Research UK | Role of altered neurogenesis in spatial memory dysfuntion in chronic TLE | £60,000 |
| Oct 2007 – Sept 2010 | W.P. Gray, P. Newland, G. Attard | Kerkut Trust | Interneuron control of stem cells | £36,000 |
| Oct 2007 – Sept 2009 | N Hanley, W.P. Gray, D. Wilson | **EPSRC** | Chameleon Spots - 3D culture of human tissue and stem cells | £1,732,570 |
| Oct 2008 – Sept 2011 | D Simpson, R. Panerai, W.P. Gray, R. Allen, A. Birch , J. Potter | **EPSRC** – EP/G008787/1, EP/G0101420/1 | New methods for assessing the control of blood flow in the brain | £400,000 |
| | | | | £2.7 million |

**Summary Curriculum Vitae - Professor Harvey Nicholas Rutt FOSA, FInstP, FIEE, SMIEEE.**

Current Post, since 1$^{st}$ January 1992 Rank Professor of Infrared Science and Technology, School of Electronics and Computer Science, University of Southampton, Highfield, Southampton, SO17 1BJ. Tel. 023 8059 3814 Fax 023 8059 7442 Email h.rutt@ecs.soton.ac.uk Head of School, Electronics and Computer Science, since 1$^{st}$ August 2007. The School has 119 academic staff, 130 research, 68 support, 268 post-graduate and over 900 undergraduate students. Turnover ˜£27 million pa. ECS holds the maximum possible 6* 'Research Assessment Rating' and maximum possible 'Teaching Quality' rating, and came top in the recent Guardian league table of Universities offering Electronics courses. At University level I am responsible for the ECS

component, ˜50%, of our new £55million clean room facility, and a member of the senior management team, Senate etc.

**Employment history 1975-1991** : UKAEA Culham Laboratory, Abingdon, Oxon, OX14 3DB. **1971-1975** : Lecturer, Federal University of Rio Grande do Sul, Porto Alegre, Brazil.

**Education** BSc First Class Honours, Zepler Prize, University of Southampton 1968. PhD 'Proustite Parametric Oscillators' University of Southampton 1972.

**Membership of learned societies, Directorships include** Fellow of the Optical Society of America
Fellow of the Institute of Physics
Fellow of the Institute of Electrical Engineering
Senior Member of the IEEE (USA)
Director, Photonics Innovations Limited from its origin in 1999. PIL is the University vehicle for funding spin-out companies in the photonics field.
Director, Stratophase Ltd, from 2003. Stratophase is a new University Photonics spin-out company.
Director, ECS Partners Ltd.
Editor in Chief of the Elsevier journal Infrared Science and Technology since approximately 2001, editor since approximately 1994.
**Research Interests** My research interests are principally in the generation, manipulation, detection and uses of infrared radiation across the entire IR spectrum from the near infrared to millimetre waves. This includes novel IR sources and lasers, new IR transparent materials in bulk, thin film and fibre form, and novel optical instruments. Applications have included ore analysis, medical diagnostic instrumentation, down-hole oil well sensors, novel infrared modulators for IR imagers, and methods of detecting the relative water content of surfaces remotely. A recent theme is the development of infrared and 'terahertz' instrumentation for medical and biological applications. This includes imaging for resection margin determination during neurosurgery, infrared measurements of abnormal proteins in early Alzheimer's Disease, and fundamental studies of protein folding. A 'terahertz microscope' is also under development. A strongly developing area of work is the use of multi-spectral imaging techniques to assist surgeons in the operating theatre. Work is in progress on neurosurgery, breast cancer surgery, and also for dermatological applications.

From 1992 to 2006, I was either Principle Investigator or co-investigator on research grants totalling £7.75 million.

**Teaching** My primary responsibilities are in the direction of the ORC, ECS, and in research. At post graduate level, I currently have five PhD students, and have

supervised nine PhD students to completion. Although management and research pressures now preclude undergraduate lecturing, in the recent past I have taught Engineering Physics, and supervised undergraduate projects.

**Summary of Publications etc.** Over 80 papers in refereed academic journals and 17 patents. More recent publications include:

Vargas-Rodriguez, E., Rutt, H., Rojas-Laguna, R. and Alvarado-Mendez, E. (2008) Calibration of a gas sensor based on cross-correlation spectroscopy. *Journal of Optics A: Pure and Applied Optics* . (In Press)

Hoy, P., Rutt, H., Gray, W. and Bulters, D. (2008) Optical Intraoperative Measurement of Function in the Human Brain. In: *Frontiers in Optics (FiO)/Laser Science XXIV (LS) Conference 2008*, 19-23 October 2008, Rochester Riverside Convention Center, USA.

Kannath, A. and Rutt, H. (2007) Development of low cost instrumentation for non-invasive detection of Helicobacter Pylori. In: *Conference on Advanced Biomedical & Clinial Diagnostic Systems*, Jan 21-23 2007, San Jose.

Vargas-Rodriguez, E. and Rutt, H. N. (2007) An analytical method to find the optimal parameters for gas detectors based on correlation spectroscopy using a Fabry-Perot interferometer. *Applied Optics*, 46 (21). pp. 4625-4632.

Rutt, H. N. (2007) The Partition Function of Large Biomolecules, and its Relevance to Infrared and Terahertz Spectroscopy. In: *IRMMW-THz 2007, The Joint 32nd International Conference on Infrared & Millimetre Waves and 15th International Conference on Terahertz Electronics*, 2-7 September 2007, Cardiff.

**Professor Harvey Nicholas Rutt Research grants and contracts**

| **Dates** | **Award Holder(s)** | **Funding Body** | **Title** | **Value** |
|---|---|---|---|---|
| 1.9.2003 | D.N. Payne, R.W. Eason, H.N. Rutt, J.S. Wilkinson, E.R. Taylor, D.J. Richardson | EPSRC | Materials and Processes for Microstructured Photonic Devices | £653,446 |
| 1.4.2004 | D.N. Payne, R.W. Eason, D. Hanna, H.N. Rutt, J.S. Wilkinson, D.W. Hewak, D.J. Richardson, P. Smith, T.M. Monro | EPSRC | Fabrication of Microstructured Glass & Crystal Photonic Materials & Devices | £2,801,404 |
| 16.1.2006 | H.N. Rutt, D.J. Richardson, K. Frampton | EPSRC | The Ultimate Soft Glass Extrusion Machine | £79,482 |
| 2006 | H. Perry, H.N. Rutt, P. Hoy, V. O'Connor, C. Cunningham, K. Hilton | CCLRC SRS | Preliminary investigation of the detection of early stage prion disease in mouse brain sections | 5 days use of synchrotron, (Ref 46086 ) |
| 2008 | H. Perry, H.N. Rutt, P. Hoy, V. O'Connor, C. Cunningham, K. Hilton | CCLRC SRS | Preliminary investigation of the detection of early stage prion disease in mouse brain sections | 5 days use of synchrotron (Ref 50105) |

# Bibliography


Adriano Aguzzi. Prions and the immue system: a trip through intestine, spleen, lymph nodes and nerves. *Rendiconti Lincei Scienze Fisiche E Naturali*, 9(14): 293–337, 2003.

Adriano Aguzzi. Prion diseases of humans and farm animals: epidemiology, genetics and pathogenesis. *Journal of Neurochemistry*, 97:1726–1739, 2006.

F. K. Albert and M. Forsting. Resection and prognosis. *Journal of Neurosurgery*, 98(1):225–226, 2003.

Friedrich K. Albert, Michael Forsting, Klaus Sartor, Hans-Peter D. Adams, and Stefan Kunze. Early postoperative magnetic resonance imaging after resection of malignant glioma: Objective evaluation of residual tumor and its influence on regrowth and prognosis. *Neurosurgery*, 34(1):45–61, 1994.

J. H. Ali, W. B. Wang, M. Zevallos, and R. R. Alfano. Near infrared spectroscopy and imaging to probe difference in water content in normal and cancer human prostate tissues. *Technology in Cancer Research and Treatment*, 3(5):491–499, 2004.

Alzheimer's Society. Alzheimer's society web page (http://alzheimers.org.uk), 2009.

M Ammirati, J.H. Galicich, E. Arbit, and Y.L. Liao. Reoperation in the treatment of recurrent intracranial malignant gliomas. *Neurosurgery*, 21: 607–614, 1987a.

M Ammirati, N Vick, Y.L. Liao, I Ciric, and M Mikhael. Effect of the extent of surgical resection on survival and quality of life in patients with supratentorial glioblastomas and anaplastic astrocytomas. *Neurosurgery*, 21(2):201–206, 1987b.

J.R. Anderson, K. C. Cain, and R.D. Gelber. Analysis of survival by tumor response. *Journal of Clinical Oncology*, 1:710–719, 1983.

J. Andreou, A. E. George, A Wise, M de Leon, I.I. Kricheff, J. Ransohoff, and S.H. Foo. CT prognostic criteria of survival after malignant glioma surgery. *American Journal of Neuroradiology*, 4(3):588–490, 1983.

Paul G. L. Andrus and Robert D. Strickland. Cancer grading by fourier transform infrared spectroscopy. *Biospectroscopy*, 4(37):46, 1997.

Susanne Astner, Susanne Dietterle, Nina Otberg, Hans-Joachim Rowert-Huber, Eggert Stockfleth, and Jurgen Lademann. Clinical applicability of in vivo fluorescence confocal microscopy for noninvasive diagnosis and therapeutic monitoring of nonmelanoma skin cancer. *Journal of Biomedical Optics*, 13(1), 2008.

A. Averbuch and Y. Keller. A unified approach to FFT based image registration, 2001.

A. Averbuch and Y. Keller. FFT based image registration. *IEEE*, 2002.

Michael Bajura and Ulrich Neumann. Dynamic registration correction in video-based augmented reality systems. *IEEE Computer Graphics and Applications*, pages 52–60, 1995.

J. Bandekar. Amide modes and protein conformation [review]. *Biochimica et Biophysica Acta*, 1120(2):123–143, 1992.

Jagdeesh Bandekar and S. Krimm. Normal mode spectrum for the parallel-chain beta-sheet. *Biopolymers*, 27:909–921, 1988.

Fred G. Barker and Susan M. Chang. Improving resection of malignant glioma. *Lancet Oncology*, 7:359–60, 2006.

Juan Manuel Benavides, Sung Chang, Sun Young Park, Rebecca Richards-Kortum, Nick Mackinnon, Calum MacAulay, Andrea Milbourne, Anais Malpica, and Michele Follen. Multispectral digital colposcopy for in vivo detection of cervical cancer. *Optics Express*, 11(10):1223–1236, 2003.

Selim Benhimane and Ezio Malis. Real-time image-based tracking of planes using efficient second-order minimization. In *2004 IEEE/RSJ international conference on intelligent robots and systems*, pages 943–949, Sendai, Japan, 2004.

Y. Bentoutou, N. Taleb, K. Kpalma, and J. Ronsin. An automatic image registration for applications in remote sensing. *Ieee Transactions on Geoscience and Remote Sensing*, 43(9):2127–2137, 2005.

Tammie L. S. Benzinger, David M. Gregory, Timothy S. Burkoth, Helene Miller-Auer, David G. Lynn, Robert E. Botto, and Stephen C. Meredith. Propagating structure of alzheimer's beta-amyloid is parallel beta-sheet with residues in exact register. *Proceedings of the National Academy of Sciences of the United States of America*, 95:13407–13412, 1998.

Hans Bernsen, Jeroen van der Laak, Benno Kusters, Abel van der Ven, and Peter Wesseling. Gliomatosis cerebri: quantitative proof of vessel recruitment by cooptation instead of angiogenesis. *Journal of Neurosurgery*, 103(4):702–706, 2005.

Peter McL Black, Thomas Moriarty, Eben Alexander, Philip Stieg, Eric J. Woodard, P. Langham Gleason, Claudia Martin, Ron Kikinis, Richard B. Schwartz, and Ference A. Jolesz. The development and implementation of intraoperative MRI and its neurosurgical applications. *Neurosurgery*, 41(4):15, 1997.

David A. Boas, Tom Gaudette, Gary Strangman, Xuefeng Cheng, John J. A. Marota, and Joseph B. Mandeville. The accuracy of near infrared spectroscopy and imaging during focal changes in cerebral hemodynamics. *NeuroImage*, 13: 76–90, 2000.

Arjen Bogaards, Abhay Varma, Sean P. Collens, Aihua Lin, Anoja Giles, Victor X. D. Yang, Juan M. Bilbao, Lothar D. Lilge, Paul J. Muller, and Brian C. Wilson. Increased brain tumor resection using fluorescence image guidance in a preclinical model. *Lasers in Surgery and Medicine*, 35:181–190, 2004a.

Arjen Bogaards, Abhay Varma, Kai Zhang, David Zach, Stuart K. Bisland, Eduardo H. Moriyama, Lothar Lilge, Paul J. Muller, and Brian C. Wilson. Fluorescence image-guided brain tumour resection with adjuvant metronomic photodynamic therapy: pre-clinical model and technology development. *Photochemical and Photobiological Sciences*, 4:438–442, 2004b.

Giovanni Bottiroli, Anna C. Croce, Donata Locatelli, Rosanna Nano, Ermanno Giornbelli, Alberto Messina, and Eugenio Benericetti. Brain tissue autofluorescence: An aid for intraoperative delineation of tumor resection margins. *Cancer Detection and Prevention*, 22(4):330–339, 1998.

S. Brandner, S. Isenmann, A. Raeber, M. Fischer, A. Sailer, Y. Kobayashi, Marino S., C. Weissmann, and Adriano Aguzzi. Normal host prion protein necessary for scrapie-induced neurotoxicity. *Nature*, 379:339–343, 1996.

Molly A. Brewer, Urs Utzinger, Jennifer K. Barton, James B. Hoying, Nathaniel D. Kirkpatrick, William R. Brands, John R. Davis, Katherine Hunt,

Sally J. Stevens, and Arthur F. Gmitro. Imaging of the ovary. *Technology in Cancer Research and Treatment*, 3(6):617–627, 2004.

Molly A. Brewer, Urs Utzinger, Elvio Silva, David Gershenson, Robert C. Bast, Michele Follen, and Rebecca Richards-Kortum. Fluorescence spectroscopy for in vivo characterization of ovarian tissue. *Lasers in Surgery and Medicine*, 29: 128–135, 2001.

Ron Brookmeyer, Elizabeth Johnson, Kathryn Ziegler-Graham, and H. Michael Arrighi. Forcasting the global burden of alzheimer's disease, 2007.

Carrie Brookner, Urs Utzinger, Michele Follen, Rebecca Richards-Kortum, Dennis Cox, and E. Neely Atkinson. Effects of biographical variables on cervical fluorescence emission spectra. *Journal of Biomedical optics*, 8(3): 479–483, 2003.

L. G. Brown. A survey of image registration techniques. *Computing Surveys*, 24 (4):325–376, 1992.

P. D. Brown, M. J. Maurer, T. A. Rummans, B. E. Pollock, K. V. Ballman, J. A. Sloan, B. F. Boeve, R. M. Arusell, M. M. Clark, and J. C. Buckner. A prospective study of quality of life in adults with newly diagnosed high-grade gliomas: The impact of the extent of resection on quality of life and survival. In *40th Annual Meeting of the American-Society-of-Clinical-Oncology*, pages 495–503, New Orleans, LA, 2004.

H.R. Bueler, Adriano Aguzzi, A. Sailer, R.A. Greiner, P Autenried, M. Aguet, and C. Weissmann. Mice devoid of prp are resistant to scrapie. *Cell*, 73: 1339–1347, 1993.

Peter C. Burger, P.J. Dubois, S.C. Schold, K.R. Smith, G.L. Odom, D.C. Crafts, and F. Giangaspero. Computerized tomographic and pathologic studies of the untreated, quiescent, and recurrent glioblastoma multiforme. *Journal of Neurosurgery*, 58(2):159–169, 1983.

Peter C. Burger and Sylvan B. Green. Patient age, histologic features, and length of survival in patients with glioblastoma multiforme. *Cancer*, 9 (1617-1625), 1987.

Pramod V. Butte, Brian K. Pikul, Aviv Hever, William H. Yong, Keith L. Black, and Laura Marcu. Diagnosis of meningioma by time-resolved fluorescence spectroscopy. *Journal of Biomedical Optics*, 10(6):064026, 2005.

Micheal D. Byler and H. Susi. Examination of the secondary structure of proteins by deconvoluted FTIR spectra. *Biopolymers*, 25:469–487, 1986.

David G. Cameron and Douglas J. Moffatt. A generalised-approach to derivative spectroscopy. *Applied Spectroscopy*, 41(4):539–544, 1987.

National Research Council Canada. Illuminating information for cardiac surgeons. Technical report, National Research Council Canada, 2002.

Cancer Research UK. www.cancerresearchuk.org, 2009.

A. F. Cannestra, S. Y. Bookheimer, N. Pouratian, Alyssa O'arrell, Nancy Sicotte, N. A. Martin, Donald P. Becker, Gregory Rubion, and Arthur W. Toga. Temporal and topographical charcterization of language cortices using intraoperative optical intrinsic signals. *NeuroImage*, 12:41–54, 2000.

Andrew F. Cannestra, Nader Pouratian, Susan Y. Bookheimer, Neil A. Martin, Donald P. Becker, and Arthur W. Toga. Temporal spatial differences observed by functional MRI and human intraoperative optical imaging. *Cerebral Cortex*, 11(8):773–782, 2001.

Joaquin Castilla, Paula Saa, Claudio Hetz, and Claudio Soto. In vitro generation of infectious scrapie prions. *Cell*, 121(2):195–206, 2005.

Byron Caughey and Gerald S. Baron. Prions and their partners in crime [review]. *Nature*, 443, 2006.

Byron Caughey and Peter T. Lansbury. Protofibrils, pores, fibrils, and neurodegeneration: separating the responsible protein aggregates from the innocent bystanders. *Annual Review of Neuroscience*, 26:267–298, 2003.

Albert E. Cerussi, Andrew J. Berger, Frederic Bevilacqua, Natasha Shah, Dorota Jakubowski, John Butler, Randall F. Holcombe, and Bruce J. Tromberg. Sources of absorption and scattering contrast for near-infrared optical mammography. *Academic Radiology*, 8(3):211–218, 2000.

R. L. Chandler. Encephalopathy in mice produced by inoculation with scrapie brain material. *The Lancet*, 1:1378–9, 1961.

Q. S. Chen, M. Defrise, and F. Deconinck. Symmetrical phase-only matched filtering of fourier-mellin transforms for image registration and recognition. *Ieee Transactions on Pattern Analysis and Machine Intelligence*, 16(12): 1156–1168, 1994.

Ying Chen, Pengwei Hao, and Chao Zhang. Shear-resize factorizations for fast image registration. In *IEEE International Conference on Image Processing (ICIP 2005)*, pages 2961–2964, Genoa Italy, 2005. IEEE.

Lin-P'ing Choo, David L. Wetzel, William C. Halliday, Michael Jackson, Steven M. LeVine, and Henry H. Mantsch. In situ characterization of -amyloid in alzheimer's deseased tissue by synchrotron fourier transform infrared microspectroscopy. *Biophysical Journal*, 71:1672–1679, 1996.

B. W. Chwirot, S. Chwirot, W. Jedrzejczyk, M. Jackowski, A. M. Raczynska, J. Winczakiewicz, and J. Dobber. Ultraviolet laser-induced fluorescence of human stomach tissues: Detection of cancer tissues by imaging techniques. *Lasers in Surgery and Medicine*, 21(2):149–158, 1997.

A. Claes, A. J. Idema, and P. Wesseling. Diffuse glioma growth: a guerilla war [review]. *Acta Neuropathologica*, 114(5):443–458, 2007.

Elizabeth B. Claus, Andres Horlacher, Liangge Hsu, Richard B. Schwartz, Donna Dello-Iacono, Florian Talos, Ference A. Jolesz, and Peter M. Black. Survival rates in patients with low-grade glioma after intraoperative magnetic resonance image guidance. *Cancer*, 103(6):1227–1233, 2005.

R.J. Coffey, L.D. Lunsford, and F.H Taylor. Survival after stereotactic biopsy of malignant gliomas. *Neurosurgery*, 22(3):465–73, 1988.

Tom Collier, Dizem Arifler, Anais Malpica, Michele Follen, and Rebecca Richards-Kortum. Determination of epithelial tissue scattering coefficient using confocal microscopy. *IEE Journal of Selected Topics In Quantum Electronics*, 9(2):307–313, 2003.

J Collinge. Molecular neurology of prion disease. *Journal of Neurology Neurosurgery and Psychiatry*, 76:906–919, 2005.

John Collinge, Miles A. Whittington, Katie C.L. Sidle, Corinne J. Smith, Mark S. Palmer, Anthony R. Clarke, and John G.R. Jefferys. Prion protein is necessary for normal synaptic function. *Nature*, 370:295–297, 1994.

H.G. Creutzfeldt. [About herdfrmige a peculiar disease of the central nervous system] uber eine eigenartige herdformige erkrankung des zentralnervensystems. *Zeitschrift ffir die gesamte Neurologie und psychiatrie*, 1920.

Anna C. Croce, Sabrina Fiorani, Donata Locatelli, Nano Rosanna, Mauro Ceroni, Flavio Tancioni, Ermanno Giombelli, Eugenio Benericetti, and Giovanni Bottiroli. Diagnostic potential of autofluorescence for an assisted intraoperative delineation of glioblastoma resection margins. *Photochemistry and Photobiology*, 77(3):309–318, 2003.

J. Cuille and P.L. Chelle. La maladie diete tremblante du mouton est-elle inoculable? *Comptes Rendus de l'Academie des Sciences*, 203:1552–1554, 1936.

J. Cuille and P.L. Chelle. Experimental transmission of trembling to the goat. *Comptes Rendus de l'Academie des Sciences*, 208:1058–1060, 1939.

C. Cunningham, R. Deacon, H. Wells, D. Boche, E. Waters, C. Picanco Diniz, H. Scott, J. N. P. Rawlins, and V. H. Perry. Synaptic changes characterize early behavioural signs in the ME7 model of murine prion disease. *European Journal of Neuroscience*, 17(10):2147–2155, 2003.

C. Cunningham, R. M. J. Deacon, K. Chan, D. Boche, J. N. P. Rawlins, and V. H. Perry. Neuropathologically distinct prion strains give rise to similar temporal profiles of behavioral deficits. *Neurobiology of Disease*, 18(2): 258–269, 2005a.

Colm Cunningham, David C. Wilcockson, Suzanne Campion, Katie Lunnon, and V. Hugh Perry. Central and systemic endotoxin challenges exacerbate the local inflammatory response and increase neuronal death during chronic neurodegeneration. *The Journal of Neuroscience*, 25(40):9275–9284, 2005b.

G. U. Dachs and G. M. Tozer. Hypoxia modulated gene expression: angiogenesis, metastasis and therapeutic exploitation. *European Journal of Cancer*, 36:1649–1660, 2000.

Phil Dadachanji. Protimeter, 2003 (personnal communication).

W.E. Dandy. Removal of right cerebral hemisphere for certain tumors with hemiplegia: preliminary report. *the Journal of the American Medical Association*, 90:823–825, 1928.

M Daneyemez, F Gezen, Z Canakci, and S Kahraman. Radical surgery and reoperation in supratentorial malignant glial tumors. *Minimally Invasive Neurosurgery*, 41(4):209–13, 1998.

E. De Castro and C. Morandi. Registration of translated and rotated images using finite fourier transforms. In *IEE transactions on pattern analysis and machine intelligence*, page 700. IEEE, 1987.

Harmen H. J. de Jongh, Erik Goormaghtigh, and Jean-Marie Ruysschaert. The different molar absorptivities of the secondary structure types in the amide i region: An attenuated total reflection infrared study on globular proteins. *Analytical Biochemistry*, 242:95–103, 1996.

Dermlite. http://www.dermlite.com, 2009.

Aichun Dong, Ping Huang, and Winslow S. Caughey. Protein secondary structures in water from second-derivative amide i infrared spectra. *Biochemistry*, 29:3303–3308, 1990.

Aichun Dong, Ping Huang, and Winslow S. Caughey. Redox-dependant changes in beta-extended chain and turn structures of cytochrome c in water solution determined by second derivative amide i infrared spectra. *Biochemistry*, 31(1): 182–189, 1992.

Janie Dubois, Richard Baydack, Eilean McKenzie, Timothy Booth, and Mike Jackson. Scrapie infection investigatie by magnetic resonance imaging and foureir transform infrared microscopy. *Vibration Spectroscopy*, 32:95–105, 2003.

H. Duffau, L. Capelle, D. Denvil, N. Sichez, P. Gatignol, M. Lopes, M-C. Mitchell, J-P. Sichez, and R. Van Effenterre. Functional recovery after surgical resection of low grade gliomas in eloquent brain: hypothesis of brain compensation. *Journal of Neurology Neurosurgery and Psychiatry*, 74:901–907, 2008.

Andrew K. Dunn, Anna Devor, Hayrunnisa Bolay, Mark L. Andermann, Michael A. Moskowitz, Anders M. Dale, and David A. Boas. Simultaneous imaging of total cerebral hemoglobin concentration, oxygenation and blood flow during functional activation. *Optics Letters*, 28:28–30, 2002.

Rainer Eckel, Hong Huo, Hong-Wei Guan, Xiang Hu, Xun Che, and Wei-Dong Huang. Characteristic infrared spectroscopic patterns in the protein bands of human breast cancer tissue. *Vibration Spectroscopy*, 27:165–173, 2001.

Heinz Fabian, Dieter Naumann, Rolf Misselwitz, Otto Ristau, Dieter Gerlach, and Heinz Welfle. Secondary structure of streptokinase in aqueous solution: A fourier transform infrared sepctroscopic study. *Biochemistry*, 31(28): 6532–6538, 1992.

Joyce Farrell. Autoexposure algorithms for digital cameras, 2004.

L.M. Fletcher, J.B. Barsotti, and J.P. Hornak. A multispectral analysis of brain tissues. *Magnetic Resonance in Medicine*, 29:8, 1993.

Gianluigi Forloni, Nadia Angeretti, Roberto Chiesa, Enrico Monzani, Mario Salmona, and Fabrizio Tagliavini. Neurotoxicity of a prion protein fragment. *Nature*, 362:543–546, 1993.

M. Forsting, F. K. Albert, S. Kunze, H. P. Adams, D. Zenner, and K. Sartor. Extirpation of glioblastomas - MR and CT follow-up of residual tumour and regrowth patterns. In *1991 Annual Meeting of the American Soc of Neuroradiology*, pages 77–87, Washington, Dc, 1991.

M. Forsting, F. K. Albert, S. Kunze, H. P. Adams, D. Zenner, and K. Sartor. Extirpation of glioblastomas: MR and CT follow-up of residual tumor and regrowth patterns. *American journal of Neuroradiology*, 14(1):77–87, 1993.

Peter T. Fox and Marcus E. Raichle. Focal physiological uncoupling of cerebral blood flow and oxdative metabolism during somatosensory stimulation in human subjects. *Proceedings of the National Academy of Sciences of the United States of America*, 83:1140–1144, 1986.

Peter T. Fox, Marcus E. Raichle, M.A. Mintun, and C. Dence. Nonoxidative glucose consumption during focal physologic neural activity. *Science*, 241 (4864):462–464, 1988.

H. Fraser, M.E. Bruce, A. Chree, I. McConnell, and G.A.H. Wells. Transmission of bovine spongiform encephalopathy and scrapie to mice. *Journal of General Virology*, 73:1891–1897, 1992.

Naoko Fujioka, Yuji Morimoto, Tsunenori Arai, and Makoto Kikuchi. Discrimination between normal and malignant human gastric tissues by fourier transform infrared spectroscopy. *Cancer Detection and Prevention*, 28(1): 32–36, 2004.

D.C. Gajdusek and V. Zigas. Degenerative disease of the central nervous system in new guinea - the endimic occurence of 'kuru' in the native population. *New England Journal of Medicine*, 257:974–978, 1957.

M.P. Garhart, M.A. Smith, K.L. Levay, and R.W. Thompson. Raw image registration (CROSS-CORR). In *International Ultraviolet explorer New spectral image processing system information manual. Version 2.0*, pages 74–81. European Space Agency, 1999.

S. C. Gebhart, W. C. Lin, and A. Mahadevan-Jansen. In vitro determination of normal and neoplastic human brain tissue optical properties using inverse adding-doubling. *Physics in Medicine and Biology*, 51:2011–2027, 2005.

C.J. Gibbs, D.C. Gajdusek, D.M. Asher, M.P. Alpers, E. Beck, P.M. Daniel, and W.B. Matthews. Creutzfeldt-jakob disease (spongiform encephalopathy): transmission to the chimpanzee. *Science*, 161:388–389, 1968.

Erik Goormaghtigh, Veronique Cabiaux, and Jean-Marie Ruysschaert. Secondary structure and dosage of soluble and membrane proteins by attenuated total reflection fourier-transform infrared spectroscopy on hydrated films. *European Journal of Biochemistry*, 193:409–420, 1990.

John C. Gore, Silvina G. Horovitz, Christopher J. Cannistraci, and Pavel Skudlarski. Integration of fMRI, NIROT and ERP for studies of human brain function. *Magnetic Resonance Imaging*, 24:507–513, 2006.

Joan C. Gorga, Aichun Dong, Mark C. Manning, Robert W. Woody, Winslow S. Caughey, and Jack L. Strominger. Comparison of the secondary structure of human class i and class II major histocompatibility complex antigens by fourier transform infrared and circular dichroism spectroscopy. *Proceedings of the National Academy of Sciences of the United States of America*, 86: 2321–2325, 1988.

J.S. Griffith. Nature of the scrapie agent: self-replication and scrapie. *Nature*, 215:1043–1044, 1967.

Amiram Grinvald, Ron D. Frostig, Ralph M. Siegel, and Eyal Bartfeld. High-resolution optical imaging of functional brain architecture in the awake monkey. *Proceedings of the National Academy of Sciences of the United States of America*, 88:11559–11563, 1991.

Amiram Grinvald, Edmund Lieke, Ron D. Frostig, Charles D. Gilbert, and Torsten N. Wiessel. Functional architecture of cortex revealed by optical imaging of intrinsic signals. *Nature*, 324:361–364, 1986.

Dirk Grosenick, Heidrun Wabnitz, K. Thomas Moesta, Jorg Mucke, Peter M. Schlag, and Hebert Rinneberg. Time-domain scanning optical mammography: II. optical properties and tissue pararmeters of 87 carcinomas. *Physics in Medicine and Biology*, 50:2451–2468, 2005.

M. M. Haglund and D. W. Hochman. Optical imaging of epileptiform activity in human neocortex. *Epilepsia*, 45(4):43–7, 2004.

M. M. Haglund, G. A. Ojemann, and D. W. Hochman. Optical imaging of epileptiform and functional activity in human cerebral cortex. *Nature*, 358: 668–671, 1992.

Walter A. Hall. Extending survival in gliomas: surgical resection or immunotherapy? *Surgical Neurology*, 61(2):145–148, 2004.

Maarouf A. Hammoud, R. Sawaya, W. Shi, Peter F. Thall, and Norman E. Leeds. Prognostic significance of preoperative MRI scans in glioblastoma miltiforme. *Journal of Neuro-Oncology*, 27(1):65–73, 1996.

K.M. Hebeda, A.E. Saarnak, M. Olivo, Henricus J. C. M. Sterenborg, and J.G. Wolbers. 5-aminolevulinic acid induced endogenous porphyrin fluorescence 9L and c6 brain tumours and in the normal rat brain. *Acta Neurochirurgica*, 140: 503–513, 1998.

Kenneth R. Hess. Extent of resection as a prognostic variable in the treatment of glioma. *Journal of Neuro-Oncology*, 42(3):227–231, 1999.

Andrew F. Hill, Martin Zeidler, James Ironside, and John Collinge. Diagnosis of new variant creutzfeldt-jakob disease by tonsil biopsy. *The Lancet*, 349:99–100, 1997.

Derek L. G. Hill, Andrew D. Castellano Smith, Andrew Simmons, Calvin R. Maurer, Timothy C.S. Cox, Robert Elwes, Michael Brammer, David J. Hawkes, and Charles E Polkey. Sources of error in comparing functional magnetic resonance imaging and invasive electrophysiological recordings. *Journal of Neurosurgery*, 93(2):214–223, 2000.

D.K. Hill and R.D. Keynes. Opacity changes in stimulated nerve. *Journal of Physiology (Cambridge)*, 108(3):278–281, 1949.

Hippocrates. Hippocratic oath (Translation from the greek by ludwig edelstein. from the hippocratic oath: Text, translation, and interpretation, by ludwig edelstein. baltimore: Johns hopkins press, 1943.), ca. 400BC.

Zhiwei Huang, Annette McWilliams, Harvey Lui, David I. McLean, Stephen Lam, and Haishan Zeng. Near-infrared raman spectroscopy for optical diagnosis of lung cancer. *International Journal of Cancer*, 107(6):1047–1052, 2003.

T. R. Husson, A. K. Mallik, J. X. Zhang, and N. P. Issa. Functional imaging of primary visual cortex using flavoprotein autofluorescence. *Journal of Neuroscience*, 27(32):8665–8675, 2007.

Michael Jackson, James R. Mansfield, Brion Dolenko, Rajmund L. Somorjai, Henry H. Mantsch, and Peter H. Watson. Classification of breast tumors by grade and steroid receptor status using pattern recognition analysis of infrared spectra. *Cancer Detection and Prevention*, 23(3):245–253, 1999.

Michael Jackson and H.H. Mantsch. The use and misuse of FTIR spectroscopy in the determination of protein structure. *Critical Reviews in Biochemistry and Molecular Biology*, 30(2):95–120, 1995.

Andreas H. Jacobs, Lutz W. Kracht, Axel Gossmann, Macia A. Ruger, Anne V. Thomas, Alexander Thiel, and Karl Herholz. Imaging in neurooncology. *NeuroRx*, 2:333–347, 2005.

A. Jakob. [About peculiar disease of the central nervous system with remarkable anatomical results. (Spastic pseudo-sclerosis encephalompelophathie with disseminated degeneration flocks)] uber eigenartige erkrankungen des zentralnervensystems mit bemerkenswertem anatomischem. befunde. (Spastische pseudosklerose-encephalompelophathie mit disseminierten

degenerationsherden). *Zeitschrift ffir die gesamte Neurologie und psychiatrie*, 64:147–228, 1921.

M. Jeffrey, W. G. Halliday, J. Bell, A.R. Johnsone, N.K. Macleod, C. Ingham, A.R. Sayers, D.A. Brown, and J.R. Fraser. Synapse loss associated with abnormal prp precedes neuronal degeneration in the scrapie-infected murine hippocampus. *Neuropathology and Applied Neurobiology*, 26:41–54, 2000.

B. Jeremic, B. Milicic, D. Grujicic, A. Dagovic, and J. Aleksandrovic. Multivariate analysis of clinical prognostic factors in patients with glioblastoma multiforme treated with a combined modality approach. *Journal of Cancer Research and Clinical Oncology*, 129(8):477–484, 2003.

Sheng Jianqiu, Shen Shijie, Li Shirong, Wu Xia, Gao Ge, Li Shiyong, and Chen Zhimin. Fourier-transform infrared spectrometric analysis for detecting colorectal carcinoma. *Chinese Journal of Digestive Diseases*, 2:179–183, 2001.

Shoji Kaminaka, Toshiaki Ito, Hiroya Yamazaki, Ehiichi Kohda, and Hiro-o Hamaguchi. Near-infrared multichannel raman spectroscopy toward real-time in vivo cancer diagnosis. *Journal of Raman Spectroscopy*, 33:498–502, 2002.

Elizabeth M. Kanter, Ross M. Walker, Samuel L. Marion, Molly Brewer, Patricia B. Hoyer, and Jennifer K. Barton. Dual modality imaging of a novel rat model of ovarian carcinogenesis. *Journal of Biomedical optics*, 11(4): 041123, 2006.

Abul B.M.F. Karim, Denes Afra, Philippe Cornu, Norman Bleehan, Simon Schraub, Olivier De Witte, Francois Darcel, Sally Stenning, Marianne PieRart, and Martine Van Glabbeke. Randomized trial on the efficacy of radiotherapy for cerebral low-grade glioma in the adult: European organization for research and treatment of cancer study 22845 with the medical research council study BR05: an interim analysis. *International Journal of Radiation Oncology Biology Physics*, 52(2):316–324, 2002.

Jyrki K. Kauppinen, Douglas J. Moffatt, H.H. Mantsch, and David G. Cameron. Fourier self-deconvolution - a method for resolving intrinsically overlapped bands. *Applied Spectroscopy*, 35(3):271–276, 1981.

G. Evren Keles, Brad Anderson, and Mitchel S. Berger. The effect of extent of resection on time to tumour progression and survival in patients with glioblastoma multiforme of the cerebral hemisphere. *Surgical Neurology*, 52(4): 371–379, 1999.

G. Evren Keles, Kathleen R. Lamborn, and Mitchel S. Berger. Low-grade hemispheric gliomas in adults: a critical review of extent of resection as a factor influencing outcome [review]. *Journal of Neurosurgery*, 95(5):735–745, 2001.

Y. Keller, A. Averbuch, and M. Israeli. Pseudopolar-based estimation of large translations, rotations, and scalings in images. *Ieee Transactions on Image Processing*, 14(1):12–22, 2005.

P.J. Kelly, C. Daumas-Duport, D.B. Kispert, B.A. Kall, B.W. Scheithauer, and J.J. Illig. Imaging-based stereotaxic serial biopsies in untreated intracranial glial neoplasms. *Journal of Neurosurgery*, 66(6):865–74, 1987.

D.F. Kennedy, M. Crisma, C. Toniolo, and D Chapman. Studies of peptides forming 310 and alpha-helices and beta-bend ribbon structures in organic solution and in model biomebranes by fourier transform infrared spectrscopy. *Biochemistry*, 30:6541–6548, 1991.

Ritu Khurana and Anthony Fink. Do parrallel beta-helix have a unique fourier transform infrared spectrum? *Biophysical Journal*, 78:994–1000, 2000.

Ralf Kleene, Gabriele Loers, Julia Langer, Yveline Frobert, Friedrick Buck, and Melitta Schachner. Prion protein regulates glutamate-dependent lactate transport of astrocytes. *The Journal of Neuroscience*, 27(45):12331–12340, 2007.

Michael Knauth, Christian R. Wirtz, Volker M. Tronnier, Nurdagul Aras, Stefan Kunze, and Klaus Sartor. Intraoperative MR imaging increases the extent of tumor resection in patients with high-grade gliomas. *American Journal of Neuroradiology*, 20:1642–1646, 1999.

Janina Kneipp, Michael Beekes, Peter Lasch, and Dieter Naumann. Molecular changes of preclinical scrapie can be detected by infrared spectroscopy. *The Journal of Neuroscience*, 22(8):2989–2997, 2002.

Janina Kneipp, Peter Lasch, Elizabeth Baldauf, Michael Beekes, and Dieter Naumann. Detection of pathological molecular alterations in scrapie-infected hamster brain by fourier transform infrared (FT-IR) spectroscopy. *Biochimica et Biophysica Acta*, 1501:189–199, 2000.

Janina Kneipp, Lisa M. Miller, Sashko Spassov, Fabian Sokolowski, Peter Lasch, Michael Beekes, and Dieter Naumann. Prion structure investigated in situ, ex vivo, and in vitro by FTIR spectroscopy. In A. Mahadevan-Jansen, Michael G. Sowa, Gerwin J. Puppels, Zygmunt Grynczynski, Tuan Vo-Dinh, and Joseph R. Lakowicz, editors, *Biomedical Vibrational Spectroscopy and Biohazard Detection Technologies*, volume 5321, pages 17–25. SPIE, 2004.

Senada Koljenovic, Lin-P'ing Choo-Smith, Tom C. Bakker Schut, Johan M. Kros, Herbert van den Berge, and Gerwin J. Puppels. Discriminating vital tumor from necrotic tissue in human glioblastoma tissue samples by raman spectroscopy. *Laboratory Investigation*, 82(10):1265–1277, 2002.

T. Kombos, B.-C. Kern, T. Holl, and M. Brock. Monopolar motor cortex stimulation: A new mapping technique? *Clinical Neurology and Neurosurgery*, 99:108, 1997.

Jilie Kong and Shoaning Yu. Fourier transform infrared spectroscopic analysis of protein secondary structures [review]. *Acta Biochimica et Biophysica Sinica*, 39(8):549–559, 2007.

Andrew Kowalczuk, R. Loch Macdonald, Chris Amidei, George Dohrmann, Robert K Erickson, MHekmatpanah, Javad, Stuart Krauss, Swarna Krishnasamy, Gregory Masters, Sean F. Mullan, Arno J. Mundt, Yatrick Sweeney, Everett E. Vokes, Bryce K.A. Weir, and Robert L. Wollman. Quantitative imaging study of extent of surgical resection and prognosis of malignant astrocytomas. *Neurosurgery*, 45(5):1028–1038, 1997.

Christoph Krafft, Stephan B. Sobottka, Gabriele Schackert, and Reiner Salzer. Analysis of human brain tissue, brain tumors and tumor cells by infrared spectroscopic mapping. *Analyst*, 129:921–925, 2004.

Christoph Krafft, Katja Thummler, Stephan B. Sobottka, Gabriele Schackert, and Reiner Salzer. Classification of malignant gliomas by infrared spectroscopy and linear discriminant analysis. *biopolymers*, 82:301–305, 2006.

Firedrich W. Kreth, Ansgar Berlis, Vicki Spiropoulou, Michael Faist, Rudi Scheremet, Reinhard Rossner, Benedikt Volk, and Christoph B. Ostertag. The role of tumor resection in the treament of glioblastoma multiforme in adults. *Cancer*, 86(10):2117–2124, 1999.

Firedrich W. Kreth, P.C. Warnke, Rudi Scheremet, and Christoph B. Ostertag. Surgical resection and radiation therapy versus biopsy and radiation therapy in the treatment of glioblastoma multiforme. *Neurosurgery*, 78(5):762–6, 1993.

Ariane Kretlow, Qi Wang, Janina Kneipp, Peter Lasch, Michael Beekes, Lisa M. Miller, and Dieter Naumann. FTIR-Microspectroscopy of prion-infected nervous tissue [review]. *Biochimica et Biophysica Acta*, 1758:948–959, 2006.

S. Krimm and J. Bandekar. Vibrational spectroscopy and conformation of peptides, polypeptides, and proteins. *Advances in Protein Chemistry*, 38: 181–364, 1986.

T. Krings, M. Schreckenberger, V. Rohde, H. Foltys, U. Spetzger, O. Sabri, M.H.T. Reinges, S. Kemeny, P.T. Meyer, W. Moller-Hartmann, M. Korinth, J.M. Gilsback, U. Buell, and A. Thron. Metabolic and electrophysoliogical validation of functional MRI. *Journal of Neurology Neurosurgery and Psychiatry*, 71:762–771, 2001.

Beat Kunz, Erika Sandmeier, and Philipp Christen. Neurotoxicity of prion peptide 106-126 not confirmed. *Federation of European Biochemical Societies Letters*, 458:65–68, 1999.

M. Kurimoto, N. Hayashi, H. Kamiyama, S. Nagai, T. Shibata, T. Asahi, N. Matsumura, Y. Hirashima, and S. Endo. Impact of neuronavigation and image-guided extensive resection for adult patients with supratentorial malignant astrocytomas: A single-institution retrospective study. *Minimally Invasive Neurosurgery*, 47(5):278–283, 2004.

Yoko Kusunoki, Fumio Imamura, Hiroshi Uda, Masayuki Mano, and Takeshi Horai. Early detection of lung cancer with laser-induced fluorescence endoscopy and spectrofluorometry. *Chest*, 118(6):1776–1782, 2000.

M. Lacroix, D. Abi-Said, D. R. Fourney, Z. L. Gokaslan, W. Shi, F. DeMonte, F. F. Lang, I. E. McCutcheon, S. J. Hassenbusch, E. Holland, K. Hess, C. Michael, D. Miller, and R. Sawaya. A multivariate analysis of 416 patients with glioblastoma multiforme: prognosis, extent of resection, and survival. *Journal of Neurosurgery*, 95(2):190–198, 2001.

S. Larsen, R. Kikinis, I.-F. Talos, D. Weinstein, W. Wells, and A. Golby. Quantitative comparison of functional MRI and direct electrocortical stimulation for functional mapping. *The international journal of medical robotics and computer assisted surgery*, 3:262–270, 2007.

Corinne Ida Lasmezas, Jean-Guy Fournier, Virginie Nouvel, Hermann Boe, Dominique Marce, Francois Lamoury, Nicolas Kopp, Jean-Jacques Hauw, James Ironside, Moira Bruce, Dominique Dormont, and Jean-Philippe Deslys. Adaptation of the bovine spongiform encephalopathy agent to primates and comparison with creutzfeldt-jakob disease: implications for human health. *Proceedings of the National Academy of Sciences of the United States of America*, 98(7):4142–4147, 2001.

Edward R. Laws. Resection of low-grade gliomas. *Journal of Neurosurgery*, 95: 731–732, 2001.

Edward R. Laws, Ian F. Parney, Wei Huang, Fred Anderson, Angel M. Morris, Anthony Asher, Kevin O. Lillehei, Mark Bernstein, Henry Brem, Andrew

Sloan, Mitchel S. Berger, and Susan Chang. Survival following surgery and prognostic factors for recently diagnosed malignant glioma: data from the glioma outcomes project. *Journal of Neurosurgery*, 99:467–473, 2003.

D.C. Lee, P. I. Haris, D Chapman, and R.C. Mitchell. Determination of protein secondary structure using factor analysis of infrared spectra. *Biochemistry*, 29 (39):9185–93, 1990.

Daniel Richard Leff, J. Warren, Oliver, Louise C. Enfield, Adam Gibson, Thanos Athanasiou, Darren K. Patten, Jem Hebden, Guang Zhong Yang, and Ara Darzi. Diffuse optical imaging of the healthy and diseased breast: A systematic review [review]. *Breast Cancer Research and Treatment*, 108:9–22, 2008.

Wei-Chiang Lin, Steven A. Toms, E. Duco Jansen, and Anita Mahadevan-Jansen. Intraoperative application of optical spectroscopy in the presence of blood. *IEEE Jounal on Selected Topics in Quantum Electronics*, 7 (6):996–1003, 2001a.

Wei-Chiang Lin, Steven A. Toms, Mahlon D. Johnson, E. Duco Jansen, and A. Mahadevan-Jansen. In vivo brain tumour demarcation using optical spectroscopy. *Photochemistry and Photobiology*, 73(4):396–402, 2001b.

Wei-Chiang Lin, Steven A. Toms, Massoud Motamedi, E. Duco Jansen, and Anita Mahadevan-Jansen. Brain tumor demarcation using optical spectroscopy; an in vitro study. *Journal of Biomedical optics*, 5(2):214–220, 2000.

Gary P Liney. Centre for MRI investigations, university of hull, 2009.

S. Lo, Simon, Kwan H. Cho, Walter A. Hall, Wilson L. Hernandez, Ronald J. Kossow, Chung K. Lee, and H.B. Clark. Does the extent of surgery have an impact on the survival of patients who receive postoperative radiation therapy for supratentorial low-grade gliomas. *International Journal of Cancer*, 96 (Suppl.):71–78, 2002.

K. Lote, T. Egeland, B. Hager, B. Stenwig, K. Skullerud, J. Berg-Johnsen, I. Storm-Mathisen, and H. Hirschberg. Survival, prognostic factors, and therapeutic efficacy in low-grade glioma: a retrospective study in 379 patients. *Journal of Clinical Oncology*, 15:3129–3140, 1997.

Cordelia Luyken, Ingmar Blumcke, Rolf Fimmers, Horst Urbach, Christian E. Elger, Otmar D. Wiestler, and Johannes Schramm. The spectrum of long-term epilepsy-associated tumors: long-term seizure and tumor outcome and neurosurgical aspects. *Epilepsia*, 44(6):822–830, 2003.

Umar Mahmood, Ching-Hsuan Tung, Alexel Bogdanov, and Ralph Weissleder. Near-infrared optical imaging of protease activity for tumor detection. *Radiology*, 213(3):866–870, 1996.

A. Mangiola, G. Maira, P. De Bonis, M. Porso, B. Pettorini, G. Sabatino, and C. Anile. Glioblastoma multiforme in the elderly: A therapeutic challenge. *Journal of Neuro-Oncology*, 76(2):159–163, 2006.

L. Marcu, J. A. Jo, P. V. Butte, W. H. Yong, B. K. Pikul, K. L. Black, and R. C. Thompson. Fluorescence lifetime spectroscopy of glioblastoma multiforme. *Photochemistry and Photobiology*, 80(1):98–103, 2004.

D. Marr and E Hildreth. Theory of edge detection. *Proceedings of the Royal Society of London. Series B: Biological Sciences*, 207(1167):187–217, 1980.

Alastair J. Martin, Walter A. Hall, Halying Liu, Christopher H. Pozza, Eduard Michel, Sean O. Casey, Robert E. Maxwell, and Charles L. Truwit. Brain tumor resection: intraoperative monitoring with high-field-strength MR imaging — initial results. *Radiology*, 215(1):221–228, 2000.

Claudia Martin, Eben Alexander, Terry Wong, Richard Schwartz, Ference A. Jolesz, and Peter M. Black. Surgical treatment of low-grade gliomas in the intraoperative magnetic resonance imager. *Neurosurgical Focus*, 4(4):8, 1998.

R. Martinez, C. Volter, and R. Behr. Parameters assessing neurological status in malignant glioma patients: prognostic value for survival and relapse-free time. *British Journal of Neurosurgery*, 22(4):557–562, 2008.

Calvin R. Maurer, Derek L. G. Hill, Robert J. Maciunas, John A. Barwise, J. Michael Fitzpatrick, and Matthew Y. Wang. Measurement of intraoperative brain surface deformation under a craniotomy, 1998.

John C. Mazziotta. Mapping human brain activity in vivo. *Neurology*, 161: 273–278, 1994.

F.B. McGillion, G.G. Thompson, and A. Goldberg. Tissue uptake of 5-aminolevulinic acid. *Biochemical Pharmacology*, 24(299-301), 1975.

Filip Meersman, Laszlo Smeller, and Karel Heremans. Comparative fourier transform infrared spectroscopy study of cold-pressure and heat-induced unfolding and aggregation of myoglobin. *Biophysical Journal*, 82:2635–2644, 2002.

Lars E. Meyer, Nina Otberg, Wolfram Sterry, and Juergen Ladermann. In vivo confocal scanning laser microscopy: comparison of the reflectance and

fluorescence mode by imaging human skin. *Journal of Biomedical Optics*, 11 (4), 2006.

K.A. Miles and M.R. Griffiths. Perfusion CT: a worthwhile enhancement? [review]. *The British Journal of Radiology*, 76:220–231, 2003.

Lisa M. Miller and Randy J. Smith. Synchrotrons versus globars, point-detectors versus focal plane arrays: Selecting the best source and detector for specific infrared microscpectroscopy and imaging applications. *Vibration Spectroscopy*, 38:237–240, 2005.

Lisa M. Miller, Qi Wang, Tejas P. Telivala, Randy J. Smith, Antonio Lanzirotti, and Judit Miklossy. Synchrotron-based infrared and x-ray imaging shows focalized accumulation of cu and zn co-localized with -amyloid deposits in alzheimer's disease. *Journal of Structural Biology*, 155:30–37, 2006.

Young-Kun Min, Tatsuya Yamamoto, Ehiichi Kohda, Toshiaki Ito, and Hiro-o Hamaguchi. 1064nm near-infrared multichannel raman spectroscopy of fresh human lung tissues. *Journal of Raman Spectroscopy*, 36:73–76, 2004.

J. F. Mineo, A. Bordron, M. Baroncini, C. Ramirez, C. A. Maurage, S. Blond, and P. Dam-Hieu. Prognosis factors of survival time in patients with glioblastoma multiforme: a multivariate analysis of 340 patients. *Acta Neurochirurgica*, 149(3):245–253, 2007.

R. Miralbell, J. Balart, X. Matias-Guiu, J. Molet, and J. Craven-Bartle. Radiotherapy for supratentorial low-grade gliomas: results and prognostic factors with special focus on tumour volume parameters. *Radiotherapy and Oncology*, 27(2):112–116, 1993.

S Mordechai, R.K. Sahu, Z. Hammody, S. Mark, K. Kantarovich, H Guterman, A. Podshyvalov, J Goldstein, and S Argov. Possible common biomarkers from FTIR microspectroscpy of cervical cancer and melanoma. *journal of Microscopy*, 215(1), 2004.

Brian J. Morris, Claudia Lee, Brian N. Nightingale, Eugen Molodysky, Lillian J. Morris, Rocco Appio, Sever Sternhell, Magnolia Cardona, Dorothy Mackerras, and Les M. Irwig. Fourier transform infrared spectroscopy of dysplastic, papillomavirus-positive cervicovaginal lavage specimens. *Gynecologic Oncology*, 56:245–249, 1995.

Carol Cruzan Morton. Aggressive surgery for low-grade brain tumor may lengthen life. *Focus Online, News from Harvard Medical, Dental and Public Health Schools*, 2005.

Y. Muragaki, H. Iseki, T. Maruyama, T. Kawamata, F. Yamane, R. Nakamura, O. Kubo, K. Takakura, and T. Hori. Usefulness of intraoperative magnetic resonance imaging for glioma surgery. In C. Fahlbusch R. Nimsky, editor, *Joint Convention of the 13th Academia-Eurasiana-Neurochirurgica/9th Germany-Academy-of-Neurosurgery*, pages 67–75, Bamberg, GERMANY, 2005.

T. Nariai, Y. Ohta, K. Hirakawa, K. Sato, I. Yazawa, S. Sasaki, K. Kamino, and K. Ohno. Intrinsic optical recording of somatosensory responses in the human cerebral cortex during brain tumor surgery. *Brain Activation and Cbf Control, Proceedings*, 1235:243–248, 2002.

Tadashi Nariai, Katsushige Sato, Kimiyoshi Hirakawa, Yoshihisa Ohta, Yoji Tanaka, Kiichi Ishiwata, Kenki Ishii, Kohtaro Kamino, and Kikuo Ohno. Imaging of somatotopic representation of sensory cortex with intrinsic optical signals as guides for brain tumor surgery. *Journal of Neurosurgery*, 103: 414–423, 2005.

J.M. Nazzaro and E.A. Neuwelt. The role of surgery in the management of supratentorial intermediate and high-grade astrocytomas in adults. [review]. *Journal of Neurosurgery*, 73(3):331–44, 1990.

NICE. Intraoperative fluorescence angiography for the evalutaion of coronary artery bypass graft patency - patient information. Technical report, NICE, 2004.

NICE. Interventional procedures overview of intraoperative fluorescence angiography for the evaluation of coronary artery bypass graft patency. Technical report, NICE, 2006.

Antonio Nicolato, Massimo A. Gerosa, Paolo Fina, Paolo Iuzzolino, Fabrizia Giorgiutti, and Albino Bricolo. Prognostic factors in low-grade supratentorial astrocytomas: a uni-multivariate statistical analysis in 76 surgically treated adult patients. *Surgical Neurology*, 44(3):208–223, 1995.

C. Nimsky, O. Ganslandt, B. von Keller, J. Romstock, and R. Fahlbusch. Intraoperative high-field-strength MR imaging: Implementation and experience in 200 patients. *Radiology*, 233(1):67–78, 2004.

Taizo Nitta and Kiyoshi Sato. Prognostic implication of the extent of surgical resection in patients with intracranial malignant gliomas. *Cancer*, 75(11): 2727–2731, 1995.

Catherine A. North, Richard B. North, Jonathon A. Epstein, Steven Piantadosi, and Moody D. Wharam. Low-grade cerebral astrocytomas: survival and quality of life after radiation therapy. *Cancer*, 66(1):6–14, 1990.

Novadaq. www.novadaq.com/, 2009.

Alexander Novotny and Walter Stummer. 5-aminolevulinic acid and the blood-brain barrier - a review. *Medical Laser Application*, 18(1):36–40, 2003.

Vasilis Ntziachristos, Christoph Bremer, and Ralph Weissleder. Fluorescence imaging with near-infrared light: new technological advances that enable in vivo molecular imaging. *European Radiology*, 13:195–208, 2002.

Keith A. Oberg and Anthony L. Fink. A new attenuated total reflectance fourier transform infrared spectroscopy method for the study of proteins in solution. *Analytical Biochemistry*, 256:92–106, 1998.

Jon D. Olson, Elyn Riedel, and Lisa M. DeAngelis. Long-term outcome of low-grade oligodendroglioma and mixed glioma. *Neurology*, 52:1442–1448, 2000.

Olympus KeyMed Group. http://www.keymed.co.uk, 2009.

Keh-Ming Pan, Micheal Baldwin, Jack Nguyen, Maria Gasset, Ana Serban, Darlene Groth, Mehlhorn Ingrid, Ziwei Huang, Robert J. Fletterick, Fred E. Cohen, and Stanley B. Prusiner. Conversion of alpha-helices into beta-sheets features in the formation of the scrapie prion proteins. *Proceedings of the National Academy of Sciences of the United States of America*, 90: 10962–10966, 1993.

Boon-Chuan Pang, Wei-Hwang Wan, Cheng-Kiang Lee, Kathleen Joy Khu, and Wai-Hoe Ng. The role of surgery in high-grade glioma - is surgical resection justified? a review of current knowledge [review]. *Annals Academy of Medicine Singapore*, 36(5):389–363, 2007.

D. J. Parekh, W. C. Lin, and S. D. Herrell. Optical spectroscopy characteristics can differentiate benign and malignant renal tissues: A potentially useful modality. *Journal of Urology*, 174(5):1754–1758, 2005.

Alexander H. Peden, Mark W. Head, Diane L. Ritchie, Jeanne E. Bell, and James W. Ironside. Preclinical vCJD after blood transfusion in a PRNP codon 129 heterozygous patient. *The Lancet*, 264:527–29, 2004.

Josep A. Perez-Pons, Esteve Padros, and Enrique Querol. Prediction and fourier-transform infrared-spectroscopy estimation of the secondary structure

of a recombinant beta-glucosidase from streptomyces sp. *Journal of Biochemistry*, 308:791–794, 1995.

V. H. Perry. personnal communication, 2009.

V. G. Peters, D. R. Wyman, M. S. Patterson, and G. L. Frank. Optical properties of normal and diseased human breast tissues in the visible and near infrared. *Physics in Medicine and Biology*, 35(9):1317–1334, 1990.

Francesco Pignatti, Martin van den Bent, Desmond Curran, Channa Debruyne, Richard Sylvester, Patrick Therasse, Denes Afra, Philippe Cornu, Michel Bolla, Charles Vecht, and Abul B.M.F. Karim. Prognostic factors for survival in adult patients with cerebral low-grade glioma. *Journal of Clinical Oncology*, 20(8):2076–2084, 2002.

N. Pouratian, N. Sicotte, D. Rex, N. A. Martin, D. Becker, A. F. Cannestra, and A. W. Toga. Spatial/temporal correlation of BOLD and optical intrinsic signals in humans. *Magnetic Resonance in Medicine*, 47(4):766–776, 2002.

Nader Pouratian, Sameer Sheth, Susan Y. Bookheimer, Neil A. Martin, and Arthur W. Toga. Applications and limitations of perfusion-dependent functional bain mapping for neurosurgical guidance. *Neurosurgical Focus*, 15 (1):1–7, 2003a.

Nader Pouratian, Sameer A. Sheth, Neil A. Martin, and Arthur W. Toga. Shedding light on brain mapping: advances in human optical imaging [review]. *Trends in Neurosciences*, 26(5):277–282, 2003b.

M.D. Prados, P.H. Gutin, T.L. Phillips, W.M. Wara, D.A. Larson, P.A. Sneed, R.L. Davis, D.K. Ahn, K. Lamborn, and C.B. Wilson. Highly anaplastic astrocytoma: a review of 357 patients treated between 1977 and 1989. *International Journal of Radiation Oncology Biology Physics*, 23(1):3–8, 1992.

Scott Prahl. http://omlc.ogi.edu/spectra/, 2001.

Steven J. Prestrelski, Micheal D. Byler, and Michael N. Liebman. Comparison of various molecular forms of bovine trypsin: correlation of infrared spectra with x-ray crstal structures. *Biochemistry*, 30:133–143, 1991.

M. A. Proescholdt, C. Macher, C. Woertgen, and A. Brawanski. Level of evidence in the literature concerning brain tumor resection. *Clinical Neurology and Neurosurgery*, 107(2):95–98, 2005.

Stanley B. Prusiner. Novel proteinaceous infectious particles cause scrapie. *Science*, 216(4542):136–144, 1982.

Stanley B. Prusiner. Prion diseases and the BSE crisis. *Science*, 278:245–251, 1997.

M.R. Quigley and J.C. Maroon. The relationship between survival and the extent of the resection in patients with supratentorial malignant gliomas [review]. *Neurosurgery*, 29(3):358–8, 1991.

B. Srinivasa Reddy and B. N. Chatterji. An FFT-based technique for translation, rotation and scale-invariant image registration. *Ieee Transactions on Image Processing*, 5(8):12661271, 1996.

John A. Reffner, Pamela A. Martoglio, and Gwyn P. Williams. Fourier transform infrared microscopial analysis with synchrotron radiation: the microscope optics and system performance. *Review of Scientific Instruments*, 66:1298, 1995.

B. Rigas, S. Morgello, I.S. Goldman, and P.T.T. Wong. Human colorectal cancers display abnormal fourier-transform infrared spectra. *Proceedings of the National Academy of Sciences of the United States of America*, 87:8140–8144, 1990.

A. Roggan, D. Schadel, U. Netz, J. P. Ritz, C. T. Germer, and G. Muller. The effect of preparation technique on the optical parameters of biological tissue. *Applied Physics B.Lasers and Optics*, 69:445–453, 1999.

T. C. Ryken, B. Frankel, T. Julien, and J. J. Olson. Surgical management of newly diagnosed glioblastoma in adults: role of cytoreductive surgery. *Journal of Neuro-Oncology*, 89(3):271–286, 2008.

P. Ryska, J. Zizka, V. Malek, V. Hobza, K. Odrazka, K. Elias, L. Klzo, A. Michl, and L. Ungermann. Early postoperative MRI in subjects with high - grade gliomas. *Ceska a Slovenska Neurologie a Neurochirurgie*, 68(1):19–25, 2005.

Michael Salcman, Herman Scholtz, Richard S. Kaplan, and Susan R.N. Kulik. Long-term survival in patients with malignant astrocytoma. *Neurosurgery*, 34 (2):8, 1994.

Ahmad Salman, Shmuel Argov, Jagannathan Ramesh, Jed Goldstein, Igor Sinelnikov, Hugo Guterman, and Shaul Mordechai. FTIR microscopic characterisation of normal and malignant humant colonic tissues. *Cellular and Molecular Biology*, 47(22):OL159–66, 2001.

Ichiro Sase, Akira Takatsuki, Junji Seki, Toshio Yanagida, and Akitoshi Seiyama. Noncontact backscatter-mode near-infrared time-resolved imaging system: preliminary study for functional brain mapping. *Journal of Biomedical Optics*, 11(5), 2006.

Katsushige Sato, Tadashi Nariai, Shinichi Sasaki, Itaru Yazawa, Hiraku Mochida, Naohisa Miyakawa, Yoko Momose-Sato, Kohtaro Kamino, Yoshihisa Ohta, Kimiyoshi Hirakawa, and Kikuo Ohno. Intraoperative intrinsic optical imaging of neuronal activity from subdivision of the human primary somatosensory cortex. *Cerebral Cortex*, 12:269–280, 2002.

Katsushige Sato, Tadashi Nariai, Yoji Tanaka, Taketoshi Maehara, Naohisa Miyakawa, Shinichi Sasaki, Yoko Momose-Sato, and Kikuo Ohno. Functional representation of the finger and face in the human somatosensory cortex: intraoperative instrinsic optical imaging. *NeuroImage*, 25:1292–1303, 2005.

R. Sawaya, Maarouf A. Hammoud, Derek Schoppa, Kenneth R. Hess, Shu Z. Wu, Wei-Ming Shi, and David M. Wildrick. Neurosurgical outcomes in a modern series of 400 craniotomies for treatment of parenchymal tumours. *Neurosurgery*, 42(5):1044–1055, 1998.

I. Schiessl, W. Wang, and N. McLoughlin. Independent components of the haemodynamic response in intrinsic optical imaging. *NeuroImage*, 39(2): 634–646, 2008.

J. P. Schneider, C. Trantakis, M. Rubach, T. Schulz, J. Dietrich, D. Winkler, C. Renner, R. Schober, K. Geiger, O. Brosteanu, C. Zimmer, and T. Kahn. Intraoperative MRI to guide the resection of primary supratentorial glioblastoma multiforme - a quantitative radiological analysis. *Neuroradiology*, 47(7):489–500, 2005.

Kevin T. Schomacker, Thomas M. Meese, Chunsheng Jiang, Charles C. Abele, Karen Dickson, Stephen T. Sum, and Ross F. Flewelling. Novel optical detection system for in vivo identification and localization of cervical intraepithelial neoplasia. *journal of Biomedical Optics*, 11(3), 2006.

Matthias L. Schroeter, Thomas Kupka, Toralf Mildner, Kamil Uludag, and D. Yves von Cramon. Investigating the post-stimulus undershoot of the BOLD signal - a simultaneous fMRI and fNIRS study. *NeuroImage*, 30:349–358, 2005.

Theodore H. Schwartz. Optical imaging of epileptiform events in visual cortex in response to patterned photic stimulation. *Cerebral Cortex*, 13(12):1287–1298, 2003.

Edward G. Shaw, R. M. Arusell, B.W. Scheithauer, J. O'Fallon, B. O'Neil, R. Dinapoli, D. Nelson, J. Earle, C. Jones, T. Cascino, D. Nichols, R. Ivnik, R. Hellman, W. Curran, and R. Abrams. Prospective randomized trial of low- versus high-dose radiation therapy in adults with supratentorial low-grade glioma: Initial report of a north central cancer treatment group/radiation

therapy oncology group/eastern cooperative oncology group study. *Journal of Clinical Oncology*, 20(9):2267–2276, 2002.

Edward G. Shaw and Jeffrey H. Wisoff. Prospective clinical trials of intracranial low-grade glioma in adults and children. *Neuro-oncology*, 5(3):153–160, 2003.

Jay R. Silveira, Gregory J. Raymond, Andrew G. Hughson, Richard E. Race, Valerie L. Sim, Stanley F. Hayes, and Byron Caughey. The most infectious prion protein particles. *Nature*, 437:257–261, 2005.

Justin S. Smith, Soonmee Cha, Mary Catherine May, Michael W. McDermott, Andrew T. Parsa, Susan M. Chang, William P. Dillon, and Mitchel S. Berger. Serial diffusion-weighted magnetic resonance imaging in cases of glioma: distinuishing tumour recurrence from postresection injury. *Journal of Neurosurgery*, 103:428–438, 2005.

Konstantin Sokolov, Michele Follen, and Rebecca Richards-Kortum. Optical spectroscopy for detection of neoplasia. *Current Opinion in Chemical Biology*, 6:651–658, 2002.

Jens Steinbrink, Arno Villringer, Florian Kempf, Daniel Haux, Stefanie Boden, and Hellmuth Obrig. Illuminating the BOLD signal: combined fMRI-fNIRS studies. *Magnetic Resonance Imaging*, 24:495–505, 2005.

Gerald Steiner, Anthony Shaw, Lin-P'ing Choo-Smith, Mario H. Abuid, Gabriele Schackert, Stephan Sobottka, Wolfram Steller, Reiner Salzer, and Henry H. Mantsch. Distinguishing and grading human glioma by IR spectroscopy. *Biopolymers*, 72:464–471, 2003.

E.O. Stejskal and J.E. Tanner. Spin diffusion mesurements: spin echoes in the presence of a time-dependant field gradient. *The Journal of Chemical Physics*, 42(1):288–292, 1965.

Matthew B. Stern. Transcranial ultrasound in parkinson's disease. *The Lancet: Neurology*, 7:376–377, 2008.

G. Strangman, J. P. Culver, J. H. Thompson, and D. A. Boas. A quantitative comparison of simultaneous BOLD fMRI and NIRS recordings during functional brain activation. *NeuroImage*, 17(2):719–731, 2002.

W. Stummer, H. J. Reulen, T. Meinel, U. Pichlmeier, W. Schumacher, J. C. Tonn, V. Rohde, F. Oppel, B. Turowski, C. Woiciechowsky, K. Franz, T. Pietsch, and A. LA-Glioma Study Grp. Extent of resection and survival on glioblastoma multiforme-identification of and adiustment for bias. *Neurosurgery*, 62(3):564–574, 2008.

Walter Stummer, Alexander Novotny, Herbert Stepp, Claudia Goetz, Karl Bise, and Hans-Jurgen Reulen. Fluorescence-guided resection of glioblastoma multiforme by using 5-aminolevulinic acidinduced porphyrins: a prospective study in 52 consecutive patients. *Journal of Neurosurgery*, 93:1003–1013, 2000.

Walter Stummer, Uwe Pichlmeier, Thomas Meinel, Otmar Dieter Wiestler, Friedhelm Zanella, and Hans-Jurgen Reulen. Fluorescence-guided surgery with 5-aminolevulinic acid for resection of malignant glioma: a randomised controlled multicentre phase III trial. *Lancet Oncology*, 7:392–401, 2006.

Walter Stummer, Susanne Stocker, Simon Wagner, Herbert Stepp, Clemens Fritsch, Claudia Goetz, Alwin Goetz, Reiner Kiefmann, and Hans J. Reulen. Intraoperative detection of malignant glioma by 5-aminolevulinic acid-induced photophyrin fluorescence. *Neurosurgery*, 42(3):518–526, 1998.

Kennichi Sugawara, Shogo Ischiuchi, Hideyuki Kurihara, Yoichi Nakazato, and Saito Nobuhito. Intraoperative fluorescence detection of malignant gliomas using 5-aminolevulinic acid. *Kitakanto Medical Journal*, 53:109–113, 2003.

Minah Suh, S Shariff, Sonya Bahar, A.D. Mehta, and T.H. Schwartz. intrinsic optical signal imaging of normal and abnormal physiology in animals and humans - seeing the invisible. *Clinical Neurosurgery*, 52:135–49, 2005.

Witold K. Surewicz, Henry H. Mantsch, and Dennis Chapman. Determination of protein secondary structure by fourier transform infrared spectroscopy: a critical assessment. *Biochemistry*, 32(2), 1993.

Witold K. Surewicz and H.H. Mantsch. New insight into protein secondary structure from resolution-enhanced infrared-spectra [review]. *Biochimica et Biophysica Acta*, 952(2):115–130, 1988.

H. Susi and Micheal D. Byler. Protein-structure by fourier-transform infrared spectroscopy 2nd derivative spectra. *Biochemical and Biophysical Research Communications*, 115(1):391–397, 1983.

H. Susi and Micheal D. Byler. Fourier-transform infrared study of proteins with parallel beta-chains. *Archives of Biochemistry and Biophysics*, 258(2):465–469, 1987.

H. Susi, Micheal D. Byler, and James M. Purcell. Estimation of beta-structure content of proteins by means of deconvoluted FTIR spectra. *Journal of Biochemical and Biophysical Methods*, 11(4-5):235–240, 1985.

Heino Susi and Micheal D. Byler. Resolution-enhanced fourier transform infrared spectroscopy of enzymes. *Methods in Enzymology*, 130:290–311, 1986.

Mehmet Teksam, Banu Cakir, and Mehmet Coskun. CT perfusion imaging in the early diagnosis of acute stroke. *Diagnostic and Interventional Radiology*, 11:202–205, 2005.

L. Terr and L.P. Weiner. An autoradiographic study of 5-aminolevulinic acid uptake by mouse brain. *Experimental Neurology*, 79(2):564–568, 1983.

The National Creutzfeldt-Jakob Disease Surveillance Unit. http://www.cjd.ed.ac.uk/, 2009.

I. Tobler, S.E. Gaus, T. Deboer, P. Achermann, M. Fischer, T. Rulicke, M. Moser, B. Oesch, P. A. McBride, and J. C. Manson. Altered circadian activity rhythms and sleep in mice devoid of prion protein. *nature*, 380: 369–642, 1996.

Steven A. Toms, Wei-Chiang Lin, Mahlon D. Johnson, Robert J. Weil, E. Duco Jansen, and A. Mahadevan-Jansen. Intraoperative detection of brain tumors using optical spectroscopy, a pilot study, in preparation.

Steven A. Toms, Wei-Chiang Lin, Robert J. Weil, Mahlon D. Johnson, E. Duco Jansen, and Anita Mahadevan-Jansen. Intraoperative optical spectroscopy identifies infiltrating glioma margins with high sensitivity. *Neurosurgery*, 57(4): 382–391, 2005.

H. Torii and M. Tasumi. Model calculations on the amide i infrared bands of globular proteins. *Journal of Chemical Physics*, 96(5):3379–3387, 1992.

Alessandro Torricelli, Antonio Pifferi, Paola Taroni, Eleonora Giambattistelli, and Rinaldo Cubeddu. In vivo optical characterization of human tissues from 610 to 1010nm by time-resolved reflectance spectroscopy. *Physics in Medicine and Biology*, 46:2227–2237, 2001.

Alexandre R. Tumlinson, Lida P. Hariri, Urs Utzinger, and Jennifer K. Barton. Miniature endoscope for simultaneous optical coherence tomography and laser-induced fluorescence measurement. *Applied Optics*, 43(1):113–122, 2003.

Geirmund Unsgaard, Steinar Ommedal, Tomm Muller, Aage Gronningsaeter, and Toril A. Nagulhus Hernes. Neuronavigation by intraoperative three-dimensional ultrasound: initial experience during brain tumour resection. *Neurosurgery*, 50(4):804–812, 2002.

Jutta Urenjak, Steve R. Williams, David G. Gadian, and Mark Noble. Proton nuclear magnetic resonance spectroscopy unambiguously identifies different neural cell types. *The Journal of Neuroscience*, 13(3):981–989, 1993.

Y Ushio, M Kochi, J Hamada, Y Kai, and H Nakamura. Effect of surgical removal on survival and quality of life in patients with supratentorial glioblastoma. *Neurologia medico-chirurgica*, 45(9):454–60, 2005.

Satoshi Utsuki, Hidehiro Oka, Sumito Sato, Sachio Suzuki, Satoru Shimizu, Satoshi Tanaka, and Kiyotaka Fujii. Possibility of using laser spectroscopy for the intraoperative detection of nonfluorescing brain tumors and the boundaries of brain tumor infiltrates, technical note. *Journal of Neurosurgery*, 104(4): 618–20, 2006.

Urs Utzinger, Douglas L. Heintzelman, A. Mahadevan-Jansen, Anais Malpica, Michele Follen, and Rebecca Richards-Kortum. Near-infrared raman spectroscopy for in vivo detection of cervical precancers. *Applied Spectroscopy*, 55(8):955–959, 2001.

Martin B. van der Mark, Anais Leproux, Tim Nielsen, Marjolein van der Voort, Leon Bakker, Michiel van Beek, Claas Bontus, Bernhard Brendel, Rik Karbers, Thomas Koehler, Falk Uhlemann, Andrea Wiethoff, Ronny Ziegler, Andy Ziegler, Lueder Fels, Martin Pessel, Stephanie van de Ven, Sjoerd Elias, Willem Mali, and Peter Luijten. Optical imaging of breast cancer by spectral and fluorescence diffuse optical tomography. In Karl Koch, editor, *Frontiers in optics 2008*, Rochester, New York, USA, 2008. OSA.

I. Vanzetta and A. Grinvald. Increased cortical oxidative metabolism due to sensory stimulation: Implications for functional brain imaging. *Science*, 286: 155–1558, 1999.

V. Vuorinen, S. Hinkka, M. Farkkila, and J. Jaaskelainen. Debulking or biopsy of malignant glioma in elderly people - a randomised study. *Acta Neurochirurgica*, 145:5–10, 2003.

T. D. Wang, J. M. Crawford, M. S. Feld, Y. Wang, I. Itzkan, and J. Van Dam. In vivo identification of colonic dysplasia using fluorescence endoscopic imaging. *Gastrointestinal Endoscopy*, 49(4):447–455, 1999.

Xuan Wang, Bin Xiao, Jian-Feng Ma, and Xiu-Li Bi. Scaling and rotation invariant analysis approach to object recognition based on radon and fourier-mellin transforms. *Pattern Recognition*, 40:3503–3508, 2007.

Masahisa Watarai, Suk Kim, Janchivdorj Erdenebaatar, Sou-ichi Makino, Motohiro Horiuchi, Toshikazu Shirahata, Suehiro Sakaguchi, and Shigeru Katamine. Cellular prion protein promotes brucella infection into macrophages. *Journal of Experimental Medicine*, 198(1):5–17, 2003.

I.R. Whittle. The dilemma of low grade glioma [review]. *Journal of Neurology, Neurosurgery and Psychiatry*, 75:31–36, 2004.

Cheryl L. Wilder, Andrew D. Friedrich, Russell O. Potts, Gaston O. Daumy, and Michael L. Francoeur. Secondary structural analysis of two recombinant murine proteins, interleukins 1alpha and 1beta: is infrared spectrsoscopy sufficient to assign structure? *Biochemistry*, 31:27–31, 1992.

Kumanan Wilson and Maura N. Ricketts. Transfusion transmission of vCJD: a crisis avoided? *The Lancet*, 364:477–479, 2004.

C. R. Wirtz, F. K. Albert, M. Schwaderer, C. Heuer, A. Staubert, V. M. Tronnier, M. Knauth, and S. Kunze. The benefit of neuronavigation for neurosurgery analyzed by its impact on glioblastoma surgery. *Neurological Research*, 22(4):354–360, 2000.

Jeffrey H. Wisoff, James M. Boyett, Mitchel S. Berger, Catherine Brant, Hao Li, Allan J. Yates, Patricia McGuire-Cullen, Patrick A. Turski, Leslie N. Sutton, Jeffrey C. Allen, J. Packer Roger, and Jonathan L. Finlay. Current neurosurgical management and the impact of the extent of resection in the treatment of malignant gliomas of childhood: a report of the children's cancer group trial no. CCG-945. *Neurosurgical Focus*, 2006.

A. Wong and D. A. Clausi. ARRSI: automatic registration of remote-sensing images. *Ieee Transactions on Geoscience and Remote Sensing*, 45(5): 1483–1493, 2007.

Bayden R. Wood, Micheal A. Quinn, Frank R. Burden, and Donald McNaughton. An investigation into FTIR spectroscopy as a biodiagnostic tool for cervical cancer. *Biospectroscopy*, 2:143–153, 1995.

Yuxiao Xie, Kaoru Sakatani, Wemara Lichty, Huancong Zuo, Zuoping Xie, and Jing Bai. Near-infrared spectroscopy studies on cerebral blood oxygenation changes during brain activation: possible limitations of blood oxygenation level dependent functional magnetic resonance imaging. *Optical Engineering*, 40 (10):2302–2307, 2001.

Xillix Technologies Corp. http://www.xillix.com, 2007.

Victor X. D. Yang, Paul J. Muller, Peter Herman, and Brian C. Wilson. A multispectral fluorescence imaging system: design and initial clinical teste in intra-operative photfrin-photdynamic therapy of brain tumors. *Lasers in Surgery and Medicine*, 32:224–232, 2003.

K. Yano, S. Ohoshima, Y. Gotou, K. Kumaido, T. Moriguchi, and H. Katayama. Direct measurement of human lung cancerous and noncancerous tissues by fourier transform infrared microscopy: can an infrared microscope be used as a clinical tool? *Analytical Biochemistry*, 287:218–225, 2000.

S-A Yeh, J-T Ho, C-C Lui, Y-J Huang, C-Y Hsiung, and E-Y Huang. Treatment outcomes and prognostic factors in patients with supertentorial low-grade gliomas. *British Journal of Radiology*, 78:230–235, 2005.

David Young. Straight lines and circle in the log-polar images. In *British Machine Vision Conference*, 2000.

Haishan Zeng, Mirjan Petek, Marjeta Tercelj Zorman, Annette McWilliams, Branko Palcic, and Stephen Lam. Integrated endoscopy system for simultaneous imaging and spectroscopy for early lung cancer detection. *Optics Letters*, 29(6):587–589, 2004.

Angelica Zepeda, Clorinda Arias, and Frank Sengpiel. Optical imaging of intrinsic signals: recent developments in the methodology and its applications [review]. *Journal of Neuroscience Methods*, 136(1):1–21, 2004.

W.G. Zijlstra, A. Buursma, and W.P. Meeuwsen-van der Roest. Absorption spectra of human fetal and adult oxyhemoglobin, de-oxyhemoglobin, carboxyhemoglobin, and methemoglobin. *Clinical Chemistry*, 37(9):1633–1638, 1991.

B. Zitova and J. Flusser. Image registration methods: a survey. *Image and Vision Computing*, 21(11):977–1000, 2003.

# Index